

**BER II
EXPERIMENTAL
REPORTS 2009**

BER II EXPERIMENTAL REPORTS

2009



Lise Meitner and Otto Hahn

edited by

A. Rödig, A. Brandt
and H.A. Graf

Berlin Neutron Scattering Center
Helmholtz-Zentrum Berlin für Materialien und Energie GmbH
in der Helmholtz Gemeinschaft

November 2010

Berichte des Helmholtz-Zentrums Berlin

HZB – 4

ISSN 1868-5781

Picture on front cover:

First glimpse of Dirac strings and magnetic monopoles in Dy₂Ti₂O₇ as seen on the flat-cone single crystal diffractometer E2 at BER II and heat capacity measurements in LaMMB.

In 1931 the physicist Paul Dirac predicted that magnetic monopoles can exist at the end of tubes – called Dirac strings – that carry magnetic field. A recent prediction in a material called spin ice showed excitations that should behave like analogies of magnetic monopoles at the end of strings, and these strings can be observed with neutron scattering.

Dysprosium titanate, Dy₂Ti₂O₇, is a spin ice with pyrochlore geometry that does not suffer from the impurity of a nuclear magnetic moment, therefore it is a clean system to look at the magnetism via diffuse neutron scattering.

The experiments have been carried out at the flat-cone single crystal diffractometer E2 at BER II (report page 20).

The results have been published as:

Dirac Strings and Magnetic Monopoles in Spin Ice Dy₂Ti₂O₇ Science 326 (2009), 411 - D.J.P. Morris, D.A. Tennant, S.A. Grigera, B. Klemke, C. Castelnovo, R. Moessner, C. Czefer-nasty, M. Meissner, K.C. Rule, J.-U. Hoffmann, K. Kiefer, S. Gerischer, D. Slobinsky, and R.S. Perry

Picture on back cover:

Sketch of the so called Dirac strings.

The cover was designed by *Screenworks*, Leibnizstraße 59, 10629 Berlin, www.screenworks.de

Editorial:

In January 2009, the former Hahn-Meitner Institute GmbH (HMI) has merged with the Berliner Elektronenspeicherring-Gesellschaft für Synchrotronstrahlung m.b.H. (BESSY) to form the new Helmholtz-Zentrum Berlin für Materialien und Energie (HZB). The HZB is a member of the Helmholtz Association of German Research Centres, Germany's largest scientific organisation with an annual budget of approximately 3 billion Euros.

The HZB is operating the neutron source BER II at the Lise-Meitner-Campus in Berlin Wannsee and the 3rd generation synchrotron source BESSY II at the Wilhelm-Conrad-Röntgen-Campus in Berlin Adlershof. The HZB User Coordination – with its two outposts in Wannsee (HZB-Neutrons) and Adlershof (HZB-Photons) – is ready to assist scientists from all over the world with applying for beam time, organising their stay at the HZB and performing their experiments at the two large-scale user facilities BER II and BESSY II.

Contact HZB Neutrons:

HZB User Coordination - Neutrons
Helmholtz-Zentrum Berlin
für Materialien und Energie GmbH
Lise-Meitner-Campus
Hahn-Meitner-Platz 1
D – 14109 Berlin

Phone: +49-30-8062 42778, - 42169, -42304, -43153

FAX: +49-30-8062 42523

Email: neutrons@helmholtz-berlin.de

Web: <http://www.helmholtz-berlin.de/userservice/neutrons>

CONTENTS

Introduction	IV
List of BER II Instruments	VII
How to apply for BER II Beam Time	XI
Acknowledgement for Support by the European Commission	XIII
List of Contributed Reports	XV

Part I: EXPERIMENTAL REPORTS 2009

Development of Instruments and Methods	1
Magnetism	13
Structure	63
Biology & Soft Matter	95
Material Science	131
Cultural Heritage	163

Part II: LIST OF BER II RELATED PUBLICATIONS

Theses	171
Publications 2009	172

AUTHOR INDEX	187
---------------------	------------

Introduction

In January 2009 two of Berlin's largest research centres, the Helmholtz-Zentrum Berlin (former Hahn-Meitner-Institut) and the Berlin synchrotron radiation source BESSY, have merged to form the new Helmholtz-Zentrum Berlin für Materialien und Energie (HZB). With this merger, a new era began for the two user facilities of the joint institute. HZB is now one of the few centres worldwide that are able to offer the whole range of instruments for neutron and synchrotron radiation experiments in one laboratory structure. Promoting the synergistic use of neutron and synchrotron radiation has become a major focus of the new institute. A common user entry point and a common Scientific Selection Panel dealing with the proposals for both facilities have been established to facilitate and encourage joint experiments with both probes. A unified user administration program for both facilities is presently developed.

Building on the 16-year-old tradition of the former "BENSC Experimental Reports" the present first "BER II Experimental Report" gives an overview on the research with neutrons carried out at the HZB in 2009. The reactor BER II was shut down for routine maintenance according to plan from January until middle of March 2009. In the rest of the year it delivered neutrons for experiments on 182 days. Fourteen instruments were fully scheduled for external user operation. The experiments performed are described by 148 reports, 94 from external users and 54 from BENSC scientists.

User Service

The HZB neutron facility BER II is open to the national and international scientific community. About 70% of the available beam time at the scheduled instruments are given to external users, 30% to in-house researchers. A fraction of the beam time for external users (up to 20% of the total beam time of an instrument) can be assigned to long-term collaborating groups from German universities and other national and international research institutions, the rest (at least 50% of the total beam time) is allocated to short term projects via a peer-review selection process.

The HZB has an outstanding tradition in providing sample environment for extreme conditions. A special emphasis is put on high magnetic fields and low and ultra low temperatures. Sample environment for high pressures up to 10 kbar and high temperatures is equally available.

More recently, a further focus in sample environment was put on the development of equipment for neutron scattering experiments under controlled gas pressure to serve a growing user

community from the fields of material science and soft condensed matter. This new "Dedicated Environment for Combined Gas Adsorption and Scattering Experiments" (DEGAS) includes humidity chambers for investigating biological samples as well as equipment for in-situ adsorption experiments on e.g. metal-organic framework systems.

For "off-beam" preliminary test experiments or additional investigations three specialised laboratories are also available for users. These are (i) the MagLab equipped with four fully operating measurement systems for magnetic fields up to 14.5 T and temperatures down to 260 mK, (ii) the GasLab equipped with a whole suite of modular experimental set-ups for experiments under controlled gas pressures and (iii) the Biolab offering a broad range of laboratory-based equipment with a focus on methods in optical spectroscopy. The access to these ancillary laboratories is mediated by the responsible instrument scientists.

A detailed technical handbook describing the existent equipment has been published by the sample environment group of HZB-Neutrons. It is continuously updated. This handbook as well as a detailed description of the neutron instruments is available on the internet under:

<http://www.helmholtz-berlin.de/userservice>

Scientific Selection Panel

To strengthen the synergetic use of neutron and synchrotron radiation, HZB has implemented a common HZB Scientific Selection Panel dealing with proposals for neutron and synchrotron radiation beamtime at the BER II and BESSY II in joint sessions. To this purpose, the HZB Scientific Selection Panel is organised in six Scientific Colleges, which are grouped according to research fields in order to facilitate discussions on the scientific merit of the proposals. All users applying for either neutron or synchrotron radiation beam time are requested to choose the appropriate Scientific College for their proposal upon on-line submission.

There are two proposal rounds per year. The deadlines for submitting the proposals are 1 March and 1 September. The proposals are allocated to the appropriate college as indicated by the proposer. Between 7 to 8 weeks after the deadlines the colleges of the Scientific Selection panel meet at the HZB and discuss and evaluate the proposals in closed sessions. They provide a priority ranking of the proposals based on their scientific merit and give advice on the appropriate amount of beamtime to be granted. Beamtime conflicts between different colleges are discussed and usually settled in a meeting of the college speakers following the college sessions. The final decision is taken by the Scientific Director of the HZB based on the recommenda-

tions of the college speakers. The results of the selection process are communicated to the proposers by the user coordinator. Rejected applicants are supplied with a written comment explaining the reasons for the refusal.

The 6 scientific colleges are:

C1 – Soft Matter and Biology

C2 – Macromolecular Crystallography

C3 – Chemistry, Catalysis

C4 – Electronic structures

C5 – Magnetism and Superconductivity

C6 – Material Science, Hard Condensed Matter

For more detailed information please see

https://www.helmholtz-berlin.de/user/user-info/colleges/index_en.html

Support for European Access to BENSC

BENSC is a major partner in the European Access programme “**Integrated Infrastructure Initiative for Neutron Scattering and Muon Spectroscopy (NMI3)**”, under the 7th EU Framework Programme (FP7), Grant Agreement number 226507-NMI3-Integrating Activities. NMI3-FP7 includes 12 different access activities offering European users approximately 1400 beam days of access to more than 150 instruments at European neutron and muon facilities with support for travel and subsistence. The programme started in February 2009 and will end in January 2011. The HZB has committed itself to provide a minimum of 240 instrument days for European users over this period of two years.

In 2009, 62 projects of 48 different European groups using 438 instrument days have been supported by BENSC. A total of 98 individual users out of 16 countries were involved. A list of the respective experimental reports included in this volume can be found on page XV.

Major Instrumental Developments

The year 2009 was characterised by finalising the plans for the large upgrade projects in the neutron guide hall I: The complete guide system from the source to the instruments shall be replaced by new supermirror coated guides and a new cold source using a focusing type moderator cell will be installed. These activities will take place between October 2010 and April 2011. In parallel some of the highly demanded user instruments in the guide hall I will be completely refurbished: The three-axes spectrometer FLEX (V2) will get an end position at its own dedicated neutron guide equipped with modern neutron optical devices such as an elliptical mirror as beam focussing element and a special polaris-

ing device. The time-of-flight spectrometer NEAT (V3) will be shifted out of the neutron guide hall I into an own new building. The chopper system and the whole secondary spectrometer of NEAT will be replaced. The tomography station CONRAD (V7) will be completely refurbished and a new detector system based on an arrangement of ³He-filled position-sensitive tubes will be installed at the small-angle scattering machine V4. An overall increase of performance by an order of magnitude can be expected by these upgrades.

The construction of two new instruments in the NGH-I has been continued in 2009. They were designed by university groups and are funded by the German Ministry of Education and Research. These instruments are (i) BioRef, a TOF reflectometer with a focus on the characterisation of bio-functional interfaces (University of Heidelberg in cooperation with HZB) and (ii) PONTO, a tomography station with a focus on the use of polarised monochromatic neutrons (Beuth University of Applied Sciences Berlin in cooperation with HZB). Both instruments will strongly profit by the new guide system.

In the new Neutron Guide Hall II (NGH-II) the final two instruments designated for this hall have been built up: the extreme-environment diffractometer EXED and the high resolution SANS machine VSANS. Both instruments have been in the commissioning phase in 2009.

Special Events

30th Berlin Neutron School

The 30th Berlin Neutron School was held at HZB from 26 March to 3 April 2009. It was attended by 30 students having backgrounds ranging from physics, materials science and engineering to chemistry, biology and soft matter. The majority were PhD students, but there were also some diploma and masters students as well as several post docs. Most of the participants came from European universities and research institutes, among them 12 from German institutions. The generous support by the European Union under its NMI3 Program is gratefully acknowledged.

The school is part of the curriculum of the Faculty of Mathematics and Sciences of the Technical University Berlin. Following suggestions by participants of previous schools, the length of the 2009 school was extended from five to nine days with more detailed lectures on all the techniques the students would encounter in the experiments. The practical sessions consisted of seven experiments on the V2/FLEX triple-axis spectrometer, the E9 powder diffractometer, the V3/NEAT time-of-flight spectrometer, the V7/CONRAD cold-neutron tomography station and the V5/SPAN neutron spin-echo spectrometer. Each practical lasted three hours, and the students were divided into groups of four people

which were rotated between all the experiments over a period of three and a half days. The last day of the school consisted of lectures on how neutron scattering is used as a research tool in the various subject areas: biology, chemistry, engineering and physics. The school was closed by an overview talk on the user service provided and the formalities to be observed when applying for beam time.

1st Joint BER II and BESSY II User Meeting

The first Joint BER II and BESSY II user meeting was held from 12 – 13 November 2009 at Berlin-Adlershof in the immediate vicinity of the Wilhelm-Conrad-Röntgen Campus of the HZB. About 300 external and 100 internal users of both facilities attended this meeting. The meeting was accompanied by an industrial exhibition featuring 49 companies.

The scientific program of the meeting was focused on topics covered by three of the six colleges of the Scientific Selection Panel:

- Soft Matter and Biology (college 1)
- Electronic Structure (college 4)
- Magnetism and Superconductivity (college 5)

A special emphasis was put on contributions dealing with the synergetic use of neutron and synchrotron radiation. Consequently, the meeting started with a key-note lecture on complementary scattering experiments with X-rays and neutrons given by O. Paris from the University of Leoben. It was followed by two reports of the representatives of the German Synchrotron community (U. Pietsch, chairman of the KFS) and the German neutron community (G. Eckold, chairmen of the KFN). The day ended with the bestowals of the Innovation Award on Synchrotron Radiation, the Ernst-Eckard-Koch prize, followed by a poster session in the BESSY II experimental Hall and a “Berliner Büffet” sponsored by the exhibitor companies. The second day started with facility reports on BESSY II and BER II and was continued with parallel sessions on Soft Matter and Life Sciences on the one hand and on Magnetism, Superconductivity and Electronic Structure on the other hand. The meeting ended with a well attended public lecture on the “Application of X-ray and Neutron Tomography in Palaeontology” given by Ch. Neumann from the Museum of Natural History in Berlin.

Conferences and Workshops

The **International Conference on Neutron Scattering** was the outstanding event in 2009. The conference was held in Knoxville, Tennessee, from 3 – 7 May 2009 and was attended by 660 participants from 29 countries. As in former international conferences on Neutron scattering, the share of the European neutron facilities in the scientific contributions and among these the

share of HZB was again remarkably high. In total, 453 poster contributions had been accepted by the program committee, of which 125 (28%) could unambiguously be attributed to one of the following major European centers: FRM II, GKSS, HZB, ILL, ISIS, JCNS and PSI. From these 125 posters by far the largest amount, namely 43 (34%), came from HZB users and in-house researchers who also gave 10% of the session talks.

Neutrons and X-rays meet biology, 25. - 27.02.2009

The international workshop was the first of its kind in-line with the new perspectives brought in by the freshly founded HZB. It was devoted to relations between structure, dynamics and function in biological systems as revealed by neutron and X-ray scattering and combinations of both.

Over 80 experts from within Europe and overseas gave an up-to-date account of the presently available results in this rapidly growing area of research in 9 keynote lectures, 28 oral and 19 poster contributions.

The scientific spectrum ranged from crystallography to large scale structures of biomolecules and their supramolecular assemblies via structure and dynamics under extreme conditions to in vivo imaging of cellular components up to living organism.

A large part of time was reserved for lively and stimulating discussions and exchanges between participants, which initiated and intensified collaborations between the different groups.

Kulturgut durchleuchtet - Strahlung trifft Kulturgut, 4. - 5.11.2009

The goal of the symposium was to foster the interdisciplinary co-operation between cultural scientists and natural scientists by presenting the broad palette of non-destructive investigation methods available in Berlin und Brandenburg on selected examples.

The examples ranged from the sky disc of Nebra over the sculpture of Queen Teje up to the paintings by the Flemish Master Steen. Each project was presented by a team: An art historian or restorer explicated the art historical issue and the conclusions deduced from the natural science findings, while a natural scientist described shortly how the measuring results were obtained.

More than 120 art historians, archaeologists, restorers, museum scientist, physicists, and chemists attended the symposium. From Berlin alone, 20 institutions were represented. The intense discussions, especially between the different disciplines during the breaks and the visit of the beam lines, showed that the goal of the symposium has been achieved.

List of BER II Instruments

Instruments in the BER II Experiment Hall (thermal neutrons) Telephone numbers: +49(0)30/8062-

	Instrument	ext.	Inst. Scientists	ext.
E1	3-Axis Spectrometer with Polarisation Analysis (limited access only in close co-operation with local staff members)	43101	A. Hoser M. Mihalik	42847 42793
E2	Flat-Cone Single Crystal Diffractometer (E2a: Crystal-Test Diffractometer)	43102	J. Hoffmann A. Hoser	42185 42847
E3	Residual Stress Analysis and Texture Diffractometer	43103	R. Wimpory	43097
E4	2-Axis-Diffractometer (E4b: Position for Single Crystal Orientation)	43104	K. Prokes S. Matas	42804 42804
E5	4-Circle Diffractometer	43104	M. Reehuis	42692
E6	Focusing Single Crystal Diffractometer	43105	N. Stüßer A. Hoser	43171 42847
E7	Residual Stress Analysis Diffractometer (limited access only in close co-operation with local staff members)	43107	R. Wimpory	43097
E9	Fine Resolution Powder Diffractometer (FIREPOD)	43106	D. Argyriou P. Henry F. Yokaichiya S. Kimber M. Tovar	43016 42686 43177 43079 42768
E10	HELINE, 3He-Diffractometer	43106	K. Siemensmeyer	42757

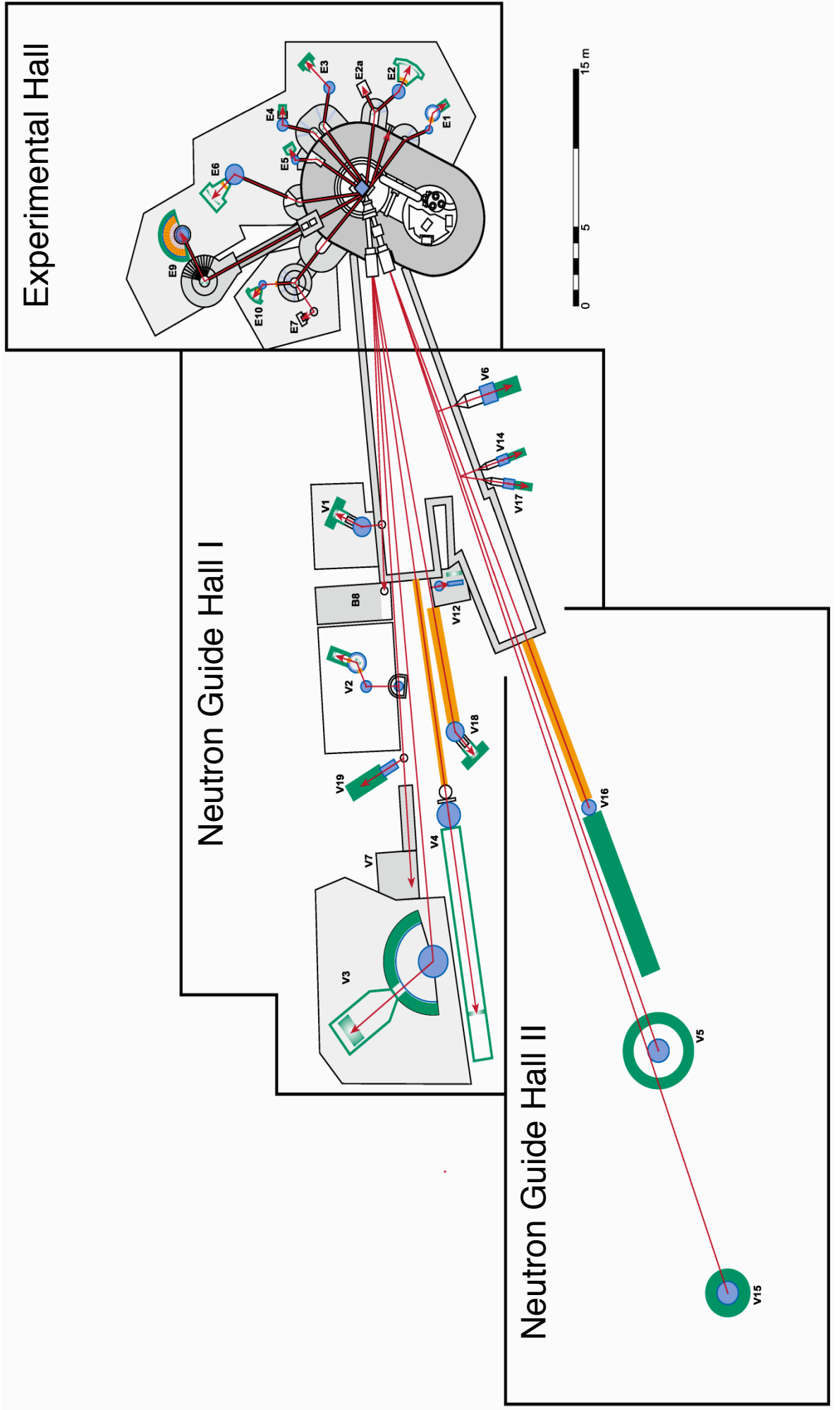
Instruments in the BER II Cold Neutron Guide Halls

Telephone numbers: +49(0)30/8062-

	Instrument	ext.	Inst. Scientists	ext.
V1	Membrane Diffractometer	43121	T. Hauß A. Buchsteiner	42071 42071
V2	I: 3-Axis Spectrometer (FLEX) II: FLEX with NRSE opt.	43122	K. Habicht K. Rule M. Skoulatos D. Le	42807 43067 42171 42803
V3	Time-of-Flight Spectrometer (NEAT)	43123	M. Russina E. Kemner Z. Izaola	43159 43073 43179
V4	Small Angle Scattering Instrument (SANS)	43124	U. Keiderling S. Prévost V. Ryukhtin A. Brandt D. Clemens K. Vogtt	42339 42339 43099 42169 42280 43022
V5	Spin-Echo Spectrometer with ToF Option (SPAN)	43125	S. Wellert B.-A. Brüning	42046 43072 43174
V6	Reflectometer	42806	R. Steitz R. Köhler A. Teichert	42149 43077 42044
V7	Cold Neutron Tomography and Radiography (CONRAD)	43327	N. Kardjilov A. Hilger M. Dawson	42298 42298
B8	Neutron-Autoradiography (limited access only in close co-operation with local staff members)	43121	A. Denker	43000
V12a	Bent-crystal Diffractometer (USANS) / Tomography	43131	W. Treimer S. Seidel	42221 43298
V14	Mirror Test Device	42284	T. Krist	42045

	Instrument	ext.	Inst. Scientists	ext.
V15	Extreme Environment Diffractometer (EXED) <i>(commissioning)</i>	43283	O. Prokhnenko H. Bleif	43068 42758
V16	Very Small Angle Neutron Scattering (VSANS) <i>(commissioning)</i>	43281	D. Clemens K. Vogtt	42280 43022
V17	Detector Test Station	43284	T. Wilpert C. Schulz S. Alimov	42743 42675 42675
V18	Reflectometer for biological applications (BioRef) <i>(under construction)</i>	****	R. Steitz M. Strobl A. Paul	42149 42490 42925
V19	Polarized Neutron Tomography (PONTO) <i>(under construction)</i>	****	W. Treimer O. Ebrahimi	42221 43076
X2	X-ray Reflectometer <i>(Sample Preparation V6, only in close co-operation with local staff members)</i>	43112	H. Bleif	42758

Floor Plan of the Neutron Instruments at the BER II



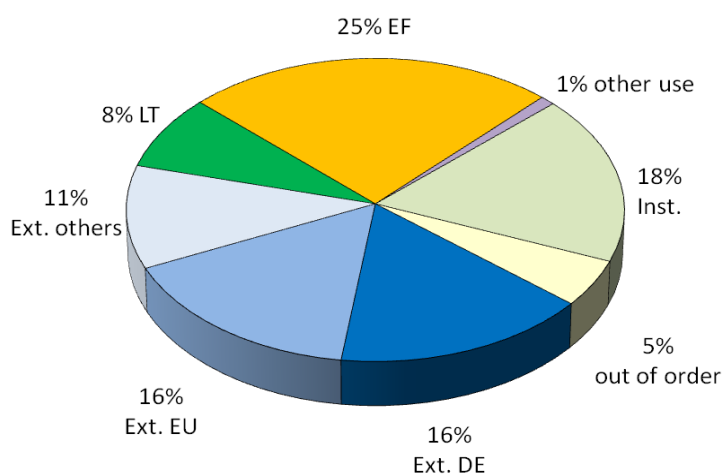
Instrument Statistics 2009

Table: Detailed statistical data on the use of the scheduled instruments

Inst.	Inst. days	EXT (DE) in %	EXT (EU) in %	EXT (other) in %	LT in %	EF in %	Other use in %	Inst in %	OOO in %
E1*	182	0	0	0	0	0	0	100	0
E2	182	19	10	15	0	35	0	21	0
E3	182	25	24	3	0	36	0	7	0
E4	182	5	13	20	0	50	0	12	0
E5	182	33	0	19	0	48	0	0	0
E6	182	9	36	9	0	27	0	18	1
E9	182	21	21	12	0	36	2	7	0
V1	178.5	25	32	10	17	9	0	8	0
V2	178.5	9	16	31	0	29	2	13	0
V3	178.5	8	36	9	0	32	0	16	0
V4*	178.5	5	5	0	2	2	0	11	75
V5	178.5	7	23	9	6	25	0	29	0
V6	178.5	38	4	8	8	24	2	17	0
V7	178.5	27	13	17	17	19	5	3	0
V12	178.5	11	10	4	69	0	0	7	0

Note: The table gives detailed statistical data on the use of the scheduled instruments. The pie chart shows the statistical data given in the table, summarized over all instruments. The meaning of the individual entries is explained in the legend below. EXT (DE), EXT (EU) and EXT (other) refer to projects performed by external users from Germany, EU or other countries via accepted "normal" short-term proposals submitted to BER II. Please note that the long-term projects are also projects performed by external user groups, where instrument time is either given on the basis of an accepted long-term proposal or on the basis of a cooperation agreement with BER II.

Overall Statistics on Instrument Use in 2009



Inst.-days	Neutron days per Instrument
EXT (DE)	German Universities, Research institutes
EXT (EU)	Universities and Research Institutes from the EU and associated states
EXT (other)	Non-EU Universities and Research Institutes
LT	Long term projects
EF	In-house projects
other use	e.g. industry, teaching (neutron school)
Inst.	Instrument time (tests, developments ...)
OOO	out of operation
E1*	under construction in 2009
V4*	technical problems in 2009

How to apply for beam time at BER II (HZB-Neutrons) and BESSY II (HZB-Photons)

The research reactor BER II is a major European neutron scattering facility with exceptional capabilities to conduct complex experiments under extreme conditions. Outstanding sample environment provides high static magnetic fields up to 17 T, high, low, and ultra-low temperatures and controlled gas pressures up to 10 kbar. The advanced and partly unique neutron scattering instrumentation and the quality of the user service attract researchers worldwide.

The storage ring BESSY II is a leading third-generation synchrotron-radiation source providing ultrabright photon beams from the long wavelength Terahertz region to hard X-rays with complete control of the polarization of the radiation and energy range. More than 50 beamlines offer a multi-faceted mixture of experimental opportunities at undulator, wiggler and dipole sources with excellent energy resolutions.

Details on the instrumentation at both sources are available on the WEB:

<http://www.helmholtz-berlin.de/userservice>

BER II and BESSY II are open to both the national and the international user community. The main fraction of the beam time is reserved for external short-term research proposals. All applications are reviewed by an international Scientific Selection Panel (SSP) twice a year. Beamtime is granted on the basis of scientific merit. To promote the synergetic use of neutron and synchrotron radiation, the Scientific Selection Panel is dealing with proposals for neutrons and synchrotron photons in joint sessions. To this purpose the Panel is divided in 6 sub-groups (colleges) each being focussed on a particular scientific field in order to facilitate in-depth discussions.

**Deadlines for the submission of proposals are
1 March and 1 September.**

The instrument responsables of HZB are asked to advise potential users and comment on the technical feasibility of the proposed experiments. For these tasks this limited class of HZB-scientists has access to the submitted proposals.

Requests for urgent or confidential experiments (Director's Discretionary Time) and for industrial use may be submitted at any time.

Applications for HZB-Neutrons as well as HZB-Photons beam time should be made by using GATE, the common user entry point for both neutron and synchrotron radiation applications

http://www.helmholtz-berlin.de/userservice/gate_en.html

Research projects for the complementary use of HZB-Neutrons and HZB-Photons are strongly encouraged.

For further information please contact:

Helmholtz-Zentrum Berlin für Materialien und Energie GmbH

HZB User Office – Neutrons
Lise-Meitner-Campus
Hahn-Meitner Platz 1
D-14109 Berlin (Wannsee)
Germany

Phone: +49 - 30 - 8062 42304 / 43153
Fax: +49 - 30 - 8062 42523
Email: neutrons@helmholtz-berlin.de

HZB User Office – Photons
Wilhelm-Conrad-Röntgen Campus
Albert-Einstein-Str. 15
D-12489 Berlin (Adlershof)
Germany

Phone: +49 - 30 - 8062-12931
Fax: +49 - 30 - 8062-14746
Email: photons@helmholtz-berlin.de

The BER II Experimental Reports are intended as interim summaries. In view of the short time available between the termination of certain experiments and the deadline for this report, the results presented here have to be considered as preliminary. The inclusion of reports in this volume does not constitute a publication in the usual sense. Final results will be submitted for publication in regular scientific journals.

Acknowledgement for Support by the European Commission

The access of users from European Community Member States and Associated States to the neutron facility BER II has been substantially supported in the past by the European Community under the Framework Programs FP5 and FP6. We gratefully acknowledge the continuation of this support under the Framework Program FP7: HZB is a partner in the EU supported network of European neutron facilities – the **Neutron and Muon Integrated Infrastructure Initiative (NMI3)** – and the access to the BER II is supported by the European Commission under the 7th Framework Program through the “Research Infrastructures” action of the “Capacities Program”, Contract No: CP-CSA_INFRA-2008-1.1.1 Number 226507-NMI3. This access program started on 1 February 2009 and will be finished on 31 January 2011.

Results of EU supported groups are contained in 39 reports of this volume.

NMI3-N^o	Page	Authors	Affiliation
1354	156	Josic et al.	PSI Villigen, CH
1363	23	Chatterji et al.	ILL Grenoble, F
1364	22	Chatterji et al.	ILL Grenoble, F
1376	167	Visser et al.	TU Delft, NL
1501	135	Schöbel et al.	TU Wien, AT
1502	71	Remhof et al.	EMPA, CH
1503	42	Nikseresht et al.	EPF, Lausanne, CH
1505	102	Preu et al.	Univ. Copenhagen, NBI, DK
1509	137	Carradó et al.	Univ. Strasbourg, F
1511	17	Comyn et al.	Univ. of Leeds, UK
1512	120	Zarbaksh et al.	QM UCL, UK
1513	104	Katsaros et al.	NCSR Demokritos, GR
1515	74	Siouris et al.	DU Thrace, GR
1517	138	Calbucci et al.	UPM Ancona, I
1521	111	Magazù et al.	Univ. of Messina, I
1523	72	Raitman et al.	LAS Riga, LV
1524	89	Kongshaug et al.	Univ. Oslo, N
1525	35	Gondek et al.	AGH-UST, Krakow, PL
1527	36	Orendáčová et al.	PJSU Kosice, SK

NMI3-N^o	Page	Authors	Affiliation
1530	150	Remhof et al.	EMPA, CH
1531	85	Remhof et al.	EMPA, CH
1533	51	Lefmann et al.	Univ. Copenhagen, DK
1535	86	Rovira-Esteva et al.	UPC Barcelona, E
1535	100	Rovira-Esteva et al.	UPC Barcelona, E
1536	114	Pérez-Hernández et al.	CSIC IIQ Sevilla, E
1540	115	Peters et al.	ILL Grenoble, F
1543	146	Davies et al.	ICL, UK
1546	147	Robinson et al.	Univ. Limerick, IE
1548	41	Levy et al.	Univ. Torino, I
1551	166	Triolo et al.	Univ. Palermo, I
1553	148	Ohms et al.	JRC Petten, NL
1555	65	Rysiakiewicz-Pasek et al.	TU Wroclaw, PL
1556	75	Baran et al.	JU Krakow, PL
1557	38	Penc et a	JU Krakow, PL
1558	39	Gil et al	JDU Czestochowa, PL
1559	87	Gondek et al.	AGH-UST, Krakow, PL
1561	76	Kuzmin et al.	Univ. of Latvia, Riga, LV
1563	157	Selvaraj et al.	AGH-UST, Krakow, PL
1564	154	Strunz et al.	ASCR NPI Rez, CZ

Notice:

The quality of figures in the electronic versions, CD and WEB (http://www.helmholtz-berlin.de/user/neutrons/reports_en.html) – especially in colour presentation – is remarkably higher than in the print version.

List of Contributed Experimental Reports

PAGE TITLE TEAM PROPOSAL

Development of Instruments and Methods

3	Optical components for the new wide angle NSE spectrometer WASP at the ILL (Cooperation contract)	C. Pappas ¹ E. Moskvina ¹ K. Andersen ² P. Fouquet ²	¹ HZB ² ILL, Grenoble, FR	V5	PHY-03-577-EF
4	Development and calibration of efficient neutron position sensitive detectors and collimators	A. Tremsin ¹ N. Kardjilov ² M. Dawson ² M. Strobl ² I. Manke ²	¹ UC Berkeley, US ² HZB	V7	MAT-04-1780
5	Dark-field neutron imaging	M. Strobl ¹⁺² I. Manke ¹ A. Hilger ¹ N. Kardjilov ¹ M. Dawson ¹ T. Kandemir ¹	¹ HZB ² Universität Heidelberg	V7	PHY-04-1866-EF
6	High-resolution neutron imaging	N. Kardjilov ¹ F. Garcia-Moreno ¹ I. Manke ¹ M. Dawson ¹ A. Hilger ¹	¹ HZB	V7	MAT-04-1867-EF MAT-04-1798-EF
7	USANS measurements to evaluate dark-field neutron imaging	M. Strobl ¹⁺⁴ S.-O. Seidel ² D. Penunadu ³	¹ HZB ² TFH Berlin ³ University of Tennessee, US ⁴ Uni Heidelberg	V12a	MAT-04-1802-EF
8	2D- reconstruction from scattering signals	S.-O. Seidel ¹ W. Treimer ¹ O. Ebrahimi ¹ N. Karakas ¹	¹ TFH Berlin	V12a	PHY-04-1849-LT
9	BioRef commissioning: first spectra measured	R. Steitz ¹ M. Grunze ¹ R. Dahint ² M. Strobl ¹⁺² M. Kreuzer ¹⁺²	¹ HZB ² Uni Heidelberg	V18	EF
10	Neutron tomography with sub-100µm spatial resolution	W. Treimer ¹⁺² O. Ebrahimi ¹⁺² S.-O. Seidel ¹⁺² N. Karakas ¹⁺²	¹ HZB ² Beuth Hochschule	V19	EF
11	First experimental results of PONTO with polarized neutrons	W. Treimer ¹⁺² O. Ebrahimi ² S.-O. Seidel ² N. Karakas ²	¹ HZB ² Beuth Hochschule	V19	EF

Magnetism

15	Tuning the ground state of pyrochlore Ho_{2-x}Y_xTi₂O₇ (x = 0.3, 1) via applied magnetic fields	Y. Su ¹ L. J. Chang ² M. R. Lees ³ A. Hoser ⁴ J.-U. Hoffmann ⁴	¹ JCNS ² Univ. Tsing Hua, TW ³ University of Warwick, UK ⁴ HZB	E2	PHY-01-2344
16	Magnetoelectric Correlations in Multiferroic DyMnO₃	M. Fiebig ¹ D. Meier ¹	¹ Uni Bonn	E2	PHY-01-2485
17	Magnetoelectric coupling in BiFeO₃ – PbTiO₃	T. Comyn ¹ T. Stevenson ¹ I. Glavatskyi ² K. Kiefer ² J.-U. Hoffmann ²	¹ University of Leeds, UK ² HZB	E2	PHY-01-2487

List of Contributed Experimental Reports

PAGE	TITLE	TEAM	PROPOSAL
18	Temperature evolution of the crystal and magnetic structures in the new Ni-Mn-Ga-(Fe, Cu) ferromagnetic shape memory alloys	I. Glavatskyi ¹ J.-U. Hoffmann ²	¹ NAS Kiev, IMP, UA ² HZB E2 PHY-01-2490
19	Magnetic order in YbCo ₂ Si ₂	K. Kaneko ¹ N. Mufti ² O. Stockert ² A. Hoser ³	¹ JAEA, JP ² MPI, CPfS, Dresden ³ HZB E2 PHY-01-2526
20	Diffuse scattering study of Dy ₂ Ti ₂ O ₇	J. Morris ¹ A. Tennant ¹ K. Rule ¹ B. Klemke ¹ S. Gerischer ¹ J.-U. Hoffmann ¹ S. Grigera ²	¹ HZB ² UNLP, AR E2 PHY-01-2546-EF
21	Change of martensite structure in Ni-Mn-Ga single crystal ingots	M. Chmielus ¹ R. Schneider ¹ I. Glavatskyi ¹ P. Müllner ²	¹ HZB ² Boise State University, US E2 MAT-01-2580-EF
22	Field dependence of the magnetic structure of the multiferroic LiCu ₂ O ₂	T. Chatterji ¹	¹ ILL, FR E4 PHY-01-2384
23	Field dependence of the magnetic structure and the (H,T) phase diagram of TbMn ₂ O ₅	T. Chatterji ¹ G. N. Iles ¹	¹ ILL, FR E4 PHY-01-2383
25	Magnetic field dependence of the antiferromagnetism in CeBiPt	O. Stockert ¹ G. Goll ² S. Mat'as ³	¹ MPI CPfS Dresden ² Uni Karlsruhe ³ HZB E4 PHY-01-2476
26	Spin re-orientation transition in jarosite	K. Matan ¹ T. J. Sato ¹ D. Grohol ² Y. S. Lee ² K. Prokes ³ S. Mat'as ³	¹ Tokyo University, JP ² MIT Cambridge, US ³ HZB E4 PHY-01-2480
27	Magnetic structure of pressure and field induced magnetically ordered phases in YbAgGe with a quasi-kagome lattice	K. Umeo ¹ T. Onimaru ¹ H. Kubo ¹ T. Takabatake ¹ K. Prokes ²	¹ Hiroshima University, JP ² HZB E4 PHY-01-2481
28	The neutron study of layered Ising magnet KEr(MoO ₄) ₂	S. Mat'as ¹ K. Prokes ¹ K. Kiefer ¹ S. Gerischer ¹ A. Orendáčová ²	¹ HZB ² PJSU Kosice, SK E4 PHY-01-2556-EF
29	CaFe ₂ As ₂ under uniaxial pressure	K. Prokes ¹ D. Argyriou ¹ S. Kimber ¹ A. Kreyssig ²⁺³ A. Goldman ²⁺³	¹ HZB ² Ames Lab, US ³ Iowa State University, US E4 PHY-01-2560-EF PHY-01-2614-EF
30	Low-Temperature Magnetic Structure of Frustrated Antiferromagnet SrYb ₂ O ₄	D. L. Quintero-Castro ¹ B. Lake ¹ M. Reehuis ¹ N. Islam ¹	¹ HZB E4/E6 /E9 PHY-01-2595-EF PHY-01-2626
31	The neutron response of layered Ising magnet K _{er} (MoO ₄) ₂	A. Orendáčová ¹ S. Mat'as ² K. Kiefer ² S. Gerischer ²	¹ PJSU Kosice, SK ² HZB E4 PHY-01-2610-EF

List of Contributed Experimental Reports

PAGE	TITLE	TEAM	PROPOSAL
32	Magnetic phase transitions and magnetic ordering in ErVO₃	C. Ulrich ¹ B. Keimer ¹ M. Reehuis ² S. Miyasaka ³ J. Fujioka ³ Y. Tokura ³	¹ MPI Stuttgart ² HZB ³ University of Tokyo, JP E5 PHY-01-2646
33	Structural and magnetic transitions in Pr_{0.80}Ca_{0.20}VO₃	C. Ulrich ¹ B. Keimer ¹ M. Reehuis ² S. Miyasaka ³ J. Fujioka ³ Y. Tokura ³	¹ MPI Stuttgart ² HZB ³ University of Tokyo, JP E5 PHY-01-2647-EF
34	Low temperature crystal structure and magnetic structure of MgV₂O₄	E. Wheeler ¹ M. Reehuis ¹ N. Islam ¹ B. Lake ¹⁺²	¹ HZB ² TU Berlin E5 PHY-01-2564-EF
35	Magnetic and crystal structure of Er₅Ni₂In₄	L. Gondek ¹ J. Czub ² A. Arulraj ³	¹ AGH-UST, Krakow, PL ² Jagiellonian University, PL ³ HZB E6 PHY-01-2514
36	Investigation of magnetic order in the quantum magnet Cu(D2O)2(en)SO₄	A. Orendáčová ¹ M. Orendáč ¹ R. Tarasenko ¹ K. Siemensmeyer ² S. Mat'áš ² K. Kiefer ² S. Gerischer ²	¹ PJSU Kosice, SK ² HZB E6 PHY-01-2515
37	Magnetism of the low-temperature phase of PrIr₂Si₂	M. Mihalik ¹ A. Hoser ¹	¹ HZB E6 PHY-01-2623-EF
38	Low temperature magnetic structure of NdPd₂Ge₂ and NdAg₂Ge₂	S. Baran ¹ B. Penc ¹ A. Hoser ² K. Kiefer ² S. Gerischer ²	¹ JU Krakow, PL ² HZB E6 PHY-01-2636
39	Neutron Diffraction Studies of RCrxGe₂ (R = Tb, Dy, Ho, Er) compounds	B. Penc ¹ A. Szytula ¹ A. Gil ² A. Hoser ³	¹ JU Krakow, PL ² JDU Czestochowa, PL ³ HZB E6 PHY-01-2637
40	Magnetism in open framework transition metal zeolitic structures with the ABW framework topology	P. Henry ¹	¹ HZB E9 PHY-01-2550-EF
41	Structure of magnetite at the Curie Temperature	D. Levy ¹ R. Guistetto ¹	¹ Università di Torino, IT E9 PHY-01-2600
42	Quantum Critical Scaling in the Model XY Antiferromagnet LiErF₄	N. Nikseresht ¹ M. Skoulatos ²	¹ EPF Lausanne, CH ² HZB V2 PHY-02-690
43	High field spin dispersion of the antiferromagnetic Heisenberg chain Cu(C₄H₄N₂)(NO₃)₂	S. Süllow ¹ K. Rule ² A. Wolter ³ C. Broholm ⁴	¹ TU Braunschweig ² HZB ³ IFW Dresden ⁴ JHU Baltimore, US V2 PHY-02-693
44	Bose-glass phase in a spin liquid with quenched disorder	T. Hong ¹ A. Zheludev ²	¹ ORNL, US ² ETH Zürich, CH V2 PHY-02-702
45	Low energy states in the frustrated and quantum critical magnet Er₂Ti₂O₇	K. Rule ¹ J. Ruff ² B. Gaullin ² P. Glancy ² K. Ross ²	¹ HZB ² McMaster Univ. Hamilton, CA V2 PHY-02-714-EF

List of Contributed Experimental Reports

PAGE	TITLE	TEAM	PROPOSAL
46	Temperature Dependence of Magnetic Excitation Spectrum of Sr₃Cr₂O₈	B. Lake ¹ D. L. Quintero-Castro ¹ N. Islam ¹ E. Wheeler ¹	¹ HZB V2 PHY-02-715-EF
47	Splitting of the Magnon Excitation Branches in BaMnF₄ investigated with NRSE	K. Habicht ¹ M. Skoulatos ¹ D. Le ¹	¹ HZB V2 PHY-02-721-EF
48	Search for Spin-Density Waves in Pb	K. Habicht ¹⁺² M. Skoulatos ¹ T. Keller ² P. Aynajian ²	¹ HZB ² MPI-FKF, Stuttgart V2 PHY-02-734-EF
49	Determination of Local Dispersion Gradients with NRSE spectroscopy	K. Habicht ¹ M. Skoulatos ¹ F. Groitl ¹	¹ HZB V2 PHY-02-735-IT
50	Magnetic excitations of alpha-CaCr₂O₄ triangular lattice antiferromagnet	B. Lake ¹ K. Rule ¹ S. Toth ¹	¹ HZB V2 PHY-02-736-EF
51	Quantum phase transition in the 1D Ising spin system CoCl₂·2D₂O	K. Lefmann ¹ S. U. H. Eisenhardt ¹ M. Sales ¹ J. Larsen ² N. B. Christensen ² K. Habicht ³ H. M. Roennow ⁴	¹ Univ. Copenhagen, DK ² DTU Risoe, DK ³ HZB ⁴ EPF, Lausanne, CH V2 PHY-02-739
52	Magnon instability in strong field in square lattice antiferromagnet	T. Masuda ¹ K. Rule ²	¹ Yokohama City University, JP ² HZB V2 PHY-02-742
53	Magnetic excitations of frustrated magnet SrYb₂O₄	B. Lake ¹ D. L. Quintero-Castro ¹ N. Islam ¹ A. Niazi ²	¹ HZB ² JMI, New Delhi, IN V3 PHY-03-647-EF
54	Spin dynamics in the ordered state of the geometrically frustrated pyrochlore, Tb₂Sn₂O₇	K. Rule ¹ E. Moskvin ¹ G. Ehlers ² J. Gardner ³	¹ HZB ² ORNL, US ³ RAL ISIS, UK V5 PHY-03-635
55	Spin dynamics in the ordered state of the geometrically frustrated pyrochlore, Dy₂Ti₂O₇	J. Morris ¹ K. Rule ¹ E. Moskvin ¹ A. Tennant ¹	¹ HZB V5 PHY-03-650-EF
56	Inverse proximity effects at the superconductor-ferromagnet interface revealed by polarized neutron	Y. Khaydukov ¹ B. Nagy ² R. Steitz ³ A. Paul ³ D. Wallacher ³	¹ JINR Dubna, RU ² KFKI Budapest, HU ³ HZB V6 PHY-04-1705
57	Magnetization reversal in exchange coupled system with field perpendicular to the cooling field	A. Paul ¹	¹ HZB V6 PHY-04-1803
58	PNR study of a BiFeO₃ multiferroic film	K. Temst ¹ M. J. Van Bael ¹ J. Demeter ¹ A. Teichert ¹⁺² R. Steitz ²	¹ KU Leuven, BE ² HZB V6 PHY-04-1808-EF
59	Simultaneous measurement of PNR and AMR on exchange bias Co/CoO bilayer	A. Teichert ¹⁺² J. Demeter ¹ D. Paramanik ¹ K. Kiefer ²	¹ KU Leuven, BE ² HZB V6 PHY-04-1894-LT

List of Contributed Experimental Reports

PAGE	TITLE	TEAM	PROPOSAL
60	Probing Magnetic Reversal Behaviour of Exchange-biased NiFe/FeMn, FeMn/CoFe bilayer and NiFe/FeMn/CoFe Trilayers with Specular Polarized Neutron Reflectivity	K.-Y. Kim ¹ J.-S. Lee ¹ H.-Ch. Choi ² Ch.-Y. You ² A. Teichert ³ R. Steitz ³	¹ KAERI, KR ² Inha University, KR ³ HZB V6 PHY-04-1907
61	Curie temperature mapping by polarised neutron imaging	M. Strobl ¹⁺² K. Rolfs ¹ M. Chmielus ¹ A. Hilger ¹ N. Kardjilov ¹ I. Manke ¹	¹ HZB ² Uni Heidelberg V7 EF
Structure			
65	Phase transformations in nanoparticles of NaNO₃	E. Pysiakiewicz-Pasek ¹ R. Poprawski ¹ A. Naberezhnov ² M. Tovar ³	¹ TU Wroclaw, PL ² RAS Ioffe PTI, RU ³ HZB E2/E3 PHY-01-2584 PHY-01-2601
66	Structural and magnetic properties of FeTe_xSe_{1-x}	D. Argyriou ¹ S. Kimber ¹ M. Reehuis ¹	¹ HZB E5 EF
67	Determination of the crystal structure of Cs₂NaAlF₆ doped with Chromium	H. N. Bordallo ¹ F. Yokaichiya ¹ S. da Silva Pedro ² L. P. Sosman ²	¹ HZB ² UERJ, Rio de Janeiro, BR E5 PHY-01-2644-EF
68	X-ray and neutron diffraction study of arrojadite	C. Kallfaß ¹ C. Hoch ¹ H. Schier ¹ H. Schubert ² M. Reehuis ³	¹ MPI Stuttgart ² TU Berlin ³ HZB E5 MAT-01-2648
69	Thermal variation of structural parameters in the cubic phase of MgV₂O₄	E. Wheeler ¹ M. Reehuis ¹ B. Lake ¹ N. Islam ¹	¹ HZB E5 PHY-01-2649-EF
70	Hydrogen bonds evaluation in the crystal structures of silicate hydrates (continuation)	O. Karimova ¹	¹ RAS IGEM Moscow, RU E5 GEO-01-2651
71	Isotope Exchange in LiBH₄	A. Remhof ¹ O. Friederichs ¹ D. Wallacher ²	¹ EMPA, CH ² HZB E6 MAT-01-2508
72	Neutron Bragg back-side scattering from the Ge single crystal excited with acoustic waves	E. Raitman ¹ V. Gavrilov ¹ D. Mjasischev ¹ A. Hoser ² N. Stüßer ² A. Arulraj ²	¹ LAS Riga, LV ² HZB E6 PHY-01-2513
73	Neutron Diffraction Studies on Nd₇Rh₃	S. Rayaprol ¹ V. Siruguri ¹ E. V. Sampathkumaran ² A. Hoser ³	¹ CSR, Mumbai, IN ² TIFR, Mumbai, IN ³ HZB E6 PHY-01-2516
74	Neutron diffraction measurements on the intermetallic Dy(Ag,In)₂ compound	I. M. Siouris ¹ K. Kosmidou ² S. Katsavounis ² A. Hoser ³	¹ DU Thrace, GR ² PME, Duth, GR ³ HZB E6 PHY-01-2529

List of Contributed Experimental Reports

PAGE	TITLE	TEAM	PROPOSAL
75	Neutron diffraction studies of tetragonal RCu_2X_2	S. Baran ¹ B. Penc ¹ A. Hoser ²	¹ JU Krakow, PL ² HZB E6 PHY-01-2634
76	Magnetic and crystal structure of $\text{La}_{1/3}\text{Sr}_{2/3}\text{FeO}_3$ -d: dependence on oxygen content	A. Kuzmin ¹ V. Sikolenko ²⁺³ V. Efimov ⁴	¹ University of Riga, LV ² ETH, Zürich, CH ³ PSI, CH ⁴ JINR Dubna, RU E9 PHY-01-2372
77	Study of the mechanism of proton conduction in ceramics	T. Scherb ¹ S. Kimber ¹ M. Russina ¹ N. Tsapasaris ¹ D. Wallacher ¹ G. Schumacher ¹ J. Serra ²	¹ HZB ² UPV-CSIC, ES E9 ART-01-2465-EF
78	Proton Mobility in Solid Super Proton Conductors	M. Lerch ¹ C. A. C. Dreismann ¹ T. Abdul-Redah ¹ M. Tovar ²	¹ TU Berlin ² HZB E9 CHE-01-2523
79	Investigation of structural trends in non-stoichiometric Cu-III-VI_2 compounds (III = In, Ca; VI=S, Se)	C. Stephan ¹ F. Yokaichiya ¹ S. Schorr ²	¹ HZB ² FU Berlin E9 MAT-01-2524
80	Structural investigation on H ₂ -sorption sites in new Li containing metal organic frameworks (MOF)	D. Wallacher ¹ D. Hims ² M. Hartmann ²	¹ HZB ² Uni Erlangen E9 PHY-01-2574-EF
81	Resolving the phase field in the materials $\text{RbCu}_x\text{Ni}_{1-x}\text{PO}_4$	P. Henry ¹	¹ HZB E9 CHE-01-2593-EF
82	Neutron diffraction study of different Cu based methanol synthesis catalysts	M. Behrens ¹ S. Kühn ¹ S. Kißner ¹ M. Tovar ² D. Wallacher ²	¹ MPG-FHI Berlin ² HZB E9 CHE-01-2597
83	Distribution of functional groups in proton-conducting mesoporous $\text{SO}_3\text{H-SiO}_2$ materials	M. Wark ¹ M. Sharifi ¹ D. Wallacher ² Th. Hauß ²	¹ Leibniz Universität Hannover ² HZB V1 MAT-01-2537-EF
84	Temperature evolution of dynamics of lead nanoparticles	A. Naberezhnov ¹ P. Parshin ² Y. Kibalin ³	¹ RAS Ioffe PTI, RU ² KI Moscow, RU ³ St. Petersburg PTU, RU V3 PHY-03-632
85	Hydrogen dynamics in liquid LiBH_4	A. Remhof ¹ P. Martelli ¹ D. Wallacher ²	¹ EMPA, Zürich, CH ² HZB V3 MAT-03-666
86	Influence of conformational disorder on the structure and dynamics of Freon 112	M. Roviera-Esteva ¹ M. D. Ruiz-Martin ¹ L. C. Pardo ¹	¹ UPC Barcelona, ES V3 PHY-03-667
87	Crystal electric field in PrT_2Ge_2 (T = Ag, Ru) compounds	L. Gondek ¹ J. Czub ¹ Z. Izaola ²	¹ AGH-UST, Krakow, PL ² HZB V3 PHY-03-670
88	Structure and dynamics of Opal: a combined USANS-QENS experiment	L. P. Aldridge ¹ P. Thomas ² A. Smallwood ² A. Ray ² H. N. Bordallo ³ E. Kemner ³	¹ ANSTO, AU ² UTS, Sydney, AU ³ HZB V3 MAT-03-671
89	Hydroxide ion dynamics in hydrated nano-porous mayenite, $\text{Ca}_{12}\text{Al}_{12}\text{O}_{33}$	C. Kongshaug ¹ N. Jalarvo ¹ D. Wallacher ²	¹ University of Oslo, NO ² HZB V5 CHE-03-643

List of Contributed Experimental Reports

PAGE	TITLE	TEAM	PROPOSAL
90	Influence of conformational disorder on the dynamics of Freon 112	M. Riviera-Esteva ¹ M. D. Ruiz-Martin ¹ L. C. Pardo ¹ H. N. Bordallo ²	¹ UPC Barcelona, ES ² HZB V5 CHE-03-676-EF
91	Study on lead single-crystals	M. Liesegang ¹ W. Treimer ¹ O. Ebrahimi ¹ S.-O. Seidel ¹ N. Karakas ¹	¹ Beuth Hochschule V12a EF
92	Structure and dynamics of Opal: a combined USANS-QENS experiment	L. P. Aldridge ¹ C. Rehm ¹ P. Thomas ² A. Smallwood ² A. Ray ² H. N. Bordallo ³ S.-O. Seidel ³ M. Strobl ³	¹ ANSTO, AU ² UTS, Sydney, AU ³ HZB V12a MAT-04-1850
93	Radiography of a diffusion process between D2O and H2O	W. Treimer ¹⁺² O. Ebrahimi ² S.-O. Seidel ² M. Konieczko-Dziadula ² N. Karakas ²	¹ HZB ² Beuth Hochschule V19 EF

Biology & Soft Matter

97	Neutron Powder Diffraction Studies of L and DL-Cysteine	H. N. Bordallo ¹ P. Henry ¹ D. N. Argyriou ¹ V. Minkov ²	¹ HZB ² NSU, Novosibirsk, RU E9 OTH-01-2554-EF
98	Structure of L-Leucine: Symmetry change or Conformational Rearrangement?	H. N. Bordallo ¹ F. Yokaichiya ¹ P. T. C. Freire ² X. Jiao ¹⁺³	¹ HZB ² UFC, BR ³ CIAE Beijing, CN E9 OTH-01-2555-EF
99	L-Methionine: Structure and Dynamics of an essential amino acid	H. N. Bordallo ¹ J. Fischer ¹⁺²	¹ HZB ² Universität Kassel E9 CHE-01-2591-EF
100	Influence of conformational disorder on the structure and dynamics of Freon 112	M. Riviera-Esteva ¹ M. D. Ruiz-Martin ¹ L. C. Pardo ¹	¹ UPC Barcelona, ES E9 PHY-01-2599
101	Structural analysis of L and DL-Serine	E. Boldyreva ¹ N. Tumanov ¹ H. N. Bordallo ² F. Yokaichiya ²	¹ NSU Novosibirsk, RU ² HZB E9 CHE-01-2602
102	The interaction of Ang II with model membranes	J. Preu ¹ Th. Gutberlet ² Th. Hauß ³	¹ University of Copenhagen, NBI, DK ² FZ Jülich ³ HZB V1 BIO-01-2535
103	Neutron diffraction study of model membranes with complex Stratum corneum-like lipid composition	T. Engelbrecht ¹ B. Dobner ¹ R. Neubert ¹ A. Buchsteiner ² Th. Hauß ²	¹ MLU Halle ² HZB V1 BIO-01-2536
104	Neutron Diffraction Studies of Polymer/Clay Nanocomposites	F. K. Katsaros ¹ T. A. Steriotis ¹ A. A. Sapalidis ¹	¹ NCSR Demokritos, GR V1 MAT-01-2539
105	Interaction of a γ-secretase inhibitor with β-amyloid and lipid membranes	Th. Hauß ¹⁺² N. A. Dencher ¹ B. Schmidt ¹ A. Buchsteiner ²	¹ TU Darmstadt ² HZB V1 BIO-01-2656-LT

List of Contributed Experimental Reports

PAGE	TITLE	TEAM	PROPOSAL
106	Quaternary Stratum corneum model membranes with or without penetration enhancers and the impact of pH	T. Engelbrecht ¹ B. Dobner ¹ R. Neubert ¹ A. Buchsteiner ² T. Hauß ²	¹ MLU Halle/Saale ² HZB V1 BIO-01-2657
107	Molecular mechanism of membrane stabilisation during dehydration by small solute (sugar) molecules	Ch. Garvey ¹ G. Bryant ² Th. Lenne ³ A. Buchsteiner ⁴	¹ ANSTO, AU ² RMIT Univ. Melbourne, AU ³ ANU Canberra, AU ⁴ HZB V1 BIO-01-2664
108	Study of the Vibrational and Structural Properties of L-leucine and L-isoleucine	H. N. Bordallo ¹ P. T. C. Freire ²	¹ HZB ² UFC, BR V3 OTH-01-2560-EF
109	Dynamical transition in a large globular protein: macroscopic properties and glass transition	A. V. Sokolova ¹ G. J. Kearley ¹ E. P. Gilbert ¹ E. Kemner ² M. Russina ²	¹ ANSTO, AU ² HZB V3 PHY-03-555
110	Study of the mechanism of proton conduction in ceramics	T. Scherb ¹ M. Russina ¹ Z. Izaola ¹ N. Tsapatsaris ¹ D. Wallacher ¹ G. Schumacher ¹ J. Serra ²	¹ HZB ² UP Valencia, ES V3 ART-03-614-EF
111	Study of the low frequency dynamics of the psychrophile enzyme alpha-amylase in bioprotectant mixtures	S. Magazu ¹ F. Migliardo ¹ M. Russina ² N. Tsapatsaris ²	¹ University of Messina, IT ² HZB V3 PHY-03-630
112	Lipid Lateral Diffusion in Phase Separated Multilamellar Systems	K. Vogtt ¹ M.-C. Bellisent-Funel ¹ E. Kemner ¹ M. Russina ¹	¹ HZB V3 BIO-03-648-EF
113	L-Methionine: Structure and Dynamics of an essential amino acid	H. N. Bordallo ¹ J. Fischer ¹⁺²	¹ HZB ² Uni Kassel V3 CHE-03-660-EF
114	Distinct Dynamics of Water Molecules in Hydrated Pores (2)	N. Pérez-Hernández ¹ J. Eckert ² N. Tsapatsaris ³	¹ CSIC, Sevilla, ES ² UCSB, US ³ HZB V3 CHE-03-668
115	Study of dynamic properties of reconstituted myelin sheath	J. Peters ¹ F. Natali ¹⁺² W. Knoll ¹ P. Kursula ³	¹ ILL, Grenoble, FR ² CNR-OGG, Grenoble, FR ³ Oulu Univ., FI V3 BIO-03-669
116	Bicontinuous phases based on sugar surfactant: Structure and influence of the co-surfactant	T. Hellweg ¹ K. v. Nessen ¹ S. Wellert ²	¹ Universität Bayreuth ² HZB V4 CHE-04-1817
117	Investigation of Preparation Techniques of Polyelectrolyte Multilayer	R. Köhler ¹ M. Kolasinska ¹ R. Krastev ² Th. Gutberlet ³⁺⁴ P. Warszynski ⁵	¹ MPI, Potsdam ² Universität Tübingen ³ ETH Zürich, CH ⁴ PSI, CH ⁵ PAS, Krakow, PL V6 BIO-04-1450-EF
118	Type of growth and water content of polyelectrolyte multilayers	S. Doodoo ¹ R. v. Klitzing ¹ R. Steitz ²	¹ TU Berlin ² HZB V6 CHE-04-1736
119	Inversion of the protein binding properties of a PAA brush	C. Czeslik ¹ F. Evers ¹ M. Tolan ¹ Ch. Reichart ¹ R. Köhler ² R. Steitz ²	¹ TU Dortmund ² HZB V6 CHE-04-1739

List of Contributed Experimental Reports

PAGE	TITLE	TEAM	PROPOSAL
120	Surfactants at the metal-oil interface	A. Zarbakhsh ¹ M. Campana ¹ R. Steitz ² A. Teichert ²	¹ QM UCL, UK ² HZB V6 CHE-04-1744
121	A Model Interface for Artificial Implants	M. Kreuzer ¹ R. Dahint ¹ R. Steitz ²	¹ RKU Heidelberg ² HZB V6 BIO-04-1805-EF
122	Continuation 2: Water at a Hydrophobic Substrate and the Effect of Pressure	M. Kreuzer ¹ R. Dahint ¹ R. Steitz ²	¹ RKU Heidelberg ² HZB V6 PHY-04-1806-EF
123	Polyelectrolyte Multilayer under Mechanical Stress	R. Köhler ¹ J. Früh ¹ R. Krastev ²	¹ MPI, Potsdam ² Uni Tübingen NMI V6 PHY-04-1891-LT
124	Interfacial Behaviour of Ionic Liquids	R. Köhler ¹ R. Krastev ² B. Saramango ³	¹ MPI, Potsdam ² Uni Tübingen NMI ³ IST Lisbon, PT V6 PHY-04-1892-LT
125	Lipid-coated surfaces exposed to joint fluid, effects of temperature and joint fluid composition	M. Kreuzer ¹ R. Dahint ¹ R. Steitz ² M. Reinhardt ²	¹ RKU Heidelberg ² HZB V6 BIO-04-1893-EF
126	Surface induced structure formation of bicontinuous microemulsions: Influence of the surface	T. Hellweg ¹ R. Stehle ¹ S. Wellert ²	¹ Universität Bayreuth ² HZB V6 ART-04-1896
127	Inhibition of insulin adsorption and aggregation at hydrophobic interfaces	C. Czeslik ¹ F. Evers ¹ M. Tolan ¹ R. Steitz ² M. Kreuzer ²	¹ TU Dortmund ² HZB V6 CHE-04-1900
128	Water transport in giant algal cells by neutron radiography	Ch. Garvey ¹ M. Strobl ²	¹ ANSTO, AU ² HZB V7 BIO-04-1882
129	SANS – Analysis of electro spun polymer fibres from PPDO/PCL	J. Körner ¹ K. Kratz ¹ S.-O. Seidel ² W. Treimer ²	¹ GKSS Teltow ² TFH Berlin V12a CHE-04-1783

Material Science

133	Determination of load-affected through-thickness residual stresses in welded Aluminium alloys	Th. Nitschke-Pagel ¹ R. C. Wimpory ²	¹ TU Braunschweig ² HZB E3 MAT-01-2428
135	Residual stresses in diamond reinforced MMC under mechanical load	M. Schöbel ¹ J. Jonke ¹ P. Dobron ¹ N. Eder ¹	¹ TU Wien, AT E3 MAT-01-2430
136	Residual stress states in case hardened discs for the validation of simulation results	J. Epp ¹ Th. Hirsch ¹ R. C. Wimpory ²	¹ Universität Bremen ² HZB E3 PHY-01-2496
137	Optimization of seamless precision drawn Copper-tubes	A. Cerradò ¹ H. Palkowski ² R. C. Wimpory ³	¹ IPCMS Strasbourg, FR ² TU Clausthal ³ HZB E3 MAT-01-2498
138	Residual stresses in butt joint and lap joint aluminium alloys welded by friction stir technique	V. Calbucci ¹ A. Manescu ¹ R. C. Wimpory ²	¹ UPM Ancona, I ² HZB E3 MAT-01-2500

List of Contributed Experimental Reports

PAGE	TITLE	TEAM	PROPOSAL		
139	Residual Stress Analysis of Drawn 1045 Steel Bars	A. da S. Rocha ¹ R. Nunes ¹ T. Hirsch ² R. C. Wimpory ³	¹ UFRGS, Porto Alegre, BR ² Universität Bremen ³ HZB	E3	MAT-01-2501
141	Three-Pass Slot Weld Specimen in Austenitic Stainless Steel	R. C. Wimpory ¹	¹ HZB	E3	MAT-01-2672-EF
142	Structure determination of unpolished Ni-Mn-Ga magnetic shape memory alloy single crystal	M. Chmielus ¹ R. Schneider ¹ R. C. Wimpory ¹ P. Müllner ²	¹ HZB ² Boise State University, US	E3	MAT-01-2673-EF
143	In-situ observation of twin structure change during loading and unloading of Ni₂MnGa Magnetic Shape Memory Alloys in a magnetic field	M. Chmielus ¹ R. Schneider ¹ R. C. Wimpory ¹ P. Müllner ²	¹ HZB ² Boise State University, US	E3	MAT-01-2673-EF
144	Residual Stress Field Measurements in Welded Steel Specimens	M. Farahian-Sohi ¹ R. C. Wimpory ²	¹ TU BRaunschweig ² HZB	E3	MAT-01-2677
145	Minimisation of spurious strains in neutron strain scanning at the surface	M. Hofmann ¹ J. Gibmeier ² R. C. Wimpory ³	¹ TU München ² TU Karlsruhe ³ HZB	E3	MAT-01-2678
146	Influence of Friction Stir Welding Parameters on the Residual Stress Distribution in Al Alloy Plates	C. M. Davies ¹ R. C. Wimpory ²	¹ ICL, UK ² HZB	E3	MAT-01-2679
147	Influence of residual stress and precipitation on the lattice parameter of aluminium alloy Jominy end quench samples	J. S. Robinson ¹ R. C. Wimpory ²	¹ University of Limerick, IE ² HZB	E3	MAT-01-2680
148	Measurements of axial residual stresses in a section of a bi-metallic piping weld	C. Ohms ¹ R. C. Wimpory ²	¹ JRC Petten, NL ² HZB	E3	MAT-01-2682
149	Influence of shifting Mn/Ga-ratio on martensite structure in Ni-Mn-Ga alloyed with 0.6% Cobalt	K. Rolfs ¹	¹ HZB	E3	MAT-01-2811-EF
150	Gas solid synthesis of LiBD₄ by borane absorption of LiD	A. Remhof ¹ O. Friederichs ¹ D. Wallacher ²	¹ EMPA, CH ² HZB	E6	MAT-01-2630
151	Residual strain-stress in anisotropic cold-rolled Zr-alloy	V. Sumin ¹ R. C. Wimpory ² A. Venter ³	¹ JINR, RU ² HZB ³ NECSA Pretoria, ZA	E7	MAT-01-2504
152	Microscopic change of carbon aerogel EDLC electrodes during charging	V. Lorrmann ¹ G. Reichenauer ¹ M. Wiener ¹ Ch. Scherdel ¹ Th. Hauß ² A. Buchsteiner ²	¹ ZAE Bayern ² HZB	V1	MAT-01-2658
153	Characterization of ODS nanoparticles in Fe-Cr model alloys	A. Ulbricht ¹ C. Heintze ¹ U. Keiderling ²	¹ FZ Dresden ² HZB	V4	MAT-04-1645
154	Stability of carbides in Co-Re-base alloy at high temperatures	P. Strunz ¹ U. Keiderling ² D. Mukherji ³	¹ ASCR NPI Rez, CZ ² HZB ³ TU Braunschweig	V4	MAT-04-1655

List of Contributed Experimental Reports

PAGE	TITLE	TEAM	PROPOSAL	
155	Research of water balance in PEM fuel cells	T. Arlt ¹ I. Manke ¹ N. Kardjilov ¹ P. Krüger ² R. Kuhn ² A. Schröder ³ T. Sanders ⁴	¹ HZB ² ZSW, ULM ³ FZ Jülich ⁴ RWTH Aachen, ISEA	V7 MAT-04-1588-LT
156	Energy selective imaging of structural materials	L. Josic ¹ E. Lehmann ¹ M. Tamaki ² N. Kardjilov ³ A. Hilger ³ M. Dawson ³	¹ PSI, CH ² Univ. Nagoya, JP ³ HZB	V7 MAT-04-1685
157	Hydrogen absorption/desorption in La Ni _{4.6} Al _{0.4} based disc-like storage tank	N. B. Selvaraj ¹ L. Gondek ¹ N. Kardjilov ²	¹ AGH-UST, Krakow, PL ² HZB	V7 MAT-04-1689
158	In-situ Stress and Structure Changes Using Portable Tensile Testing System and Large Chamber SEM	D. Penunadu ¹ R. Woracek ¹ N. Kardjilov ² M. Dawson ²	¹ University of Tennessee, US ² HZB	V7 MAT-04-1781
159	Influence of magneto-mechanical cycling on the initialization and growth of crack in Ni ₂ MnGa magnetic shape-memory single crystal specimens	M. Chmielus ¹ R. Schneider ¹ A. Paulke ¹ A. Hilger ¹ P. Müllner ¹	¹ HZB	V7 MAT-04-1863-EF
160	Visualisation of magnetic domains by dark-field neutron imaging	M. Strobl ¹⁺² I. Manke ¹ A. Hilger ¹ N. Kardjilov ¹ M. Dawson ¹	¹ HZB ² Universität Heidelberg	V7 OTH-04-1871-EF
161	CO ₂ -deposition-evacuation in spherical particles for correlations with thermal conductivity models	M. Geisler ¹ G. Reichenauer ¹ N. Kardjilov ² M. Dawson ²	¹ ZAE Bayern ² HZB	V7 PHY-04-1874
162	Use of Neutron Tomography to Study the Effects of Microporosity in Binary Aluminum Alloy Castings	D. Penunadu ¹ J. Bunn ¹ N. Kardjilov ² M. Dawson ² A. Hilger ²	¹ University of Tennessee, US ² HZB	V7 MAT-04-1885

Cultural Heritage

165	Report on use of μ -ct scans for research under GEO-04-1870 and GEO-04-1774	Ch. Neumann ¹ P. Giere ¹ Th. Lehmann ² N. Kardjilov ³ A. Hilger ³ A. Paulke ¹	¹ HU Berlin ² FI Senckenberg ³ HZB	V7 GEO-04-1870 GEO-04-1774
166	Archaeometric characterization by Neutron tomography of recovered underwater items	R. Triolo ¹ I. Ruffo ² F. Wieder ³ M. Dawson ³ N. Kardjilov ³	¹ Univ. Palermo, IT ² ITC Don L. Sturzo, Bagheria, IT ³ HZB	V7 ART-04-1877
167	Neutron Tomography study of pottery fragments from Vörs-Máriaasszonysziget: 5600 BC – 300 AD	D. Visser ¹ N. Kardjilov ²	¹ TU Delft, NL ² HZB	V7 ART-04-1686

Development of Instruments and Methods

	EXPERIMENTAL REPORT Optical components for the new wide angle NSE spectrometer WASP at the ILL (Cooperation contract)	Proposal: PHY-03-577-EF Instrument: V5 Local Contact: E. Moskvina, C. Pappas
	Principal Proposer: Catherine Pappas, HZB Experimental Team: Ken Andersen, Institute Laue-Langevin Peter Fouquet, Institute Laue-Langevin Evgeny Moskvina, HZB	Date(s) of Experiment 26.05.2008 – 08.06.2008 11.06.2008 – 23.06.2008

Date of report: 08.12.2009

The results of this experiment have already been published in Review of Scientific Instruments [1]. We included the abstract of this paper as experimental report.

This paper describes the design and experimental tests of a novel neutron spin analyzer optimized for wide angle spin echo spectrometers.

The new design is based on nonremanent magnetic supermirrors, which are magnetized by vertical magnetic fields created by NdFeB high Field permanent magnets.

The solution presented here gives stable performance at moderate costs in contrast to designs invoking remanent supermirrors.

In the experimental part of this paper we demonstrate that the new design performs well in terms of polarization, transmission, and the high quality neutron spin echo spectra can be measured.

Reference:

[1] P. Fouquet, Bl Rarago, K.H. Anderson, P.M. Bentley, G. Pastrello, I. Sutton, E. Thaveron, F. Thomas, E. Moskvina and C. Pappas.

Design and Experimental Tests of a Novel Neutron Spin Analyzer for Wide Angle Spin Echo Spectrometers

Rev. Sci. Instrum. **80**, 095105 (2009)

 HELMHOLTZ ZENTRUM BERLIN für Materialien und Energie NEUTRONS	EXPERIMENTAL REPORT Development and calibration of efficient neutron position sensitive detectors and collimators	Proposal: MAT-04-1780 Instrument: V7 Local Contact: N. Kardjilov
	Principal Proposer: A. Tremsin, University of California at Berkley, USA Experimental Team: N. Kardjilov, HZB M. Dawson, HZB M. Strobl, HZB I. Manke, HZB	Date(s) of Experiment 17.11.2009 – 24.11.2009

Date of report: 04.12.2009

The experiment conducted at CONRAD beamline mostly concentrated on the two applications: **dynamic imaging of varied magnetic field with polarized neutrons and rejection of scattered neutrons by the microchannel plate collimators.**

The imaging of a static magnetic field has already been published by the HZB team [Kardjilov et al., Nature Physics 4 (2008) 399]. The high resolution of our microchannel plate (MCP) based neutron counting detector enabled dynamic imaging of an alternating magnetic field varying with the frequency of 3 kHz. The unique capability of our detection system to register both time (with $\sim 1 \mu\text{s}$ accuracy) and position ($\sim 55 \mu\text{m}$) of each detected neutron allowed us to acquire images with 2 μs time duration. High detection efficiency (exceeding 50% for cold neutron spectrum), the absence of readout noise and fast readout electronics (although limited to only 360 μs time range by the current implementation of electronics) enabled acquisition of enough neutron statistics in order to visualize the state of neutron polarization in each pixel of the acquired 2- μs images. The detector measured the time of neutron arrival at the detection plane relative to the trigger of pulse generator, used to set up the voltage in a ~ 12 -loop coil (Fig. 1). A large



Fig. 1. Photograph of a coil, which produced an alternating magnetic field. 10 A current was varied with frequency of 3 kHz.

fraction of neutrons was registered by the detector which was capable of operation at 50% duty cycle (only 50% of acquisition time was spent on the data readout). However, a higher neutron flux at the detection plane would have led to a much worse duty cycle due to the speed of the readout electronics requiring 30 ms for each readout frame. We plan to work on a much faster implementation

(use full parallel readout mode available at the ASIC level).

The images of the magnetic field generated by the coil are shown in Fig. 2. Examples of four frames acquired during the 3-kHz cycle are shown.

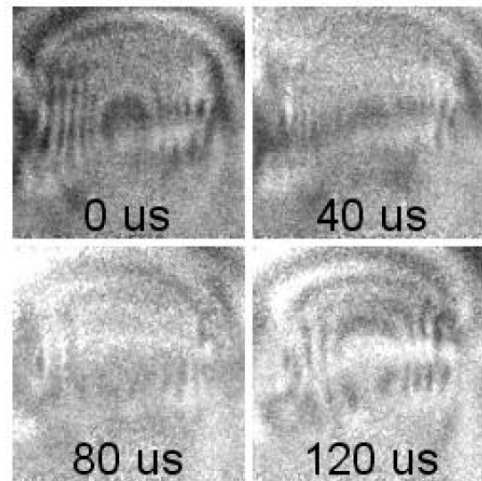


Fig. 2. Stroboscopic images of magnetic field measured with the spin-polarized neutron beam and an analyzer installed in front of neutron counting detector with microchannel plates. Continuous sequence of frames, each 2 μs in duration, was acquired for the entire 333 μs -long cycle. Only 4 frames out of the entire sequence are shown. The legend indicates the time delay from the beginning of the AC cycle. The amplitude of the AC current was 10 A.

MCP-based collimators were also tested for the first time for the possibility to remove scattered neutrons from the detection plane in cases when objects with large scattering cross sections are to be imaged (e.g. objects containing plastics, water). It was found that quantitative analysis of sample thicknesses can be performed after the scattering component was removed from the images. The compactness of our MCP collimators (~ 1 mm thick for aspect ratios of 100:1) enables very close distances to be preserved between the imaging objects and the detection plane. These collimators do not introduce any image distortions due to the small size of MCP pores ($< 10 \mu\text{m}$) and collimation in two dimensions is performed simultaneously.

 HELMHOLTZ ZENTRUM BERLIN für Materialien und Energie NEUTRONS	EXPERIMENTAL REPORT Dark-field neutron imaging	Proposal: PHY-04-1866-EF Instrument: V7 Local Contact: N. Kardjilov
	Principal Proposer: M. Strobl, Uni Heidelberg and HZB Experimental Team: I. Manke, HZB, A. Hilger, HZB N. Kardjilov, HZB, M. Dawson, HZB T. Kandemir, HZB	Date(s) of Experiment 11.12.2009 – 16.12.2009

Date of report: 12.01.2010

Recently a grating interferometer has been set-up that can be installed at the CONRAD imaging beamline in order to perform differential phase contrast imaging and - like could be demonstrated with this set-up – also dark-field contrast imaging [1]. Dark-field contrast imaging enables the detection of micro-structural inhomogeneities in a sample with structure sizes smaller than the spatial resolution of the imaging set-up.

Radiographic measurements have been performed to study the homogeneity of a BiSn sheets of approximately 1 mm thickness. While the attenuation and differential phase images did not provide any contrast (Fig. 1a), porous structures could be identified in the dark field contrast image of one of the sheets (Fig. 1b)[2]. The found structures correspond well to control measurements performed using high resolution x-ray radiography ($U=150$ keV, micro focus tube with a spatial resolution of $22 \mu\text{m}$) (Fig. 1c), which was feasible only due to the low thickness of the sample [2].

Another kind of samples were Al fatigue test specimen. Several samples have been exposed to radiographic and tomographic measurements. A micro-crack due to fatigue test loading was found in one of the samples in radiographic as well as tomographic images (Fig. 2 a, b) [2]. Additionally, the dark-field contrast of one of the samples differs significantly from the others (Fig. 2c, 2nd from top). This reveals a different microstructure with less inhomogeneities. This finding could be confirmed by energy dispersive x-ray (EDX) measurements (Fig. 2 d,e), which prove that the porosity in the specific sample is much lower as well as the number of precipitates. Additionally the precipitates in this sample contain less Cu, which reduces its scattering length density as compared to the surrounding matrix. As a consequence of these facts this sample causes significantly less ultra-small angle scattering and can hence be distinguished in dark-field contrast images [2].

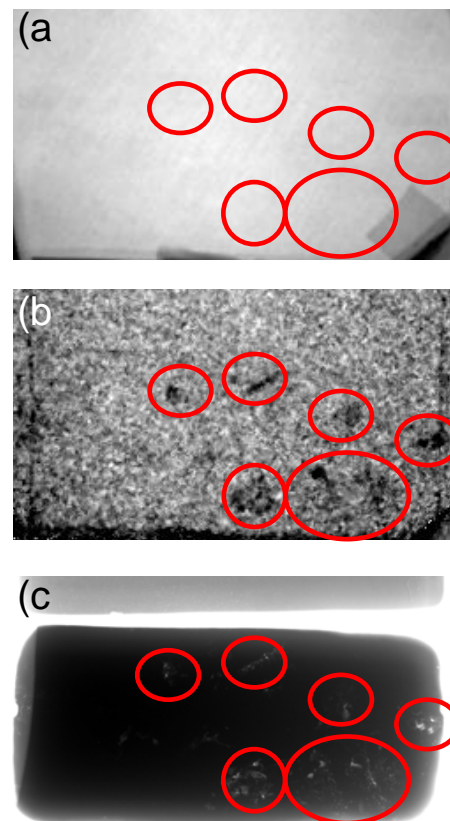


Fig. 1 Neutron attenuation, dark-field and x-ray image of BiSn sheet [2]

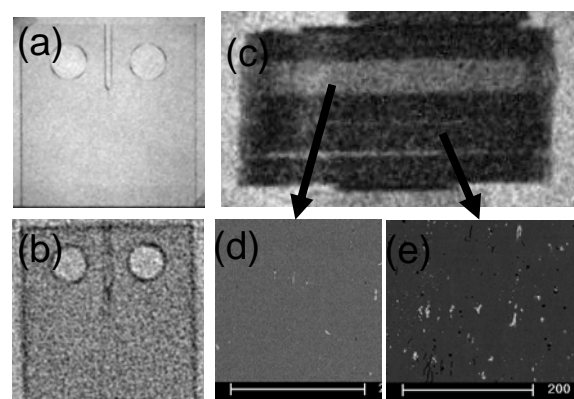


Fig. 2 Dark-field images and EDX of Al samples [2]

References

- [1] M. Strobl et al., PRL 101, 123902 (2008)
- [2] A. Hilger et al. JAP in the press

	EXPERIMENTAL REPORT High-resolution neutron imaging	Proposal: MAT-04-1867-EF MAT-04-1798-EF Instrument: V7 Local Contact: N. Kardjilov
Principal Proposer: Experimental Team:	N. Kardjilov, F. Garcia-Moreno, I. Manke, HZB N. Kardjilov, HZB M. Dawson, HZB A. Hilger, HZB	Date(s) of Experiment 23.05.2009 – 24.05.2009 13.12.2009 – 17.12.2009

Date of report: 26.01.2010

Introduction

A detector system for high-resolution neutron imaging was recently set up at the neutron tomographic instrument CONRAD, V7 at HZB [1]. It is a CCD-camera-based detector system using a 10 μm thick Gadox ($\text{Gd}_2\text{O}_2\text{S}(\text{Tb})$) screen, 200 mm Nikon lens (AF Micro-Nikkor 200 mm f/4D) and 2048x2048 pixel CCD camera (Andor DW436N-BV). The pixel size for the presented system is 13.5 μm , resulting in a field of view of 28 x 28 mm^2 . The achieved spatial resolution was 25 μm .

Experiment and results

Tomographic experiments performed with cold neutrons on CONRAD (V7) using the high-resolution detector system and with X-rays using a micro-focus tube and a flat panel detector have been compared.

The first example shows a compacted silica (SiO_2) sample with water (H_2O) where the goal of the investigation was to discern individual particles from one another and to clearly show water films and their distribution.

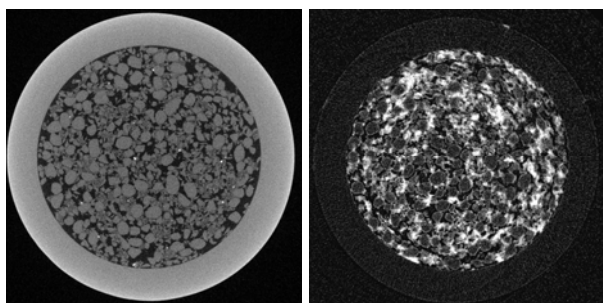


Fig. 1 Tomographic slices of a compacted silica sample with water measured by (left) X-rays (pixel size: 12 μm ; exposure time: 2.5 s; 1000 projections) and (right) cold neutrons (pixel size: 13.5 μm ; exposure time: 120 s; 500 projections). The diameter of the Al container is 10 mm. (courtesy of Dr. D. Penumadu, University of Tennessee).

As seen in Fig. 1 the high resolution neutron tomography provides comparable resolution to the X-ray measurement. The neutron tomography experiment shows the silica grains and the water distribution as well.

The second example shows an investigation of borated aluminum foam by X-ray and neutron tomography.

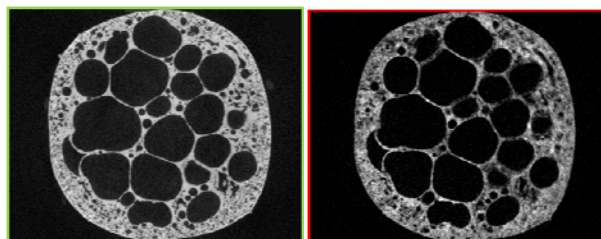


Fig. 2 Tomographic slices of borated aluminum foam by (left) X-rays (pixel size: 12 μm ; exposure time: 2.5 s; 1000 projections) and (right) cold neutrons (pixel size: 13.5 μm ; exposure time: 120 s; 500 projections). The foam size is 6 mm in the horizontal direction.

The X-ray tomography shows the structure of the foam with a high resolution. The resolution of the neutron tomography is comparable but, in addition, the boron distribution (bright areas) can be recognized.

Conclusion

The high resolution detector for neutron imaging provides comparable results with the X-ray tomographic investigations. In addition the complementary contrast provided by neutrons helps to resolve structures and distributions of light elements such as hydrogen and boron, which is not possible using X-rays.

References

[1] BENS Report 2008, p. 12

Principal Proposer: M. Strobl, Uni Heidelberg and HZB
Experimental Team: S.-O. Seidel, TFH
D. Penumadu, Univ. of Tennessee

Date(s) of Experiment

23.03.2009 – 31.03.2009

Date of report: 14.01.2010

Dark field imaging has been introduced as USANS (ultra small angle neutron scattering) contrast imaging in double crystal diffractometers [1]. Recently a more efficient method that enables even three-dimensional tomographies on reasonable time scales, could be realised using a grating interferometer in conventional neutron imaging instruments [2]. However, the new method cannot yet resolve the scattering pattern. In order to investigate respectively to compare the information content several samples that have earlier been imaged with the grating interferometer have now been exposed to USANS measurements at the V12a diffractometer.

First several steel plates, i.e. different stainless steel (304) plates with a thickness of 0.5 mm and low carbon steel (1018) plates of 1.3 mm, which provided no dark-field contrast and exceeded dark-field contrast, respectively, in the imaging experiments.

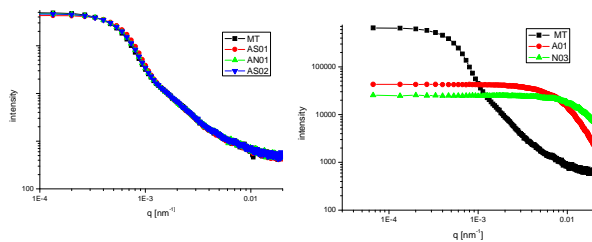


Fig. 1 USANS curves of stainless steel (left) and low carbon steel (right) compared to instrumental curve

In accordance to these earlier results the thin stainless steel plates display low scattering contributions, while the low carbon steel scatters strongly to relatively high q -values (Fig. 1). Consequently, these measurements constitute upper and lower limits of the grating set-up.

More measurements have been performed with both instruments on well defined scattering particles of different concentrations in solution. However, these data are still under evaluation, while radiographic dark-field images taken in the double crystal diffractometer and at the cold neutron radiography instrument CONRAD with

a grating interferometer of four cylindrical AISi casts [3] can be compared in Fig. 2. Obviously, although the sample geometry and different scattering contributions could be visualised accordingly, the spatial resolution in the USANS instrument (Fig. 2 top) is not sufficient to resolve micro-structural inhomogeneities revealed with the grating interferometer (Fig. 2 bottom) [3].

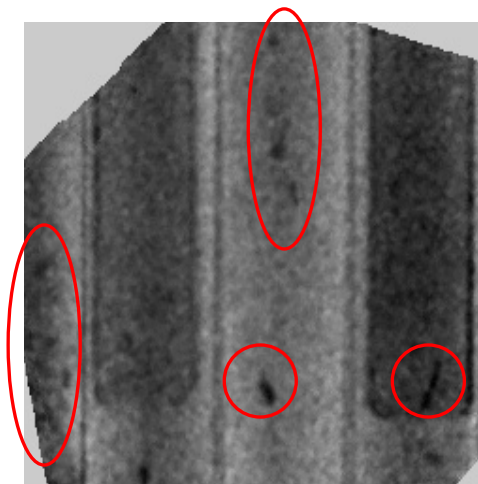
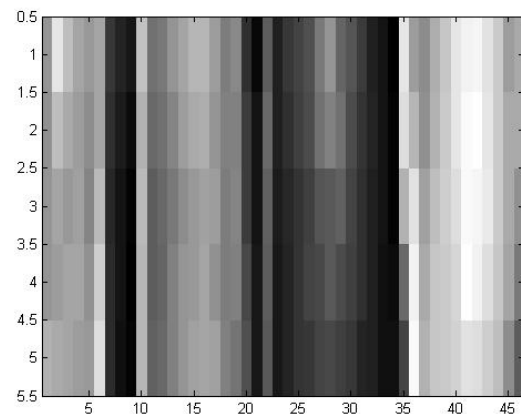


Fig. 2 Dark-field (USANS) radiography of cylindrical AISi samples taken in the double crystal diffractometer V12a (top), and corresponding measurement [3] with a grating interferometer at the radiography instrument CONRAD (bottom) Note that the grey scale is inverse as compared to the upper image.

References

- [1] M. Strobl et al. APL 85, 3 (2004)
- [2] M. Strobl et al., PRL 101, 123902 (2008)
- [3] A. Hilger et al., JAP in the press

Principal Proposer: S.-O. Seidel, W. Treimer, University of Applied Science
 Experimental Team: S.-O. Seidel, University of Applied Science
 W. Treimer, University of Applied Science
 O. Ebrahimi, University of Applied Science
 N. Karakas, University of Applied Science

Date(s) of Experiment

03.08.2009 – 23.08.2009
 23.11.2009 – 23.12.2009

Date of report: 12.01.2010

The investigations of USANS – or dark field tomography were continued on the basis of the first results from experiments of neutron tomography reconstruction from scattering signals [1]. Now the measurements were performed with the 2D-detector in order to get information about scattering at different sample heights. A similar specimen with the dimensions of (H x D) of 24 x 20 mm² with three different samples (Fe, Ni, Cu) inside were adjusted. A vertical slit (width = 1mm) in front of the sample, perpendicular to the incident beam, was shifted in 23 steps, and for each step the total scattering curve was measured.

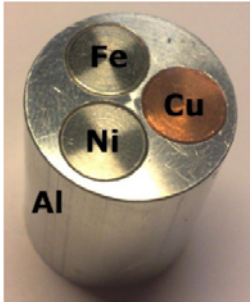


Fig.1: Sample

This measurement has been carried out with 60 rotation steps over an angular range of 360°. Figure 2 shows a test measurement for three different angle positions from 0 up to 180 deg, to find the centre of rotation. Figure 3 shows the appropriate absorption profile for comparison between measurement and theory. According to this measurement, with a number of around 1,4x10³ files for the whole sample size, a programme routine had to be developed in order to prepare data in such a way that they further could be processed with standard software. To solve this special problem of reconstruction three-dimensionally the numbers of files will rise up to at least 50 x10³ files.

In principal there are 3 parameters which have to be extracted from the data [2]. Therefore a fit function for all scattering curves was chosen, to get information about the imaging signals which corresponded to the attenuation, refraction and the ultra small angle scattering of neutrons. The model in the Fig.4 depicts one slice of the sample with corresponding calculated attenuation coefficients for each material (left part), the right part shows the calculated Radon transform and taking projections of the sample under different angles.

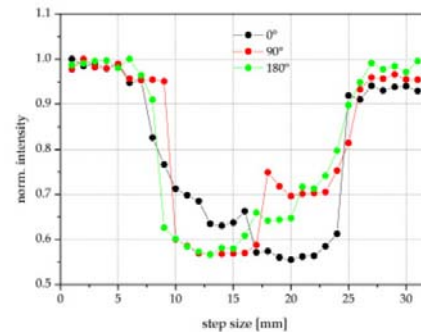


Fig.2: Absorption scans for three angle positions

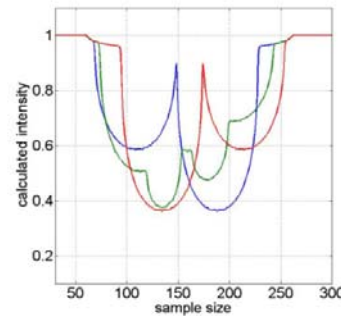


Fig.3: Absorption profiles without convolution with scan slit geometry for 0, 90° and 180°

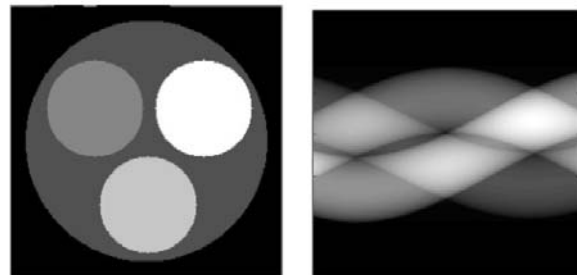


Fig.4: left: Calculated model of sample, right: Radon transform of the left image

[1] M. Strobl, W. Treimer, A. Hilger, Appl. Phys. Lett. 85 (3) (2004) 488-490

[2] W. Treimer, M. Strobl, A. Hilger, C. Seifert, U. Feyer-Treimer, Appl. Phys. Lett. 83 (2) (2003) 398

This work was financed by the BMBF project 05KN7KF1

 Neutrons	EXPERIMENTAL REPORT BioRef commissioning: first spectra measured	Proposal: EF Instrument: V18 Local Contact: M. Strobl
	Principal Proposer: M. Strobl, Uni Heidelberg and HZB Experimental Team: R. Steitz, HZB R. Dahint, Uni Heidelberg M. Kreuzer, Uni Heidelberg and HZB M. Grunze, HZB	Date(s) of Experiment November 2009

Date of report: 12.01.2010

Only two years and a few months after the project was started in summer 2007 the first reflectivity measurements could be performed at the time-of-flight (TOF) neutron reflectometer BioRef (V18) [1].

The TOF reflectometer consists mainly of a three chopper system, a frame overlap mirror, a slit collimation system and a 30 x 30 cm² area detector on the arm of a theta-2theta sample stage (Fig.1). An outstanding feature of the instrument will be the set-up of an infrared spectrometer to achieve additional conformation information on samples in-situ. The two pulse shaping choppers can be set to variable distances by moving the second chopper on a linear stage in order to choose a constant wavelength resolution between 1% and 5% [2]. Relaxed resolutions can be achieved by using one of them alone. This however means giving up the constant wavelength resolution on the used wavelength band which is defined by the third chopper. The choppers run at identical frequency of up to 100Hz, allowing to choose wavelength bands with widths from 4Å up to 16Å usually starting from 4Å. That permits

to make a choice of q-range probed simultaneously in one instrumental setting, i.e. at a constant scattering angle. Hence, measurements can be focused on a q-range with maximum efficiency. A first reflectivity measurement of a Si wafer as a reference, taken with 5 angular settings and a wavelength band from 4Å to 8Å, demonstrates the envisaged ability of measuring reflectivities at least down to 10⁻⁶ despite the fact that the final shielding is not in place yet.

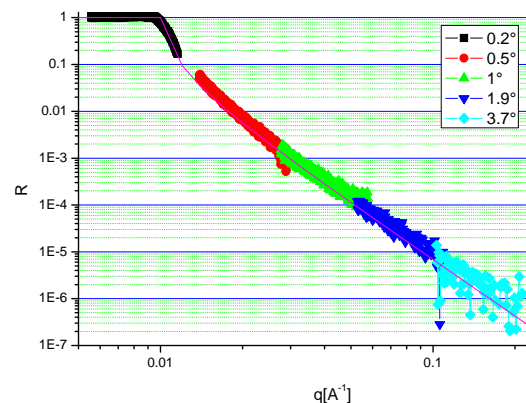


Fig. 2 First measurement of Si-wafer & theory (line)

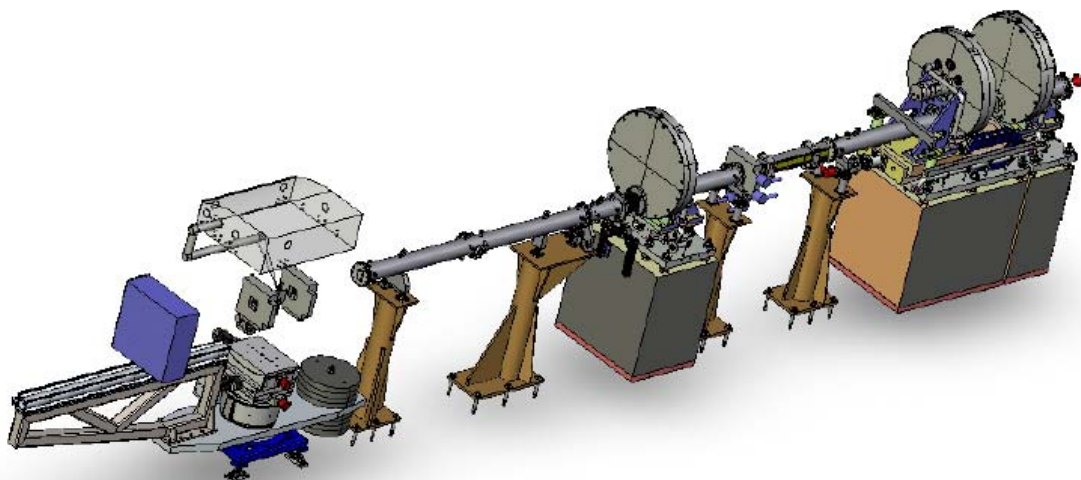


Fig. 1 Schematic drawing of BioRef

- [1] A.A van Well, Physica B 180 & 181 (1992) 959
 [2] M. Strobl et al., J. of Phys. (conf. series) in press

	EXPERIMENTAL REPORT Neutron tomography with sub-100µm spatial resolution	Proposal: EF Instrument: V19 Local Contact: W. Treimer
	Principal Proposer: W. Treimer, O. Ebrahimi, S.-O. Seidel, N. Karakas, Beuth Hochschule für Technik Berlin, & HZB Experimental Team: O. Ebrahimi, Beuth Hochschule für Technik & HZB N. Karakas, Beuth Hochschule für Technik & HZB S.-O. Seidel, Beuth Hochschule für Technik & HZB W. Treimer, Beuth Hochschule für Technik & HZB	Date(s) of Experiment 05.05.2009 – 24.05.2009 03.06.2009 – 21.06.2009 01.07.2009 – 20.07.2009

Date of report: 12.01.2009

The new instrument PONTO (“Polarized neutron tomography”) is a neutron tomography setup dedicated to radiography and tomography with polarized neutrons. It works with monochromatic neutrons coming from a graphite crystal ((002) reflection, the size was (65x40x4) mm³.) using continuously a wavelength range between 3.7 Å - 4.3 Å. To investigate and improve the spatial resolution several scintillator materials and optical objectives were tested.

Neutrons were detected and converted with a ⁶Li scintillator finally with a thickness of 50µm. The detecting optics were a mirror, an objective and a CCD-camera with a pixel field of (1024x1024) pixels. The spatial resolution was determined by measuring the edge spread function with a Gd-edge of 500µm thickness and deducing from radiogram the resulting modulation transfer function (MTF). The corresponding spatial resolution (line pair/mm) at the 10% MTF was found for the given geometry (L ~ 2000mm, L+l=const.) with ≥ 5lp/mm, much better than expected from the geometrical L/D.

This results can't be explained by the assumed conventional monochromatic tomography based on the beam divergence given by the convolution $\phi_{\text{guide}} \otimes \phi_{\text{mosaic}}$ and given by conventional pin hole L/D. Therefore D must be about 3 - 4 times smaller than (65x40) mm² reflecting crystal area. This improvement can be seen in the reconstructed images of an old watch that had details smaller than 100µm which one can only see with a spatial resolution > 5 lp/mm.

The tomography was performed with 301 projections each with an exposure time of 4 min. The reconstruction was performed with the standard software “Octopus”, the images in Fig. 1 and Fig.2 with VG Studio. Comparing these two reconstructions one realizes the improved spatial resolution mainly based on the higher flux and so the thinner converter foil used.



Fig.1 Reconstruction of an old watch with 85µm resolution with PONTO, size of the watch ~ 40mm

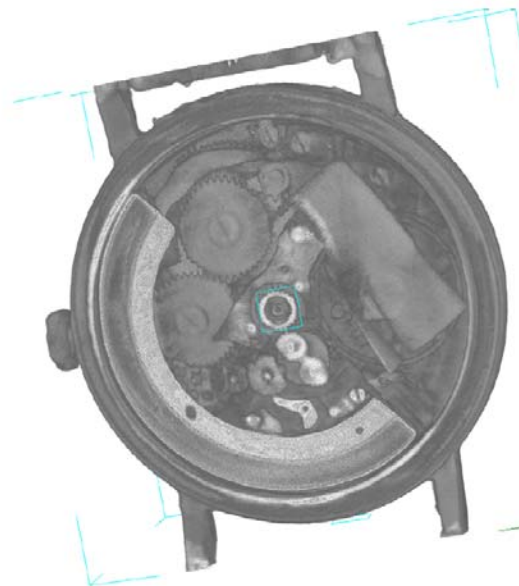


Fig.2 The same watch as in Fig.1 but with 180µm resolution with the V12c set up.

This work is part of the BMBF project 05KN7KF1

Principal Proposer: W. Treimer, Beuth Hochschule für Technik & HZB
O. Ebrahimi, N. Karakas, S.-O. Seidel, Beuth Hochschule für Technik
Experimental Team: W. Treimer, Beuth Hochschule für Technik & HZB
O. Ebrahimi, N. Karakas, S.-O. Seidel, Beuth Hochschule für Technik

Date(s) of Experiment
21.07.2009 – 26.07.2009
03.08.2009 – 23.08.2009
15.09.2009 – 31.10.2009

Date of report: 12.01.2010

In the frame of the BMBF project 05KN7KF1 the instrument PONTO (“polarized neutron tomography”) was installed at the NL1b neutron guide and we report about the first results. A (002) graphite monochromator (mosaic spread $\sim 0.4^\circ$) served as monochromator (wavelength 0.392(2) nm), and the reflected beam was collimated (divergence = 0.1°) in front of the polarizer. The cross section was (30x30) mm² which was reduced due to geometrical reasons. The collimator and polarizer were placed in a massive shielding box consisting of from B₄C and lead. Between polarizer and analyzer magnetic guide fields should avoid the depolarization of the beam. The degree of polarization was determined in two independent ways. The first measurement was the “shim-test” with an iron shim plate of 2mm thickness, which depolarized the beam more than 99%. The shim was put between polarizer and analyzer. The result is corrected with the flip-ratio of the analyzer.

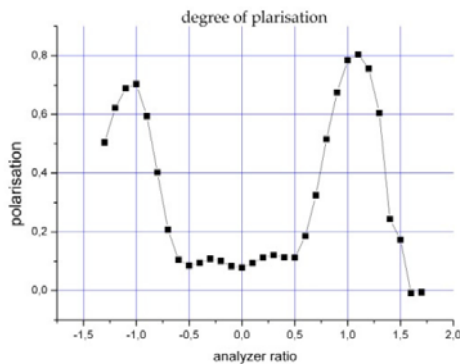


Fig.1: degree of polarization with ‘shim-method’

The second method is the π - flip method using two coils (compensation and flip-coil). At first the theoretical magnetic fields of the coils were calculated and then experimentally via iterative method adjusted. To appoint the quality of the π -Flipper, the determinations of the flipper efficiently and flip ratio are necessary.

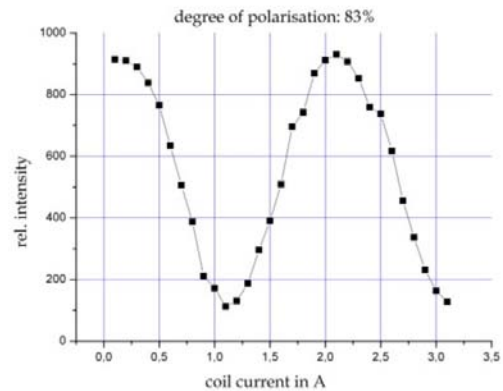


Fig.2 Spin rotation measurement with flip coils

Due to the size of the analyzer in front of the detector and a fixed L/D ratio, the spatial resolution for tomographies with polarized neutrons is much inferior to non-polarized neutrons. To image magnetic domains in sample like in a Fe crystal or fields in coils, a resolution well below 200 μ m is desirable. Within first experiments with a special short analyzer we achieved a spatial resolution for polarized neutrons below 150 μ m. The resolution was measured with a gadolinium-edge (500 μ m thickness) 10mm apart from the analyzer. From the edge image the corresponding MTF function & 10% was calculated. Fig.3 shows the depolarization image of the resulting magnetic field of two small magnets.

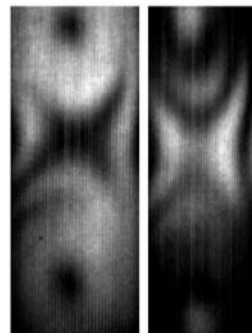


Fig.3: Image of the 2D depolarisation due to the magnetic-fields of two permanent magnets. Left: Incident neutron spin up, right spin down.

This work was part of the BMBF project 05KN7KF1

Magnetism

	EXPERIMENTAL REPORT Tuning the ground state of pyrochlore Ho_{2-x}Y_xTi₂O₇ (x = 0.3, 1) via applied magnetic fields	Proposal: PHY-01-2344 Instrument: E2 Local Contact: A. Hoser
	Principal Proposer: Yixi Su, JCNS, Outstation at FRM-II, Germany Experimental Team: L. J. Chang, National Tsing Hua University, TW M. R. Lees, University of Warwick, UK A. Hoser, HZB J.-U. Hoffmann, HZB	Date(s) of Experiment 14.10.2009 – 22.10.2009

Date of report: 9.03.2010

In spin-ice pyrochlore compounds $\text{Ho}_2\text{Ti}_2\text{O}_7$, spin correlations are determined by the “ice rule” organizing principle that stabilizes a magnetic ground state with the same zero-point entropy as water ice. Recently, Castelnovo *et al.* predicts that magnetic monopoles could emerge in spin ice as a consequence of the local violation of the “ice rule” due to excitations [1]. Another fascinating issue is possible quantum phase transitions driven by the chemical disorder and external magnetic field on the true ground state of spin ice materials. In our recent diffuse neutron scattering experiments carried out in zero magnetic field [2], we have observed that the chemical disorders introduced via the substitutions of Ho^{3+} with nonmagnetic Y^{3+} induce changes of the ground state of spin-ice $\text{Ho}_2\text{Ti}_2\text{O}_7$. The new ground states can also emerge upon the application of magnetic fields [3].

The diffuse neutron scattering experiment has been performed at E2 in order to investigate the magnetic ground states of the diluted spin-ice pyrochlore single crystal $\text{Ho}_{1.7}\text{Y}_{0.3}\text{Ti}_2\text{O}_7$ in the application of magnetic fields. A neutron wavelength of 2.4 Å was selected throughout the experiment. A 5-Tesla vertical field cryomagnet and a $^3\text{He}/^4\text{He}$ dilution insert have been used. The magnetic field has been aligned along the [111] direction of the crystal.

The results obtained at 40 mK in zero field and 1 Tesla are shown in the figure 1. At zero field, broad diffuse scattering with three-fold symmetry was observed. This pattern corresponds to the short-range spin correlations in the stacked Kagome and triangle layers in the (111) plane. It has been observed that the magnetic diffuse scattering has been drastically

changed under 1 Tesla field. The presence of long-range magnetic ordering and the “Bow-tie” like diffuse scattering as well as so-called pinch point indicates the complex nature of spin correlations in the spin-ice compounds under applied magnetic fields. More detailed analysis is under way.

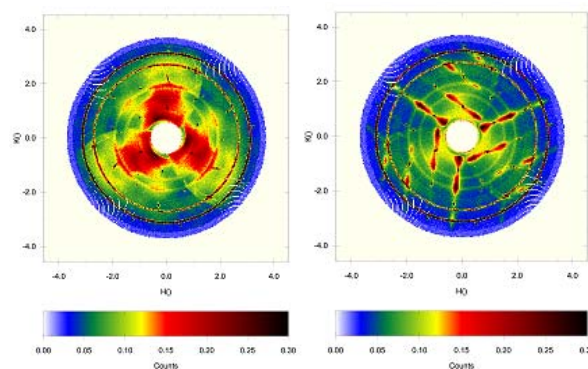


Figure 1. The contour plot of the diffuse neutron scattering of the (111) orientated $\text{Ho}_{1.7}\text{Y}_{0.3}\text{Ti}_2\text{O}_7$ at 40 mK at zero field (left), and 1 Tesla field (right).

References

- [1] C. Castelnovo, R. Moessner and S.L. Sondhi, *Nature* **451**, 42 (2008).
- [2] L.-J. Chang, Y. Su, M. R. Lees *et al.* (unpublished).
- [3] T. Fennell, S. T. Bramwell *et al.*, *Nature Physics* **3**, 566 (2007).

	EXPERIMENTAL REPORT Magnetolectric Correlations in Multiferroic DyMnO₃	Proposal: PHY-01-2485 Instrument: E2 Local Contact: J.-U. Hoffmann
	Principal Proposer: Manfred Fiebig, HISKP, Universität Bonn Experimental Team: Dennis Meier, HISKP, Universität Bonn	Date(s) of Experiment 06.07.2009 – 13.07.2009

Date of report: 27.11.2009

In our experiment the competition of the magnetic 3d and 4f sublattices of hexagonal DyMnO₃ was investigated to complete our study on the microscopy of magnetolectric interactions in the RMnO₃ series. For this purpose, measurements were performed using an Orange Cryostat in combination with a He³/He⁴ dilution stick at E2. This enabled measurements down to 30 mK, where DyMnO₃ is fully ordered, exhibiting ferroelectricity, antiferromagnetic Mn³⁺ ordering and magnetic ordering at the two Dy³⁺ sites.

Use of the flat cone geometry allowed full scans of the (h0l)-plane at different temperature, which reveal the symmetry of the different ordered phases. In addition, the intensity of certain reflexes giving access to specific aspects of the multiple order, was traced between 3 mK and 80 K.

A detailed quantitative analysis of the data gained on DyMnO₃ and a comparison to the data gained on ErMnO₃ (PHY-01-2341) is still in progress. However, important open questions about the rare-earth ordering on hexagonal RMnO₃ can already be answered. Surprisingly, the previously gained neutron data on DyMnO₃ samples of rather poor quality (PHY-01-1641) suggested the same magnetic symmetry considering the order of the rare-earth moments (4f) in ErMnO₃ and DyMnO₃.

In contrast, the repeated measurements on high-quality crystals of DyMnO₃ now clearly reveal that this result no longer holds. Various details indicate that DyMnO₃ exhibit a different magnetic symmetry regarding the rare-earth moments, although we have not solved the magnetic structure in detail yet. Most significant is the absence of different reflexes in DyMnO₃ that are characteristic for the rare-earth order of ErMnO₃. The (301)-reflex for instance, indicating the rare-earth ordering on the 2a-site in ErMnO₃, is absent in DyMnO₃.

Moreover, significant differences regarding the interplay of the rare-earth magnetism and the ordered Mn moments are obtained at low temperature. This is shown in figure 1, displaying the temperature dependence of the (102)- and the (100)-reflex, being sensitive to the ordering of the Mn³⁺ moments (3d) in ErMnO₃ and DyMnO₃.

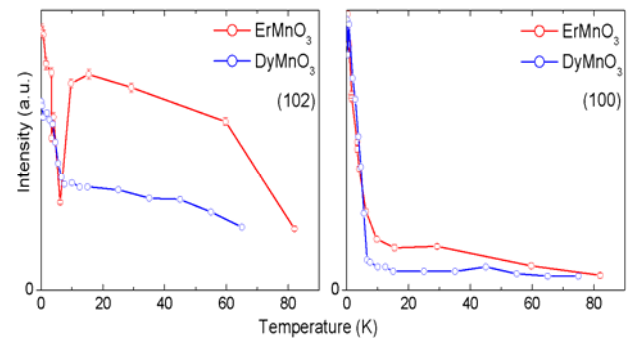


Figure 1: Temperature dependence of the (102) and (100)-reflex in ErMnO₃ and DyMnO₃. The reflexes probe different components of the Mn moments.

Each measurement clearly shows an increase of the detected intensity below 10 K, which correlates to the onset of the magnetic long-range order of the rare earth spins. First of all, this observation indicates a pronounced 3d-4f coupling. A comparison of DyMnO₃, ErMnO₃ and HoMnO₃ [1] (not shown) reveal a completely different temperature behaviour regarding the (102)-reflex at low temperature. As shown in figure 1, ErMnO₃ reveals a breakdown of the detected intensity as the rare-earth subsystem orders. In contrast, no similar effect is observed in DyMnO₃. We attribute these differences to the specific interactions of the 3d and 4f moments in the two compounds caused by the different symmetry of the rare earth subsystems. This interpretation is supported by since SHG measurements that reveal the same symmetry regarding the Mn moments in ErMnO₃ and DyMnO₃ above the ordering temperature of the rare-earth spins.

Further optical second harmonic generation experiments will allow for clarifying the obtained subtle differences regarding the temperature dependence of the magnetic order of the Mn moments and may reveal possible changes in the symmetry at 10 K.

Reference

1. T. Lonkai: *Electric and Magnetic Order Parameters in the Multiferroic Hexagonal RMnO₃ System*, PhD thesis (Universität of Tübingen, 2003)

	EXPERIMENTAL REPORT Magnetolectric coupling in BiFeO₃ – PbTiO₃	Proposal: MAT-01-2487 Instrument: E2 Local Contact: J.-U. Hoffmann
	Principal Proposer: Tim Comyn, University of Leeds, UK Experimental Team: Tim Stevenson, University of Leeds, UK Illya Glavatskyi, HZB Klaus Kiefer, HZB Jens-Uwe Hoffmann, HZB	Date(s) of Experiment 02.06.2009 – 10.06.2009 22.07.2009 – 24.07.2009

Date of report: 12.08.2009

The aims of this experiment were to provide an understanding of the link between crystallographic structure, electric and magnetic ordering in the perovskite bismuth ferrite lead titanate (BFPT).

BFPT is a multiferroic, displaying both ferroelectric and antiferromagnetic ordering. For the composition $0.7\text{BiFeO}_3 - 0.3\text{PbTiO}_3$, $T_C = 638^\circ\text{C}$ and $T_N = 370^\circ\text{C}$. We have shown using a range of experiments that this composition has a significant enhancement in resistivity and ease of synthesis compared to pure BiFeO_3 . In addition, this composition shows large (>1 GPa) internal strain levels due to phase coexistence (rhombohedral, R3c and tetragonal, P4mm), which drives an enhancement in ferroelectric, piezoelectric and magnetic properties.

The experiment used the E2 powder diffractometer, with an Orange cryostat and 6.5 kV amplifier to apply an electric field to the sample. The cryostat sample 'stick' was modified by the sample environment team to support a Teflon block to insulate the sample from the stick. From the Teflon an aluminium paddle and Teflon coated wire protodes to introduce an electric field across the sample.

For the experiment, we used discs of the composition 70% $\text{BiFeO}_3 - 30\%$ PbTiO_3 , 28 mm in diameter, 500 μm thick and electroded on both sides with silver. These dimensions were selected as a compromise to keep the samples thin enough to apply a large electric fields (> 10 MVm^{-1}) but thick enough to provide sufficient data statistics; each disc was measured in 5 hour periods in 1 kV increments steps.

In order to prevent breakdown through the air around the sample, the cryostat was pumped down to $<5.0 \times 10^{-4}$ mbar. It was noted that applying fields of 6 MVm^{-1} and higher (3000V), began to resistively heat the sample, as no mechanism was present to remove the heat; these samples failed. In subsequent measurement, the sample environment was cooled from room temperature to 250 K. This relatively small drop of ca. 50 K increases the

resistivity of the ceramic sample by ca. 4 orders of magnitude, without providing a significant modification to the ferroelectric or magnetic properties.

Figure 1 shows the diffraction data collected from 0 kV to 5 kV in steps of 1 kV. The magnetic peak at 4.6 Å shows that with increasing voltage, the magnetisation of the material increases steadily. Extremely care was taken during these measurements to ensure that the sample temperature remained steady; we were able to achieve this to within ± 0.5 K.

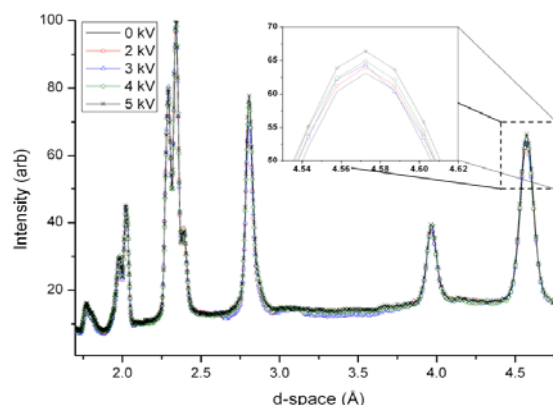


Figure 1; Neutron diffractogram of $0.7\text{BiFeO}_3-0.3\text{PbTiO}_3$ with applied field

The observations can be better defined in figure 2, when comparing the material with 5 kV field and subtracting the difference from the sample with no applied field.

Here the material is clearly observed to have an increased intensity in magnetic peak, as well as an increasing difference in the (110) and (111) structural peaks.

We are thus able to directly show a correlation between an applied electric field and the magnitude of the magnetic peak. The alteration in the nuclear peaks suggest that this is due to an increase in the concentration of R3c phase. The R3c phase is antiferromagnetic, whereas the P4mm phase is paramagnetic

Acknowledgement

This research project has been supported by the European Commission under the 7th Framework Programme through "Research Infrastructures" action of the "Capacities" Programme, contract number CP-CSA_INFRA-2008-1.1.1. Number 226507-NMI

	EXPERIMENTAL REPORT Temperature evolution of the crystal and magnetic structures in the new Ni-Mn-Ga-(Fe, Cu) ferromagnetic shape memory alloys	Proposal: PHY-01-2490 Instrument: E2 Local Contact: J.-U. Hoffmann
	Principal Proposer: I. Glavatskyi, Institute for Metal Physics, UA Experimental Team: I. Glavatskyi, Institute for Metal Physics, UA Jens-Uwe Hoffmann, HZB – M-I1	Date(s) of Experiment 19.05.2009 – 24.05.2009

Date of report: 10.07.2009

The temperature evolution of the crystal structure of the Ni-Mn-Ga based magnetic shape memory alloys had been a topic of severe discussion over the last years, producing a bunch of publications based on the experimental and ab-initio theoretical studies, often with contradictory results. However, this subject is of particular importance, both for the fundamental and applied points, due to high technological potential of such multifunctional alloys. Thus, we aimed our studies to resolve the conflicts and clarify the crystal structure of the martensite in Ni₂-Mn-Ga-(Cu,Fe) alloys [1] by the neutron powder thermo-diffractometry.

Experiment: For the experimental studies with E2 diffractometer at $\lambda=1.2$ and 2.4\AA , powder specimens were prepared by high impact ball milling, followed by 800°C annealing in Ar atmosphere. Measurements were performed during cooling and heating cycles, using the Orange Cryofurnace.

Results: From the obtained diffraction patterns vs. temperature the notable changes in the peak profiles are observed. Thus, while the crystal structure is conserved over the entire temperature interval of the martensite phase existence, the strong changes in the (020) and (211) and smaller satellite peaks are believed to be caused by the short-range ordering of the stacking faults along [010], due to the anisotropic temperature dependence of the martensite lattice parameters [2], and thus – changes of the energy of the stacking faults, which is already very low for the martensite phase of the material. Such changes in the crystal structure affect the microstructure of the martensite as well, having the hierarchical twinning morphology from nano- to macro-scale. Such changes in the defect structure of the martensite, affecting the microstructural level, bring up changes in the transport (magnetic, electric etc.) properties, being often mistakenly considered in literature as signs of the intermartensitic phase transitions, e.g. in [3].

For the first time in this alloy system, the experimental evidence of the antiferromagnetic order is observed (e.g. Fig.1). The AFM phase appears on cooling at $T\sim 100\text{K}$ and co-exists with ferromagnetic ordering till the ground state. The appearance of the AFM ordering is proved for the quaternary Ni-Mn-Ga-(Cu,Fe) as well as for the ternary Ni-Mn-Ga alloys. However, in the Cu-alloyed case, the AFM transition temperature is found to be the highest observed.

Another intriguing feature observed of the thermal evolution is that Ni-Mn-Ga-Cu alloys did not show any

significant shift of the diffraction peaks, contrary to the ternary Ni-Mn-Ga alloys, where thermal expansion of the martensite is strong and highly anisotropic (Fig.2).

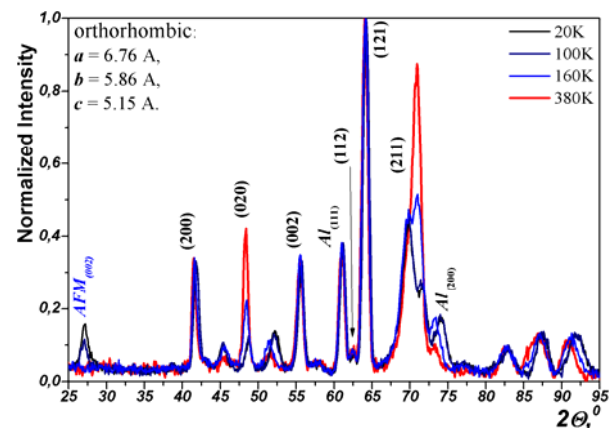


Fig.1. Thermal evolution of the powder diffraction pattern of the Ni-Mn-Ga-Cu(2.7at.%) alloy.

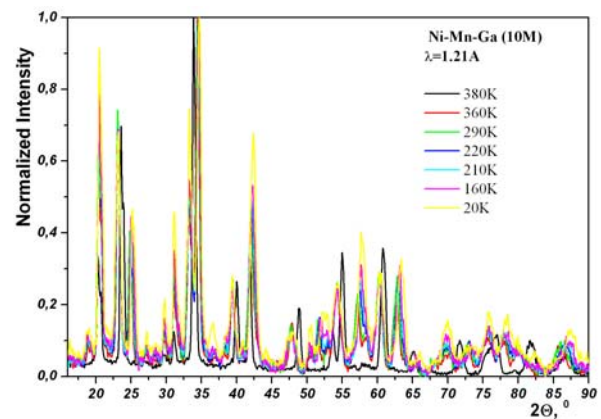


Fig.2. Thermal evolution of the powder diffraction pattern of the Ni-Mn-Ga alloy.

References:

- [1] Glavatskyy I., Glavatska N., Soderberg O., Hannula S.-P., Hoffmann J.-U. // Scripta Mater., 54 (2006), 1891-1895.
- [2] I. Glavatskyy, N. Glavatska, I. Urubkov, J.-U. Hoffman, F. Bourdarot // Mat. Sci. Eng. A, 481-482 (2008), 298-301.
- [3] O. Heczko, N. Lanska, O. Soderberg, K. Ullakko // J. Magn. Magn. Mater. 242-245 (2002) 1446-1449.

 Neutrons	EXPERIMENTAL REPORT	Proposal: PHY-01-2526
	Magnetic order in YbCo₂Si₂	Instrument: E2 Local Contact: A. Hoser
Principal Proposer: Koji Kaneko, Advanced Science Research Center, Japan Atomic Energy Agency Experimental Team: Nandang Mufti, Max-Planck-Institut CPfS, Dresden Oliver Stockert, Max-Planck-Institut CPfS, Dresden Andreas Hoser, HZB	Date(s) of Experiment 06.05.2009 – 11.05.2009	

Date of report: 4.03.2010

Recently the heavy-fermion compound YbRh₂Si₂ has attracted much attention due to its close vicinity to a quantum critical point (QCP) [1,2]. However, the weak antiferromagnetism in YbRh₂Si₂ with T_N = 70 mK and a small ordered moment makes it difficult to study in more detail the unusual properties of this compound. One way to overcome these difficulties is to stabilize the AFM state and increase both, T_N and the size of the ordered moment by application of positive chemical pressure. Our recent studies show that substitution of Rh by isoelectronic Co stabilizes the AFM state and enhances T_N [3]. Therefore we started to study YbCo₂Si₂ which gives useful information on the magnetic interactions in the YbT₂Si₂ systems in general and serves as a reference for the (almost) quantum critical YbRh₂Si₂.

A powder neutron diffraction experiment was performed on the diffractometer E2 with a neutron wavelength λ = 2.41 Å. Approximately 7 gram of YbCo₂Si₂ powder was sealed in a Cu container and mixed with a small amount of deuterated methanol – ethanol mixture. The sample was mounted on ³He insert inside a vertical magnet and allowed measurements in the temperature range between 0.4 and 2 K and in magnetic fields up to 2.5 T.

Figure 1 displays the neutron powder diffraction pattern of YbCo₂Si₂ recorded at three different temperatures, corresponding to the ground state (T = 0.45 K), the intermediate phase (1.1 K) and the paramagnetic phase (2.0 K). The data below 2.0 K clearly reveal additional Bragg peaks of magnetic origin. In order to obtain the pure magnetic signal, the diffraction pattern at 0.45 K and 1.1 K were subtracted from the data at 2.0 K. The magnetic peaks at lowest temperature can be indexed with a

propagation vector $k_1 = (\frac{1}{4}, \frac{1}{4}, 1)$. For the intermediate phase, the analysis yields a propagation vector $k_2 = (\frac{1}{4}, 0.08, 1)$. The temperature dependence of the magnetic reflections shows a dramatic drop at T_L = 0.9 K as shown in figure 2. These results indicate that the commensurate-incommensurate phase transition at T_L is first order in nature. Magnetic intensity vanishes at T_N = 1.7 K in close agreement with thermodynamic and transport measurements.

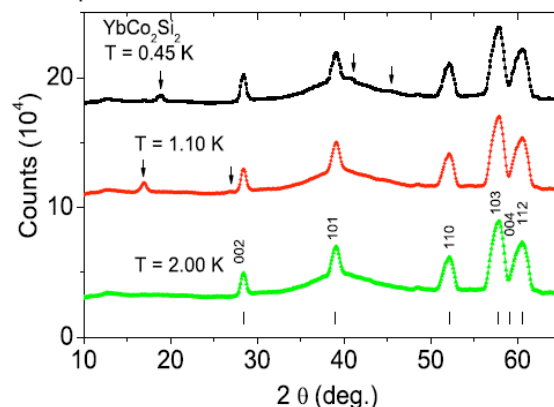


Figure 1. Neutron diffraction pattern of YbCo₂Si₂ recorded at different temperatures.

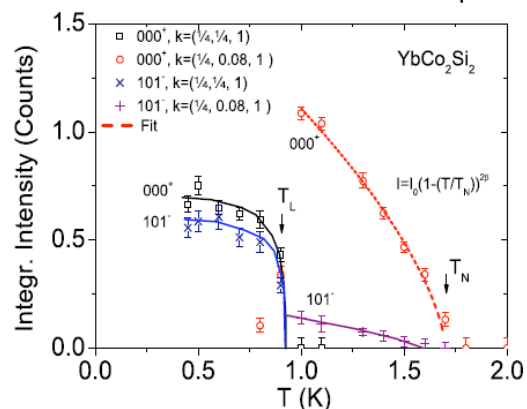


Figure 2. Temperature dependence of the (000⁺), (101⁻) integrated intensity of YbCo₂Si₂

- [1] J. Custers et al., Nature 424, 524 (2003).
- [2] P. Gegenwart et al., Nature Phys. 4, 186 (2008).
- [3] T. Westerkamp et al., Physica B 403, 1236 (2008).

 Neutrons	EXPERIMENTAL REPORT	Proposal: PHY-01-2546-EF
	Diffuse scattering study of Dy₂Ti₂O₇	Instrument: E2 Local Contact: Jens-Uwe Hoffmann
Principal Proposer: Experimental Team:	Jonathan Morris, HZB Alan Tennant, HZB Santiago Grigera, Instituto de Física de Líquidos y Sistemas Biológicos, La Plata, Argentina Kirrily Rule, HZB Bastian Klemke, HZB Sebastian Gerischer, HZB Jens-Uwe Hoffmann, HZB	Date(s) of Experiment 30.03.2009 – 09.04.2009

Date of report: 27.11.2009

Spin ice is a system where the magnetic moments have a geometry which mimics the hydrogen configuration in water ice. This frustration and geometry gives the system some fascinating physics.

Dysprosium titanate, Dy₂Ti₂O₇, is a spin ice with the pyrochlore geometry. Which does not suffer from the impurity of a nuclear magnetic moment, therefore this a clean system to look at the magnetism via diffuse neutron scattering. The VM4 magnet with dilution insert is used to take the sample below 1K in order to reach the spin-ice regime.

Predictions of magnetic monopoles and Dirac strings in such materials has increased interest, and the purpose of this experiment was to look for signatures of such exotic excitations. The collaborations previous experiment on E2 allowed us to measure the scattering from the Dirac strings when a field is applied to the sample nominally along [100] direction (fig. 1). Due to demagnetisation effects the magnetic field was actually tilted away from the [100] by around 10 degrees and this gave us a useful test of the hypothesis showing how strings align against the field. Here we probe the strings with a field along [100] where the sample geometry has changed and the demagnetisation does not misalign the field by more than a degree or two.

These Dirac strings are strings of spins which align anti-parallel to the applied magnetic field. Also they are tensionless and therefore can meander within the plane as they grow along the field direction. The prediction therefore is for a cone of scattering from the ensemble of these strings (fig. 2).

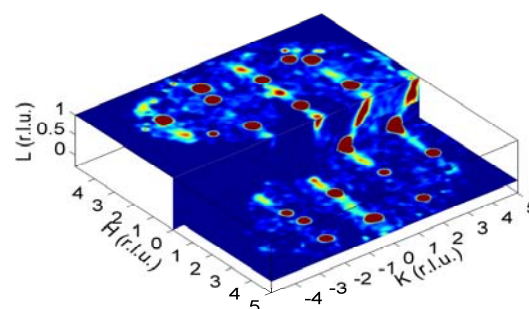


Fig. 1. E2 data from Dy₂Ti₂O₇ with the internal magnetic field tilted away from the [100] direction showing walls of diffuse scattering (Oct 2008)

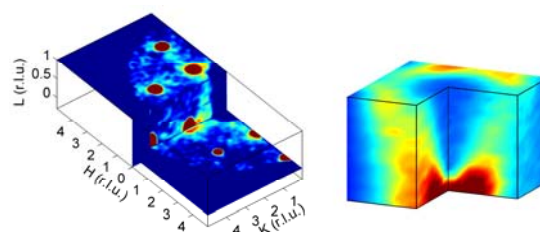


Fig. 2. (left) Neutron scattering revealing the cone of intensity expected for strings of spins along random walks along the applied field direction. (right) Calculation of the expected scattering around the (020) position showing the cone of scattering. (Apr 2009)

Working with a wavelength of 2.39Å, temperatures above the spin-freezing temperature of 0.6K and a magnetic field of 0.5T we measured the predicted cone. This experiment has given extra weight to the idea of excitations resembling Dirac strings and magnetic monopoles in spin-ice. It also improves our understanding into the Kasteleyn transition that leads to these quasiparticles.

Publications resulting from this experiment:
 D.J.P. Morris et al. Science 326, 411 (2009)

	EXPERIMENTAL REPORT Change of martensite structure in Ni-Mn-Ga single crystal ingots	Proposal: MAT-01-2580-EF Instrument: E2 Local Contact: I. Glavatskyi, J.-U. Hoffmann
	Principal Proposer: Markus Chmielus, HZB Experimental Team: Markus Chmielus, HZB Rainer Schneider, HZB Illia Glavatskyi, HZB Peter Müllner, Boise State University	Date(s) of Experiment 26.10.2009 - 31.10.2009

Date of report: 21.01.2010

Magnetic shape memory alloys (MSMA) with twinned martensite tend to deform in response to an external magnetic field reversibly (elastic), irreversibly (plastic), or as a combination of both. In 1996, the first results of the magnetoplastic effect and MFIS for a Ni₂MnGa Heusler alloy were published [1]. Since then, the interest in MSMA has grown, and large MFIS of around 10% in a rotating magnetic field were published in 2002 [2].

The single crystal samples studied in the DFG priority program SPP1239 subproject B2 are produced using the SLARE technique [3]. While this single crystal growth technique is designed to reduce Mn loss, inclusions, and impurities, solidification segregation during the growth process causes a composition gradient in growth direction. Depending on the nominal composition, the segregation results in different phase transformation temperatures and, more importantly, different martensite structures. Finally, that leads to different magneto-mechanical behaviours. The right column of fig. 1 shows the change of the composition, measured with calibrated EDS, (top) and phase transformation/Curie temperature, measured with DSC, (bottom) throughout a Ni-Mn-Ga single crystal ingot. In growth direction, Ni content changed 2 at.-%, Mn increased 3 at.-%, and Ga decreased 2.5 at.-%. The martensite phase

transformation temperature rose from 77 °C to 111 °C and the Curie temperature decreased from 100 °C to 92 °C and then below the martensite phase transformation temperature. The composition change resulted not only in a change of the phase transformation temperature but also in a change of the martensite structure as shown in the left two columns of fig. 1. While the samples examined from slice 1 and 3 showed four modulation reflections between the fundamental structure peaks, which is an indication for a 10M martensite, samples from slice 5 and 7 showed six modulation reflections, which indicates a 14M martensite. The change of martensite structure within growth direction from 10M to 14M martensite was also found in two other single crystal ingots that were examined during the reported time period (not shown here). The knowledge of the change of martensite structure is most important for the standardization process of MSMA and future applications.

References:

- [1] K. Ullakko et al., Appl Phys Lett, 69(13), 1966-1968 (1996)
- [2] A. Sozinov, Appl Phys Lett, 80(10), 1746-1748 (2002)
- [3] A. Mecklenburg et al., patent DE102004018664A1; 2005

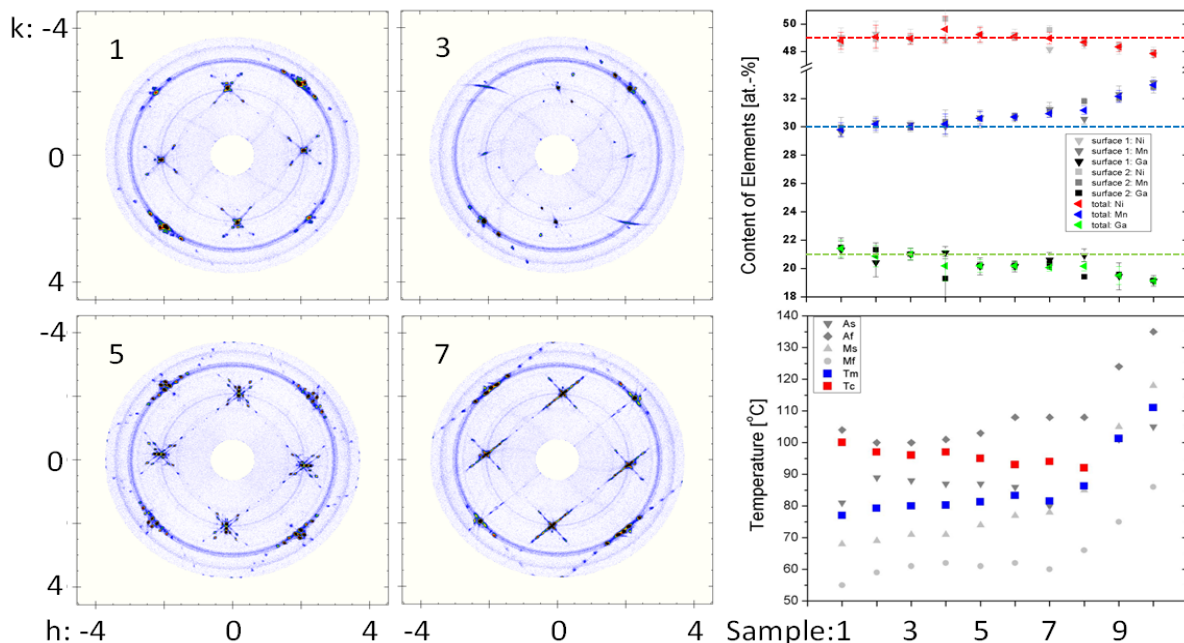


Figure 1: The left two columns show $hk0$ planes of samples of slice 1, 3, 5, and 7 of the same single crystal ingot, of which the composition (top, dashed lines indicate nominal composition of Ni₄₉Mn₃₀Ga₂₁) and phase transformation temperatures (bottom) are given in the right column. The numbers below the right column graphs indicate slices of the ingot corresponding to the $hk0$ plane diffractions. In the composition graph, the green triangles represent the Ga content, the blue ones the Mn content, and the red ones the Ni content. In the transformation/Curie temperature graph, the blue squares are indicating the martensite phase transformation temperature and the red square the Curie temperature.

 Neutrons	EXPERIMENTAL REPORT Field dependence of the magnetic structure of the multiferroic LiCu₂O₂	Proposal: PHY-01-2384 Instrument: E4 Local Contact: K. Prokes
	Principal Proposer: Tapan Chatterji, ILL – Grenoble, France Experimental Team: Tapan Chatterji; ILL – Grenoble, France	Date(s) of Experiment 28.10.2008 - 04.11.2008

Date of report: 17.12.2009

Introduction:

Ferroelectricity had been known to be mutually exclusive to magnetism, because, for example, in the class of transition metal oxides, to which most ferroelectrics belong, the nonzero d electrons, required for the presence of magnetic moments, tend to reduce the energy gain associated with ferroelectric distortion [1,2]. Therefore, only a limited number of compounds, the so-called multiferroics, exhibit the coexistence of magnetism and ferroelectricity. Multiferroics with enhanced cross-coupling effects exhibit magnetic order with broken centrosymmetry. It turns out that the lattice relaxation through exchange striction is associated with the magnetic orders with noncentrosymmetry is the origin of magnetism-induced ferroelectricity [3-6]. The exchange coupling between spins, where exchange striction is associated, is a tensorial quantity, and has symmetric parts as well as asymmetric parts. The symmetric part seems to be relevant to multiferroicity in RMn₂O₅ (R = rare-earth element) [7], and the antisymmetric parts, which constitute the Dzyoloshinskii-Moriya (DM) interaction, become active when ferroelectricity is induced by spiral-magnetic orders in systems such as RMnO₃, Ni₃V₂O₈, delafossite CuFeO₂, hexaferrite (Ba, Sr)₂Zn₂Fe₁₂O₂₂, spinel CoCr₂O₄ and MnWO₄.

Park et al. [8] reported recently the surprising discovery of ferroelectricity in the quantum $S = 1/2$ linear chain compound LiCu₂O₂ at temperature at which the spiral magnetic order sets in. Electric polarization (P) emerges along the c direction below the spiral magnetic order temperature, but changes from the c to the a axis when magnetic fields (H) are applied along the b direction. They also found that P_c increases with H_c, and P_a appears with H_a. These results are in contradiction with the proposed magnetic structure model in which the spiral plane is the a-b plane. Park et al. [8] proposed a different spiral structure in zero field consistent with the presence of a finite electric polarization (P) along the c axis. They also proposed the spiral spin structure in magnetic field H = 9 T.

Experimental results:

To resolve the above controversy, we did neutron diffraction experiment on LiCu₂O₂ at zero field and also under magnetic field up to 12 Tesla. Three single crystals of LiCu₂O₂ was oriented and tested on the two-axis diffractometer E2 of Berlin Neutron Scattering Centre. All these crystals were found to be twinned but the twinning in one of these crystals was small. We selected this crystal for further investigation and placed the crystal inside the 15 T vertical cryomagnet with the [001] axis of the crystal parallel to the ω -axis of the diffractometer. We measured the temperature dependence of the magnetic -0.5, 0.826,0 reflection at zero magnetic field H = 0 and also at H = 12 T

shown in Fig. 1 (top). We measured the field dependence of the -0.5, 0.826,0 reflection at T = 2 K as a function of applied magnetic field shown in Fig. 1 (bottom). We were disappointed to observe very weak field dependence of the magnetic field applied along the [001] axis as high as 12 T. We could not apply magnetic field along the b-axis with vertical cryomagnet, because in that case the b-axis of the crystal had to be mounted parallel to the ω -axis of the two-axis diffractometer. However this geometry does not allow one to measure any magnetic reflection in the horizontal scattering plane. The diffractometer D15 of the Institut Laue-Langevin with a tilting detector will enable one to measure magnetic reflections with magnetic field parallel to the b-axis of the crystal albeit in the magnetic field range of 0 - 6 T only.

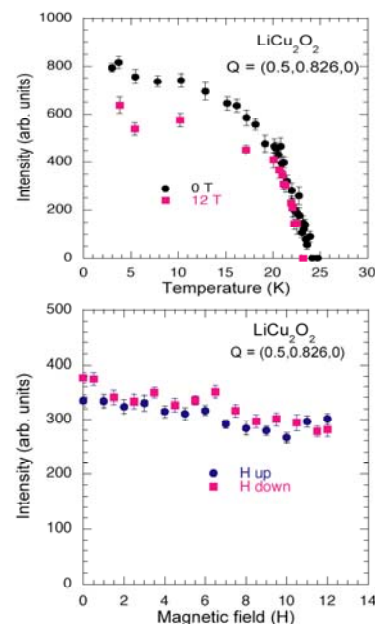


Fig. 1. – (Top) Temperature variation of the -0.5,0.826,0 reflection at H= 0 and 12 T. (Bottom) Magnetic field variation of the -0.5,0.826,0 reflection at T = 2 K.

References:

1. N.A. Hill, J. Phys. Chem. b **104**, 6694 (2000)
2. D.I. Khomskii, J. Mag. Magn. Mater. **306**, 1 (2006).
3. H. Katsura, N. Nagaosa and A.V. Balatsky, Phys. Rev. Lett. **95**, 057205 (2005).
4. I.A. Sergienko and E. Dagotto, Phys. Rev. B **73**, 094434 (2006).
5. M. Mostovoy, Phys. Rev. Lett. **96**, 067601 (2006).
6. A.B. Harris et al., Phys. Rev. B **73**, 184433 (2006).
7. P.G. Radaelli et al., Phys. Rev. Lett. **101**, 067205 (2008).
8. S. Park et al., Phys. Rev. Lett. **98**, 057601 (2007).

Acknowledgement: This research project has been supported by the European Commission under the 6th Framework Programme through the Key Action: Strengthening the European Research Infrastructures. Contract n°: RII3-CT-2003-505925 (NMI 3).

	EXPERIMENTAL REPORT Field dependence of the magnetic structure and the (H,T) phase diagram of TbMn₂O₅	Proposal: PHY-01-2383 Instrument: E4 Local Contact: K. Prokes
	Principal Proposer: Tapan Chatterji, ILL – Grenoble, France Experimental Team: Tapan Chatterji, ILL – Grenoble, France Gail N. Iles, ILL – Grenoble, France	Date(s) of Experiment 23.07.2008 - 02.08.2008

Date of report: 17.12.2009

There is a great deal of current interest in materials that exhibit interplay between electrical, magnetic and structural order parameters. In particular, the small group of materials known as magnetoelectric multiferroics, in which magnetism and ferroelectricity coexist and are mutually coupled, are being extensively investigated. These materials display phenomena such as the control of electrical polarization by the application of an external magnetic field, providing an additional degree of freedom for the design of new devices. Recent work on TbMnO₃ [1], TbMn₂O₅ [2] and isostructural compounds with other rare earths (*RE*) has suggested that systems with frustrated magnetic order may be good candidates in which to look for multiferroic properties. Several other systems, including Ni₃V₂O₈ (Kagomé staircase), CoCr₂O₄ (spinel) and CuFeO₂ (delafossite) have later been shown to display similar properties. All these systems are improper ferroelectrics, with the main order parameter being magnetic, and are characterized by magnetic lattices that are either frustrated or display strongly competing interactions, giving rise to complex magnetic structures, often evolving in intricate phase diagrams. Manganese oxides with the general formula *REMn₂O₅* (*R* = La, Y, Bi or rare-earth) simultaneously display long-range magnetic order and electrical polarisation at low temperature [3,4]. Although the magnitude of the polarisation (**P**) is 2 or 3 orders of magnitude smaller than in typical ferroelectrics, there is growing evidence that **P** is strongly coupled to the magnetic order. *REMn₂O₅* are insulators consisting of Mn⁴⁺O₆ octahedra and Mn³⁺O₅ pyramids linked through edge- and cornersharing networks. There are 5 nearest-neighbour magnetic interactions, giving rise to complex antiferromagnetic (AFM) order below 50 K.

According to initial work on these systems *REMn₂O₅* appears to have unique properties among known multiferroics. Whereas all other materials display some form of spiral magnetic structure (cycloidal, conical etc.) in the ferroelectric phase, *REMn₂O₅* orders either as a constant-moment, quasi-collinear AFM or as an incommensurate

SDW. The transition between the two phases, which unusually takes place on *cooling*, has a dramatic effect on the ferroelectric properties, whereby the polarization is strongly reduced and changes sign. This and most other observations can be explained within the framework of a simple, symmetric-exchange model, in which polarization is generated by superexchange striction that would be effective even in the presence of perfectly collinear spins [5-7]. This is in sharp contrast with *REMnO₃* and other materials, for which spin non-collinearity is purported to be a key ingredient not only to break inversion symmetry, but also to generate atomic displacements, e.g. through the inverse Dzyaloshinsky-Moriya effect [8,9]. If *REMn₂O₅* were indeed to prove the sole known representative of a “symmetric exchange” class of multiferroics, it would be natural to search for other compounds of this class, redirecting part of the research effort that is currently devoted to screen all known oxide spiral phases systematically. It is therefore of crucial importance that magnetic structures and the (H,T) phase diagram of the *REMn₂O₅* are established beyond doubt.

We investigated the magnetic structure and (H,T) phase diagram of TbMn₂O₅ by single crystal neutron diffraction on the two-axis single crystal diffractometer E4 of BENSCH. The TbMn₂O₅ single crystal with its b axis vertical was fixed to the sample stick of the 15 T vertical cryomagnet such that the magnetic field could be applied parallel to the b-axis of the single crystal. In order to construct the (H,T) phase diagram we measured the temperature and magnetic field dependence of a few nuclear and magnetic reflections. Fig. 1 shows the magnetic field dependence of (left) 001 nuclear and (right) the 002⁻ magnetic satellite reflection of TbMn₂O₅. We constructed the (H,T) phase diagram of TbMn₂O₅ which is shown in Fig. 2. Nothing drastically happens to the magnetic structure up to a field of 14.5 T.

However, the stability range of the commensurate ferroelectric phase increases and that of the two incommensurate phases decreases at higher magnetic field.

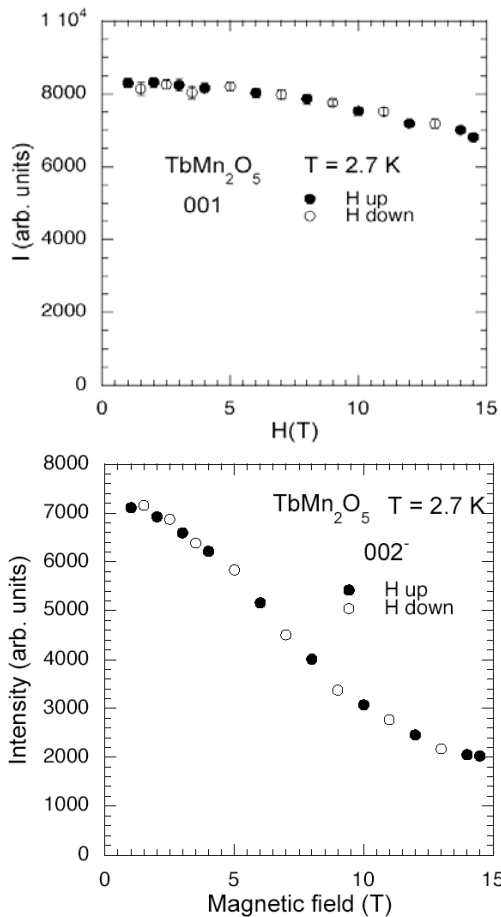


Fig. 1 - Magnetic field variation of (left) 001 nuclear and (right) the 002⁻ magnetic satellite reflection of TbMn₂O₅ at T = 2.7 K.

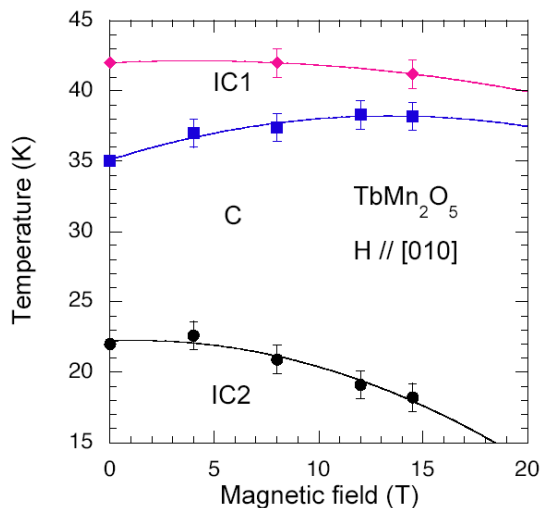


Fig. 2 – The (H,T) phase diagram of TbMn₂O₅ with magnetic field applied parallel to the b-axis.

References

1. T. Kimura et al, *Nature (London)* 426, 55 (2003)
2. H. Hur et al, *Nature (London)*, in press (2004)
3. I. Kagomiya et al, *Ferroelectrics* 280, 131 (2002)
4. A. Inomata et al, *J. Phys.: Condens. Matter* 8, 2673 (1996).
5. L. C. Chapon, G. R. Blake, M. J. Gutmann, et al., PRL 93, art. no. 177402 (2004).
6. G. R. Blake, L. C. Chapon, P. G. Radaelli, et al., PRB 71, art. no. 214402 (2005).
7. L. C. Chapon, P. G. Radaelli, G. R. Blake, et al., PRL 96, art. no. 097601 (2006).
8. I. A. Sergienko and E. Dagotto, PRB 73 (2006).
9. I. K. Sawada and N. Nagaosa, Phys. Rev. Lett. 95 (2005).

Acknowledgement:

This research project has been supported by the European Commission under the 6th Framework Programme through the Key Action: Strengthening the European Research Infrastructures.

Contract n°: RII3-CT-2003-505925 (NMI 3).

 Neutrons	EXPERIMENTAL REPORT	Proposal: PHY-01-2476
	Magnetic field dependence of the antiferromagnetism in CeBiPt	Instrument: E4 Local Contact: S. Matas
Principal Proposer: Experimental Team:	O. Stockert, Max-Planck-Institut CPfS Dresden O. Stockert, Max-Planck-Institut CPfS Dresden G. Goll, Karlsruhe Institute of Technology, Karlsruhe S. Matas, HZB	Date(s) of Experiment 03.04.2009 – 09.04.2009

Date of report: 19.12.2009

The equiatomic ternary RBiPt intermetallic compounds (R = rare-earth elements) crystallize in the cubic MgAgAs-type structure (space group $F\bar{4}3m$) and show a variety of low temperature properties ranging from semiconductor or semimetal-like behavior of NdBiPt to magnetism and heavy fermion-like behavior in YbBiPt with one of the highest measured specific heat coefficients $\gamma = C/T = 8 \text{ J/molK}^2$.

CeBiPt orders antiferromagnetically in an AF-type I structure with an ordered moment of $0.6 \mu_B$ below the Néel temperature $T_N = 1.15 \text{ K}$ as yielded by single crystal and powder neutron diffraction. Thermodynamic measurements show marked discrepancy in the critical magnetic fields needed to suppress antiferromagnetism. Therefore we performed a single crystal diffraction experiment on E4 in magnetic fields applied along $[0 0 1]$ and $[1 1 0]$ to measure the critical fields to suppress antiferromagnetic order, to map the (B, T) phase diagram and to study the origin of the finite magnetic domain sizes found previously.

In our measurements we focused on three magnetic peaks, namely $(1 1 2)$ for magnetic field along $[0 0 1]$, and $(1 1 0)$ and $(2 2 1)$ for fields along $[1 1 0]$. For magnetic fields along $[0 0 1]$ we found a continuous decrease of the magnetic intensity with field and the magnetic intensity vanishes around $B = 0.5 \text{ T}$. Surprisingly, a large hysteresis between increasing and decreasing magnetic field has been detected and the line width of the peaks seems to be become smaller in fields. This suggests an increase in the domain size of the magnetic domains with field which is inline with the difference in intensity for increasing and decreasing magnetic fields. Fig. 1 shows the results for magnetic fields along $[1 1 0]$. For this field direction the mag-

netic intensity vanishes at much higher fields of $B = 1 - 1.5 \text{ T}$, but displays a pronounced maximum around $B = 0.7 \text{ T}$ at lowest $T = 0.05 \text{ K}$ shifting to lower fields with increasing temperatures. In addition, the hysteretical behavior for sweeping the magnetic field up and down is strongest at $T = 0.05 \text{ K}$ becoming quite small at higher temperatures. The origin for this behavior is suggested to be caused by the different domain formation and population in magnetic fields. Currently the data are further analyzed.

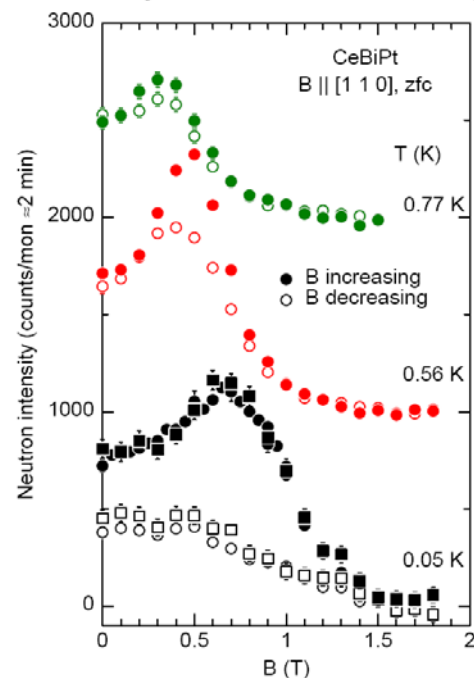


Fig. 1: Magnetic field dependence of the magnetic $(1 1 0)$ peak at different temperatures for fields applied along the $[1 1 0]$ direction after subtracting the paramagnetic intensity. The crystal was first cooled in zero magnetic field (zfc) from above T_N to the desired temperature and then the magnetic field was increased and decreased again (measured on E4 with $\lambda \approx 2.4 \text{ \AA}$, data for different T are shifted by 1000 counts with respect to each other).

 Neutrons	EXPERIMENTAL REPORT	Proposal: PHY-01-2480 Instrument: E4 Local Contact: K. Prokes
	Spin re-orientation transition in jarosite	Date(s) of Experiment 13.07.2009 - 21.07.2009
Principal Proposer: Experimental Team:	Kittiwit Matan, Univ. Tokyo, ISSP, JP Karel Prokes, Slavomir Matas, HZB Taku J. Sato, Univ. Tokyo, ISSP, JP Daniel Grohol, Young S. Lee, MIT Cambridge, USA	

Date of report: 05.01.2010

We performed elastic neutron scattering measurements at the spectrometer E4 in a high magnetic field on a single crystal sample of the kagome antiferromagnet $\text{KFe}_3(\text{OH})_6(\text{SO}_4)_2$ to study the H-T phase diagram. In this experiment, we measured the (1,1,0) magnetic Bragg intensity as a function of temperature at several fields between 5 T and 14.5 T. We mounted the sample inside the magnet VM1 such that the c-axis of the sample is along the vertical axis of the magnet. The DM interaction in this system causes the spins on each triangle in jarosite to form an umbrella-like structure and gives each kagome plane a net ferromagnetic moment. However, the interlayer coupling in iron jarosite causes the ferromagnetic moments to couple antiferromagnetically between layers in the absence of an applied field. In the applied field exceeding a critical field H_c , all spins on the previously oppositely canted layers rotate 180° resulting in the change in magnetic Bragg peaks from half integer, e.g. (1,1,3/2), to whole integer, e.g. (1,1,0), along the L direction. Our previous neutron scattering at BENSCH confirms this spin transition.

The results of this experiment are shown in Figures 1. Figure 1(a) shows scattering intensity of the (1,1,0) magnetic Bragg peak in the ferromagnetic state. The intensity drops sharply on the low temperature side, indicative of the transition between the antiferromagnetic to ferromagnetic state due to the 180° spin rotation. On the high temperature side, the transition becomes broad, implying a crossover behavior between the 3D magnetic ordered state and 2D short-range disordered state. Figure 1(b) shows a H-T phase diagram of jarosite. Black squares and red circles denotes the results from magnetization measurements of the critical field performed on a pulsed-field facility at Institute for Solid State Physics, The university of Tokyo and on PPMS, respectively. The contour map shows the intensity profile of the (1,1,0) Bragg intensity measured in this experiment. The agreement between these two sets of data confirms that the ferromagnetic transition observed in the magnetization measurements corresponds to the spin re-orientation caused by the 180° rotation of spins on an alternating plane.

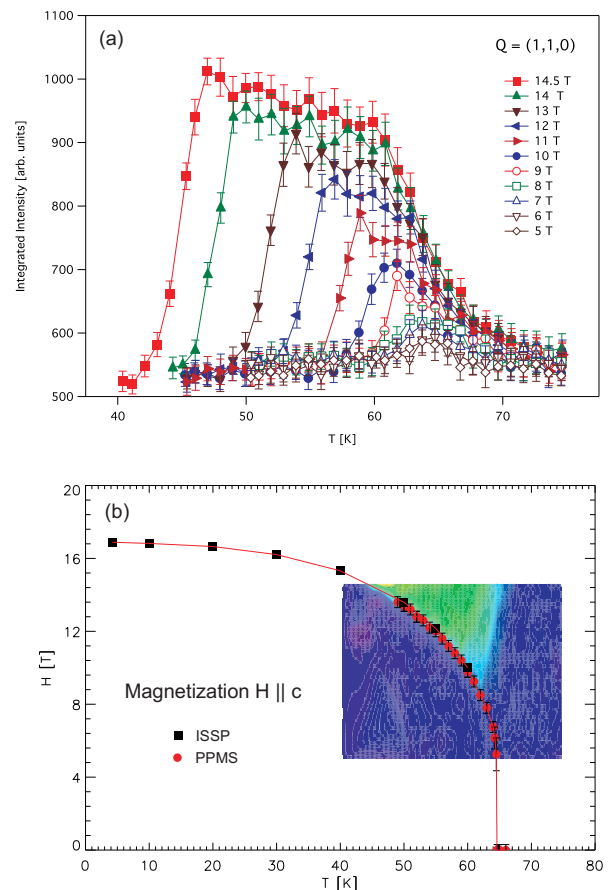


Figure 1 (a) shows scattering intensity measured at (1,1,0) at the base temperature and at several field. (b) shows a contour plot of the (1,1,0) intensity as a function of temperature and field overlaying the phase diagram. Green denotes high intensity and blue low intensity.

	EXPERIMENTAL REPORT	Proposal: PHY-01-2481
	Magnetic structure of pressure and field induced magnetically ordered phases in YbAgGe with a quasi-kagome lattice	Instrument: E4 Local Contact: K. Prokes
Principal Proposer: K. Umeo, Hiroshima University, JP Experimental Team: K. Prokes, HZB T. Onimaru, Hiroshima University, JP H. Kubo, Hiroshima University, JP T. Takabatake, Hiroshima University, JP	Date(s) of Experiment 05.08.2009 – 11.08.2009	

Date of report: 15.01.2010

The intermetallic compound YbAgGe, crystallising in the hexagonal ZrNiAl-type structure, is a candidate of the magnetically frustrated 4f-electron system. This compound undergoes two antiferromagnetic transitions at $T_{M1} = 0.8$ K and $T_{M2} = 0.65$ K. Applying pressures above $P^* = 1.6$ GPa, the magnetic entropy S_m at T_M rises continuously, whereas the Kondo temperature does not change. These facts strongly suggest that the magnetic structure changes above P^* by the release of the magnetic frustration. The aim of the present experiments was to detect the pressure-induced change of the magnetic structure by means of neutron diffraction.

A single crystal of YbAgGe of 2.8 mm in diameter and 3.9 mm in height was aligned so that the $a^* - c^*$ plane is the horizontal scattering plane. The sample was set in a piston cylinder-type cell with size of 14 mm in diameter and 50 mm in height, which was placed on the mixing chamber of a dilution refrigerator. The wave length of neutron beam was 2.45350 Å and the collimation was 40' - Open - S - 80' on E4.

We observed magnetic peaks characterized by the propagation vector $\mathbf{k}_1 = [1/3, 0, 1/3]$ at 0.7 GPa. Fig. 1 shows the profile scan of the magnetic Bragg peak at $\mathbf{Q} = (2/3, 0, 2/3)$ at 0.07 K and 0.7 GPa. In spite of large background scattering due to the pressure cell, a clear peak could be observed. The magnetic

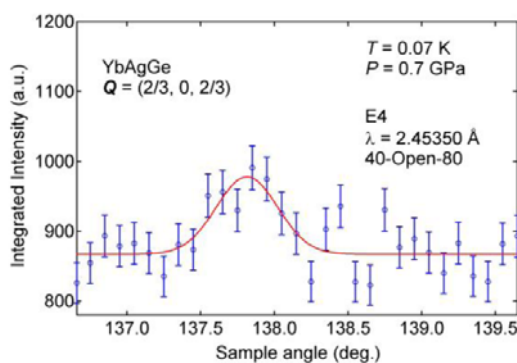


Fig. 1. Profile scan of the magnetic Bragg peak at $\mathbf{Q} = (2/3, 0, 2/3)$ at 0.07 K and 0.7 GPa. The solid curve indicates a fitting using the Gaussian function.

field dependence of the profile scans of the magnetic peak at $\mathbf{Q} = (2/3, 0, 2/3)$ are shown in Fig. 2. The peak at $(2/3, 0, 2/3)$ disappears above 2.0 T. These results are consistent with the $B - T$ phase diagram under pressure determined by our magnetoresistance and magnetization measurements.

We regret that we were unable to perform scheduled measurements due to the shutdown (about 40 hours) of the atomic reactor in the beam time. In the next time, we should observe the pressure-induced change of the magnetic structure above 1.6 GPa.

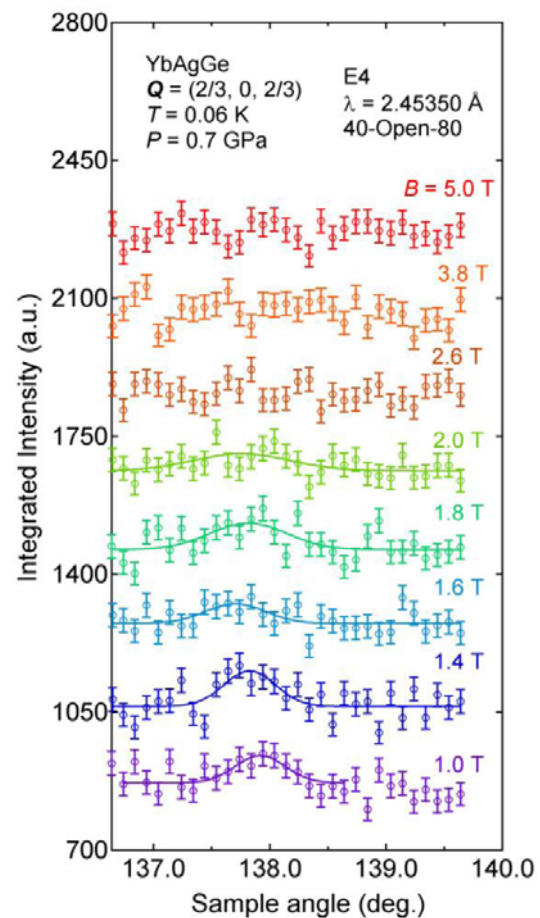


Fig. 2. Profile scans of the magnetic peak at $\mathbf{Q} = (2/3, 0, 2/3)$ at 0.06 K and 0.7 GPa in various magnetic fields up to 5 T. The solid curve show fitting with the Gaussian function.

**The neutron study of layered Ising magnet
KEr(MoO₄)₂**

Proposal: PHY-01-2556-EF

Instrument: **E4**

Local Contact:
K. Prokes/S. Mat'as

Principal Proposer: S. Mat'as, HZB
Experimental Team: A. Orendáčová, UPJŠ, Košice, Slovakia
K. Prokes, HZB
K. Kiefer, HZB
S. Gerischer, HZB

Date(s) of Experiment

17.12.2008 – 21.12.2008
19.06.2009 – 21.06.2009

Date of report: 17.12.2009

The KEr(MoO₄)₂ belongs to a family 2D compounds of double rare-earth molybdates MR(MoO₄)₂, where R- rare-earth, M- alkali metal. They crystallize in variety of layered structures, exhibit strong anisotropy and often are close to ideal 2D Ising system. The magnetic susceptibility measurements taken on KEr(MoO₄)₂ system show [1-4] the magnetic phase transition to an antiferromagnetic ordered state at about T_N = 0.9 K. A non-collinear magnetic structure (6AF-12, ref. [1,2]) with magnetic moments lying in the ac-plane having an angle about ±9 degree with [001] direction has been suggested by Anders et al. [1,2] in zero field.

Experiment: The experiment was carried out at E4 diffractometer at wavelength λ = 2.43 Å. The following experimental set up has been chosen: PG filter - 40' collimation - sample - open-2D detector. A vertical magnet VM2 together with the low temperature dilution insert LT-DS1 were used to reach desired fields ≤ 6 T and temperatures < 100 mK. The single crystal KEr(MoO₄)₂ with room temperature lattice cell parameters a = 5.063 Å, b = 18.25 Å, c = 7.917 Å and size of 12 mm x 0.67 x 12 mm mm was mounted so that the reflections in the a*-b* scattering plane were accessible, a vertical external magnetic field was applied parallel to the c*-axis.

Results: We have explored the contribution to the scattering at temperatures 70 mK and 1.8K well below and above the magnetic transition temperature. The zero field magnetic structure (6AF-12) [1,2] imposes an appearance of additional magnetic reflections described by τ = (½, ½, 0). However, we did not find any magnetic contribution at any of following positions (1.5, 1.5, 0), (1.5, -1.5, 0), (0.5, k, 0), k = 0.5, 1.5, 2.5, 3.5 and 4.5. The critical field of KEr(MoO₄)₂ system is of the order of ~100 mT. One can only speculate that possibly due to a high remanent field of the VM2 magnet the

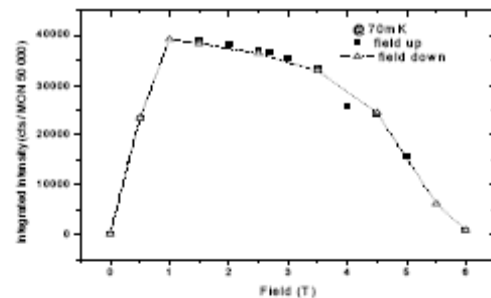


Fig. 1 : The field dependence at forbidden nuclear reflection (030) and temperature 70 mK, the line is guide to the eye.

zero field phase did not fully developed. Contrary to that, the magnetic contributions have been identified at several forbidden nuclear reflection positions as (030), (050), (070), (090) and on top of allowed nuclear reflections. This would correspond to the magnetic phase assigned by Anders et al. as "1FM-1 phase" [2]. In Fig.1 is shown the field dependence for the forbidden reflection (030) at 70 mK. Integrated intensity for (030) reflection approaches quickly maximum and for higher magnetic fields again decreases (H > 3.5 T). The measured data are under analysis. Appropriate model of magnetic structure is to be refined taking into account all known experimental facts. In fact, the experiment without magnet for the a*-b* crystal orientation and also the experiment for a*-c* crystal orientation at 70 mK temperature is highly desired.

References

- [1] A.G. Anders et al. Low Temp. Phys. 20 (2) 1994,105
- [2] A.G. Anders et al. Low Temp. Phys. 20 (2) 1994,137
- [3] E.N. Khatsko et al, Low Temperature Physics, vol.30 No.2 (2004) 133
- [4] E.N. Khatsko et al, Low Temperature Physics, vol.19 No.11 (1993) 1217-1222

Acknowledgement:

S.M. and A.O. would like to thank A.G. Anders for providing the single crystal for the neutron scattering experiment.

Principal Proposer: K. Prokes, HZB
Experimental Team: D. Argyriou, HZB
S. Kimber, HZB
A. Kreyssig, Iowa State University & Ames Labs, USA
A. Goldman, Iowa State University & Ames Labs, USA

Date(s) of Experiment
15.06.2009 – 18.06.2009
01.07.2009 – 07.07.2009

Date of report: 19.01.2010

The observation of pressure-induced superconductivity in AF₂As₂ (A=Ca, Ba or Sr) [1-2] has opened an exciting new avenue for investigations of the relationship among magnetism, superconductivity, and lattice instabilities. Superconductivity is reported to appear either at a critical doping or above some critical hydrostatic pressure which is in the CaFe₂As₂ about 0.4 GPa. This pressure corresponds to a structural transition from low-temperature orthorhombic phase (O) (that is antiferromagnetic in contrast to a so called collapsed tetragonal (cT) phase because of much smaller c axis parameter.

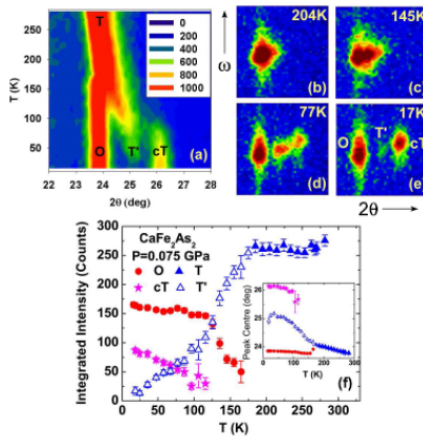


Fig. 1: Color map (counts per monitor are color-coded in the inset) showing the temperature dependence of a portion of the diffraction pattern taken on the E4 diffractometer within the range of various structural (002) reflections of CaFe₂As₂. (b)-(e) 2θ - μ -1 plots at selected temperatures showing the angular distribution of peaks tracked in (a). Panel (f) shows the temperature dependence of the integrated intensities and positions of reflections shown in panels (a)-(e).

Recently, high-pressure susceptibility and transport studies on CaFe₂As₂, using helium as the pressure medium have been performed suggesting that no signature of bulk superconductivity was found under strictly hydrostatic conditions in this material. [4]. For uniaxial pressure it was expected that CaFe₂As₂ should develop very quickly the cT phase that should be superconducting. However, we have observed on E4 using 2.4 Å wavelength that

the high-temperature tetragonal phase is stabilized (Fig. 1). In situ electrical resistance measurements showed also that this phase is hosting the superconductivity (Fig. 2) [5].

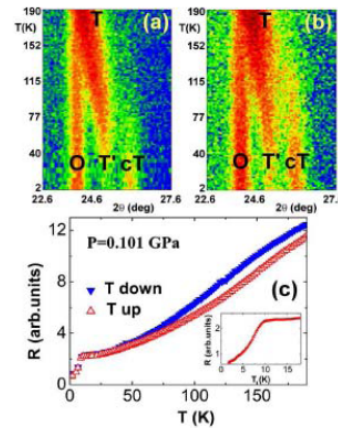


Fig.2: Color map showing the temperature dependence of a portion of the diffraction pattern taken at E4 in that covers various structural (002) reflections of CaFe₂As₂ under uniaxial pressure of 0.101 GPa along the c axis measured with (a) decreasing and (b) increasing temperature. The simultaneously measured electrical resistance is shown in panel (c). The inset to (c) shows the low-temperature detail of the electrical resistance data taken upon heating.

However, we have been able to cover only the beginning of the „superconducting bubble“. In order to map the development of the superconducting transition temperature as the function of the applied pressure, smaller sample crosssections (leading to necessity for larger diffraction counting times) are needed (currently being performed).

[1] M. S. Torikachvili et al., Phys. Rev. Lett. **101**, 057006 (2008).
[2] P. Alireza et al. [arXiv:0807.1896](https://arxiv.org/abs/0807.1896).
[3] A. I. Goldman et al. Phys. Rev. B **79**, 024513 (2009)
[4] W. Yu, A. A. Aczel, T. J. Williams, S. L. Bud'ko, N. Ni, P. C. Canfield, and G. M. Luke Phys. Rev. B **79**, 020511 (R) (2009).
[5] K. Prokes et al., submitted to Phys. Rev. Lett.

Principal Proposer: Diana Lucia Quintero Castro, HZB
Experimental Team: Bella Lake, HZB
Manfred Reehuis, HZB
Nazmul Islam, HZB

Date(s) of Experiment
29.09.2009 – 04.10.2009
10.11.2009 – 16.11.2009
18.08.2009 – 20.08.2009

Date of report: 02.12.2009

SrYb₂O₄ is a frustrated, low dimensional antiferromagnet. The magnetic Yb³⁺ ions have angular momentum $S=1/2$, $L=3$ and $J=7/2$ and form sub-lattices of double chains running parallel to the crystallographic c -axis. There are two inequivalent although highly similar chains due to the two inequivalent Yb³⁺ ions per unit cell. These chains suggest the presence of frustrated first and second neighbour magnetic interactions. Moreover the coupling between the chains is also frustrated and the Yb³⁺ ions form a hexagonal structure around the Sr ions.

Powder and single crystal neutron diffraction measurements have been performed on three different diffractometers at HZB in order to determine the crystal and magnetic structure of the compound. The compound orders antiferromagnetically at a temperature of 0.9 K according to heat capacity measurements (see inset figure 2). For all the diffraction experiments we have used a dilution stick to reach temperatures below and above this phase transition.

For the experiment on E6 we have used an initial wavelength of 2.4 Å and the sample mass was 12 g. For this experiment we used an aluminium sample container, which consisted in a cylindrical shell of 2 mm thickness. The container was filled with the powder sample, sealed under a He4 atmosphere and filled with He3 to ensure the thermal conductivity. The container was design for inelastic neutron scattering and not for diffraction therefore the Bragg peaks were wider and the resolution was not as good as expected. We took patterns at 40 mK, 200 mK, 400 mK, 600 mK, 800 mK and 1000 mK.

On E9 we have used a cylindrical Cu sample can and this was fill with the powder sample and a mixture of deuterated ethanol and methanol to ensure the thermal contact. Unfortunately, the diffraction pattern show a bump of incoherent scattering around 2 \AA^{-1} due to the alcohol mixture as is showed on the inset in figure 1. The data were collected at two temperatures 0.03 K and 10 K.

For the single crystal neutron diffraction experiment on E4 we have used a initial wavelength of 2.43 Å and we have measured in two scattering planes (OKL) and (HK0). The single crystal was a cylinder of mass 3.2 g mounted in a copper holder. We measured a total 82 reflections and we followed the temperature dependence of the intensity on 4 reflections as showed in figure 2.

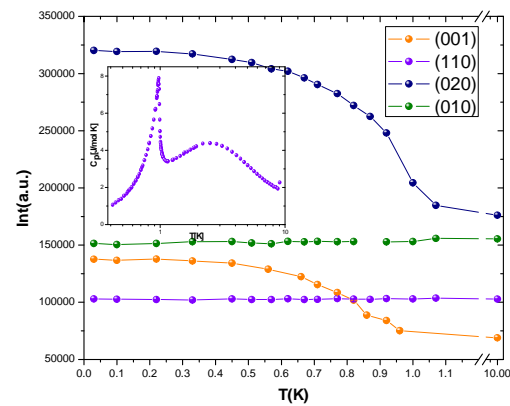


Fig 2. Temperature dependence of the intensity of four reflections measured in E4. Two of them are pure nuclear reflections (110) and (010). And the other two have magnetic and nuclear component, showing a transition around 0.9 K in agreement with the heat capacity measurement (inset).

The results proved that antiferromagnetic order occurs below 0.9 K with ordering wavevector $\mathbf{k}=0$. Both Yb ions order, this differs from the magnetic structure of the isostructural compound SrEr₂O₄ where the two Er sites are inequivalent [1]. On the single crystal experiment we found intensity on some reflections forbidden for the space group, this suggests a crystal distortion. The data analysis is in progress.

Reference:

[1] O. A. Petrenko et al . Phys. Rev. B **78**, 184410 (2008).

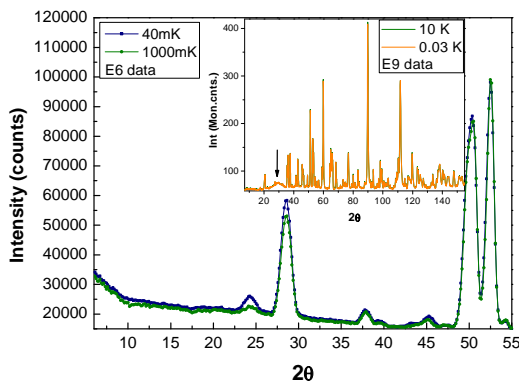


Fig 1. Diffraction patterns acquired in E6 (main figure) and E9 (inset). The main figure shows the low 2theta patterns for the lowest and higher temperature.

 Neutrons	EXPERIMENTAL REPORT The neutron response of layered Ising magnet $\text{Ker}(\text{MoO}_4)_2$	Proposal: PHY-01-2610-EF Instrument: E4 Local Contact: K. Prokes
	Principal Proposer: S. Mat'as, HZB Experimental Team: A. Orendáčová, UPJŠ Košice, Slovakia K. Prokes, HZB K. Kiefer, HZB S. Gerischer, HZB	Date(s) of Experiment 27.10.2009 – 01.11.2009

Date of report: 17.12.2009

Double rare – earth molybdates $\text{MR}(\text{MoO}_4)_2$ (R- rare-earth , M- alkali metal) crystallize in a large variety of layered structures. Some species of this group are close to ideal 2D Ising system, however, there are also exceptions. The single crystal $\text{KEr}(\text{MoO}_4)_2$ is very anisotropic and undergoes a Jahn – Teller (JT) phase transition ~ 0.95 K on cooling in zero magnetic field. The JT phase transition, however, can be induced above T_N by applying moderate external magnetic field [1-4].

Experiment: The experiment was carried out at E4 instrument (BERII reactor) at wavelength $\lambda = 2.43$ Å. The following experimental set up has been chosen: *PG filter - 40' collimation sample-open-2D detector*. A vertical magnet VM2 together with the low temperature dilution insert *LT-DS1* were used to reach desired fields ≤ 6 T and temperatures < 100 mK. The single crystal $\text{KEr}(\text{MoO}_4)_2$ with room temperature lattice cell parameters $a = 5.063$ Å, $b = 18.25$ Å, $c = 7.917$ Å and size of 12 mm x 0.67 x 12 mm was mounted so that the reflections in the (b^*c^*) scattering plane were accessible, a vertical external magnetic field was applied parallel to the a^* -axis. In addition we measured crystal for the other orientation e.g. reflections in the (a^*c^*) scattering plane were accessible.

Results: In a zero magnetic field and at low temperature, well below T_N , an ordered state is manifested by additional scattered signal at forbidden nuclear reflection positions of the (0K0) $K=\text{odd}$ type. Our magnetic model with wave vector $k=(0,0,0)$ proposes the magnetic moments alignment according the symmetry mode $\tau_4: A_x C_z (+ - - +)_x (+ + - -)_z$ [5] where only magnetic moments at the erbium atom positions are assumed: (0, y, 0.25), (0, 1-y, 0.75), (0.5, 0.5-y, 0.75), (0.5, 1+y, 0.25), $y = 0.008$. This model, however, describes the magnetic structure only qualitatively. The additional signal at (030) reflection appears not only at the low temperature in zero field, but also above the

transition temperature when the moderate

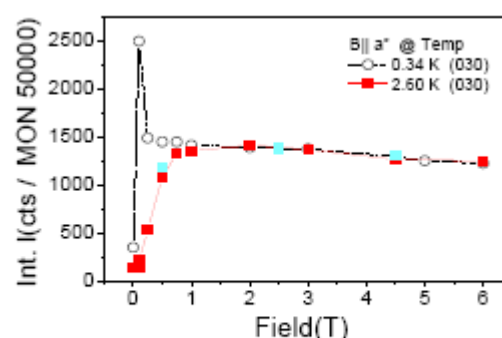


Fig. 1 Integrated intensity at (030) forbidden nuclear reflection for magnetic field $B||a^*$.

magnetic field is applied There are still several issues to be answered:

- first of all, what is the origin of observed (0K0) reflections. Is the origin magnetic, structural or contains both components?

This can not be answered on the basis of our non-polarized neutron data, the polarisation analyses or synchrotron experiment can well separate charge and magnetic contributions

- second, can molybdenum atom in the environment of oxygen atoms possess a magnetic moment or is non-magnetic?

We believe that the resonant X-ray experiment if combined with polarized neutron diffraction on E4 at low temperatures and in magnetic fields, should be able to give decisive insights into the interplay between structural and magnetic degrees of freedom of $\text{KEr}(\text{MoO}_4)_2$.

References:

- [1] A.G. Anders et al. *Low Temp. Phys.* 20 (2) 1994,105
- [2] A.G. Anders et al. *Low Temp. Phys.* 20 (2) 1994,137
- [3] E.N. Khatsko et al, *Low Temperature Physics*, vol.30 No.2 (2004) 133
- [4] E.N. Khatsko et al, *Low Temp. Physics*, vol.19 No.11 (1993) 1217-1222
- [5] Sikora W., Białas F. and Pytlík L. 2004 *Journal of Applied Crystallography*, **37** 1015

 Neutrons	EXPERIMENTAL REPORT Magnetic phase transitions and magnetic ordering in ErVO₃	Proposal: PHY-01-2646 Instrument: E5 Local Contact: M. Reehuis
	Principal Proposer: Experimental Team:	C. Ulrich, B. Keimer, MPI Stuttgart M. Reehuis, HZB S. Miyasaka, J. Fujioka, Y. Tokura – Department of Applied Physics, University of Tokyo, Japan M. Reehuis, HZB

Date of report: 11.01.2010

In the last years we have started to investigate intensively the structural and magnetic properties of vanadates RVO_3 ($R = Y$ or rare-earth element) [1-4]. These compounds exhibit many exciting properties, which can be related to orbital or spin rearrangements. A phase transition from an orthorhombic to a monoclinic structure sets in at T_{S1} . Below T_N , in the monoclinic phase, the vanadium moments show antiferromagnetic ordering with the modes C_x , C_y and G_z , where the z -component is the weakest [2, 3]. Some of the vanadates exhibit an additional structural phase transition at T_{S2} , which sets in well below T_N . This transition can only be observed for the vanadates with smaller R^{3+} -ions ($R^{3+} = Y^{3+}, Dy^{3+} - Lu^{3+}$) [3]. Here the crystal structure changes again to the orthorhombic structure, in which the vanadium moments are purely G -type ordered along the z -direction [1-3].

In the present study we have investigated the magnetic phase transitions of $ErVO_3$. A single-crystal neutron diffraction study of this vanadate has been performed on the instrument E5 (PG-monochromator: $\lambda = 2.38$ Å). The used cylindrical single-domain crystal of $ErVO_3$ with the dimensions of $d = 3$ mm and $h = 5$ mm was grown by the floating zone technique [1]. In order to observe magnetic phase transitions we have measured the T -dependence of prominent magnetic reflections. In Fig. 1 it can be seen that magnetic intensity appears at the Néel temperature $T_N = 112(1)$ K. This value is similar to $T_N = 110(1)$ K obtained earlier from specific heat measurements [1]. On the other hand the second structural phase transition (55 K $< T_{S2} < 61$ K) of $ErVO_3$ sets in at much lower temperature than in YVO_3 (73.7 K $< T_{S2} < 76.2$ K). A much stronger reduction of T_{S2} could be observed recently in $HoVO_3$ (23.5 K $< T_{S2} < 35.5$ K) [5]. Further it can be seen that a reduction of T_{S2} leads to stronger hysteresis effects. These effects can be ascribed to strong exchange interactions between the ordered V-moments and the paramagnetic Ho^{3+} - and Er^{3+} -ions. In the case of YVO_3 these interactions are negligible, since Y^{3+} is diamagnetic.

The presence of the reflections 100 and 010 clearly suggests the C -type ordering of the V-moments in the ab -plane. At 57 K the moments reach the values $\mu_x = 0.69(3)$ μ_B and $\mu_y = 1.55(3)$ μ_B , respectively. A similar value $\mu_x = 0.79(3)$ μ_B could be found for the x -component in YVO_3 . On the other hand the y -component $\mu_y = 1.21(3)$ μ_B of the yttrium compound was found to be slightly smaller. This can be ascribed to the fact that the Er-moments are slightly polarized by the ordered V-sublattice. For both YVO_3 and $ErVO_3$ weak magnetic intensities appear at T_N at the position of the reflection 011, suggesting the

presence of a G_z -component. It is interesting to see that the magnetic intensity is decreasing again at lower temperatures. At about 85 K the moments reach the maximum values $\mu_z = 0.19(3)$ μ_B (YVO_3) and $\mu_y = 0.15(3)$ μ_B ($ErVO_3$), respectively. Below T_{S2} the magnetic intensity of the 011 decreases spontaneously (Fig. 1). In the pure G -type phase the V-atoms reach a moment value $\mu_z = 1.47(3)$ μ_B . This value is very similar to $\mu_z = 1.49(3)$ μ_B obtained for YVO_3 .

The onset of long-range magnetic ordering of the Er-sublattice in $ErVO_3$ could not be observed down to 6 K. It is interesting to see that magnetic ordering of the R^{3+} -ions in $DyVO_3$ and $HoVO_3$ sets in at the relatively high temperatures 23 K and 36 K, respectively.

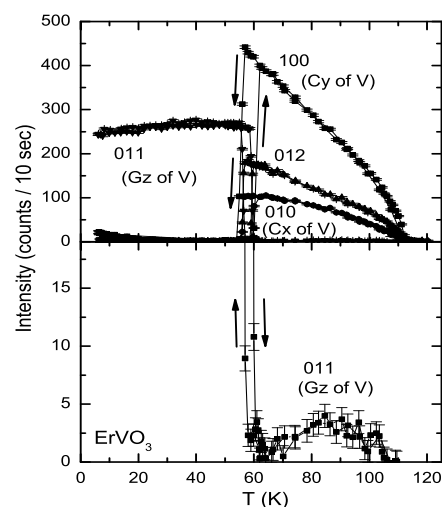


Fig 1. T -dependence of the magnetic intensity of the Bragg reflections 100, 010, 011 and 012 of $ErVO_3$.

References

- [1] S. Miyasaka, Y. Okimoto, M. Iwama, Y. Tokura, Phys. Rev. B **68**, 100406(R) (2003).
- [2] C. Ulrich, G. Khaliullin, J. Sirker, M. Reehuis, M. Ohl, S. Miyasaka, Y. Tokura, B. Keimer, Phys. Rev. Lett. **91**, 257202 (2003).
- [3] M. Reehuis, C. Ulrich, P. Pattison, B. Ouladdiaf, M.C. Rheinstädter, M. Ohl, L.P. Regnault, S. Miyasaka, Y. Tokura, B. Keimer, Phys. Rev. B **73**, 094440 (2006).
- [4] M. Reehuis, C. Ulrich, P. Pattison, S. Miyasaka, Y. Tokura, B. Keimer, Eur. Phys. J. B **64** (2008) 27.
- [5] M. Reehuis, C. Ulrich, K. Prokeš, J. Fujioka, S. Miyasaka, Y. Tokura, B. Keimer, in preparation.

 Neutrons	EXPERIMENTAL REPORT	Proposal: PHY-01-2647-EF
	Structural and magnetic transitions in $\text{Pr}_{0.80}\text{Ca}_{0.20}\text{VO}_3$	Instrument: E5 Local Contact: M. Reehuis
Principal Proposer:	C. Ulrich, B. Keimer – MPI Stuttgart M. Reehuis – HZB	Date(s) of Experiment
Experimental Team:	J. Fujioka, S. Miyasaka, Y. Tokura – Department of Applied Physics, University of Tokyo, Japan M. Reehuis – Helmholtz-Zentrum Berlin	17.05.2009 – 24.05.2009 03.08.2009 – 09.08.2009

Date of report: 07.01.2010

Recently we have started to investigate the structural and magnetic properties of PrVO_3 and the Ca-doped vanadate $\text{Pr}_{0.90}\text{Ca}_{0.10}\text{VO}_3$ [1]. It could be seen that the crystal and magnetic structures of these compounds are very similar to those observed earlier for CeVO_3 [2]. In the low-temperature monoclinic phase the magnetic moments of the V^{3+} -ions were found to be purely C-type ordered in the ab -plane. Antiferromagnetic interactions between magnetic moments of the vanadium and lanthanide ions induce a progressive magnetic polarization of the lanthanide sublattice at lower temperature, resulting in a ferrimagnetic structure.

In the present single-crystal neutron diffraction study, carried out on the instrument E5 ($\lambda = 2.38 \text{ \AA}$, PG-monochromator), we have studied the higher-doped vanadates $\text{Pr}_{1-x}\text{Ca}_x\text{VO}_3$ with $x = 0.80$ and $x = 0.70$, respectively. For $\text{Pr}_{0.80}\text{Ca}_{0.20}\text{VO}_3$ it can be seen in Fig. 1, that magnetic intensity appears at the Néel temperature $T_N = 117 \text{ K}$ at the position of the reflection 100. A spontaneous change of intensity could be observed for the strong nuclear reflection 022 at the structural phase transition temperature $T_S = 108 \text{ K}$. These transitions have been observed at considerably lower temperatures than for PrVO_3 ($T_S = 180 \text{ K}$, $T_N = 140 \text{ K}$) and $\text{Pr}_{0.80}\text{Ca}_{0.20}\text{VO}_3$ ($T_S = 135 \text{ K}$, $T_N = 117 \text{ K}$), respectively. For the higher-doped vanadate $\text{Pr}_{0.70}\text{Ca}_{0.30}\text{VO}_3$ not any phase transitions could be detected.

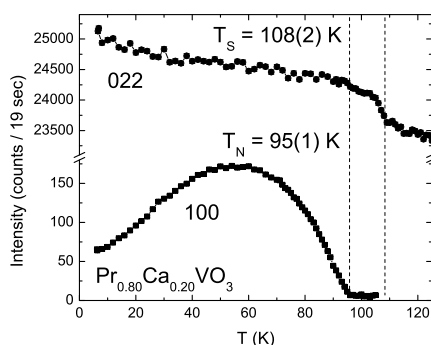


Fig 1. T -dependence of the magnetic intensities of the nuclear and magnetic reflections 022 and 100 of $\text{Pr}_{0.80}\text{Ca}_{0.20}\text{VO}_3$.

From the refinements of the magnetic structures we were able to determine the components of the magnetic moments of both the Pr- and the V-atoms. These magnetic moments could be deduced from the magnetic intensities of the reflections 100, 010, 012, 102, 200, 020 and 110. The obtained T -dependence of the magnetic moments, shown in Fig. 2, is similar to that observed for

$\text{Pr}_{0.90}\text{Ca}_{0.10}\text{VO}_3$ [1]. Therefore an increasing Ca-doping level does not result in a discernible change of the magnetic ordering parameters of both the V^{3+} - and the Pr^{3+} -ions. But on the other hand the transition temperatures T_S and T_N show a strong reduction. We found that the magnetic moments of the V-atoms are aligned predominantly along the b -axis, reaching a moment $\mu_y = 0.83(3) \mu_B$. The moment along the a -axis is $\mu_x = 0.22(3) \mu_B$ and the total moment is $\mu_{\text{exp}} = 0.86(3) \mu_B$. This moment is significantly smaller than $\mu_{\text{exp}} = 1.17(3) \mu_B$ found for $\text{Pr}_{0.90}\text{Ca}_{0.10}\text{VO}_3$. This shows that the V-moments also show a reduction with increasing Ca-doping.

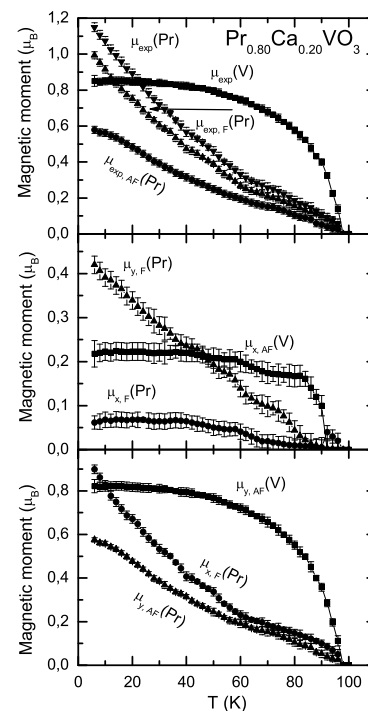


Fig 2. T -dependence of the magnetic moments of the V-atoms in $\text{Pr}_{0.80}\text{Ca}_{0.20}\text{VO}_3$. The C_y -component of the vanadium induces a ferrimagnetic order of the Pr-moments with the modes C_y and F_x ; accordingly the C_x -component of the vanadium induces a ferrimagnetic order of the Pr-moments with the modes C_x and F_y .

References

- [1] C. Ulrich, B. Keimer, J. Fujioka, S. Miyasaka, Y. Tokura, M. Reehuis, Eur. Phys. BENSX Exp. Report 2008, p 53 and p. 54.
- [2] M. Reehuis, C. Ulrich, P. Pattison, M. Miyasaka, Y. Tokura, B. Keimer, Eur. Phys. J. B. **64** (2008) 27.

	EXPERIMENTAL REPORT	Proposal: PHY-01-2564-EF
	Low temperature crystal structure and magnetic structure of MgV₂O₄	Instrument: E5 Local Contact: M. Reehuis
Principal Proposer: E. Wheeler, HZB Experimental Team: M. Reehuis, HZB E. Wheeler, HZB B. Lake, TU Berlin and HZB N. Islam, HZB		Date(s) of Experiment 18.03.2009 – 31.03.2009

Date of report: 13.01.2010

At room temperature cubic MgV₂O₄ crystallizes in the space group $F\bar{4}3m$ [1], which is a close to the typical spinel structure with the space group $Fd\bar{3}m$. This compound shows a structural phase transition to a lower symmetry tetragonal phase at 64 K [2]. The V³⁺-ions form a corner-sharing tetrahedral network and are octahedrally coordinated by six oxygen ions. Tetrahedral networks of localized spins with antiferromagnetic couplings are governed by strong geometrical frustration and can reveal fascinating ground states. At $T_N = 42$ K MgV₂O₄ undergoes a second transition to a magnetically ordered state [2]. In this work we continued our investigations of the low temperature crystal structure and magnetic ordering of the V-sublattice.

Single crystals of MgV₂O₄ were mounted on the four-circle diffractometer E5. We used a small aluminium pressure cell (uniaxial pressure along 001) to have a single-domain sample in the low temperature tetragonal phase. We set up the instrument with a Cu-monochromator selecting the neutron wavelength $\lambda = 0.89$ Å.

Low-temperature tetragonal phase

A data set of MgV₂O₄ was collected at 6K, well below the structural phase transition, with a total of 1328 (295 unique) reflections. Structural refinements were carried out in the space group $I\bar{4}m2$. In this space group the two different Mg1 and Mg2 atoms are located at the Wyckoff positions $2a$ (0,0,0) and $2c$ (0,1/2,1/4); the V-, O1- and O2-atoms at the position $8i$ (x,0,z). The refinement of the overall scale factor and the positional and anisotropic thermal parameters resulted in the very satisfactory residuals $R_F = 0.047$ ($R_w = 0.042$). The results of the refinements are presented in Table 1.

Magnetically ordered phase

We had established from powdered neutron diffraction that the ordering wave vector was $\mathbf{k} = (0,0,1)$ [3]. Measuring a multi-domain sample at low temperature enabled us to identify the magnetic moment direction. Because we had a single-domain crystal, we were able to observe strong magnetic intensities on the positions of the magnetic reflections 100 and 010. The data analysis showed that the V-spins are predominantly aligned parallel to the c-axis, with a moment value $\mu_z = 0.47(1) \mu_B$. But it was interesting to see that the 001-reflection (also a structural absence) carried a weak magnetic intensity, resulting in a moment value $\mu_{x(y)} = 0.065(3) \mu_B$. Therefore V-moments show a small tilt from the c-axis of 8(1) deg. The magnetic structure is sketched in Fig. 1.

Table 1

Results of the single-crystal neutron diffraction study of MgV₂O₄ at 6 K.

MgV ₂ O ₄ at 6 K	
a [Å]	5.9857(7)
c [Å]	8.4020(1)
V [Å ³]	301.03(8)
O1(x,y,z)	0.2743(2), ½, 0.1164(2)
O2(x,y,z)	0.2649(2), 0, 0.1374(2)
V(x,y,z)	0, 0.242(4), 0.622(3)
d(Mg1-O2)	1.961(1) x 4
d(Mg2-O1)	1.989(1) x 4
d(V-O1)	1.982(17) x 2 and 2.005(30)
d(V-O2)	2.092(17) x 2 and 2.027(30)
O1-V-O1	85.9(9) 86.6(9) x 2
O1-V-O2	94.73(6) x 2 95(1) x 2 94(1) x 2
O2-V-O2	84.5(8) 83.6(9) x 2

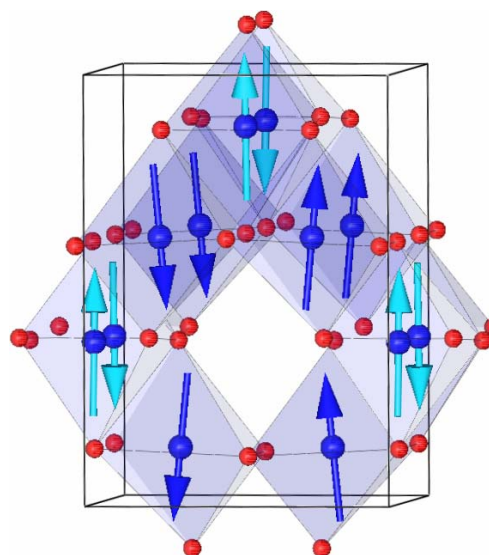


Fig. 1. Crystal and magnetic structure of MgV₂O₄. Blue balls indicate vanadium ions, red balls indicate oxygen ions. The Mg-ions are not shown to simplify the picture. Light/dark blue spins indicate perpendicular chains.

References

- [1] B. Lake, E. Wheeler, N. Islam, M. Reehuis, BENSIC Exp. Report 2008, p. 116. PHY-01-2291-EF
- [2] B. Lake, E. Wheeler, N. Islam, M. Reehuis, H.J. Bleif, BENSIC Exp. Report 2008, p. 117. PHY-01-2291-EF
- [3] B. Lake, E. Wheeler, N. Islam, M. Reehuis, BENSIC Exp. Report 2008, p. 77. PHY-01

 Neutrons	EXPERIMENTAL REPORT	Proposal: PHY-01-2514
	Magnetic and crystal structure of Er₅Ni₂In₄	Instrument: E6 Local Contact: A. Arulraj
Principal Proposer: Experimental Team:	Ł. Gondek, AGH-UST, Krakow, Poland J. Czub, Jagiellonian University, Poland A. Arulraj, HZB	Date(s) of Experiment 30.03.2009 – 02.04.2009

Date of report: 01.01.2010

Er₅Ni₂In₄ sample belongs to a very novel family of compounds crystallizing within the orthorhombic crystal unit cell (Space group *Pbam*) with following lattice constants (XRD at 300K): $a = 17.7138\text{\AA}$; $b = 7.8587\text{\AA}$ and $c = 3.5560\text{\AA}$. The synthesized sample was of a very good quality, it exhibits no impurities. From magnetometric studies it turned out, that the sample orders at temperature of roughly 20 K (see figure 1).

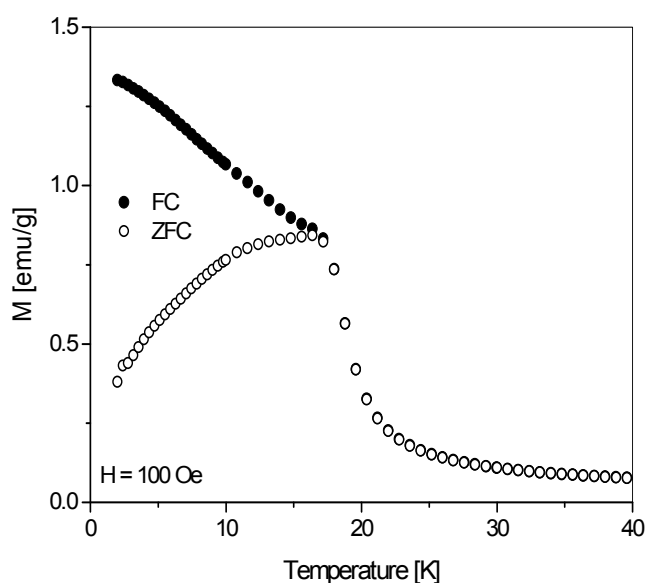


Fig. 1 ZFC and FC magnetization versus temperature for Er₅Ni₂In₄.

In this sample there are three different Er positions, thus the expected magnetic structure might be extremely complex. Neutron diffraction experiments were carried to approach determining of the magnetic structure. The data were collected at several temperatures between 1.5 – 24 K. The corresponding neutron diffraction patterns are presented in the figure 2.

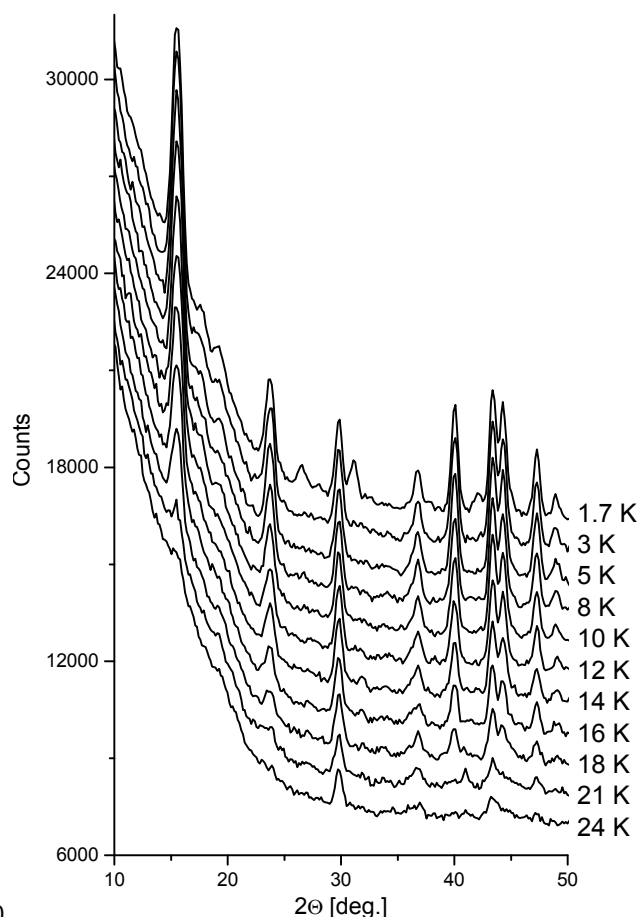


Fig. 2 Neutron diffraction patterns of Er₅Ni₂In₄ at different temperatures.

The preliminary data treatment revealed, that below 21 K two Er sublattices are ordered, whereas below 3 K the third one becomes ordered as well.

This research project has been supported by the European Commission under the 7th Framework Programme through "Research Infrastructures" action of the "Capacities" Programme, contract number CP-CSA_INFRA-2008-1.1.1. Number 226507-NMI3

Principal Proposer: A. Orendáčová, P.J. Šafárik University, Košice, Slovakia
Experimental Team: M. Orendáč, P.J. Šafárik University, Košice, Slovakia
K. Siemensmeyer, S. Maňáš, K. Kiefer, S. Gerischer, HZB
R. Tarasenko, P.J. Šafárik University, Košice, Slovakia

Date(s) of Experiment

05.07.2009 – 14.07.2009

Date of report: 15.12.2009

Previous studies showed the compound represents an $S = 1/2$ Heisenberg square lattice with an intralayer coupling, $J/k_B \approx 3$ K and ordering temperature, $T_N = 0.9$ K [1]. Elastic neutron scattering experiment was focused on the determination of the magnetic order established below the phase transition.

The $\text{Cu}(\text{D}_2\text{O})_2(\text{C}_2\text{D}_{12}\text{N}_2)\text{SO}_4$ compound crystallizes in $C2/c$ space group, room temperature unit cell parameters $a=7.192$ Å, $b=11.680$ Å, $c=9.737$ Å, $\beta=105.5^\circ$. Diffraction patterns were taken at the powder diffractometer E6 equipped with the vertical magnet VM2 and He^3 -insert. The powder sample of total mass 1.6 g was prior pressed into a pellet and stored in the copper can filled with He^3 exchange gas. The sets of powder diffraction patterns were recorded at low and high temperatures in a zero magnetic field. Further comparative runs were also performed in the magnetic field $B = 3$ and 6 T at the lowest temperature 0.45 K. Each of run lasted 12 hours. Within the used statistics, no additional peaks except the nuclear ones were observed at the lowest temperature (Fig.1).

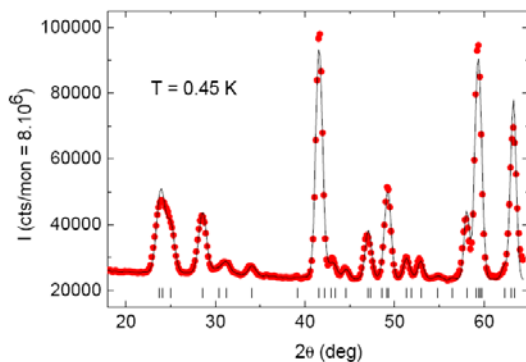


Fig.1: Example of a powder diffraction pattern recorded at $B=0$ and $T=0.45$ K.

Our analysis performed by means of Fullprof program revealed the monotonic decrease of

a - and b - lattice parameters with decreasing temperature, a maximum at about 20-30 K (Fig. 2) was observed for c - parameter. The position of the maximum can be correlated with rapid changes of g -factor and resonance line-width as indicated by X-band electron paramagnetic resonance spectra [2].

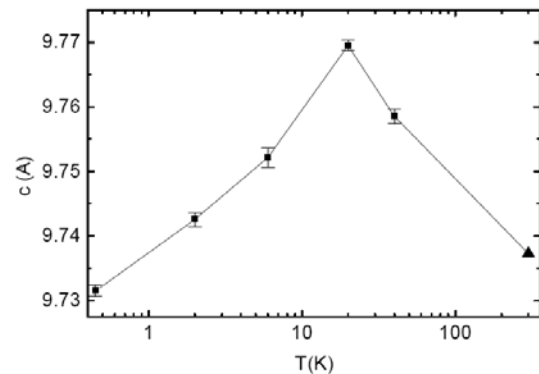


Fig.2: Temperature dependence of c parameter. A triangle corresponds to X-ray study at $T=300$ K.

In conclusion, further experiments on sufficiently large single crystals are necessary for determination of magnetic structure formed below the phase transition.

This project has been supported by the European Commission under the 7th Framework Programme through the Key Action: Strengthening the European Research Infrastructures. Contract n^o: CP-CSA_INFRA-2008-1.1.1 Number 226507-NMI3. M. Orendáč acknowledges financial support of VEGA 1/0078/09.

[1] M. Kajňaková, et al., Phys. Rev. B 71 (2005) 014435.

[2] R. Tarasenko et al., manuscript in preparation.

	EXPERIMENTAL REPORT	Proposal: PHY-01-2623-EF
	Magnetism of the low-temperature phase of PrIr₂Si₂	Instrument: E6 Local Contact: Andreas Hoser
Principal Proposer: M. Mihalik, HZB Experimental Team: A. Hoser, HZB		Date(s) of Experiment 13.10.2009 – 22.10.2009

Date of report: 03.12.2009

The PrIr₂Si₂ compound belongs to the family of polymorphic compounds, which can adopt both, ThCr₂Si₂- (α -phase) and CaBe₂Ge₂-type (β -phase) crystallographic structure. The β -phase of this compound was found to be paramagnetic down to 2 K, however the α -phase was found to undergo two magnetic phase transitions at $T_N = 45.5(1)$ and $T_t = 23.7(2)$ K. The magnetic phases at magnetic field $B = 0$ T were already studied by the powder neutron diffraction (proposal PHY-01-2396). We have found that the compound orders as simple antiferromagnet (magnetic moments aligned along the c -axis) at $T < T_t$ and adopts the longitudinal sine-modulated magnetic structure with the magnetic propagation vector $\mathbf{k} = (0\ 0\ 5/6)$ at temperatures $T_t < T < T_N$.

To understand better the magnetic phase transitions in α -PrIr₂Si₂ we have performed the single crystal neutron experiment on the E6 diffractometer using the HM-1 horizontal magnet. For the experiment we had used scattering plane defined by the (002) and (110) reciprocal vectors, and we have studied $(-1\ -1\ 0+q)$ magnetic reflection. Our first goal was to apply the magnetic field along the c -axis, but the accessible \mathbf{Q} -space didn't allow such an experiment. Instead of this we had to rotate the sample in the magnet 4° out of the magnetic field, and the only possible way, how to scan through the magnetic reflection was to rotate the sample inside the magnet. This resulted to the variation of the misalignment of the magnetic field with respect to c -axis in range from -12 to +4 degrees. We have performed the zero-field-cooled (ZFC) and field cooled (FC) scans in the applied magnetic field of 4, and 6 T and in temperatures lower than 50 K.

The temperature evolution of $(-1\ -1\ 1)$ reflection (Fig. 1) confirmed that the simple antiferromagnetic phase is stable up to magnetic field of 6 T, but exhibits hysteresis features between the ZFC and FC scans. This we consider as a proof of correctness of region I and II of our previously-published magnetic phase diagram [1]. To sample the region III in the magnetic phase diagram, we have made 6 T FC scans around the $(-1\ -1\ 5/6)$ magnetic reflection (Fig. 2). We have

found some magnetic signal, but the statistic is rather poor. These data indicate that the region III in the phase diagram might be correct, but we can not consider it as a final proof.

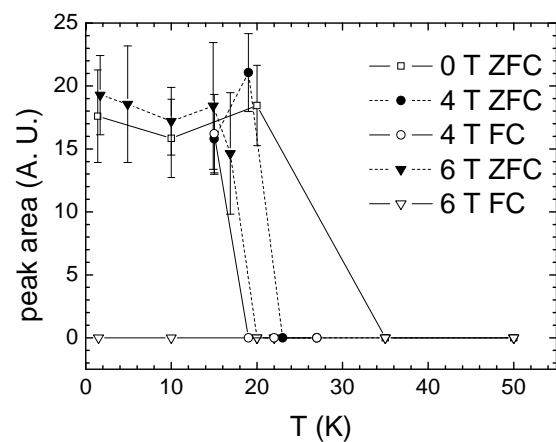


Fig. 1: The temperature evolution of the intensity of the $(-1\ -1\ 1)$ magnetic reflection.

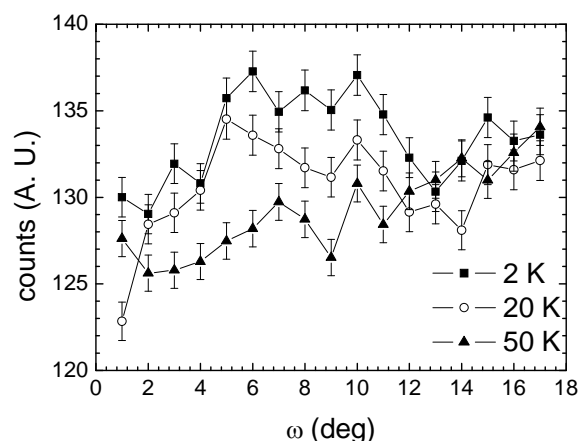


Fig. 2: The raw data ω scans in the $B = 6$ T; FC scan. The mask on the 2D detector was centered to 50.4°. The position $\omega = 9^\circ$ is than the diffraction position for the $(-1\ -1\ 5/6)$ reflection.

References:

- [1] M.Mihalik, M. Diviš, V. Sechovský, J. Magn. Magn. Mater, doi:10.1016/j.jmmm.2009.06.005

	EXPERIMENTAL REPORT Low Temperature magnetic structure of NdPd₂Ge₂ and NdAg₂Ge₂	Proposal: PHY-01-2636 Instrument: E6 Local Contact: A. Hoser
	Principal Proposer: B. Penc, Jagiellonian University, Krakow, Poland Experimental Team: S. Baran, Jagiellonian University, Krakow, Poland A. Hoser, HZB K. Kiefer, HZB S. Gerischer, HZB	Date(s) of Experiment 29.09.2009 – 04.10.2009

Date of report: 22.01.2010

Structural and magnetic properties of the ternary intermetallic compounds NdT₂Ge₂ (T=Pd, Ag) are reported. The magnetic and specific heat studies indicate that both compounds exhibit antiferromagnetic ordering below T_N equal to 1.5 K for NdPd₂Ge₂ and 1.8 K for NdAg₂Ge₂.

The neutron diffraction data were collected at several different temperatures between 0.47 K and 4 K using an ILL – type cryostat with a ³He insert. The data from T = 4 K confirm for both compounds the tetragonal structure of ThCr₂Si₂ – type (space group: I4/mmm). In the unit cell, the Nd atoms occupy the 2(a) sites: (0, 0, 0), the Ag or Pd atoms are located at the 4(d) sites (0, ½, ¼) and (½, 0, ¼), while the Ge atoms occupy the 4(e) sites: (0, 0, z) and (0, 0, -z) (the atoms are located at these and the symmetry equivalent positions). In order to determine the magnetic contributions the neutron diffraction patterns are collected at 0.47 K and 1 K for NdPd₂Ge₂ and 0.47 K for NdAg₂Ge₂. In the case of NdPd₂Ge₂, two peaks at 2θ equal 16.3 and 18.1 deg can be noticed in the 0.47 K pattern while only one broad feature at 2θ = 17.8 deg can be resolved at 1 K pattern (Fig. 1). From this data it is not possible to determine the

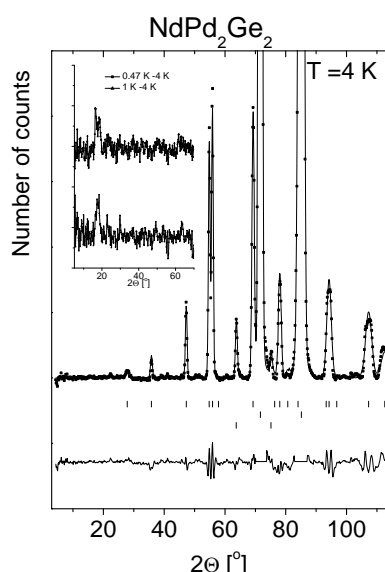
magnetic structure of this compound. For NdAg₂Ge₂ the pattern at 0.47 K contains several additional peaks of the magnetic origin (Fig. 2). Their analysis give a collinear antiferromagnetic structure described by the propagation vector **k** = (½, 0, ½). The Nd magnetic moments located at the (0, 0, 0) and (½, ½, ½) positions are equal to 2.24(5) μ_B. The moments are aligned along the a-axis and have a (+ –) sequence within the crystallographic unit cell.

These data and these from the magnetic, specific heat and electrical resistivity are given in work [1].

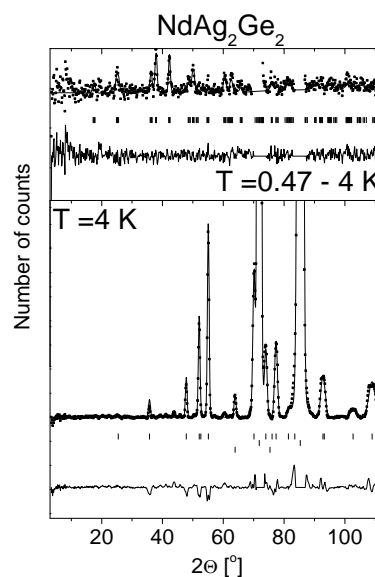
[1] Ł. Gondek, B. Penc, D. Kaczorowski, S. Baran, A. Hoser, A. Szytuła, S. Gerischer, Magnetic and thermodynamic properties of NdT₂Ge₂ (T = Pd, Ag) compounds in J. Solid State Chem. (in press).

Acknowledgement

This research project has been supported by the European Commission under the 7th Framework Programme through “Research Infrastructures” action of the “Capacities” Programme, contract number CP-CSA_INFRA-2008-1.1.1. Number 226507-NMI



Neutron diffraction pattern of NdPd₂Ge₂ collected at 4 K. The inset presents the difference patterns 0.47 – 4 K and 1 – 4 K



Neutron diffraction pattern of NdAg₂Ge₂ collected at 4 K (lower panel) and the difference pattern 0.47-4 K (upper panel).

	EXPERIMENTAL REPORT Neutron Diffraction Studies of RCr_xGe₂ (R = Tb,Dy,Ho,Er) compounds	Proposal: PHY-01-2637 Instrument: E6 Local Contact: A. Hoser
	Principal Proposer: A. Gil, Jan Długosz University, Częstochowa, Poland Experimental Team: A. Hoser, HZB B. Penc, Jagiellonian University, Kraków, Poland A. Szytuła, Jagiellonian University, Kraków, Poland	Date(s) of Experiment 25.11.2009 – 29.11.2009

Date of report: 30.01.2010

Experiment

Polycrystalline samples of the RCr_{0.3}Ge₂ (R =Tb, Dy, Ho, Er) crystallize in the orthorhombic CeNiSi₂-type structure (space group Cmcm), in which the rare earth atoms occupy the 4c crystallographic positions (0,y,¼). Their structure was examined by X-ray powder diffraction.

They were also studied with magnetometric, electrical resistivity and neutron diffraction methods.

Neutron diffraction patterns at several different temperatures between 1.5 K and 25 K were collected in HZB with the use of E6 diffractometer (wavelength $\lambda=2.45$ Å).

Results

The compounds investigated order antiferromagnetically below their Néel temperatures and have different magnetic orderings at low temperatures.

Table 1 presents a summary concerning the determined parameters of the magnetic structures.

Table 1. Summary of the determined magnetic structures of RCr_xGe₂ (R = Tb, Ho, Er).

Compound	T _N [K]	Propagation vector k (k _x , k _y , k _z)	μ [μ_B]	Magnetic moment arrangement
TbCr _{0.3} Ge ₂	18,2	k=(½;0;0)	7,65	(+ + - -) c
HoCr _{0.3} Ge ₂	5,8	k=(½;½;0)	6,99	(+ - - -) c
ErCr _{0.3} Ge ₂	3,2	k=(0;0;0,42)	8,32	(+ + - -) a

At paramagnetic state only the Bragg reflections of nuclear origin are present whereas at lower temperatures additional magnetic reflections appear. The changes of relative intensities of magnetic reflections, the calculating values of magnetic moment and the values of lattice parameters in function of temperature give us the information about the transition temperatures and are in good

agreement with magnetic susceptibility and electrical resistivity data.

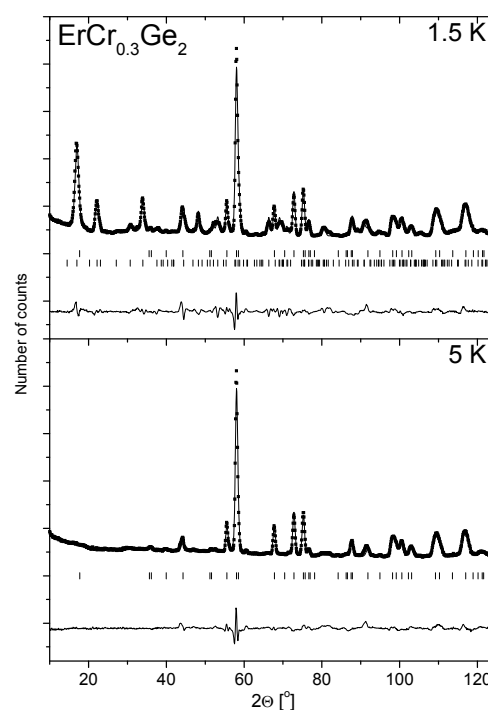


Fig 1.:

Neutron diffraction patterns of ErCr_{0.3}Ge₂ collected at 1.5 and 5 K. The squares represent experimental points, the solid curves are the calculated profiles for the crystal and magnetic structure and the differences between the observed and calculated intensities are plotted at the bottom of each diagram. The vertical bars indicate the Bragg peaks of nuclear and magnetic origin.

Acknowledgement:

This research project has been supported by the European Commission under the 7th Framework Programme through "Research Infrastructures" action of the "Capacities" Programme, contract number CP-CSA_INFRA-2008-1.1.1. Number 226507-NMI

	EXPERIMENTAL REPORT Magnetism in open framework transition metal zeolitic structures with the ABW framework topology	Proposal: PHY-01-2550-EF Instrument: E9 Local Contact: P. Henry
	Principal Proposer: Paul Henry, HZB Experimental Team: Paul Henry, HZB	Date(s) of Experiment 03.07.2009 - 08.07.2009

Introduction and initial aims

The unit cell type exhibited by RbCuPO₄, as made, is highly dependent on the cooling regime. X-ray diffraction showed that the fast cooled sample is a mixture of 2 phases, denoted **I** and **II**, where **I** has a monoclinic unit cell and **II** has an orthorhombic unit cell. **I** can be converted into **II** at RT by the application of mechanical pressure, either by grinding or by pelletisation. In addition, variable temperature X-ray measurements on **II** show that there are 5 distinct phases in the temperature range RT - 550 °C - RT. We had previously published the structure of **II** from PXD [1] but unpublished powder neutron data had revealed a more complex superstructure was present.

Several other materials with the general stoichiometry ABPO₄ (A = Rb, Cs; B = Ni, Cu Co) show similar behaviour and with the recent reports of interesting magnetic properties in the related LiNiPO₄ system [2-3], it was decided to revisit this class of materials. The aims of the experiment were to probe the two RT stable phases at low temperatures to probe for possible magnetic ordering and also to redetermine the structures at RT for publication.

Experiment

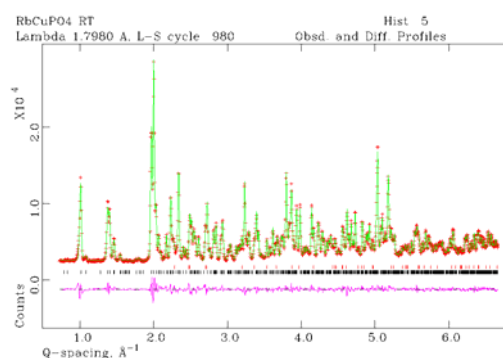
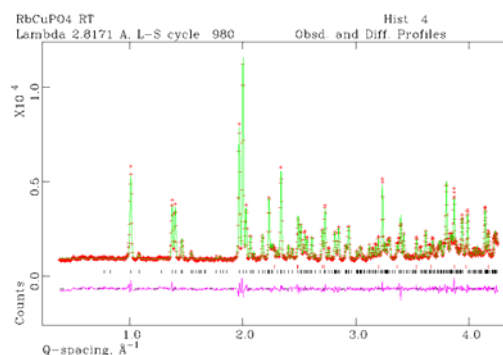
RbCuPO₄ **II** was initially chosen for measurement. Problems were encountered with the interface between the sample environment and CARESS such that no temperature control could be performed. Therefore, the experiment was changed and data were collected on the superstructure sample of **II** at RT at the wavelengths $\lambda = 2.8 \text{ \AA}$ and 1.797 \AA . Data were also collected on CsNiPO₄ and RbNiPO₄ at long wavelength to compliment previous PND data collection from other sources and to search for superstructure peaks.

Results

The figures (right) show the fit to the Rietveld refinement of the data sets of

Date of report: 13.01.2010

RbCuPO₄ collected at the two wavelengths. Analysis of the data collected here with that from PXD and a RT PND dataset at $\lambda = 1.87 \text{ \AA}$ from D20 at ILL allowed the superstructure to be determined and the model to be refined free from any chemical, occupancy and bond length constraints. A publication detailing these results is in preparation. Data analysis of the RbNiPO₄ and CsNiPO₄ are continuing as each shows a superstructure of the simple ABW zeotype that remain unsolved.



References

- [1] Henry PF, Hughes RW, Ward SC, Weller MT Chem. Commun. 2000, No. 19, 1959-60.
- [2] Jensen, T.B.S., et al., PRB, 2009. **79**(9), 092413.
- [3] Jensen, T.B.S., et al., PRB, 2009. **79**(9), 092412

 Neutrons	EXPERIMENTAL REPORT Structure of magnetite at the Curie Temperature	Proposal: PHY-01-2600 Instrument: E9 Local Contact: A. Hoser
	Principal Proposer: Davide Levy, Università di Torino Experimental Team: Roberto Guistetto, Università di Torino	Date(s) of Experiment 15.09.2009 – 18.09.2009

Date of report: 22.2.2010

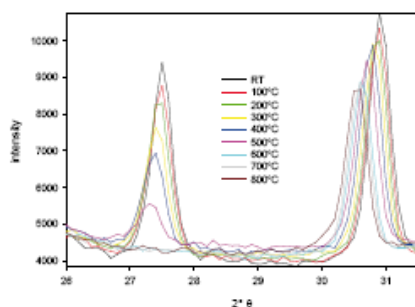
The experiment was performed on two natural magnetite samples. Two sets of data have been collected from room temperature to 800°C with neutron powder diffraction techniques under vacuum. Since both samples are magnetic, three magnetic diffraction peaks are present and their intensities decrease with temperature (fig.1). The diffraction patterns of the first sample show some small peaks, not indexable with the classical cubic structure of magnetite. Further work has to be performed to better describe the related structure.

The second sample does not present extra peaks. The thermal expansion curve shows a slope change at 500°C, due to the magnetic structure relaxation during the transformation from an anti-ferromagnetic to a paramagnetic phase. Diffraction patterns of this sample have been used to extract structure changes during the phase transition by means of Rietveld refinement.

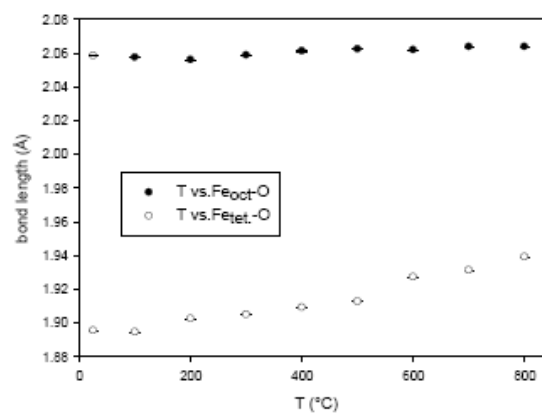
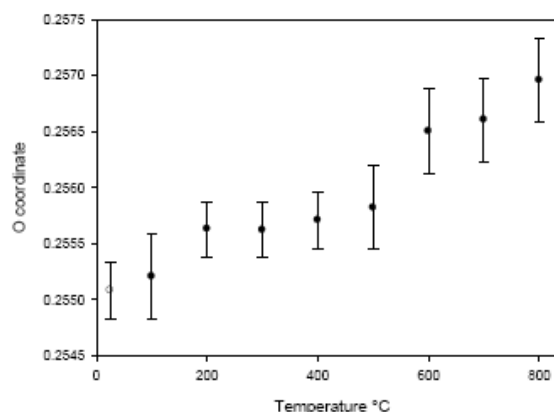
Most significant considerations that can be done on the structural evolution of the studied magnetite as a function of temperature are:

- 1- the thermal expansion presents a slope change at the Curie temperature, as reported by previous experiments (Levy *et al.*, 2004);
- 2- a drastic change of oxygen coordinates after the phase transition occurs (fig.2)
- 3- a contraction of the tetrahedral site is observed (fig.3);
- 4- site occupancy fractions do not change over all the studied temperature range.

Analysis of the commented results is still in progress.



Temperature vs. oxygen coordinate



Bibliography

Levy, D., G. Artioli, et al. (2004). "The effect of oxidation and reduction on thermal expansion of magnetite from 298 to 1173 K at different vacuum conditions." *Journal of Solid State Chemistry* 177(4-5): 1713-1716.

Acknowledgement:

This research project has been supported by the European Commission under the 7th Framework Programme through "Research Infrastructures" action of the "Capacities" Programme, contract number CP-CSA_INFRA-2008-1.1.1. Number 226507-NMI

	EXPERIMENTAL REPORT Quantum Critical Scaling in the Model XY Antiferromagnet LiErF4	Proposal: PHY-02-690 Instrument: V2 Local Contact: Klaus Habicht
	Principal Proposer: N. Nikseresht, EPF Lausanne, Switzerland Experimental Team: N. Nikseresht, EPF Lausanne, Switzerland M. Skoulatos, HZB	Date(s) of Experiment 14.07.2009 – 26.07.2009

Date of report: 14.12.2009

LiErF4 as an example of a dipolar coupled planar antiferromagnet orders at $T_c=375$ mK, and shows a quantum phase transition by applying the 4kOe field along the crystallographic c axis. The higher achievable signal to noise intensity which can be obtained from V2 comparing to E4 by optimizing collimators, encouraged us to continue our critical scattering investigation in order to have more accurate physical explanations of the system close to the thermal phase transition. This knowledge would lead us to introduce LiErF4 as a model which belongs to a different universality class.

Our recent studies on LiErF4 [1,2,3,4] is one step forward in better understanding the consequence of dipole-dipole interaction in quantum magnetism [5]. Through neutron scattering investigations, mostly at HZB, we could obtain the magnetic structure, the temperature-field phase diagram and furthermore completely characterized the Hamiltonian of the system and we believe that by complementary measurements we would be able to establish a model giving more information about purely dipolar coupled antiferromagnets and critical alternations close to phase transitions. Studying the critical exponents of order parameter and specific heat gave us interesting information about the system dimensional decoupling probability near thermal phase transition. In order to reach to an exact conclusion, we should complete our investigation by looking at critical scattering and extracting exponents for the correlation length (ν) as a factor of resp. T and H , and for the spatial correlation function (η) at the critical points.

To probe these facts in continuation of our prev. experiment on E4, (PHY-01-2475), we measured the same sample on V2, which demonstrated high quality data with much better signal to noise ratio compared to E4. Fig. 1 shows a typical scan, from which the correlation length was extracted. Already this preliminary scan reveal a lineshape deviating from simple Lorentzian, suggesting that extracting the exponent η for the spatial correlation function at the critical points will be possible. The obtained correlation lengths appear to follow powerlaw (Fig. 2), but unfortunately, despite using the same sample as on E4, we faced poor thermalisation, which prevented us obtaining enough data to determine T_N with sufficient accuracy. Fig. 3 shows how exponent for correlation length depends on exact value of T_N .

We have now improved the thermalisation by sputtering gold on thin crystal slices sandwiched by copper foils and squeezed together in a copper coffin. Furthermore, an additional thermometer and heater is mounted on the sample, which will allow firstly more accurate recording of sample temperatures, secondly simultaneous recording of specific heat providing independent determination of T_N and H_c . Hence, to continue our investigation of critical scattering, we submitted a new proposal on V2 (proposal no. PHY-02-753).

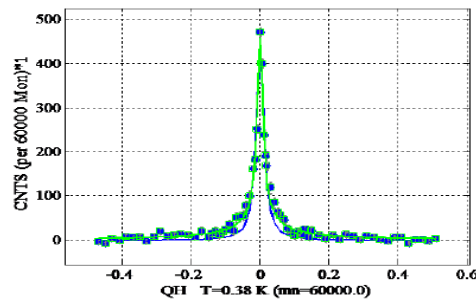


Fig.1. Typical scan, from which correlation length was extracted.

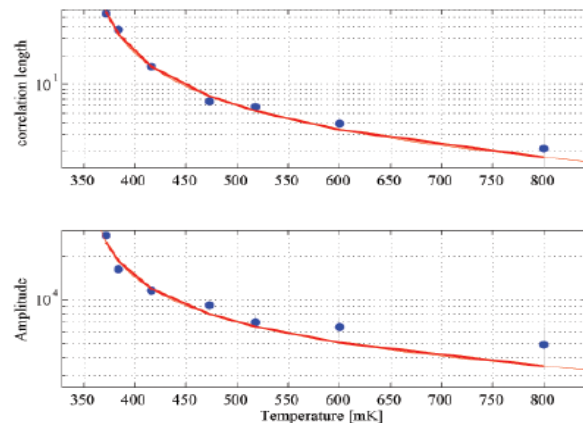


Fig.2. Powerlaw fits to the obtained correlation length and amplitude.

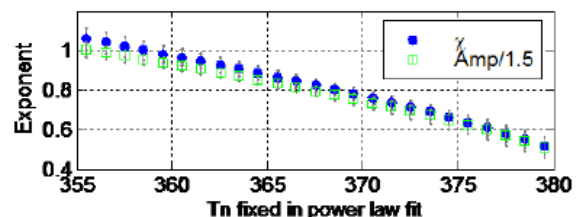


Fig.3. Exponent for correlation length depends on exact value of T_N

References:

- [1] C. Kraemer et al., in preparation for Nature Physics
- [2] https://documents.epfl.ch/users/r/ro/ronnow/www/LiREF4/Thesis_Conradin2006.pdf
- [3] C. Kraemer et al., in preparation for PRL.
- [4] C. Kraemer, PhD Thesis, 2009, in preparation
- [5] J. M. Luttinger and L. Tisza, Phys. Rev. 70, 954 (1946)

This research project has been supported by the European Commission under the 7th Framework Programme through "Research Infrastructures" action of the "Capacities" Programme, contract number CP-CSA_INFRA-2008-1.1.1. Number 226507-NMI

Principal Proposer: Stefan Söllow, TU Braunschweig
Experimental Team: Kirrily Rule, HZB
Anja Wolter, IFW Dresden
Collin Broholm, John Hopkins University, USA

Date(s) of Experiment
14.12.2009 – 23.12.2009

Date of report: 01.03.2010

We have carried out inelastic neutron scattering experiments on a single crystalline sample of deuterated copper pyrazine dinitrate $\text{Cu}(\text{C}_4\text{H}_4\text{N}_2)(\text{NO}_3)_2$ (CuPzN). CuPzN crystallizes in an orthorhombic structure and has been considered a good example of a 1D Heisenberg antiferromagnetic chain (1D HAFC) where Cu^{2+} ions form chains along the crystallographic a-axis. The magnetic coupling along the chain has been determined to be $J/k_B = 10.3\text{K}$, yielding a critical field B_C of moment saturation of about 15T [1,2,3].

Measurements were taken using the cold-neutron triple axis spectrometer, FLEX, with high magnetic fields up to $B > B_C$ used to probe ferromagnon excitations in the saturated phase. To facilitate the extreme magnetic fields the 15T magnet, VM1B, was used with the custom made dysprosium pole pieces which are able to increase the magnetic field at the sample position by 2.5T. However, with this extreme environment set up, the sample space is limited to a cylinder with 6mm diameter and 4mm height. This constraint coupled with limited access to deuterated crystals restricted our sample mass to about 0.07g. The sample consisted of two co-aligned crystals with a mosaic spread of around 2° which was considered acceptable for inelastic neutron scattering measurements where Q-resolution is not so important. FLEX was calibrated with collimations of 60° -open-open after the vertically focused monochromator, sample and horizontally focused analyzer respectively. The experiments were conducted with a k_f fixed at 1.55\AA^{-1} , and 1.3\AA^{-1} which gave an energy resolution of 0.13 and 0.09 meV, respectively.

The nuclear Bragg reflections observable within the (HK0) plane showed the crystals to be well aligned even in high magnetic fields (fig. 1).

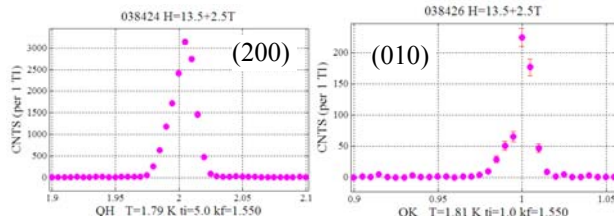


FIG1: Bragg reflections at 16T, (200) left and (010) right

Initial investigations of the 1D HAFC in zero field yielded no discernable features due to the extremely small sample size which contributes only weak scattering from the spinon continuum.

With an applied field of 17.3T very weak scattering was observed at the AFM zone boundary (Fig. 2) and zone centre (Fig 3) in this sample. From Fig. 3 the energy gap

of the dispersion at 17.3T is around 0.3meV. To maximize the intensity at the detector, we used a conventional parallel beam configuration in which the projection of the instrumental resolution ellipsoid on the scattering plane was maximized along the chain direction.

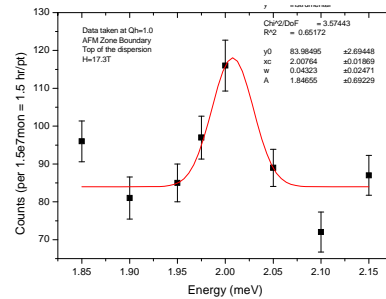


FIG 2: Scattering observed at the zone boundary, $q/\pi = 2$ ($Qh = 1.0$). The peak at $E=2\text{meV}$ represents the top of the dispersion curve.

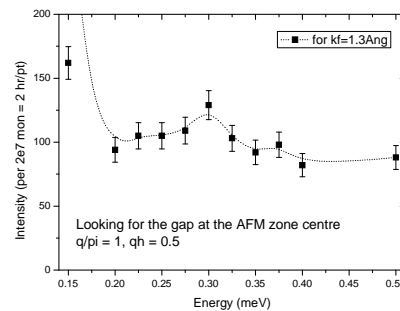


FIG 3: Scattering observed at the zone centre, $q/\pi = 1$ ($Qh = 0.5$). $E=0.3\text{meV}$ is the expected energy of the energy gap at 17.3T. Dashed line is a guide to the eye.

With counting times of approximately 1.5-2 hours per data point required, it is clear that this experiment is hindered by the extremely small sample size. To fully map out the dispersion in the saturated phase, a larger sample mass and longer counting time are needed. For this, we intend to submit a continuation proposal for the next proposal round. Further to this, adjustments to the Dy-booster set up are also planned to maximize the sample volume seen by the neutrons.

- [1] P.R. Hammar, et al., Phys. Rev. B **59** (1999) 1008
- [2] H. Kuehne, et al., cond-mat:0804.2170
- [3] A.V. Sologubenko, et al., Phys. Rev. Lett. **98** (2007) 107201

 Neutrons	EXPERIMENTAL REPORT	Proposal: PHY-02-702 Instrument: V2 Local Contact: Markos Skoulatos
	Bose-glass phase in a spin liquid with quenched disorder	Date(s) of Experiment 12.05.2009 – 24.05.2009
Principal Proposer: Experimental Team:	Tao Hong, ORNL, USA Andrey Zheludev, ETH Zürich, Switzerland	

Date of report: 19.12.2009

We performed neutron scattering experiment at Flex, HZB. The sample used for the experiment consists of 4-coaligned single crystals with a total mass ~ 1 g. The mosaic of the sample is $\sim 3^\circ$. The focusing analyzer was used with final energy fixed at $E=3.7$ meV and the horizontal scattering plane is $(h,k,0)$ plane. We measured the gap mode of 5% Br IPA-Cu(Cl_{1-x}Br_x)₃ samples with applied magnetic field from $H=0$ up to 14.6 T. Fig.1 shows the typical energy scans at zone center $Q=(1.5, 0.5, 0)$ at $H=3$ T and 6 T respectively.

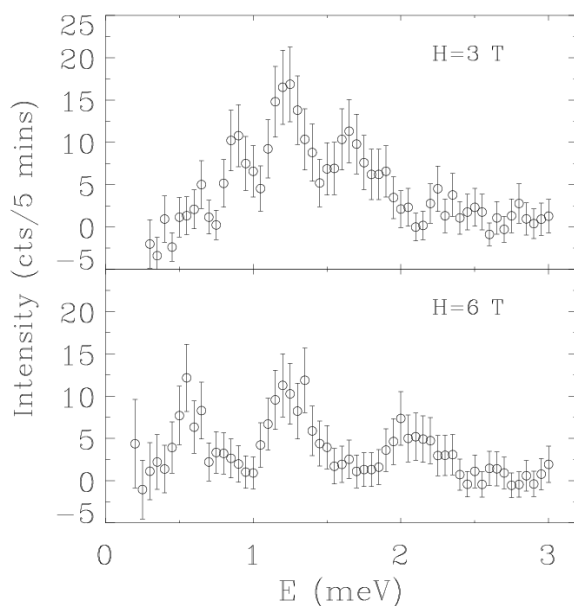


Fig. 1 Typical E-scans at $Q=(1.5, 0.5, 0)$ at $T=50$ mK with the applied magnet fields $H=3$ and 6 T respectively. The shown data are after background subtraction.

The determined field dependence of spin gap Δ is summarized in Fig. 2. The gap of lowest branch $S_z=1$ is softened at a critical field $H_0=10.1(1)$ T using a linear fit.

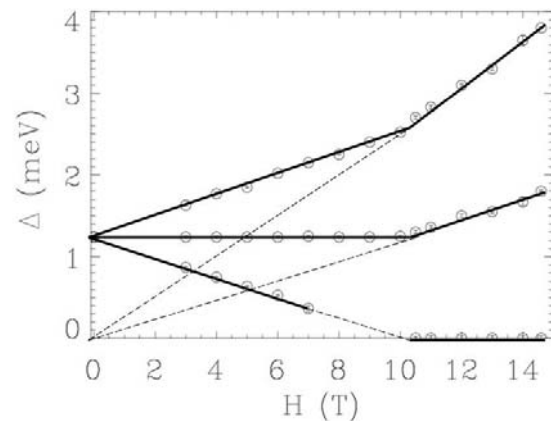


Fig. 2 Measured spin gap Δ as a function of applied magnetic field H at $T=50$ mK.

Fig.3 shows the measurements of field dependence of the magnetic Bragg peak $(0.5, 1.5, 0)$ intensity. The big difference between the field cooling (FC) and zero field cooling (ZFC) indicate the intermediate Bose-glass phase between the spin-liquid phase and Bose-Einstein Condensation (BEC) phase. The second critical field H' where the staggered moment starts to appear is determined to be $10.6(1)$ T by fitting to the power law $(H-H')^{2\beta}$.

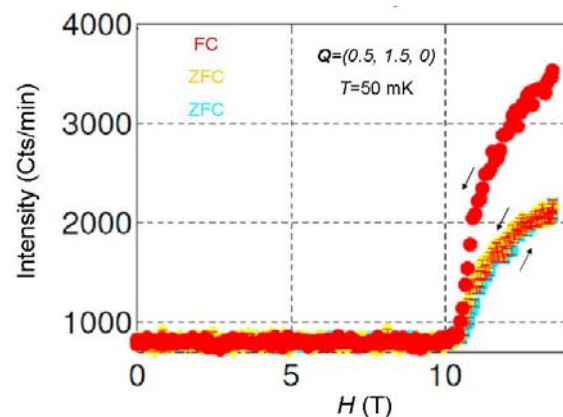


Fig. 3 Field cooling (FC) and Zero field cooling (ZFC) of field dependence of the magnetic Bragg peak $(0.5, 1.5, 0)$ intensity measured at $T=50$ mK.

	EXPERIMENTAL REPORT Low energy states in the frustrated and quantum critical magnet Er₂Ti₂O₇	Proposal: PHY-02-714-EF Instrument: V2 Local Contact: Kirrily Rule
	Principal Proposer: Kirrily Rule, HZB Experimental Team: Jacob Ruff, McMaster University, Hamilton, Canada Bruce Gaullin, McMaster University, Hamilton, Canada Pat Glancy, McMaster University, Hamilton, Canada Kathryn Ross, McMaster University, Hamilton, Canada	Date(s) of Experiment 18.03.2009 – 25.03.2009

Date of report: 30.11.2009

We have investigated the geometrically frustrated magnet erbium titanate (Er₂Ti₂O₇) using the cold-neutron triple axis spectrometer, FLEX at HZB. Er₂Ti₂O₇ has been put forth as a candidate material where long-range magnetic order is induced by quantum fluctuations in an example of order-by-disorder [1]. The phase diagram of this system is exotic, revealing coexisting short range and long range magnetic order in zero applied field. In previous TOF measurements, a finite magnetic field was applied along the crystallographic [110] direction, which induced a quantum phase transition between magnetic order and a quantum paramagnetic state, with a critical field value of H_c ~ 1.6 Tesla. This previous data lacked a detailed field dependent investigation of the short range order and the evolution of the energy gap. Both elastic and inelastic neutron scattering measurements were performed on a single crystal of Er₂Ti₂O₇ aligned within the [HHL] scattering plane. Applied field measurements were taken with vertical fields of up to 5T applied along the [110] direction. Elastic measurements of the nuclear and magnetic Bragg peaks were performed with a tight collimation of 60°-60°-60°. For the inelastic measurements, constant-Q, energy-transfer scans were performed between 0 and 3 meV. The experiments were conducted with a k_f fixed at 1.55 Å⁻¹, which gave an energy resolution of 0.13. Scans were taken with a base temperature of ~50mK to ensure that the sample was close to the quantum critical point.

Figure 1:

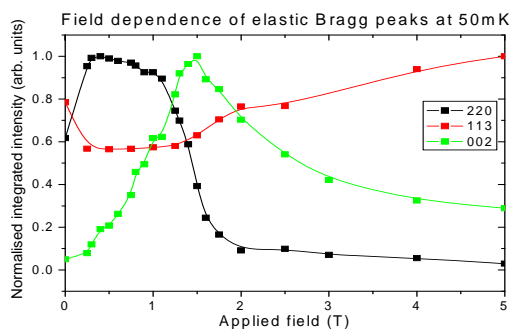
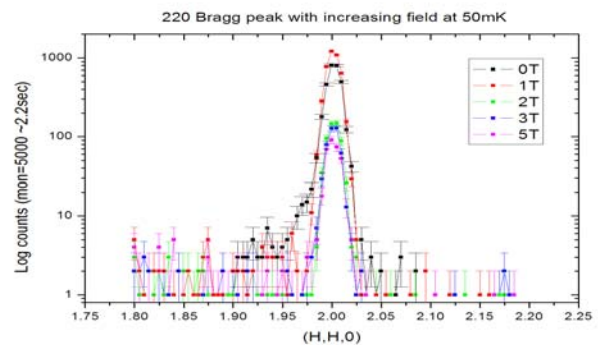


Figure 1 shows the field evolution of three different Bragg peaks, including the structurally forbidden reflection (002). The behaviour of each peak corresponds well with the previously observed trends [2]. The previously observed diffuse scattering around the tail of the (220) peak was not observed in these

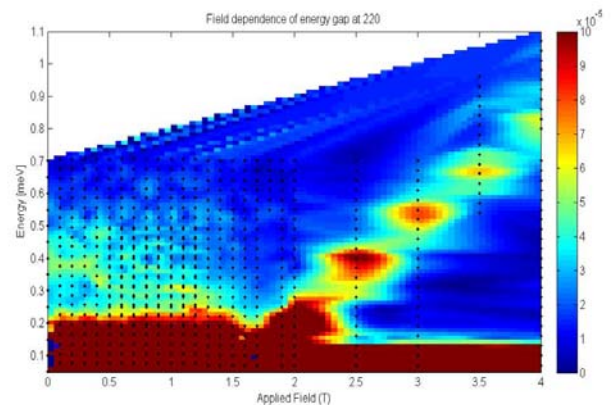
measurements (Fig. 2). This may be due to a coarser resolution in the current experimental set-up. Thus a detailed investigation of the diffuse scattering could not be performed.

Figure 2:



Finally, inelastic measurements clearly mapped out the excitation spectrum in Er₂Ti₂O₇. With extremely fine steps in magnetic field we can observe the transition into the magnetic ordered state at 1.6T. Below this field there is significant diffuse scattering up to ~0.5meV which may result from the dynamic frustration in the paramagnetic state. A second critical field, expected at approximately 0.5T, was not observed in these measurements however a detailed analysis of the raw data is still required.

Figure3:



[1] J.D.M. Champion et al. Phys. Rev. B 68, 020401(R) (2003).

[2] J.P.C. Ruff et al. Phys. Rev. Lett. 101, 147205 (2008)

	EXPERIMENTAL REPORT	Proposal: PHY-02-715-EF
	Temperature Dependence of Magnetic Excitation Spectrum of Sr₃Cr₂O₈	Instrument: V2 Local Contact: Kirrily Rule
Principal Proposer: Experimental Team:	Bella Lake, HZB Diana Lucia Quintero Castro, HZB Nazmul Islam, HZB Elisa Wheeler, HZB	Date(s) of Experiment 03.04.2009 – 09.04.2009

Date of report: 01.12.2009

Sr₃Cr₂O₈ consist of a lattice of spin-1/2 Cr⁵⁺ ions, which form hexagonal bilayers and which are paired into dimers by the dominant antiferromagnetic intrabilayer coupling. The dimers are coupled three-dimensionally by frustrated interdimer interactions. A structural distortion from hexagonal to monoclinic leads to orbital order and lifts the frustration giving rise to spatially anisotropic exchange interactions. Different neutron scattering experiments performed so far, revealed three gapped and dispersive singlet to triplet modes arising from the three twinned domains that form below the transition thus confirming the picture of orbital ordering [1].

We performed an experiment on the triple axis spectrometer FLEX at BENSC, HZB. For our investigation we used two single crystal of Sr₃Cr₂O₈ of mass 3.69 g and 4.04 g, respectively. FLEX was operated in the W configuration (+ - +). The collimation settings were guide-60'-open-open, meaning that the beam was collimated only after the monochromator. The measurements were performed with a fixed final wavevector $k_f = 1.2 \text{ \AA}^{-1}$ and 1.55 \AA^{-1} .

In the previous experiment at Flex we investigated the magnetic excitation spectrum along the (H,0,L) scattering plane. This time, we investigated the spectrum along the (H,H,L) scattering plane (Figure 1). The new data together with the data from the previous experiment provided us with enough information to fit the data to a model and to find the different magnetic couplings in the system [1].

In addition to the scans at 2K, we measured the temperature dependence of the excitations. We explored the linewidth broadening for 11 different temperatures (2K, 5K, 10K, 15K, 20K, 25K, 30K, 40K, 75K, 100K).

We were especially interested in the linewidth broadening at the minimum and maximum of the excitation, and therefore we measured the (0.5,0.5,3) point which contains both features. It was also interesting to measure the linewidth broadening for the (0,0,3) point as at this point the mode is degenerate and there is just one branch which lies in the middle of the bandwidth.

Theory and experimental measurements for the one-dimensional dimer chain compound (Cu(NO₃)₂) show that the thermal broadening is asymmetric quite unlike the symmetric Lorentzian broadening expected in a classical magnet [2].

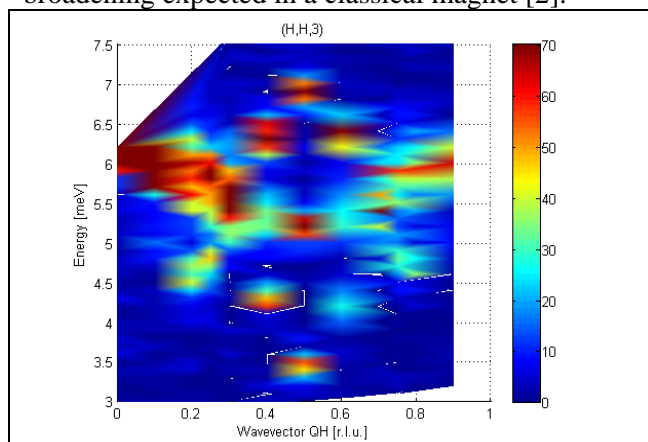


Fig 1. One-magnon excitation spectrum as a function of energy and wavevector in the $(h,h,3)$ direction at 2K.

The temperature dependence of the mode at (0,0,3) is shown in figure 2. Data analysis is ongoing to determine whether the lineshape is asymmetry.

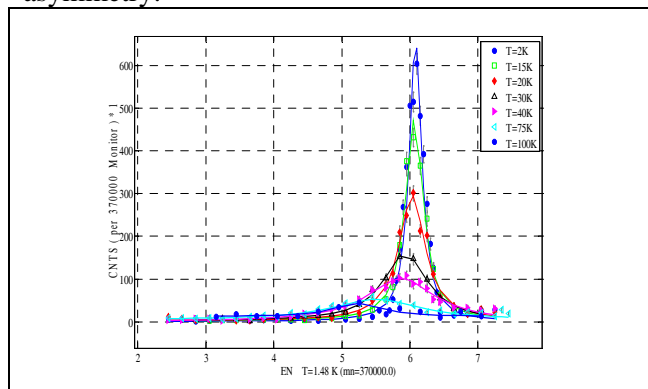


Fig 2. Temperature dependence of the excitation at (0,0,3).

The experiment was completely successful and we got enough data to find the magnetic exchange constants in this material. Further analysis must be done to understand the temperature dependence.

Reference:

- [1] D. L. Quintero-Castro, B. Lake, E. M. Wheeler, A.T.M.N. Islam, et al. *Phy. Rev. B* in press 2009.
- [2] A. J. A. James, F. H. L. Essler, R. M. Konik *Phys. Rev. B* **78**, 094411 (2008).

	EXPERIMENTAL REPORT Splitting of the Magnon Excitation Branches in BaMnF₄ investigated with NRSE	Proposal: PHY-02-721-EF Instrument: V2 Local Contact: K. Habicht
	Principal Proposer: K. Habicht, HZB; Experimental Team: K. Habicht, HZB M. Skoulatos, HZB D. Le, HZB	Date(s) of Experiment 09.06.2009 – 16.06.2009

Date of report: 12.01.2010

This experiment is part of an extended programme aimed at investigating the potential of the neutron resonance spin echo (NRSE) technique beyond lifetime determination. NRSE spectroscopy is a unique experimental tool to measure life times of dispersive elementary excitations over extended regions in the Brillouin zone with resolution in the μeV range. It is thus natural exploring the application of the technique for resolving modes with a separation in energy which is less than the resolution of standard spectrometers. While we have worked out an advanced theoretical description, experimental evidence is still sparse due to lack of data. Here we have chosen BaMnF_4 which shows splitting of the dispersion branches presumably induced by the superstructure present below the structural phase transition at $T \sim 250 \text{ K}$ [1]. The signature of a mode doublet measured by NRSE is a sinusoidal modulation of the exponentially decaying polarization as has already been detected during earlier experiments [2].

FLEX with its NRSE option installed was operated in a configuration with scattering senses (SM=-1, SS=-1, SA=-1) with an experimental transverse Q-resolution of about 0.005 \AA^{-1} FWHM at fixed incident $k_i = 1.7 \text{ \AA}^{-1}$. No additional collimators were used besides Mezei cavity polarizers inserted behind the PG monochromator and behind the PG analyzer. Second-order contamination is substantially suppressed by the curved neutron guide. A different crystal than in the earlier measurements [2] was used for the present experiment with a substantially smaller sample mass of 0.835 g. The sample was mounted with the [hkk] plane as the scattering plane and kept at base temperature $T=1.8\text{K}$ throughout the experiment. We concentrated on the dispersionless excitation at $E = 0.14 \text{ meV}$ at the Brillouin zone center $Q=(0 \ 0.5 \ 0.5)$ of the gapped dispersion (see insert in Fig.2) due to the weak inelastic intensity. Interestingly the large splitting formerly observed at $(1 \ 0.5 \ 0.5)$ (with a different crystal) was not observed at $(0 \ 0.5 \ 0.5)$. A calibration curve was recorded using the elastic signal at $Q=(0 \ 0.5 \ 0.5)$. The elastic polarization was measured to be $\sim 65\text{-}70\%$ while the inelastic signal dropped to 50% of this value. This is indicative of a 1:1 mixture of spin-flip to non-spin-flip scattering.

Fig. 1 shows the individual NRSE scans covering a range of spin-echo times from 166.25 ps to 20 ps.

The echo amplitude was extracted from the background-corrected signal. Fitting an exponential decay to the echo amplitudes normalized to the elastic calibration curve we obtain a Lorentzian HWHM $\Gamma = 1.1 \pm 1.3 \mu\text{eV}$ (Fig. 2). No splitting could be detected up to 166.25 ps excluding signal splitting on a $50 \mu\text{eV}$ sensitivity level.

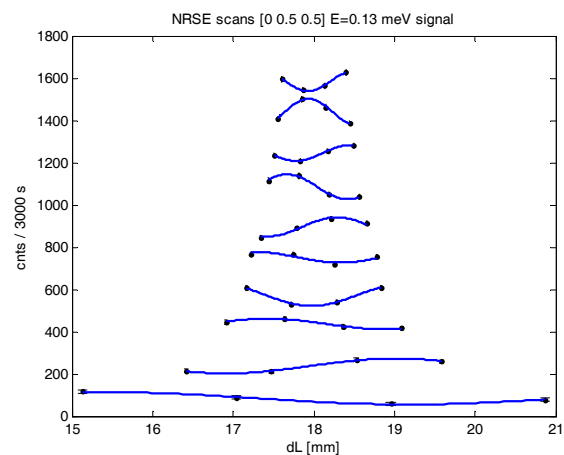


Fig. 1: Top to bottom: NRSE scans at spin-echo times $\tau = 166.25 \text{ ps}, 150 \text{ ps}, \dots, 20 \text{ ps}$. Scans are offset by 150 cnts for clarity.

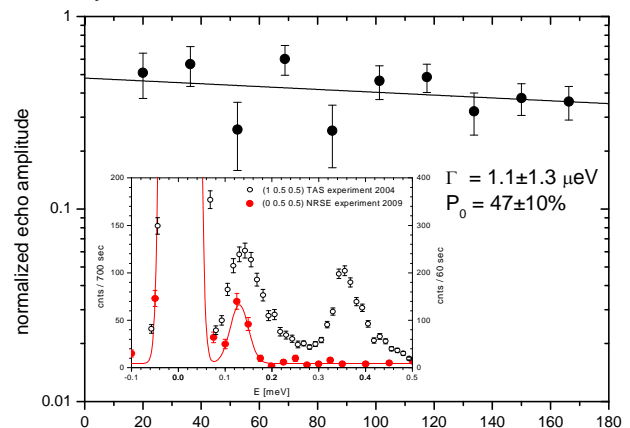


Fig. 2: Background corrected echo amplitude at $Q=(0 \ 0.5 \ 0.5)$ r.l.u., $E=0.14 \text{ meV}$ fitted to an exponential decay. Insert: Red solid circles: const.-Q scan at $Q=(0 \ 0.5 \ 0.5)$ compared to $Q=(1 \ 0.5 \ 0.5)$ r.l.u. data from earlier TAS measurements (black open circles).

We are indebted to H. Nunes Bordallo for loan of the BaMnF_4 crystal.

[1] M. Yoshimura, M. Hidaka, *J. Phys. Soc. Japan* **74** 1181 (2005).

[2] S. P. Bayrakci *et al.*, *BENSC Experimental Reports* (2003).

 Neutrons	EXPERIMENTAL REPORT	Proposal: PHY-02-734-EF
	Search for Spin-Density Waves in Pb	Instrument: V2 Local Contact: K. Habicht
Principal Proposer:	K. Habicht, HZB; T. Keller, P. Aynajian - MPI-FKF Stuttgart	Date(s) of Experiment
Experimental Team:	K. Habicht, HZB M. Skoulatos, HZB	13.10.2009 – 19.10.2009

Date of report: 08.01.2010

A recent detailed experimental study of the wave vector and temperature dependence of the lifetimes of transverse acoustic phonons in the elemental superconductors Pb and Nb found that the superconducting energy gap coincides with sharp Fermi-surface anomalies [1]. Despite known Kohn-anomalies a new energetically low-lying anomaly in the dispersion with reduced lifetime was found which is not reproduced by theoretical calculations and its origin remains unexplained. The aim of this experiment was to explore one possible scenario for the microscopic origin of the anomaly, which is based on the existence of spin-density waves (SDW) as predicted by Overhauser [2, 3]. The search for SDWs in elemental Pb has led to conflicting experimental results and has been discussed controversially [4, 5, 6]. Overhauser [6] explained the absence of elastic satellites to the (210) Bragg peak in an early NIST experiment with a longitudinal polarization state of the SDW resulting in zero intensity. He also showed that it is possible that a magnetic field can rotate the polarization vector resulting in a transverse component which renders a SDW visible to neutrons

We have extended our previous measurements [7] to test the SDW scenario using high magnetic fields. Gridded elastic Q-scans were performed operating FLEX in a configuration with scattering senses (SM=-1, SS=-1, SA=+1) at $k_i = k_f = 2.66 \text{ \AA}^{-1}$. A single PG filter was used in the first arm to suppress second order contamination. The Pb sample was mounted in the (hk0) scattering plane in the horizontal field magnet HM1. The accessible wavevector space close to the (210) Bragg peak has been mapped out at zero field and B=5T and T=2K. The magnetic field was oriented at 41.5° relative to the crystallographic (210) direction. The data shows strong contamination from powder scattering which is attributed to either Al powder lines or double scattering involving scattering from a Pb Bragg peak and Al powder scattering. In addition we have raised the temperature to 15 K which left the elastic intensity unchanged. No field dependent elastic signal indicative of a SDW could be found within the accessible Q-range at 41.5° field angle with a sensitivity level of 10^{-6} relative to the intensity of the (200) Bragg peak which was measured to be 200000 cnts/s with a calibrated

absorber. Additional elastic measurements were performed close to (110) with the field at 60° relative to the (110) direction. Elastic Peaks have been found at (1.1 0 75 0) and (0.75 1.1 0) showing neither field nor temperature dependence between 0 and 5 T and 2K and 15 K respectively (see Fig.). Careful spurious checks at different incident wavelengths demonstrated however that the apparent incommensurate signal is likely to arise from double-Bragg scattering. Furthermore we conducted a search for dynamic spin correlations performing const.-Q-scans in the energy range 0-3 meV at (1 1 0) and const.-E-scans in the Q-range (0.9 1 0) to (1.1 1 0) at energies 1 and 2 meV. These and similar scans at (1.5 0 0) and (0.5 0.5 0) led to negative results. We thus conclude that static spin correlations can be excluded as a possible scenario for the lifetime anomaly observed in Pb and have no indication of dynamic spin correlations.

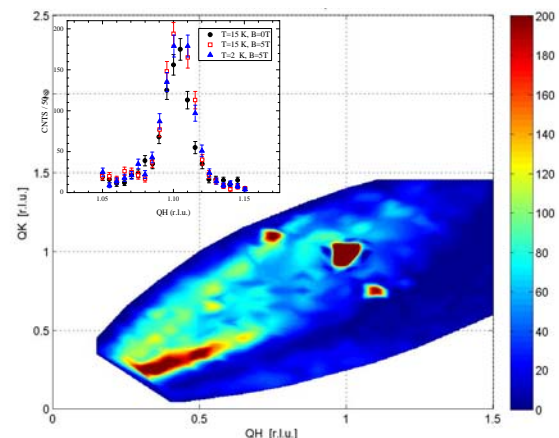


Fig.: Map of the accessible wavevector space close to the (1 1 0) measured at B=5T and higher resolution scans at (1.1 0.75 0) (insert).

- [1] P. Aynajian, T. Keller, S.M. Shapiro, K. Habicht and B. Keimer, *Science* **319**, 1509 (2008).
- [2] A. W. Overhauser, *Phys. Rev.* **128**, 1437 (1962).
- [3] A. W. Overhauser, L. L. Daemen *Phys. Rev. Lett.* **61**, 1885 (1988).
- [4] A. W. Overhauser, T. M. Giebultowicz, *Phys. Rev. B* **47**, 14338 (1993).
- [5] J.D. Short, J. P. Wolfe, *Phys. Rev. Lett.* **24** (2000).
- [6] J. P. Wolfe, T. L. Head, *J. Phys. Conference Series* **92**, 012097 (2007)
- [7] K. Habicht *et al.*, *BENSC Experimental Reports* (2008).

Determination of Local Dispersion Gradients with NRSE spectroscopy

Proposal: PHY-02-735-IT

Instrument: V2

Local Contact:
K. Habicht

Principal Proposer: K. Habicht, HZB
Experimental Team: K. Habicht, HZB
M. Skoulatos, HZB
F. Groitl, HZB

Date(s) of Experiment

10.11.2009 – 23.11.2009

Date of report: 08.01.2010

This experiment is part of an extended programme aimed at a thorough experimental confirmation of resolution effects in neutron resonance spin-echo (NRSE) type experiments. We have recently generalized the resolution formalism developed earlier [1-3] to include non-satisfied spin echo conditions and arbitrary oriented local gradients of the dispersion surface [4]. In this particular experiment we focused on phase-sensitive NRSE measurements on the reasonably well characterized model dispersion surface of Pb. The orientation of the local gradient of the dispersion can be simply controlled by rotating the sample.

FLEX was operated in a configuration with scattering senses (SM=-1, SS=-1, SA=+1) with an experimental transverse Q-resolution of about 0.01 \AA^{-1} FWHM at fixed incident $k_i = 1.7 \text{ \AA}^{-1}$. No additional collimators were used besides Mezei cavity polarizers inserted behind the PG monochromator and behind the PG analyzer. Second-order contamination is substantially suppressed by the curved neutron guide. The background TAS parameters and the NRSE parameters were fixed at their nominal values for the (2 0.1 0) excitation which was experimentally found at 0.97 meV at T=100K. The required tilt angles of the RF-flippers were calculated from linear fits to dispersion data from earlier experiments, $\theta_1 = -27.9^\circ$, $\theta_2 = +24.17^\circ$ were used. A large Pb single crystal of high quality w.r.t. mosaicity was mounted with the [hk0] plane as the scattering plane. The phase was extracted from standard NRSE scans (see insert in Fig.1) as a function of sample rotation around all three possible axes (A3, GU, GL) with counting times of 900 s per point and 24 points covering roughly 2.5 periods of the echo signal. The bulk of the measurements were done at a spin-echo time $\tau=20$ ps, additional data was collected at $\tau=30$ ps. A sample temperature of T=100K was used which provided a reasonable compromise between thermal population and loss of echo-amplitude due to anharmonic effects.

Fig. 1 shows the phase shift as a function of rocking angle dominated by a linear coefficient in the phase but deviations from linear behaviour are clearly visible. As expected, the phase shift due to moving the dispersion surface varying the sample goniometer is much less (Fig. 2). For the

preliminary data analysis we have so far only considered the data at $\tau=20$ ps. Adding the $\tau=30$ ps data set shall reduce the statistical error.

The data collected during the course of the experiment will allow a more detailed comparison to our theoretical results than previously possible.

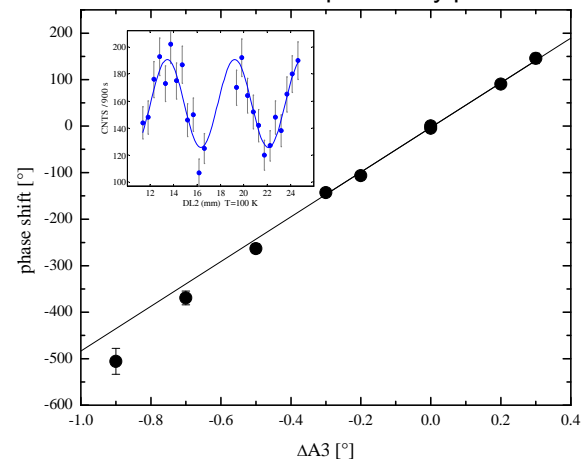


Fig 1.: Phase shift as a function of rocking angle at (2 0.1 0) E=0.97 meV and typical SE signal (insert).

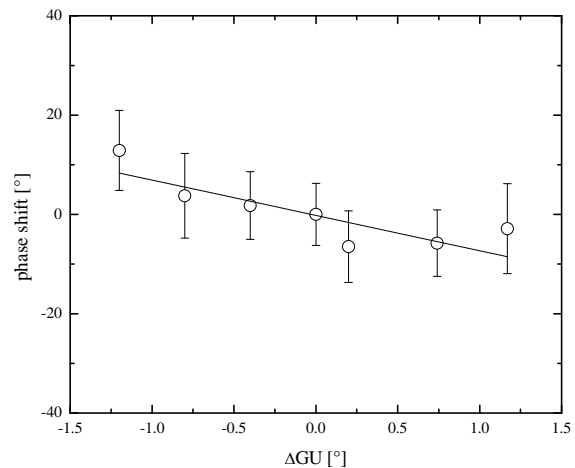


Fig 2.: Phase shift as a function of sample goniometer angle GU at (2 0.1 0) E=0.97 meV.

- [1] K. Habicht, R. Golub, T. Keller, *J. Appl. Cryst.* **36**, 1307 (2003).
- [2] K. Habicht, R. Golub, F. Mezei, B. Keimer, T. Keller, *Phys. Rev. B.* **69**, 104301 (2004).
- [3] K. Habicht, T. Keller, R. Golub, *Physica B* **350**, E803-E806 (2004).
- [4] K. Habicht *et al.* submitted to proceedings of the PNSXM 2009 to be published in *J. Phys. J. of Phys. Conf. Series*.

 Neutrons	EXPERIMENTAL REPORT Magnetic excitations of alpha-CaCr2O4 triangular lattice antiferromagnet	Proposal: PHY-02-736-EF Instrument: V2 Local Contact: K. Rule
	Principal Proposer: Bella Lake, HZB Experimental Team: Sandor Toth, HZB Bella Lake, HZB Kirrily Rule, HZB	Date(s) of Experiment 27.10.2009 – 02.11.2009

Date of report: 15.01.2010

α -CaCr2O4 is a distorted quasi 2D Heisenberg triangular lattice antiferromagnet. The crystal structure is orthorhombic ($Pmmn$). The Cr^{3+} $S=3/2$ magnetic ions are arranged into triangular layers that form the **b-c** plane and which are stacked antiferromagnetically along the **a** axis. The crystal orders magnetically below $T_N=41$ K with a magnetic ordering wavevector of $\mathbf{k}=(0 \ 2/3 \ 0)$. Strong direct exchange interactions which are both isotropic and antiferromagnetic are expected between the magnetic ions within the **b-c** while antiferromagnetic superexchange interactions are expected along **a** which are much weaker due to the longer interplane Cr-Cr distance. This system is interesting because of its potential for frustration, non-collinear magnetic ordering and strong magnon-magnon interactions.

We measured a single crystal sample ($m=340$ mg), at the base temperature of 2K well below the Neel temperature using the FLEX triple axis spectrometer. The sample was oriented with $(h,k,0)$ as the horizontal scattering plane and the spectrometer was used in W configuration for optimum resolution with the final wavelength fixed and collimation of (60°) before the sample. Most of the data were collected with final wavevector $k_F=1.55 \text{ \AA}^{-1}$, which gave a vanadium width of 0.2 meV FWHM. To check certain linewidths we used $k_F=1.2 \text{ \AA}^{-1}$, where the energy resolution was 0.1 meV FWHM. In the low resolution mode, the maximum possible energy transfer was 11 meV.

In accordance with expectations, a steep dispersion is observed along $(1 \ k \ 0)$ due to the strong exchange interactions within the plane. (see figure 1). The top of the dispersion is much higher than the instrumental limit. Assuming a undistorted triangular antiferromagnet, the in-plane spin-spin coupling is estimated to be 23 ± 3 meV by fitting the expression $E=J|\sin(2\pi Q)|$ to the dispersion along $(1 \ k \ 0)$.

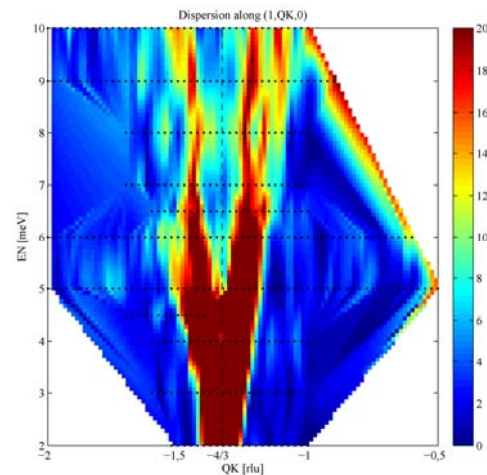


Fig. 1. Dispersion along $(1 \ k \ 0)$.

We also measured the spin wave dispersion along the $(h \ -1.33 \ 0)$ direction, in order to probe the interplanar interactions (see Fig. 2). The measured linewidths are resolution limited and the top of the dispersion is around 4 meV. A small energy gap of 0.5 meV was observed at $(1 \ -1.33 \ 0)$ above the magnetic Bragg-peak.

Data analysis is underway to determine the exchange interactions and the nature of the excitations.

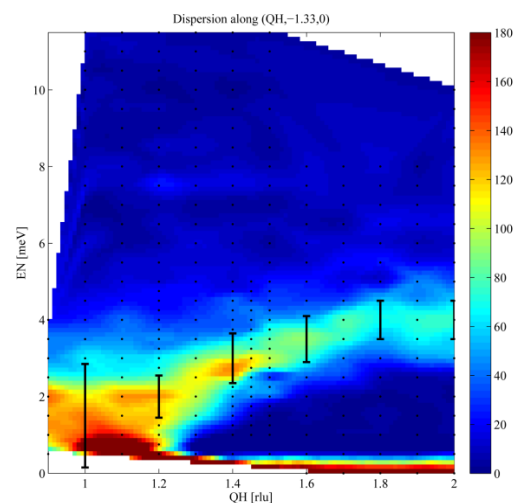


Fig. 2. Spinwave dispersion along **a**, error bars are simulated instrumental resolution where the broadening due to the strong dispersion in the **b-c** plane has been taken into account.

Quantum phase transition in the 1D Ising spin system $\text{CoCl}_2 \cdot 2\text{D}_2\text{O}$

Proposal: PHY-02-739

Instrument: **V2**

Local Contact: K. Habicht,
M. Skoulatos

Principal Proposer: Kim Lefmann, University of Copenhagen
Experimental Team: Jacob Larsen, Risø DTU National Laboratory for Sustainable Energy
Sara U. H. Eisenhardt, University of Copenhagen
Moren Sales, University of Copenhagen
Klaus Habicht, HZB, Markos Skoulatos, HZB
Henrik M. Rønnow, École Polytechnique de Lausanne
Niels B. Christensen, Risø DTU National Laboratory for Sustainable Energy

Date(s) of Experiment

25.11.2009 – 29.11.2009
07.12.2009 – 14.12.2009

Date of report: 11.01.2010

Modern research into solid state physics seeks the fundamental understanding of the quantum mechanics of many interacting particles, and how the quantum critical properties of solids may hold the key to phenomena such as high-temperature superconductivity [1]. $\text{CoCl}_2 \cdot 2\text{D}_2\text{O}$ is well known as a quasi one-dimensional Ising-like system [2]. The spins pointing along the crystallographic b -axis are arranged in ferromagnetic Ising-chains (along with the crystallographic c -axis) with antiferromagnetic (AFM) interchain couplings (Fig. 1) giving rise to AFM order below $T_N=17.5\text{K}$. Theory predicts a quantum phase transition from the AFM phase to a completely polarized quantum paramagnetic state when a sufficiently strong magnetic field is applied transverse to the easy axis.

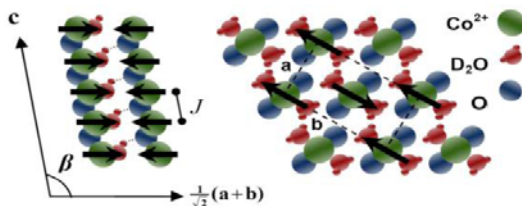


Figure 1: The magnetic unit cell of $\text{CoCl}_2 \cdot 2\text{D}_2\text{O}$ also showing the chemical elements. The unit cell belongs to the monoclinic space group $C_{2/m}$.

We used elastic neutron scattering to measure the antiferromagnetic order parameter. Close to the critical point the measured intensity follows $I \sim (1 - H/H_c)^{2\beta}$ (Fig. 2) with $H_c=16\text{ T}$ in agreement with [3]. In the second part of the experiment we used inelastic neutron scattering to measure the spin wave energy as function of field. There exists two spin wave modes and our model predicts one spin wave mode to go soft at the quantum critical point. By careful background subtraction we found the soft mode at $\Delta E = 0.80\text{ meV}$ in 15.2T which agrees well with both our earlier measurements and our theoretical model [4].

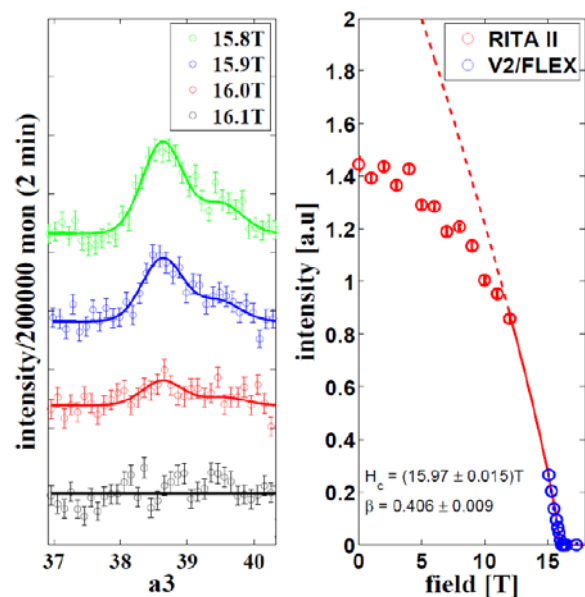


Figure 2: Left: Examples of scans at $q_{\text{AFM}} = (211)$ close to the quantum critical point, shown with an offset for clarity. Right: The integrated intensity measured from 0T to 17.3T. The high field data was measured in this experiment and the low field data is taken from [4].

- [1] S. Sachdev, Quantum Phase Transitions, Cambridge (1999).
- [2] J. K. Kjems et al. Phys. Rev. B **12**, 5190 (1975).
- [3] H. Mollmotto et al. J. Phys. Soc. Jpn. **49**, 108 (1980).
- [4] J. Larsen, M.Sc. thesis, University of Copenhagen (2009)

This research project has been supported by the European Commission under the 7th Framework Programme through "Research Infrastructures" action of the "Capacities" Programme, contract number CP-CSA_INFRA-2008-1.1.1. Number 226507-NMI3

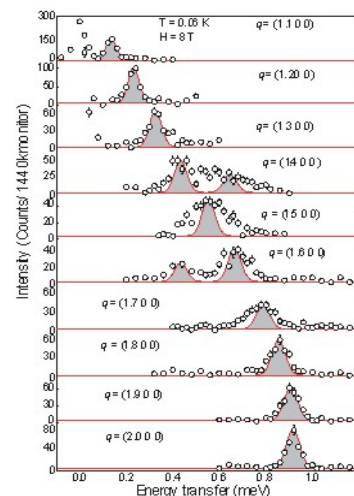
	EXPERIMENTAL REPORT Magnon instability in strong field in square lattice antiferromagnet	Proposal: PHY-02-742 Instrument: V2 Local Contact: Klaus Habicht
	Principal Proposer: T. Masuda, Yokohama City University, Japan Experimental Team: T. Masuda, Yokohama City University, Japan Kirrily Rule, HZB	Date(s) of Experiment 14.08.2009 – 23.08.2009

Date of report: 14.12.2009

Some of interesting phenomena in condensed matter science are explained by universal natures of quasiparticle, quantized element excitation with a certain energy and wave vector. For example antiferromagnetic order is a result of Bose condensation of magnon[1,2] and superfluidity is those of phonon[3]. The quasiparticles in the material, however, can be unstable and decayed if it is allowed by conservation laws. Such phenomena was initially predicted in the superfluid Helium and it was identified by a termination of the excitation at the twice energy of roton[4]. The magnon version of the spectral termination was observed in a few quantum magnets, where one magnon branch crosses the lower boundary of two magnon continuum [5,6]. Recently the instability of magnon with a similar mechanism is predicted in 2D square lattice Heisenberg antiferromagnets (SLHAF) in high magnetic field [7-10]. At zero field two magnon continuum spreads in higher energy region for all wave vector \mathbf{q} and there is no decay channel for one magnon. With increasing field one magnon branch moves higher around $\mathbf{q} \sim (\pi, \pi)$ and eventually overlaps with the continuum at a threshold field $H \sim 0.76 H_C$. The hybridization of one-magnon and two-magnon continuum induces instability of the one-magnon state. While most theoretical calculations including spin-wave[7,9], Monte Carlo[8], exact diagonalization[10] are for $S=1/2$ spin case, the field induced magnon instability is universal to 2D and 3D AFMs with general spins. It is the change of the curvature of AF magnon dispersion from downward at low field to upward at higher field that qualitatively explains the kinematical instability of magnon [4,7]. Here we report the experimental observation of the magnon instability in $S=5/2$ SLHAF $\text{Ba}_2\text{MnGe}_2\text{O}_7$ at V2/FLEX spectrometer in Helmholtz Zentrum Berlin. Dr. Kirrily Rule, Dr. Klaus Kiefer, Dr. Duc Le, Mr. Kitaoka and Dr. Masuda participated in the experiment.

Single crystal with $7 \times 7 \times 80 \text{ mm}^3$ was grown by floating zone method. To obtain the precise peak profile of the magnetic excitation we put tight collimations, guide-60'-60'-60' and use the $\text{\$E_F\$}$ = 2.6 meV mode, which gives the best resolution in practical use of 3-axis spectrometer. Field was applied in the c direction. Constant \mathbf{q} scans at $\mathbf{q}=(h \ 0 \ 0)$ at $H = 8 \text{ T}$ and $T = 0.06 \text{ K}$ are shown in the Figure. At $h < 1.3$ and $h > 1.8$ the excitations are

within the calculated experimental resolution shown by shaded area. Meanwhile, at $1.4 < h < 1.7$ we clearly observe the broadening of the peaks. Shoulder structure at $h = 1.4$ and 1.6 are contribution from another mode. We numerically calculated the allowed decay channel for one-magnon by conservation laws. We confirmed that the obtained \mathbf{q} region for the broad peak is consistent with the calculated decay channel. Additionally we performed a series of constant \mathbf{q} scans at $H=6$ and 10 T . Detail data will be displayed in forthcoming publication [11]. In this report, we simply mentioned that we observed the field induced one-magnon instability in $S=5/2$ 2D-SLHAF $\text{Ba}_2\text{MnGe}_2\text{O}_7$ at V2/FLEX spectrometer in Helmholtz Zentrum Berlin.



References

- [1] T. Giamarchi and A. M. Tsvelik, Phys. Rev. B 59, 11398 (1999).
- [2] T. Nikuni, M. Oshikawa, A. Oosawa, and H. Tanaka, Phys. Rev. Lett. 84, 5868 (2000).
- [3] F. London, Nature 141, 643 (1938).
- [4] E. Lifshits and L. Pitaevskii, Statistical Physics II (Pergamon, Oxford, 1980).
- [5] M. B. Stone, I. A. Zalitznyak, T. Hong, C. L. Broholm, and D. H. Reich, Nature 440, 187 (2006).
- [6] T. Masuda, A. Zheludev, H. Manaka, L.-P. Regnault, J.-H. Chung, and Y. Qiu, Phys. Rev. Lett. 96, 047210 (2006).
- [7] M. E. Zhitomirsky and A. L. Chernyshev, Phys. Rev. Lett. 82, 4536 (1999).
- [8] O. F. Syljuåsen, Phys. Rev. B 78, 180413(R) (2008).
- [9] A. V. Syromyatnikov, Phys. Rev. B 79, 054413 (2009).
- [10] A. Lüscher and A. M. Läuchli, Phys. Rev. B 79, 195102 (2009).
- [11] T. Masuda et al., to be published.

 HELMHOLTZ ZENTRUM BERLIN für Materialien und Energie NEUTRONS	EXPERIMENTAL REPORT	Proposal: PHY-03-647-EF
	Magnetic excitations of frustrated magnet SrYb₂O₄	Instrument: V3 Local Contact: N. Tsapatsaris M. Russina
Principal Proposer: Bella Lake, HZB Experimental Team: Diana Lucia Quintero Castro, HZB Nazmul Islam, HZB Asad Niazi, JMI, New Delhi, India		Date(s) of Experiment 02.06.2009 – 04.06.2009

Date of report: 01.12.2009

SrYb₂O₄ is a frustrated, low dimensional antiferromagnet (see fig 1). The magnetic Yb³⁺ ions have angular momentum $S=1/2$, $L=3$ and $J=7/2$ and form sub-lattices of double chains running parallel to the crystallographic c -axis (see figure 1). There are two inequivalent although highly similar chains due to the two inequivalent Yb³⁺ ions per unit cell. These chains suggest the presence of frustrated first and second neighbour magnetic interactions. Moreover the coupling between the chains is also frustrated and the Yb³⁺ ions form a hexagonal structure around the Sr ions. Heat capacity measured down to 0.3 K shows a lambda anomaly at 0.965 K which we attribute to a phase transition to long-range antiferromagnetic order. In addition a broad feature at $T \sim 2.5$ K is observed, which is characteristic of low-dimensional magnets with short-range correlations above T_N .

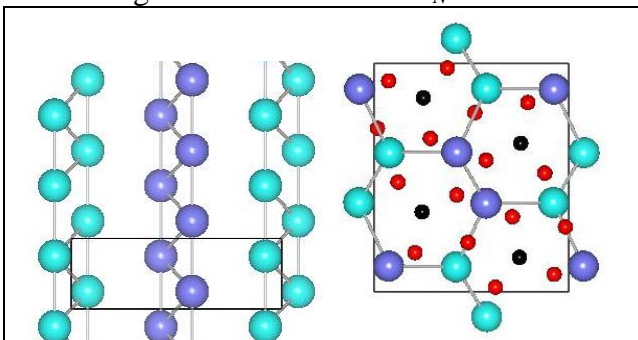


Fig 1. Structure of SrYb₂O₄ pale blue and lilac represent the two inequivalent Yb sites, red – O, black – Sr. The left panel show the double chains running along c . The right panel shows the 'hexagonal' structure perpendicular to c .

We have used the time of flight spectrometer V3-Neat, together with a dilution stick to reach temperatures below the phase transition, e.g. 0.055 K. For this experiment we used a range of different incident energies to determine the energy scale of the magnetic excitations. The incoming wavelengths were: 1.5 \AA^{-1} , 2.5 \AA^{-1} , 3.2 \AA^{-1} , 3.8 \AA^{-1} . With the different data sets acquired we measured

mainly quasielastic scattering below 2 meV, which is most intense for $Q=1 \text{ \AA}^{-1}$, this wavevector coincides with the Q vector of the peaks with magnetic contributions. The data is showed in figure 2.

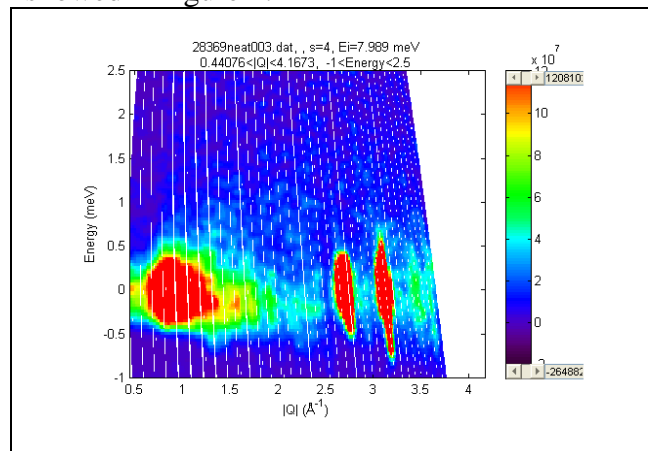


Fig. 2. Inelastic neutron scattering data measured on a powder sample. The data was collected on NEAT at 0.05 K and the incident energy was 7.989 meV. The intensity is in arbitrary units.

This measurement suggested that the magnetic structure is antiferromagnetic with an ordering wavevector of $k=0$. It also revealed the low energy scale of the system ~ 2 meV. We plan further measurements in the future using single crystals.

Reference:

- [1] H. Karunadasa et al. Phys. Rev. B **71**, 144414 (2005).
- [2] O. A. Petrenko et al. Phys. Rev. B **78**, 184410 (2008).

Neutron spin echo (NSE) measurements have been performed on polycrystalline $Tb_2Sn_2O_7$ at temperatures above and below the phase transition, $T_N = 0.87K$, to investigate the spin dynamics in the magnetically ordered state. These results show a distinct Q -dependence in the dynamics indicating a coexistence of static ferromagnetism and dynamically fluctuating spins present at 30 mK. The aim of this experiment was to investigate the Q -dependence of the spin dynamics of a 30g sample of $Tb_2Sn_2O_7$. This was loaded into a Cu sample can within a dilution cryostat. The spin echo spectrometer, SPAN, was calibrated with 4.5\AA neutrons and the three detector banks were moved during the experiment to cover the Q -range represented by the black bars in figure 1 below.

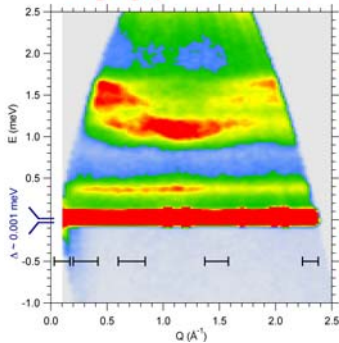
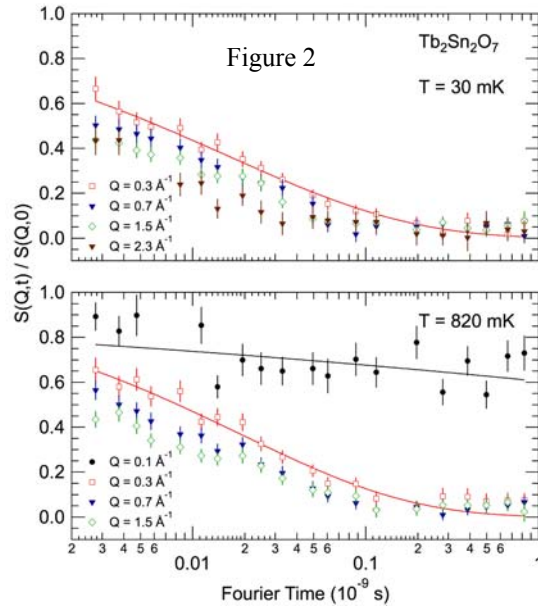


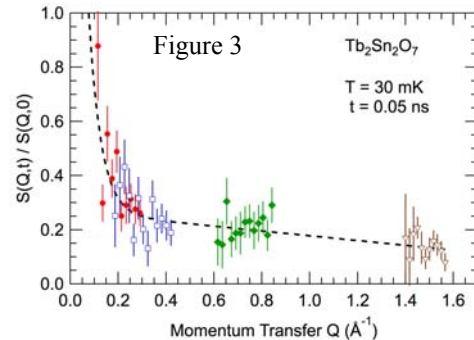
Fig. 1: Polarized TOF showing magnetic scattering from D7 at ILL. Black bars indicate the Q -space covered by SPAN. Care was taken to avoid magnetic Bragg peaks.

NSE results for the normalized intermediate scattering function, $S(Q,t)/S(Q,0)$, of $Tb_2Sn_2O_7$ are shown in figure 2 illustrating the temporal spin correlations at 30 mK and 820 mK. Groups of 7 detectors were binned together to give an average $|Q|$ as indicated in the figure. A data set at $|Q| = 2.3$ and $T = 820$ mK was omitted as it is virtually indistinguishable from data at lower $|Q|$ at this temperature. These measurements show that there is an initial, fast relaxation of the $S(Q,t)/S(Q,0)$ signal which occurs outside the time window of the NSE measurement (at $t < 2 \times 10^{-12}$ s), which is consistent with the observation of inelastic scattering due to CF transitions (figure 1). With the exception of the lowest Q , within the time window of our NSE measurements (2×10^{-12} s $< t < 1 \times 10^{-9}$ s) we see a full relaxation of the $S(Q,t)/S(Q,0)$ signal from $\sim 60\%$ of its $t = 0$ value to zero. For a phenomenological description, these data were

fitted with a stretched exponential function, $S(Q,t)/S(Q,0) = \exp[-(t/\tau)^\beta]$, to reveal a spin relaxation with a similar time scale to that observed in $Tb_2Ti_2O_7$ ².



The Q -dependence of the dynamics (figure 3) show that the static moments only contribute to the scattering at very low $|Q|$ (ferromagnetic forward scattering), and at the Bragg peaks.



These results highlight that $Tb_2Sn_2O_7$ contains static components to the magnetic moments which are responsible for the observed magnetic Bragg peaks, as well as dynamic components coexisting at the lowest temperatures.

¹ K. C. Rule et al., Phys. Rev. B 76, 212405 (2007).
² J.S. Gardner et al., Phys. Rev. B 68, 180401(R) (2003)

	EXPERIMENTAL REPORT Spin dynamics in the ordered state of the geometrically frustrated pyrochlore, Dy₂Ti₂O₇	Proposal: PHY-03-650-EF Instrument: V5 Local Contact: E. Moskvin
	Principal Proposer: Jonathan Morris, HZB Experimental Team: Kirrily Rule, HZB Evgeny Moskvin, HZB Alan Tennant, HZB	Date(s) of Experiment 10.07.2009 – 15.07.2009

Date of report: 20.07.2009

Spin-ice Dy₂Ti₂O₇ is a clean pyrochlore system which incorporates interesting physics. The spin diffusion rate is slow and metastable states have been observed below a Kagome ice region of the phase diagram. Our aim was to look at the spin dynamics via the quasi-elastic scattering at special points in Q-space, as determined previously with diffuse scattering from E2 (see figure 1). We also planned to utilise the polarised neutrons in V5 to look at simplified spin structure factors in the elastic data. From this we wished to determine whether our understanding of the E2 data, and the theory upon which it is based, is valid.

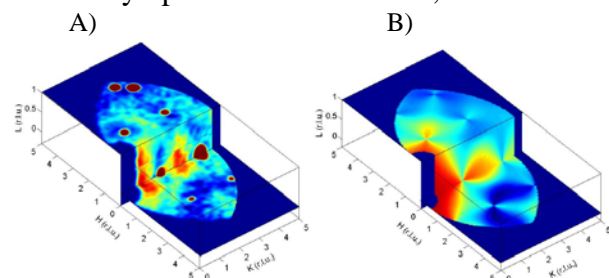


Figure 1: Three dimensional rendering of the dipolar correlations in reciprocal space (hkl) of spin ice at 0.7 K. A) Neutron diffraction data taken at 0.7 K and 0.0 T on E2, HZB, with the diffuse peaks at (003) and minima in (3/2 5/2 0) positions. B) Pinch points are found in the correlation functions and these are three dimensional in nature, with the diffuse scattering constricting at the reciprocal lattice point (200) and its equivalents. Diffuse peak and scattering minima positions agree with data.

The small single crystal of Dy₂Ti₂O₇ was mounted within a ³He-stick to achieve temperatures close to the spin freezing temperature of 0.6K. It was mounted such that the (H00) and (OK0) vectors were within the scattering plane.

The spin echo spectrometer, SPAN, was calibrated with 4.5Å neutrons and the three detector banks were moved during the experiment to cover the scattering angles required to observe the Bragg reflections (002) and (004) as well as the diffuse scattering region around the (003).

Care was taken to make sure that the sample was completely illuminated with neutrons. Unfortunately for the entire duration of this experiment, no nuclear Bragg reflections were observed which could have been due to numerous obstacles:

- The sample size was extremely small.
- The goniometers were only able to move $\pm 0.8^\circ$ in each direction.
- The Bragg peaks expected within the (HK0) plane were also extremely weak.

Thus after 5 days of optimizing the instrument and searching for Bragg reflections, we discovered that this experiment was not feasible on SPAN with the current configuration. Perhaps after checking the alignment of the sample again, and with computer control of the omega motor on SPAN this experiment may have been more successful.

NB – After removing the ³He-stick, we found that our sample had in fact fallen off the sample stick and broken in half. We believe this happened during height adjustments on the third day of the experiment.

	EXPERIMENTAL REPORT Inverse proximity effects at the superconductor-ferromagnet interface revealed by polarized neutron	Proposal: PHY-04-1705 Instrument: V6 Local Contact: A. Teichert
	Principal Proposer: Khaydukov Yu, FLNP, JINR, RU Experimental Team: Nagy, B., RMKI KFKI, HU Steitz, R., HZB Paul, A., HZB Wallacher, D., HZB	Date(s) of Experiment 18.05.2009 – 24.05.2009

Date of report: 17.12.2009

Experimental description

Sample – 8104B, nominal structure
 Cu(33nm)/V(40nm)/57Fe(1nm)/MgO
 Instrument – V6,
 Sample plane – horizontal
 Polarizer – magnetic mirror, polarization > 95%
 Analyzer – stack of mirrors, polarization >90%
 Detector – 2D PSD, area 190x190 mm²
 Neutron wavelength – 4.66 Å.
 Cryostat:
 Closed cycle cryostat, minimum temperature
 1.4K. Approximate time for cooling down to
 minimum and warming up to room temperature
 is 8-10 hours.

Short diary of the experiment

May 18

11.00 – Start of the cryostat installation
 17.55 – The cryostat has been installed.
 Search for the neutron reflection
 21.45 – Reflected beam has been found, start
 of the measurement of reflectivity curves in (+
 +) and (- -) in the region $\theta_1 = 0.01^\circ \div 2^\circ$ at
 magnetic field $H = 1$ kOe (current - 25 amps)
 applied parallel to the surface.

May 19

14.00. Scan has been finished. Specular beam
 is blocked at small incident angles (< 0.02°)
 was observed
 Beam stop has been moved out. Measurement
 has been repeated at small angles only.
 18.00. Cryostat with the sample has been
 rotated 90° along the axis perpendicular to
 beam path. Magnetic field of 2 kOe (50 Amps)
 has been applied for 1 min and then released.
 Cryostat rotated back. Check for the presence
 of reflected beam - measuring of reflectivity
 curves in guide field 20 ± 0.5 Gs.
 23.30. Measurement finished. Resolution is not
 enough for waveguide features (dip at (+ +)
 and (- -) and peak at (+ -) and (- +)). Adjusting
 S1 slit width's to increase resolution

May 20

01 15 Cooling's started. After cooling to helium
 temperature sample stick has been
 deformed and reflection has been lost.

Repeat procedure of reflection adjustment at
 small temperatures

May 21

11.15 At T=30K cryostat 90° rotated,
 magnetized for 2 min in field of ~ 1kOe, then
 released and rotated back.

16.00. Started measuring of (+ +) and (- +)
 reflectivity curves around the resonant peak (θ
 $\approx 0.2^\circ$) at temperatures 1.4K – 3.8K (step 0.2K)
 and 4.0K – 6K (step 0.5K)

May 22

Re-measure of T = 1.9K, T=2.4K and T =2.8K
 Before it, temperature has been set to T =30K
 and remagnetizing procedure has been done.

May 23 – May 24.

The measurements of reflectivity curves at T =
 1.6K, T = 2.6K and T = 4.5K. Last point later
 has been changed to T = 8K due to
 temperature jump.

Reflectivities has been measured at (+ +), (+ -
) and (- -) channels.

Main results

a) Reflectivity curves at T=1.6K, T=2.6K has
 been measured in big Q region. Shift of
 oscillations at spin asymmetry at change of
 temperature from T =1.6K and T =2.6K has
 been proven. Unfortunately reflectivity at T >
 Tc has not been finished due to reactor cycle
 end.

b) Temperature evolution of the spin flip
 resonance peak has been investigated.
 Previous result at ADAM reflectometer has
 been proven.

In addition, temperature evolution of diffuse
 scattering has been collected. However no
 significant change of it has been detected.

 HELMHOLTZ ZENTRUM BERLIN für Materialien und Energie NEUTRONS	EXPERIMENTAL REPORT Magnetization reversal in exchange coupled system with field perpendicular to the cooling field	Proposal: PHY-04-1803-EF Instrument: V6 Local Contact: A. Teichert
	Principal Proposer: Amitesh Paul, HZB Experimental Team: Amitesh Paul, HZB	Date(s) of Experiment 23.03.2009 – 29.03.2009

Date of report: 24.09.2009

In this experiment, we have shown, that for an exchange coupled Antiferro (AF)-Ferromagnetic (FM) system, we could directly manipulate the uncompensated moments in the AF - resulting in induced magnetism within the AF layer. This is done by applying an in-plane magnetic field perpendicular to the cooling field but the field being in the plane of the cooling field. The neutron measurements along the cooling field direction enabled us to investigate the new state of interface due to the application of a perpendicular field in a trained state of the specimen.

It was found that an in-plane magnetic field perpendicular to the cooling direction, does not restore the untrained state or the asymmetry in reversal, but only redefines the state of interface - inducing a FM order within the AF layer. Due to a modified state of interface, after application of the perpendicular field, the ratio of the rotational anisotropy and the unidirectional anisotropy is also expected to be redefined. The angular variation of the net magnetization, as deduced from the fits to the specular reflectivity patterns, indicates that the reversal mechanism is predominantly via the uniform way (rotational reversal).

This variation can also be seen following the SF (spin-flip) intensities at a particular Q value. The increase in signal during the second field cycling is greatly reduced after the perpendicular field cycling. Apparently, this reduction can be mistaken as an indication of reversal via non-uniform way. But a deeper insight into the reflectivity patterns reveals it to be otherwise. This is in contradiction to the claim of restoration of asymmetric reversal, as in that case, the magnetization in the decreasing branch should have been reversed via the non-uniform way. However, induced by perpendicular field cycling - the magnetism is owed to the plausible controlled rearrangements of AF moments at the interface which can have significant effects on the overall characteristics of the exchange coupling. This can therefore be regarded as

the basis in realizing the idea of interfacial engineering in exchange bias systems in a controlled way.

The induced magnetism within the AF layer is significantly interesting, as an external field could bring in rearrangements of uncompensated spins that were frozen while field cooling. In Figure 1 we show the comparative reflectivity profile for the specimen before and after the perpendicular field cycling. Fig. 1a shows the state when it is cooled at 4000 Oe and measured at 10K at 4000 Oe. Fig. 1b, on the other hand, shows the spectra after the induced magnetism has crept in within the AF layer, causing a significant change in its profile.

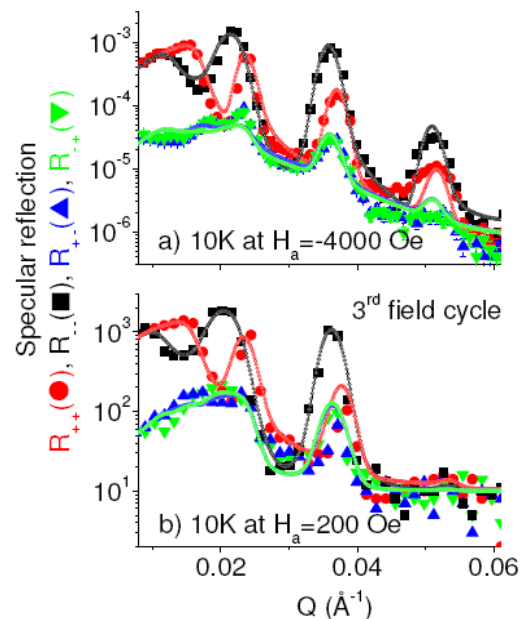


Fig. 1. a) Specular reflectivity patterns (solid symbols) along with their fits (open symbols) for the NSF [R_{++}] (red) and R_{--}] (black)] and SF [R_{-+}] (green) and R_{+-}] (blue)] channels measured from Co/CoO/Au ML at different conditions as indicated a) after cooling at +4.0-kOe and measured at negative saturation (10-K). b) This is followed by measuring after negative saturation and during the 3rd field cycle (after 90 degree field cycling) at $H_a=200$ -Oe. Solid symbols are data and open circles are fits to a model.

 HELMHOLTZ ZENTRUM BERLIN für Materialien und Energie NEUTRONS	EXPERIMENTAL REPORT	Proposal: PHY-04-1808-EF
	PNR study of a BiFeO₃ multiferroic film	Instrument: V6 Local Contact: A. Teichert
Principal Proposer: K. Temst & M.J. Van Bael – KU Leuven, B Experimental Team: J. Demeter – KU Leuven, B A. Teichert – HZB & KU Leuven, B R. Steitz – HZB	Date(s) of Experiment 03.04.2009 – 09.04.2009	

Date of report: 15.01.2010

Multiferroic BiFeO₃ films are gaining a lot of interest because of their magnetoelectrical properties, in which ferroelectricity and (anti)ferromagnetism are coexisting. As a consequence the magnetization can be switched by applying an electric field. The aim of this experiment was to study the magnetic properties of BiFeO₃ films by polarized neutron reflectometry (PNR). Based on results from a previous PNR study (PHY-04-1712-LT) on BiFeO₃ films, experiments were continued on films with an improved stoichiometry. Results of this previous PNR study showed ferromagnetic order in the film, indicated by a clear splitting between the uu- and dd- signal. The BiFeO₃ film measured in this experiment was prepared by a sol-gel method at UHasselt. X-ray diffraction and SQUID measurements were performed at KU Leuven to fully characterize the film. The thickness of the film was 80 nm and it had a polycrystalline structure. SQUID measurements indicated that the sample was ferromagnetic and that there was no difference between field cooling and zero-field cooling. The measurements were performed on the V6-instrument ($\lambda = 4.66 \text{ \AA}$), using a helium bath cryostat between 1.5 K and 55 K. The resolution of the instrument was 0.002 \AA^{-1} .

A series of reflectivity scans was performed at different temperatures. First, the sample was cooled down to 1.5 K without an applied field. The sample was measured in the demagnetized state, at saturation and at remanence. In none of these cases a splitting between non-spin flip neutrons (uu and dd) was observed. Secondly, the sample was cooled down to 1.5 K in saturation, at 3700 Oe. The sample was consecutively measured at 1.5 K, 12 K, 35 K and 55 K, each time in saturation. These reflectivity scans neither showed any splitting between the uu- and dd-signal, similar as after the zero-field cooling. The previous PNR-experiments did show a clear splitting between uu and dd signal at 12 K, where this was not observed for this film.

Nevertheless, the preparation method and characteristics of this film were comparable to the previous one. Despite this inconsistency with previous measurements, the reflectivity measurements will be fitted in detail to extract the structural depth profile.

In conclusion, the PNR study of BiFeO₃, prepared by a sol-gel method, could not give a clear indication for ferromagnetism in the film. Reasons can be an incorrect stoichiometry of the film or a different origin of the ferromagnetic signal observed in the SQUID measurements. Another possible cause can be an incorrect position of the temperature sensor inside the cryostat. A more definite installation of the sensor close to sample could lead to an improvement in the temperature read-out.

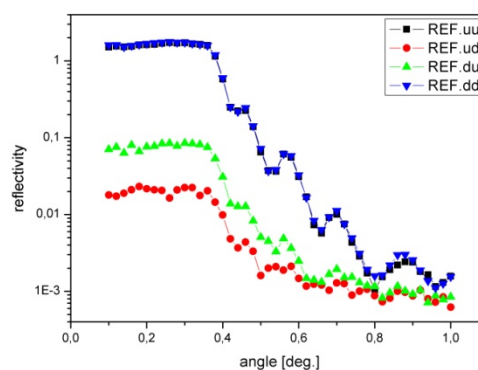


Fig. 1: Reflectivity measurement of the sample at 12K after field cooling. No clear splitting between uu- and dd- signal is observed.

In cooperation Agreement between KU Leuven and HZB

	EXPERIMENTAL REPORT	Proposal: PHY-04-1894-LT
	Simultaneous measurement of PNR and AMR on exchange bias Co/CoO bilayer	Instrument: V6 Local Contact: A. Teichert
Principal Proposer: Experimental Team:	A. Teichert, HZB & KU Leuven, B J. Demeter, KU Leuven, B D. Paramanik, KU Leuven, B A. Teichert, HZB & KU Leuven, B K. Kiefer, HZB	Date(s) of Experiment 14.09.2009 – 21.09.2009

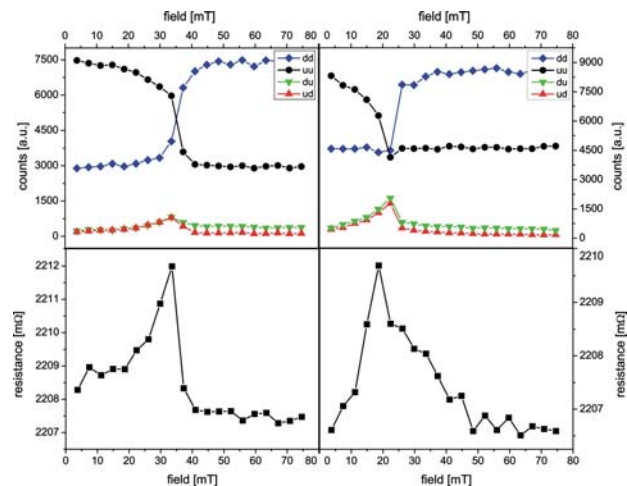
Date of report: 06.01.2010

The aim of this experiment was to study the feasibility of performing Polarized Neutron Reflectometry (PNR) simultaneously with Anisotropic Magnetoresistance (AMR) measurements on the V6 instrument. This method gives the possibility of using two independent techniques, which provide complementary information, on one single sample in exactly the same conditions. Moreover the use of an electrical transport measurement technique during a neutron scattering experiment can act as a 'diagnostics tool'. This technical development was first applied on a system where the use of these two techniques has an important scientific interest. Both PNR [1] and AMR [2] have been used in the past to study the magnetization reversal mechanism in exchange bias (EB) bilayers, but were never measured simultaneously.

The measurements were performed on a Co/CoO EB bilayer. This MBE-grown thin film consisted of a 50 nm Co layer, grown with a 45 nm thick Cu buffer, on a Si(100) substrate. The Co-layer was subsequently oxidised in a reduced oxygen atmosphere to form a 3 nm thick CoO layer at the surface. This configuration was also of particular interest since it acts as a reference for a previous PNR study performed on the V6-instrument (PHY-04-1720-LT). Magnetic and structural characterisations of the sample were performed in advance by respectively SQUID and XRD/XRR. UV lithography was used to form a narrow current path on the side of the sample to measure the resistance. This part of the sample was shielded from the neutron beam.

First of all *specular reflectivity measurements* were performed at specific magnetic fields. These measurements show interesting features and will be fitted in detail to reveal the magnetic depth profile. Secondly *magnetic field scans* were performed in which the reflectivity was measured at well-chosen

scattering angles, while varying the magnetic field. During these measurements we simultaneously performed the AMR measurements. The successful performance of these measurements shows the feasibility of this method and extends the possibilities of the V6 instrument. The crossing of the uu- and dd-signal corresponds with the peak in the AMR-measurements, both indicating the coercive field. Both the PNR and AMR measurements indicate a change in the magnetisation reversal mechanism, occurring during the consecutive branches: the contribution of coherent rotation increases. This is observed by an increasing du- and ud- signal in the PNR measurements and an increasing peak height in the AMR-signal. These findings agree with knowledge from literature on similar Co/CoO bilayers [1,2].



- [1] F. Radu, *et. al.*, Phys. Rev. B **67**, 134409 (2003)
 [2] S. Brems, *et. al.*, Phys. Rev. Lett. **95**, 157202 (2005)

In Cooperation Agreement between KU Leuven and HZ Berlin

	EXPERIMENTAL REPORT Probing Magnetic Reversal Behavior of Exchange-biased NiFe/FeMn, FeMn/CoFe bilayer and NiFe/FeMn/CoFe Trilayers with Specular Polarized Neutron Reflectivity	Proposal: PHY-04-1907 Instrument: V6 Local Contact: A. Teichert
Principal Proposer: Experimental Team:	Ki-Yeon Kim, KAERI, Republic of Korea Hyeok-Cheol Choi, Inha University, Republic of Korea Chun-Yeol You, Inha University, Republic of Korea Jeong-Soo Lee, KAERI, Republic of Korea A. Teichert, HZB, R. Steitz, HZB	Date(s) of Experiment 12.08.2009 – 18.08.2009

Date of report: 07.12.2009

Exchange bias (EB) effect is originated from the exchange coupling at the interface between ferromagnet (F) and antiferromagnet (AF) in F/AF bilayers or multilayers. It brings about the shift of magnetic hysteresis loops along the origin, that is, exchange bias field along with the increased coercivity. Although EB effect has been considered to be the interfacial effect, recent experimental reports put this into question. In this connection, we recently investigated the magnetization reversal behaviour due to the EB at F/AF interface in 30-nm NiFe/ t_{AF} -nm FeMn/30-nm CoFe trilayer (t_{AF} :0~30) as well as 30-nm (NiFe, CoFe)/15-nm FeMn bilayers grown on optically transparent substrate by measuring the longitudinal and transverse magneto-optic Kerr (MOKE) hysteresis loop from each F layer. We witnessed that EB at two neighbouring F/AF interfaces in NiFe/FeMn/CoFe trilayers considerably affects magnetic reversal behaviour of the adjacent layer across the FeMn thickness as thick as 15 nm.

Polarized neutron reflectivity (PNR) has proven to be very useful of distinguishing between different magnetization reversal behaviours in magnetic thin films and multilayers via non-spin flip (R^{++} , R^{-}) and spin flip (R^{+} , R^{+-}) reflectivities, where first (second) superscript denote spin polarization direction of incident (reflected) neutrons and +(-) denote the spin-up (spin-down) of the neutrons. We carried out the PNR experiment on 3 different magnetic thin films such as (30-nm NiFe/15 nm FeMn), (15-nm FeMn/30-nm CoFe) bilayers and (30-nm NiFe/15-nm FeMn/30-nm CoFe) trilayers for 7 days. One of experimental results is shown in Figure 1. Apart from non-spin flip intensity variation, any spin flip intensity at both coercivities is not observed in CoFe/FeMn bilayer, indicating that magnetization reversal takes place through nucleation and domain wall motion. Meanwhile, spin-flip reflectivities at both coercivities are

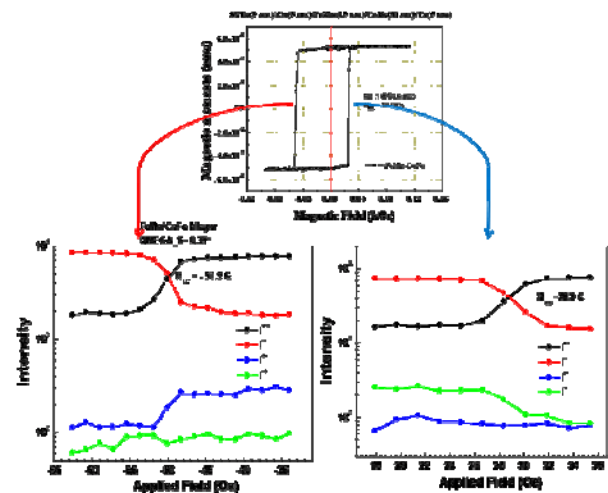


Figure 1. The upper figure is the magnetic hysteresis loop of 15-nm FeMn/30-nm CoFe bilayer. The lower two figures are the non-spin flip (I^{++} , I^{-}) and spin flip (I^{+-} , I^{+}) neutron intensity as a function of an applied field at left (red arrow, left figure) and right coercivities (blue arrow, right figure). I^{++} (black line), I^{+-} (blue line), I^{+} (green line), I^{-} (red line) are displayed in the graph.

pronounced in NiFe/FeMn bilayer. This means that magnetization reversal occurs via the magnetic rotation. Interestingly enough, it is found that spin flip intensities exist at both left and right coercivities of a corresponding NiFe/FeMn/CoFe trilayer. This tells us that CoFe layer as well as NiFe layers exhibit the similar magnetization reversal behaviour accompanying magnetic rotation. We can conclude that PNR experiment results corroborate MOKE experiment results. Therefore, we clearly observed the interlayer exchange bias coupling between two F layers across a thick AF layer in F/AF/F trilayers by measuring magnetization reversal behaviour with a combination of MOKE and PNR experiments. In addition, we present the novel approach to study the interlayer exchange bias coupling via magnetization reversal other than exchange bias field and coercivity.

	EXPERIMENTAL REPORT Curie temperature mapping by polarised neutron imaging	Proposal: EF Instrument: V7 Local Contact: N. Kardjilov
	Principal Proposer: M. Strobl, Uni Heidelberg and HZB Experimental Team: K. Rolfs, M. Chmielus HZB A. Hilger, HZB N. Kardjilov, HZB I. Manke, HZB	Date(s) of Experiment 20.12.2009 – 21.12.2009

Date of report: 21.01.2010

Magnetic shape memory alloys (MSMA) single crystals tend to deform up to 10% in a magnetic field. The magnetic field-induced strain (MFIS) strongly depends on composition, crystal structure, crystal quality, and training [1]. Therefore a homogeneous distribution of the elements (Ni, Mn, Ga and Co) over the crystal volume is essential. One indicator for a possible composition change within the samples is the Curie temperature, which strongly depends on the content of Ni and Co. Using polarized neutrons, it is now possible to investigate the Curie temperature distribution within massive samples non destructively with three dimensional resolution [2]. The sample is imaged with a polarized incident neutron beam. The final polarisation is analysed in front of the imaging detector. Consequently the depolarisation can be measured spatially resolved. As long as the sample is in the ferromagnetic state the magnetic domains depolarize the beam and hence add significantly to the attenuation signal. A series of images will be recorded for each sample at different temperatures around the Curie temperature T_c . When the sample, respectively a sample region, becomes paramagnetic the beam polarisation is not further affected and hence the transmission at the analyser increases. Using this technique of T_c mapping different Ni-Co-Mn-Ga MSMA crystals and growth techniques shall be investigated in upcoming experiments. Here we have performed a feasibility study using 4 small crystals and were able to observe the phase transition with spatial resolution (Fig. 1).

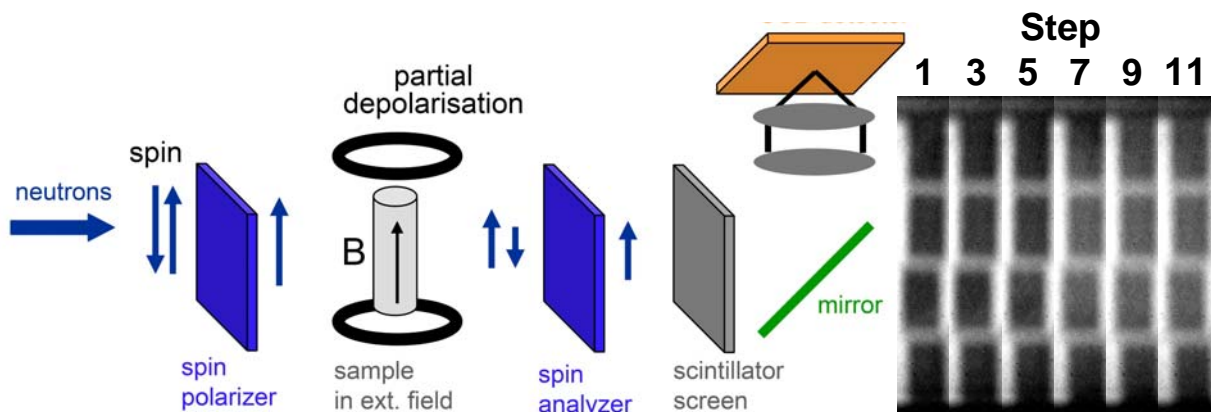
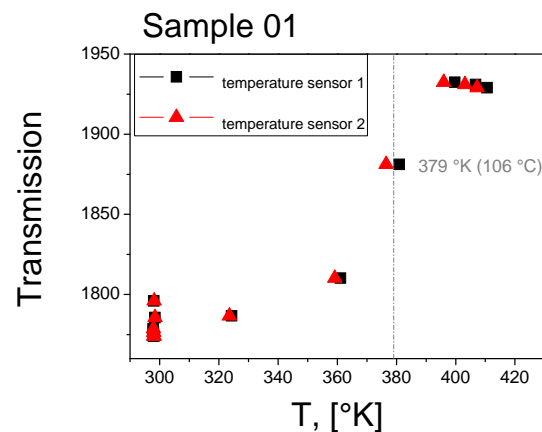
Fig. 1 Imaging set-up and results for selected temperature steps

The temperature resolution was not yet sufficient but spatial differences of the Curie temperature could be visualised (Fig. 1 and 2) produced using two different single crystal growth techniques.

Fig. 2 Temperature dependent transmission

References

- [1] Chmielus, M. et al., Eur. Phys. J. (2008)
- [2] N. Kardjilov et al. Nat. Phys. 4 (2008)



Structure

	EXPERIMENTAL REPORT	Proposal: PHY-01-2584 PHY-01-2601
	Phase transformations in nanoparticles of NaNO₃	Instrument: E2, E9 Local Contact: M. Tovar, I. Glavatskyi
Principal Proposer:	E. Rysiakiewicz-Pasek, Institute of Physics, Wroclaw, Poland	Date(s) of Experiment
Experimental Team:	A. Naberezhnov, Ioffe Phys. – Tech. Institute, Russia R. Popravski, Institute of Physics, Wroclaw, Poland M. Tovar, I. Glavatskyi, HZB	17.09.2009 – 21.09.2009 18.11.2009 – 23.11.2009

Date of report: 28.12.2009

NaNO₃ undergoes orientational order-disorder PT at 549 K and melts at ~580 K. Earlier the melting-freezing transition for sodium nitrate embedded into porous glasses with pore radii 2.5, 5, 10 and 20 nm has been studied by differential scanning microscopy and Raman spectroscopy [1]. For NaNO₃ within 2.5 nm pores no melting transition has been observed and the authors have suggested that NaNO₃ within these porous glasses exists as disordered aggregates. Within glasses with 2.5 < r_p < 20 nm NaNO₃ exists in a new phase stabilized by surface OH groups of the porous silica. However the study of temperature evolution of structure of these confined materials has not been carried out. In our samples we have avoided the influence of absorbed OH radicals and studied the “pure” confined material. We have studied the temperature evolution of structure of NaNO₃, embedded into porous glasses with pore diameters 320, 46 and 7 nm, on powder diffractometers E2 (λ=2.38 Å) and E9 (λ=1.79 Å). The diffraction patterns for the bulk NaNO₃ and sodium nitrate within 320 and 7 nm glasses at room temperature are presented in Fig.1.

The principle results are:

1 – For all samples the crystal structure corresponds to the structure of sodium nitrate.

We did not observe any new phase for NaNO₃ within 7 nm porous glasses.

2 – The melting temperatures decrease on 15 degrees for 320 nm glasses and on 50 K (down to ~530 K) for NaNO₃ within 7 nm glasses.

3 – Sodium nitrate within 320 nm glasses is textured strongly and there are the visible stresses.

4 – The temperatures of order-disorder phase transition decrease on decreasing of pore diameters (from ~10 K for 320 nm to ~25 K for 7 nm).

5 – The amplitudes of thermal motion of constituent ions for NaNO₃ within 46 and 7 nm glasses are essentially larger than in the bulk.

[1] R. Mu, F. Jin, S.H. Morgan et al., J. Chem. Phys 100, 7749 (1994)

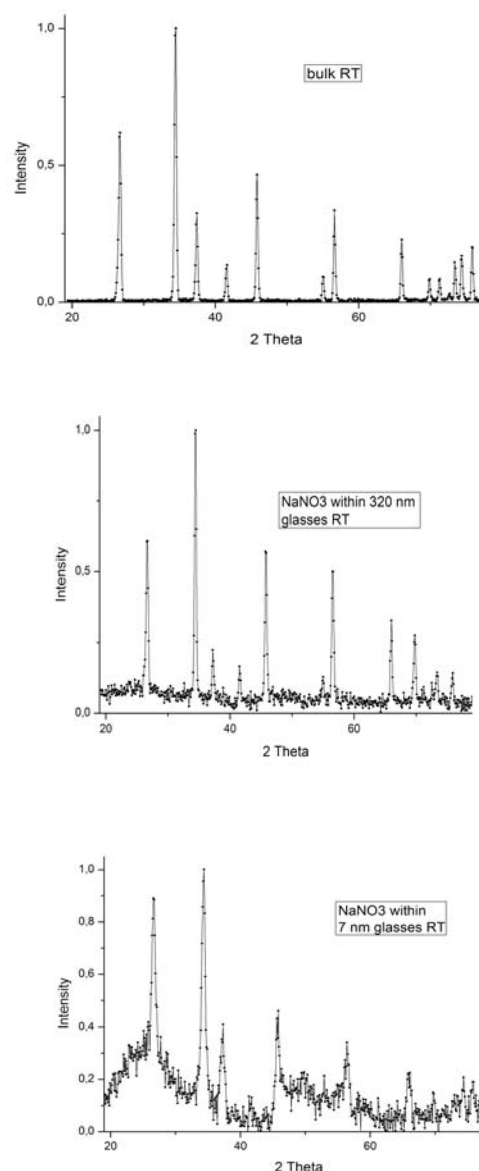


Fig.1

This research project has been supported by the European Commission under the 7th Framework Programme through “Research Infrastructures” action of the “Capacities” Programme, contract number CP-CSA_INFRA-2008-1.1.1. Number 226507-NM13

 Neutrons	EXPERIMENTAL REPORT	Proposal: EF
	Structural and magnetic properties of FeTe_xSe_{1-x}	Instrument: E5 Local Contact: M. Reehuis
Principal Proposer: D. Argyriou, HZB Experimental Team: S. Kimber, HZB M. Reehuis, HZB		Date(s) of Experiment 19.10.2009 – 01.11.2009

Date of report: 20.11.2009

At room temperature FeTe and the doped compounds FeTe_xSe_{1-x} crystallize in the tetragonal space group *P4/nmm* [1]. In the present work we have investigated the crystal structure of FeTe_{0.93}Se_{0.07} using a plate-like single crystal with the dimensions 10.5 × 5.5 × 1.3 mm³. Neutron diffraction experiments were carried out on the 4-circle diffractometer E5 of the BER II reactor at the Helmholtz-Zentrum Berlin, which uses a Cu-monochromator selecting the neutron wavelength $\lambda = 0.896$ Å. A full data set of FeTe_{0.93}Se_{0.07} [922 (195 unique) reflections] has been collected. The refinement of the crystal structure was carried out with the program *Xtal* 3.4. [2]. The crystal structure of this compound could be successfully refined in the space group *P4/nmm* resulting in the residuals $R_F = 0.079$ and $R_w = 0.063$, respectively. In this structure type the Fe-atoms are located in the Wyckoff position $2a(\frac{1}{2}, \frac{1}{4}, 0)$ and the Te/Se-atoms in $2c(\frac{1}{4}, \frac{1}{4}, z)$, respectively. A difference-fourier synthesis clearly showed one additional density peak at the same Wyckoff position $2c(\frac{1}{4}, \frac{1}{4}, z)$ as found for the Te/Se-atoms, but with a large Δz of 0.4374. In agreement with Ref. [1] we assumed that an additional content of iron (Fe2) occupies this position. The refinement of *occ*(Fe2) finally resulted in a considerable improvement of the refinements resulting in the residuals $R_F = 0.060$ and $R_w = 0.042$, respectively. But this position only shows an occupancy of 5.1(3) %. Recently, occupancies of 8.8(4) % and 5.4(5) % were found for the compounds FeTe_{0.416}Se_{0.584} and FeTe_{0.493}Se_{0.507}, respectively [1]. The results of our refinements are given in Table 1.

At lower temperature the crystal structure of FeTe_xSe_{1-x} ($0 \leq x \leq 0.09$) changes spontaneously to a monoclinic structure with the space group *P2₁/m*, where the monoclinic *b*-axis is significantly smaller than the *a*-axis. The angle between the *a*- and *c*-axes (monoclinic plane) is slightly smaller than 90°. Below the structural phase transition a second magnetic transition occurs, indicating the onset of magnetic ordering of the Fe-sublattice. A collinear antiferromagnetic with a propagation vector $\mathbf{k} = (\frac{1}{2}, 0, \frac{1}{2})_M$ was observed earlier, where the Fe-spins are aligned parallel to the monoclinic *b*-axis [1]. The tetragonal-monoclinic structural transition gives rise to two domains in the *ab*-plane occupying equal volume fractions. Therefore we have observed both reflections the $(\frac{1}{2}, 0, \frac{1}{2})_M$ and $(0, \frac{1}{2}, \frac{1}{2})_M$, respectively. Magnetic reflections have been collected on E5 using the larger neutron wavelength $\lambda = 2.38$ Å (PG-monochr.). For our studies we also used single crystals of FeTe_xSe_{1-x}. ($x = 0.05, 0.06, 0.08, 0.09$) with dimensions similar to those of FeTe_{0.93}Se_{0.07}. With the knowledge of the magnetic structure we were able to deduce the magnetic moments of the Fe-atoms in the system FeTe_xSe_{1-x}. The *T*-dependence of the magnetic moments of the different samples is shown in Fig. 1. It can be seen that both the magnetic moments of the Fe-atoms as well

as the Néel-temperatures are strongly decreasing with a doping level from $x = 0.05$ up to $x = 0.09$.

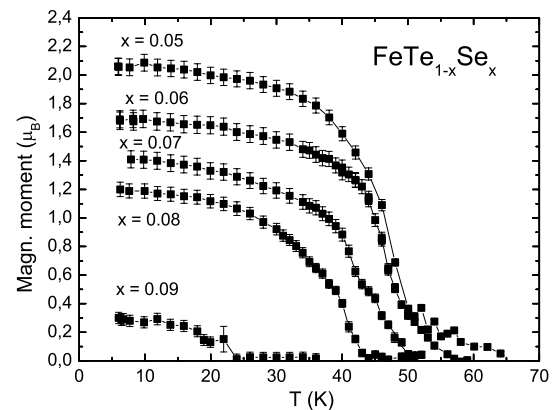


Fig. 1. *T*-dependence of the magnetic peak $(\frac{1}{2}, 0, \frac{1}{2})_M$ of FeTe_xSe_{1-x} ($0.05 \leq x \leq 0.09$).

Table 1

Results of the single-crystal neutron diffraction study of FeTe_{0.93}Se_{0.07} at 295 K. The thermal parameters U_{ij} are in the form $\exp[-2\pi^2(U_{11} h^2 a^{*2} + \dots + 2U_{13} hla^*c^*)]$. For symmetry reasons all values U_{12} and U_{23} as well as the values U_{13} of the Fe- and Te/Se-atoms are equal to zero in this structure. The shortest interatomic distances ($d \leq 3.0$ Å) between the Fe- and Te/Se-atoms are also listed.

<i>P4/nmm</i> (No. 129)	FeTe _{0.93} Se _{0.07} , 295K
<i>a</i> [Å]	3.8127(9)
<i>b</i> [Å]	6.2556(16)
<i>V</i> [Å ³]	90.94(5)
<i>z</i> (Te/Se)	0.2778(3)
<i>z</i> (Fe2)	0.715(3)
<i>occ</i> (Fe2)	0.051(3)
$U_{11}(\text{Fe1}) = U_{22}(\text{Fe1})$ [100 Å ²]	1.78(3)
$U_{33}(\text{Fe1})$ [100 Å ²]	2.31(4)
$U_{11}(\text{Te/Se}) = U_{22}(\text{Te/Se})$ [100 Å ²]	1.74(5)
$U_{33}(\text{Te/Se})$ [100 Å ²]	2.61(7)
$d(\text{Fe1}-\text{Te/Se}) \times 4$ [Å]	2.5796(13)
$d(\text{Fe2}-\text{Te/Se}) \times 4$ [Å]	2.6963(5)
$d(\text{Fe2}-\text{Te/Se}) \times 1$ [Å]	2.736(19)

References

- [1] S. Li, C. de la Cruz, Q. Huang, Y. Chen, J.W. Lynn, J. Hu, Y.-L. Huang, F.-C. Hsu, K.-W. Yeh, M.-K. Wu, P. Dai, *Phys. Rev. B* 79 (2009) 054503.
- [2] S. R. Hall, G S D King, and J. M. Stewart, Eds., *Xtal* 3.4 User's Manual. University of Australia: Lamb, Perth (1995).

	EXPERIMENTAL REPORT	Proposal: PHY-01-2644-EF
	Determination of the crystal structure of Cs₂NaAlF₆ doped with Chromium	Instrument: E5 Local Contact: Manfred Reehuis
Principal Proposer: Experimental Team:	Heloisa N. Bordallo, HZB Sandra da Silva Pedro, UERJ, BR Fabiano Yokaichiya, HZB Lilian P. Sosman, UERJ, BR Heloisa N. Bordallo, HZB	Date(s) of Experiment 09.11.2009 – 20.11.2009

Date of report: 15.01.2010

Cs₂NaAlF₆ is a perovskite related compound belonging to the A₂BMX₆ family of materials, where A, B and M are metal cations or more complex molecular ions and X is a halogen anion or an oxygen atom. These minerals have been classified as part of the elpasolites group. In doped elpasolites the physical properties are related to point defects that arise during the compound's formation process by the insertion of interstitial impurities into the host lattice [1].

In this report we present the results of our neutron single crystal results on Cs₂NaAlF₆:Cr³⁺. Based on SQUID results magnetic fluctuations were clearly observed in samples with high Cr³⁺ content [2]. The main objective of this experiment was to obtain additional information on the crystalline structure as well as completely new results on the magnetic properties for these samples.

A total of 141 (54 unique) reflections been collected on Cs₂NaAlF₆:50% Cr³⁺ at 100 K. using the instrument E5 with a neutron wavelength $\lambda = 2.38 \text{ \AA}$. The crystal structure was refined with the program FullProf. Initial refinements were made based on the structural information previously obtained at 300 K for the same sample but with lower concentration [3].

Our results indicate that either the sample with 50% Cr³⁺ does not crystallize in the $R\bar{3}m$ space group or that the lattice parameters are very different from the ones found in the literature [3, 4, 5]. As shown in Figure 1, where the observed structure factor is plotted against the calculated, the experimental points do not follow in the line indicating that the refinement is not converging.

In order solve the structure it is crucial to conduct a new measurement of neutron diffraction in this sample at room temperature with a better accuracy.

However, our second question related to magnetic response of the crystalline lattice could be partially answered. Based on these results no changes in the structure that would suggest the development of long range magnetic structure could be observed between 300K and 100K.

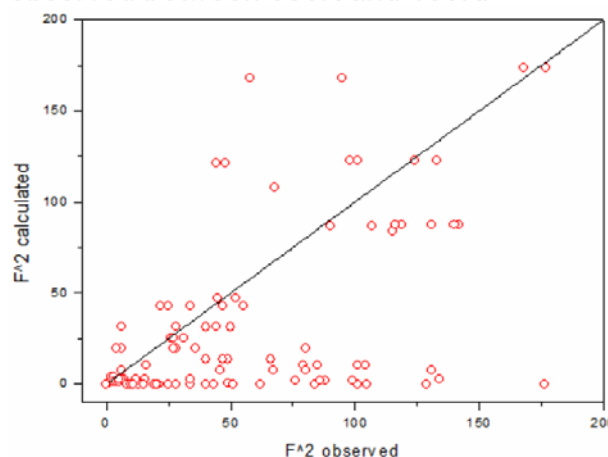


Figure 1: Observed vs Calculated structure factor for Cs₂NaAlF₆:50% Cr³⁺. The graph shows that the refinement is not converging.

[1] Henderson B and Imbusch G F 1989 *Optical Spectroscopy of Inorganic Solids* (Oxford: Clarendon) and references therein.

[2] L. P. Sosman et al, JMMM **2009**, 321, 2210

[3] H. N. Bordallo et al, J. Chem. Phys. **2001**, 115, 4300

[4] H. N. Bordallo et al, J. Phys: Condens. Matter **2002**, 14, 12383

[5] A. C. Doriguetto et al, J. Chem. Phys. **2004**, 121, 3184.

**X-ray and neutron diffraction study
of arrojadite**

Proposal: MAT-01-2648

Instrument: **E5**

Local Contact:
Manfred Reehuis

Principal Proposer: C. Kallfaß, C. Hoch, H. Schier, MPI Stuttgart
H. Schubert, TU Berlin, M. Reehuis, HZB
Experimental Team: M. Reehuis, HZB

Date(s) of Experiment

01.07.2009 – 26.07.2009

Date of report: 26.08.2009

The crystal structure of the manganese and iron containing mineral arrojadite is complex, and has been the centre of interest by several independent research groups during the last 30 years [1-3]. In the present work we have investigated the crystal structure of arrojadite by X-ray and neutron diffraction, where a lithium enriched sample was used.

Single-crystal neutron diffraction data of arrojadite have been collected at 300 K on the four-circle diffractometer E5. Using the neutron wavelength $\lambda = 0.8839 \text{ \AA}$ (Cu-monochr.) a total of 2176 (662 unique) reflections was measured. The crystal structure of arrojadite could be successfully refined in the space group $C2/c$. In our X-ray study we were able to measure a much larger number of 5379 unique reflections. Consequently the refined positional and thermal parameters here reached a much better accuracy. But it could be seen that the refined parameters are in a very good agreement. Therefore for the refinement of the neutron data we have used the fixed positional and thermal parameters and only the overall scale factor and the occupancies of the metal atoms were allowed to vary. Table 1 shows that especially the occupancies of the Fe- and Mn-atoms could be well determined from our neutron diffraction study. Further the position of one H-atom has been precisely determined. But not any new position could be detected for the Li^+ -ions. However the refinements showed that Li^+ -ions possibly occupy the positions of the Na-, K- and Cr1-sites, respectively.

Tab. 1: Results of the different refinements of single-crystal data (X-ray and neutron) of arrojadite.

	Parameters			X-ray data		ND data	
	x	y	z	element	Occ.	element	occ.
Na1	0	0	0	Na	1.0	Na	1.0
Na2	0.13390	0.48530	0.11940	Na	1.0	Na Li	0.9607 0.0393
K1	0	0.49620	1/4	K	1.0	K	1.0
K2	0	0.33390	1/4	K	0.2129	K Li	0.4773 0.5227
Mn1	0.20448	0.30069	0.35175	Mn	1.0	Mn Fe	0.7268 0.2732
Mn2	0.28068	0.20576	0.15669	Mn	1.0	Mn Fe	0.7540 0.2460
Mn3	0.28728	0.49229	0.23232	Mn	1.0	Mn Fe	0.3412 0.6588
Fe4	0.10679	0.01421	0.63925	Fe	1.0	Fe Mn	0.8749 0.1251
Fe5	0.03349	0.25655	0.40052	Fe	1.0	Fe Mn	0.9844 0.0156
Fe6	0.47775	0.25053	0.09635	Fe	1.0	Fe Mn	0.9180 0.0820
Fe7	0.21878	0.09530	0.47164	Fe	0.7644	Fe	0.5454

						Mn	0.4546
Al1	0	1/2	0	Al	1.0	Al	1.0
Cr1	0.26856	0.27854	0.01563	Cr	0.5	Al Li	0.5621 0.4379
P1	0.12588	0.25146	0.53842	P	1.0	P	1.0
O11	0.59467	0.10480	0.03610	O	1.0	O	1.0
O12	0.08478	0.16660	0.57459	O	1.0	O	1.0
O13	0.27815	0.24800	0.43761	O	1.0	O	1.0
O14	0.10697	0.18990	0.47949	O	1.0	O	1.0
P2	0.13043	0.27542	0.21144	P	1.0	P	1.0
O21	0.13970	0.12440	0.20834	O	1.0	O	1.0
O22	0.13150	0.32040	0.27000	O	1.0	O	1.0
O23	0.20429	0.33990	0.19366	O	1.0	O	1.0
O24	0.04880	0.32050	0.17050	O	1.0	O	1.0
P3	0.35711	0.20346	0.29534	P	1.0	P	1.0
O31	0.28520	0.14620	0.31799	O	1.0	O	1.0
O32	0.35010	0.35560	0.29500	O	1.0	O	1.0
O33	0.34860	0.15060	0.23673	O	1.0	O	1.0
O34	0.44180	0.16100	0.33473	O	1.0	O	1.0
P4	0.10272	0.23270	0.04721	P	1.0	P	1.0
O41	0.40350	0.31370	0.01237	O	1.0	O	1.0
O42	0.19365	0.26370	0.07686	O	1.0	O	1.0
O43	0.04673	0.35750	0.04795	O	1.0	O	1.0
O44	0.06634	0.12880	0.07952	O	1.0	O	1.0
P5	0.36993	0.03318	0.07556	P	1.0	P	1.0
O51	0.29017	0.03780	0.02677	O	1.0	O	1.0
O52	0.37140	0.15510	0.11369	O	1.0	O	1.0
O53	0.44968	0.05600	0.05526	O	1.0	O	1.0
O54	0.12124	0.40220	0.39257	O	1.0	O	1.0
P61	0.3853	0.49081	0.13219	P	0.6425	P	0.6987
P62	0.08180	0.00590	0.33720	P	0.3575	P	0.3013
O61	0.38832	0.64040	0.13637	O	1.0	O	1.0
O62	0.02463	- 0.06130	0.36725	O	1.0	O	1.0
O63	0.35740	0.42310	0.17818	O	1.0	O	1.0
O614	0.31980	0.45390	0.07790	O	0.6425	O	0.6987
O624	0	- 0.15270	1/4	O	0.3575	O	0.3013
O7	0.23126	- 0.00130	0.13780	O	1.0	O F	0.4949 0.5051
H1	0.22240	0	0.09000			H	0.4949

- [1] Krutik et al, *Kristallografiya* **24** (1979), 743.
[2] Merlino et. al, *Acta Cryst. B* **37** (1981), 1733.
[3] Moore et al., *Am. Mineral.* **66** (1981) 1034.

	EXPERIMENTAL REPORT Thermal variation of structural parameters in the cubic phase of MgV₂O₄	Proposal: PHY-01-2649-EF Instrument: E5 Local Contact: M. Reehuis
	Principal Proposer: E. Wheeler, HZB Experimental Team: M. Reehuis, HZB E. Wheeler, HZB B. Lake, HZB N. Islam, HZB	Date(s) of Experiment 20.11.2009 – 29.11.2009 07.12.2009 – 15.12.2009

Date of report: 02.01.2010

Recently we found that cubic MgV₂O₄ crystallizes in the space group $F\bar{4}3m$ [1] and not in the higher-symmetric one with the space group $Fd\bar{3}m$ as given earlier [2, 3]. Due to the fact that we clearly found weak intensities at the positions of forbidden reflections 200, 600, 420, 820 the d -glide plane symmetry is violated. In the present study we have investigated in detail the cubic crystal structure in the temperature range between 100 K and 700 K. Single-crystal diffraction data have been collected on the four-circle diffractometer E5 using the neutron wavelength $\lambda = 0.89 \text{ \AA}$. For the experiment we have used a high-quality single crystal of MgV₂O₄ with the dimensions $5.3 \times 5.9 \times 6.1 \text{ mm}^3$. In order to see changes in the crystal structure we first measured the T -dependence of the strong reflection 222 as well as the T -dependence of the 020 reflection which is forbidden in $Fd\bar{3}m$. In Fig. 1 it can be seen that a spontaneous change of intensity sets in at the structural phase transition at $T_S = 60 \text{ K}$ (from the cubic to tetragonal phase) and the Néel temperature $T_N = 38 \text{ K}$ (magnetic order of the V-moments). Above T_S the intensities of both reflections 222 and 020 show a smooth decrease up to 600 K and 700 K, respectively. Further it can be seen that the intensity of the 020 does not vanish up to the highest temperature of 700 K.

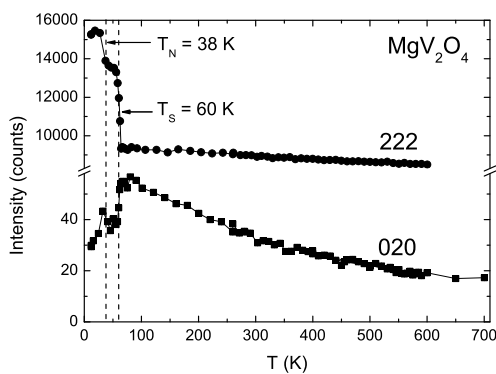


Fig. 1. T -dependence of the intensities of the reflections 022 and 020 of MgV₂O₄.

In order to find systematic changes of structural parameters in the cubic phase of MgV₂O₄ we have collected full data sets of Bragg reflections at 100 K (1046 122 unique), 300 K (984, 121 unique) and 600 K (643, 118 unique). Structure refinements were carried out in space group $F\bar{4}3m$, where two different Mg1 and Mg2 atoms are located at the Wyckoff positions $4a(0,0,0)$ and $4c(\frac{1}{4},\frac{1}{4},\frac{1}{4})$; the V-, O1- and O2-atoms at the

position $16e$. The refinement of the overall scale factor and the positional and anisotropic thermal parameters resulted in satisfactory residuals $R_F = 0.031$ ($R_w = 0.032$) at 100 K, $R_F = 0.028$ ($R_w = 0.037$) at 300 K, and $R_F = 0.018$ ($R_w = 0.025$) at 600 K, respectively. The results of the refinements are presented in Table 1. It can be seen that the two different metal-O-bond distances show a large discrepancy at 100 K. With increasing temperature these two values become more and more similar. The T -dependence of the reflection 020 (Fig. 1) shows that this reflection possibly disappears at about 900 K. Then the crystal structure can be refined in the higher-symmetric space group $Fd\bar{3}m$, where the two bond distances are due to symmetry reasons exactly the same.

Table 1

Results of the single-crystal neutron diffraction study of MgV₂O₄ at different temperatures. The crystal structure has been refined in the space group $F\bar{4}3m$. The thermal parameters U_{ij} (given in 100 \AA^2) are in the form $\exp[-2\pi^2(U_{11}h^2a^{*2} + \dots + 2U_{13}hla^*c^*)]$; for symmetry reasons one finds: $U_{11} = U_{22} = U_{33}$ (for all atoms) and $U_{12} = U_{13} = U_{23}$ (for the O-atoms); $U_{12} = U_{13} = U_{23} = 0$ (for the Mg-atoms). Due to the weak scattering power of vanadium the positional and thermal parameters of this element were not allowed to vary. The shortest interatomic distances (in \AA) as well as the O-V-O bond angle (in $^\circ$) are also listed.

	MgV ₂ O ₄ at 100 K	MgV ₂ O ₄ at 300 K	MgV ₂ O ₄ at 600 K
a [\AA]	8.4415(1)	8.4415(1)	8.4415(1)
V [\AA^3]	601.53(1)	601.53(1)	601.53(1)
x (O1)	0.38642(11)	0.38623(10)	0.38576(12)
x (O2)	0.86651(10)	0.86623(9)	0.86584(12)
U_{11} (Mg1/Mg2)	0.31(3)	0.51(3)	0.94(2)
U_s (V)	0.30	0.50	0.30
U_{11} (O1 / O2)	0.38(2)	0.55(3)	0.96(2)
U_{12} (O1 / O2)	-0.024(9)	-0.058(10)	-0.079(8)
d (Mg11-O2)	1.9518(9)	1.9559(8)	1.9616(10)
d (Mg12-O1)	1.9946(10)	1.9918(9)	1.9849(10)
d (V-O1) ($\times 3$)	2.0186(10)	2.0200(9)	2.0236(10)
d (V-O2) ($\times 3$)	2.0412(9)	2.0390(8)	2.0360(10)
O1-V-O1 ($\times 3$)	84.40(4)	84.50(3)	84.75(4)
O1-V-O2 ($\times 6$)	94.84(4)	94.87(3)	94.84(4)
O2-V-O2 ($\times 3$)	85.91(3)	85.76(3)	85.57(4)

References

- [1] B. Lake, E. Wheeler, N. Islam, M. Reehuis, BENSCH Exp. Report 2008, p. 116.
- [2] M. Onoda, H. Imai, Y. Amako, H. Nagasawa, Phys. Rev. B. **56** (1997) 3760.
- [3] O. Tchernyshyov, Phys. Rev. Lett. **93** (2004) 157206.

	EXPERIMENTAL REPORT Hydrogen bonds evaluation in the crystal structures of silicate hydrates (continuation)	Proposal: GEO-01-2651 Instrument: E5 Local Contact: M. Reehuis
	Principal Proposer: O. Karimova, RAS IGEM Moscow, RU Experimental Team: O. Karimova, RAS IGEM Moscow, RU	Date(s) of Experiment 17.08.2009 – 23.08.2009

Date of report: 15.01.2010

A crystal of mineral catapleiite was studied by single crystal neutron diffraction at low temperature (6K). An experiment was performed at the four circle E5 diffractometer of the BER II reactor. A monochromated beam with $\lambda=0.89491$ was attained by reflection from the (220) plane of a copper single crystal. The data were collected using an area position-sensitive ^3He -detector. Total amount of 3152 reflections were collected.

Mineral catapleiite was studied by X-ray before. Sodium variety of mineral, $\text{Na}_2\text{ZrSi}_3\text{O}_9\cdot 2\text{H}_2\text{O}$, was solved in monoclinic cell [1], calcium variety, $\text{CaZrSi}_3\text{O}_9\cdot 2\text{H}_2\text{O}$ - in orthorhombic cell [2].

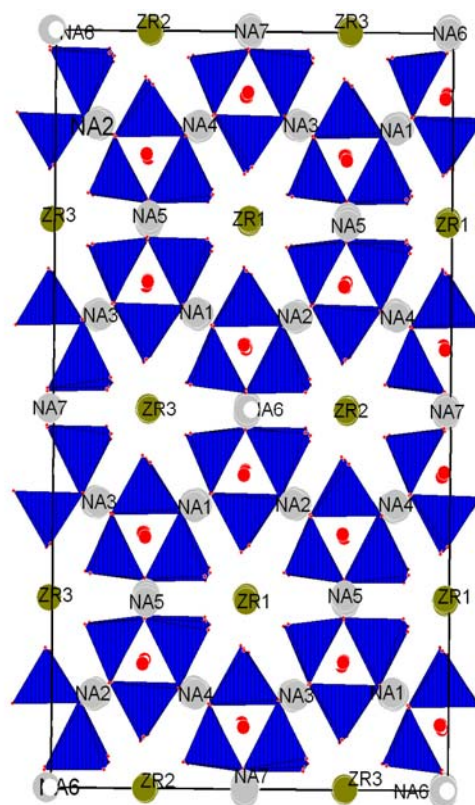
Our crystal is characterized by unusual composition: following formula was given SEM analysis – $\text{Na}_{2.52}\text{Ca}_{0.22}\text{Zr}_2\text{Si}_6\text{O}_{17}(\text{OH})_4\text{H}_2\text{O}$. It characterizes by deficit in sodium position, which compensate particularly by calcium.

Crystallographic characteristics for that variety of mineral (cell parameters, space group and atom coordinates) were determined by X-ray analysis. First, refinement of the structure was performed in the orthorhombic cell from [2]. But, it was not successful. Then, a modified model was found: changing in composition caused doubling of the unit cell (see table 1). Refinement in a cell and space group gave good results. Received data was used for further refining of structure features using neutron diffraction data. There are seven possible sodium positions in the structure. A distribution of sodium, calcium and vacancies over these positions will be defined. Also anisotropic thermal parameters for protons will be determined. Further refinement is ongoing.

Table 1.

$\text{Na}_2\text{ZrSi}_3\text{O}_9\cdot 2\text{H}_2\text{O}$ [1]	$\text{CaZrSi}_3\text{O}_9\cdot 2\text{H}_2\text{O}$ [2]	$\text{Na}_{2.52}\text{Ca}_{0.22}\text{Zr}_2\text{Si}_6\text{O}_{17}(\text{OH})_4\text{H}_2\text{O}$
$a=23.917 \text{ \AA}$	$a=7.378 \text{ \AA}$	$a=20.100 \text{ \AA}$
$b=20.148 \text{ \AA}$	$b=12.779 \text{ \AA}$	$b=25.673 \text{ \AA}$
$c=7.432 \text{ \AA}$	$c=10.096 \text{ \AA}$	$c=14.822 \text{ \AA}$
$\lambda=147.46^\circ$		
$z=8$	$z=4$	$z=24$
<i>sp. gr.</i> $B2/b$	<i>sp. gr.</i> $Pbnn$	<i>sp. gr.</i> $Fdd2$

Fig.1 Projection of catapleiite structure along (100).



Acknowledgement:

This research project has been supported by the Helmholtz-Center Berlin for Materials and Energy.

References:

- Ilushin, Cryst. Reports 260 (1981) 623.
- Merlino, Can. Miner. 42 (2004) 1037.

 Neutrons	EXPERIMENTAL REPORT	Proposal: MAT-01-2508
	Isotope Exchange in LiBH₄	Instrument: E6 Local Contact: Andreas Hoser
Principal Proposer: Experimental Team:	Arndt Remhof, EMPA Arndt Remhof, EMPA Oliver Friederichs, EMPA Dirk Wallacher, HZB	Date(s) of Experiment 08.06.2009 – 15.06.2009

Date of report: 09.07.2009

H/D isotope exchange measurements are suitable to study the hydrogen transport within hydrides. While the transport of hydrogen in metals and intermetallic compounds is well understood, little is known about the properties of complex hydrides [1,2].

In the present experiment we examined the H/D exchange of LiBH₄. LiBH₄ is an ionic solid, consisting of Li⁺ and BH₄⁻ ions. We examined a D enriched LiBH₄ (~60%D) sample in an applied H atmosphere of 40 bar at 250°C. The exchange reaction was monitored via the change of the Bragg reflected intensities.

Let us briefly discuss two models. In the first (M1) we assume a mix of LiBH₄ and LiBD₄, i.e. each anion contains only one species (H or D). In this case we expect a decrease of the Bragg reflected intensities, which is proportional to the amount of LiBH₄. In the second model (M2) we assume a completely random distribution of H and D within the sample. In this case we expect the structure factors to decrease linearly with increasing H content. Consequently, the reflected intensities in M2, which are proportional to the squares of the structure factors, decay faster than in M1.

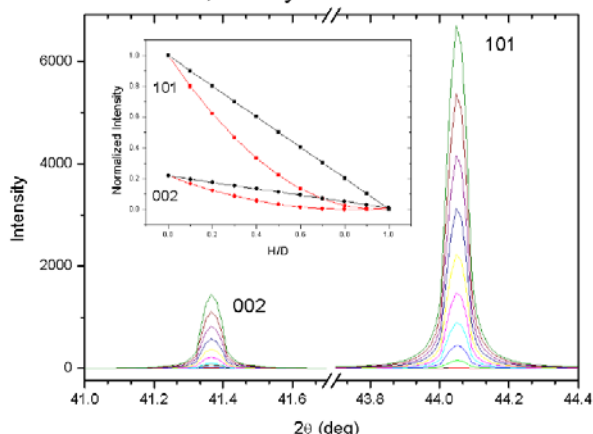


Fig. 1: Effect of H/D exchange (simulated)

Figure 1 shows the calculated (002) and (101) Bragg reflections for M2. The inset shows the normalized intensities (I_{002} and I_{101}) of the respective reflections during the exchange reaction for M1 (black) and for M2 (red). The

ratio of the intensities I_{101}/I_{002} is a clear indication for the validity of the models. The ratio decreases monotonously from its initial value of 4.62 in M1, while it increases in M2 until H/D~70/30, where it reaches a maximum.

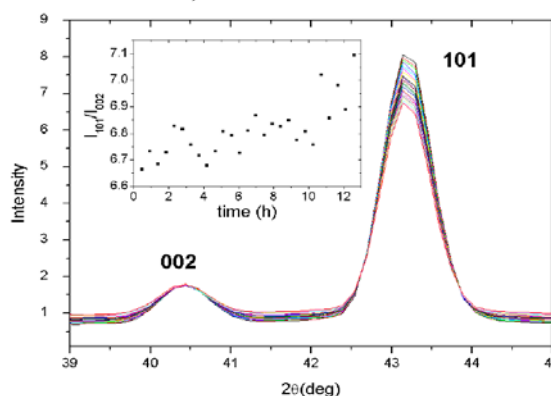


Fig. 2: Subsequently recorded diffractograms during the H/D exchange.

Figure 2 shows the measured data. From the intensity ratio (>6) and its increase with time (i.e. with increasing H content) we can exclude M1. Assuming the validity of M2 we estimate the initial H/D ratio of about 40/60, which is in agreement with gravimetric measurements.

The measurement clearly shows that:

- Isotope exchange occurs well below the melting point and well below the decomposition temperature of LiBH₄.
- During the exchange H and D are randomly distributed.
- There must be a mechanism allowing the exchange of single atoms within the anion without breaking it.
- There is no observable change in lattice parameter

References:

- [1] A. Borgschulte et al., *J. Phys. Chem. A*, (2008), **112**, 4749.
 [2] A. Borgschulte et al., *Appl. Phys. Lett.*, (2009), **94**, 111907.

Acknowledgement

This research project has been supported by the European Commission under the 7th Framework Programme through "Research Infrastructures" action of the "Capacities" Programme, contract number CP-CSA_INFRA-2008-1.1.1. Number 226507-NMI

	EXPERIMENTAL REPORT Neutron Bragg back-side scattering from the Ge single crystal excited with acoustic waves	Proposal: PHY-01-2513 Instrument: E6 Local Contact: Norbert Stüßer
	Principal Proposer: E. Raitman, LAS Riga, LV Experimental Team: E. Raitman, LAS Riga, LV V. Gavrilov, LAS Riga, LV D. Mjasischev, LAS Riga, LV A. Hoser, HZB N. Stüßer, HZB A. Arulraj, HZB	Date(s) of Experiment 02.04.2009 – 07.04.2009

Date of report: 17.12.2009

Experiments were aimed to obtain new data on Bragg's reflected neutrons space distribution from single crystals excited by ultrasound.

The intensities of neutron Bragg diffracted from the front (FFS) and back faces (BFS) of a 22 mm thick perfect Ge (220) crystal undergoing on ultrasound excitation has been measured at the BENS E6 diffractometer and calculated theoretically. It was shown that at the same time with acoustic wave amplitude growing the main Bragg's peak increases but the back face peaks becomes asymmetric and has more complicated behaviour. Within frameworks the dynamic theory of neutron scattering this features can be described by first order Bessel functions.

The main experimental results are shown on Figs.

Fig. Space distribution of the diffracted beam vs generator voltage, on the left parts scaled-up back-face scattering (BFS) is shown.

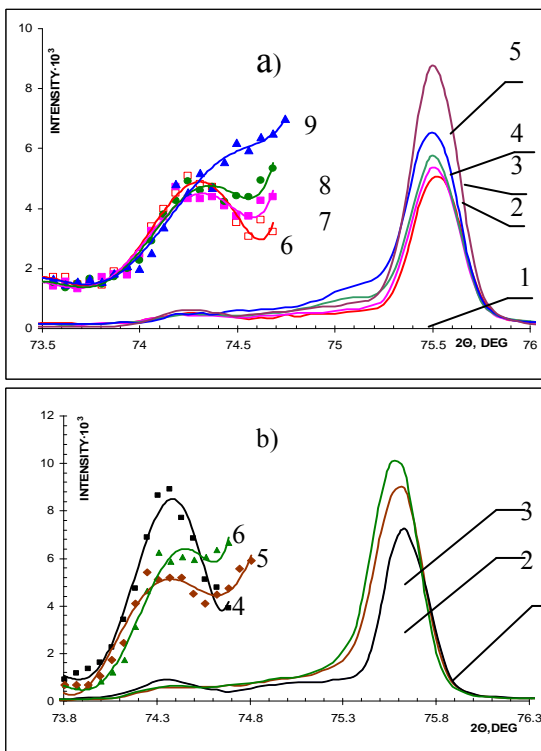
a) for longitudinal acoustic waves (LAW); right part for FFS: 1 (—) -0V, 2 (—) -1V, 3 (—) -2V, 4 (—) -4V, 5 (—) -6V; left part for BFS: 6 (□) -0V, 7 (■) -1V, 8 (■) -2V, 9 (▲) -4V

b) the same as a) for transverse acoustic waves (TAW); right part for FFS: 1 (—) -0V, 2 (—) -1V, 3 (—) -2.5V; left part for BFS: 4 (■) -0V, 5 (◆) -1V, 6 (▲) -2.5V

The obtained results are submitted as a paper to the journal *Europhysics Letters*.

Acknowledgement

This research project has been supported by the European Commission under the 7th Framework Programme through "Research Infrastructures" action of the "Capacities" Programme, contract number CP-CSA_INFRA-2008-1.1.1. Number 226507-NMI



Principal Proposer: Sudhindra Rayaprol, UGC-DAE CSR, Mumbai, India
Experimental Team: Vasudeva Siruguri, UGC-DAE CSR, Mumbai, India
E. V. Sampathkumaran, TIFR, Mumbai, India
Andreas Hoser, HZB

Date(s) of Experiment

30.06.2009 – 04.07.2009

Date of report: 17.12.2009

The phenomenon of electronic phase separation has been extensively studied in giant magnetoresistive manganites. This is observed across the first order metal-insulator transition driven by temperature or magnetic field resulting in percolative conduction. Recent magnetic measurements on a polycrystalline [1, 2] and single crystal [3] Nd₇Rh₃ exhibit the magnetic-field-induced first-order-phase-transition (FOPT). Magnetization data on Nd₇Rh₃ show that the zero-field state is antiferromagnetic below 32 K. However, M vs. H data at 1.8 K indicates that there is a field-induced transition to a ferromagnetic state at H = 1 T.

In order to explore whether Nd₇Rh₃ exhibit magnetic field induced first-order transition by undergoing structural transition / disorder at low temperatures or in applied magnetic field we have carried out neutron diffraction (ND) experiments at low temperatures (2 – 45 K) and externally applied magnetic fields (0 – 1.5 Tesla).

The sample Nd₇Rh₃ was prepared in bulk form by arc melting Nd and Rh metals in stoichiometric ratio. The ND experiments were carried out on the powdered sample obtained by coarse grinding. Sample for ND measurement was placed in a 7 Tesla cryostat and ND patterns were recorded using a wavelength of 2.45Å.

The Nd₇Rh₃ compound crystallizes in a hexagonal unit cell of Th₇Fe₃ type structure. Nd ion has three independent crystallographic positions and Rh ion has one position. Contrary to the results on other isostructural compounds such as Nd₇Ni₃ [4], Er₇Rh₃ [5], Nd₇Rh₃ does not exhibit antiferromagnetic peak at low angles even at 2 K (see Fig. 1). The ND patterns recorded at all temperatures could be refined to a hexagonal unit cell, and does not exhibit any traces of structural transformation or sample degradation.

The application of magnetic field enhances the intensity of the Bragg peaks. The magnetic Bragg peaks ride over the nuclear Bragg

peaks indicating the ferromagnetic state. The application of magnetic field transforms the magnetic moment from one crystallographic Nd site to another.

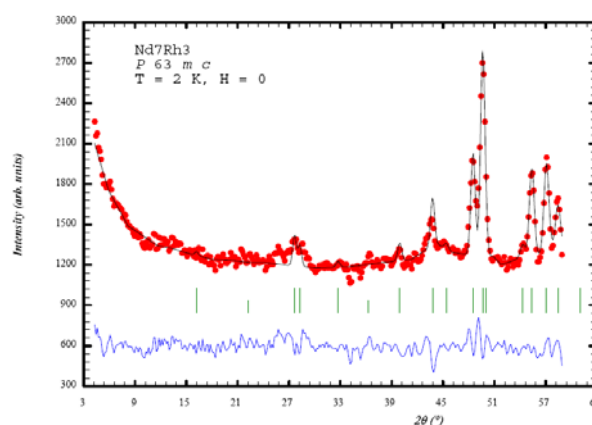


Fig. 1 ND pattern for Nd₇Rh₃ recorded at 2 K

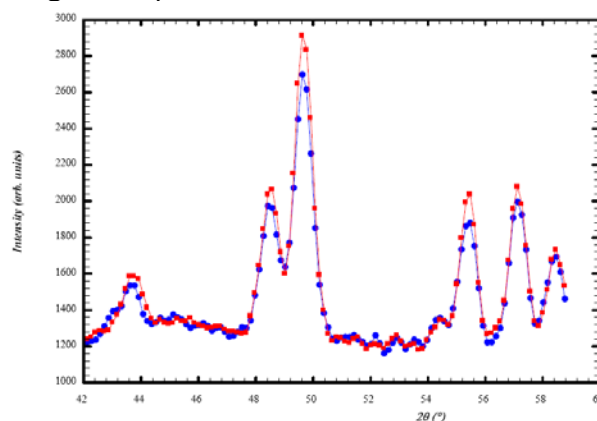


Fig. 2 ND pattern for Nd₇Rh₃ recorded at 2 K in H = 0 (blue circle) and 1.5 Tesla (red square) fields.

More detailed neutron diffraction experiments are planned for getting better statistics on Nd₇Rh₃ and for better understanding of magnetism of this compound.

This research project has been supported by Department of Science & Technology, Govt. of India by providing financial assistance. The project has also been supported by HZB by providing local hospitality.

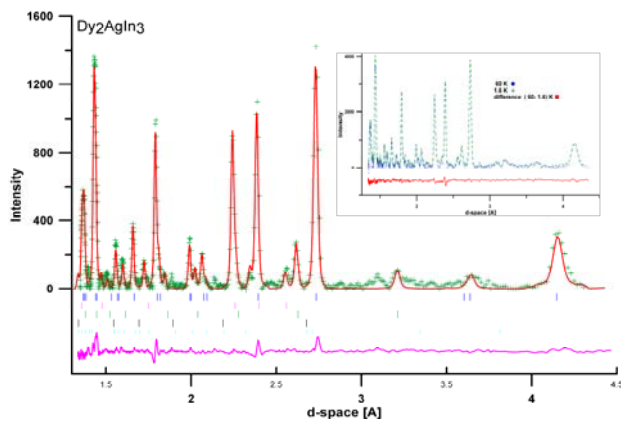
Principal Proposer: I.M. Siouris, Dept. of Production and Management Engineering, Democritus University of Thrace – Greece.
Experimental Team: K. Kosmidou, PME, Duth –Greece.
S. Katsavounis, PME, Duth –Greece.
A. Hoser, HZB

Date(s) of Experiment

13.07.2009 – 16.07.2009

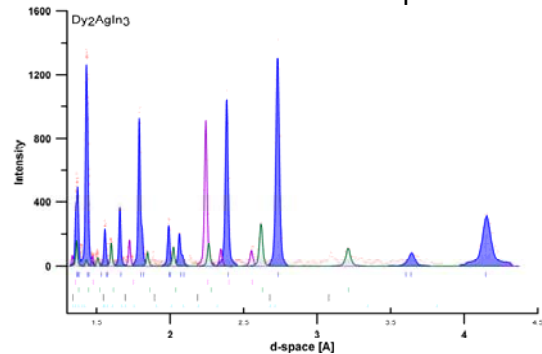
Date of report: 28.11.2009

Two samples of Dy(Ag,In)₂ prepared by arc melting in Ar/He atmospheres and annealed at 700°C for 7 and 24 days respectively, were measured on the powder diffractometer E6, at the BER-2 reactor in the Helmholtz Centrum Berlin. For each sample, ten diffraction patterns (2θ = 10° - 130°), were collected, from 2 K to 60 K with a neutron wavelength λ = 2.44 Å, in 2 hour measurements. Additional data was taken at 1.6K and 30 K. Profile inspection revealed that each sample contained several phases. So far, data analysis has concentrated on obtaining structural information, the cell parameters and the fractional atomic position dependence of the phases present. The diffraction profile analysis was based on full pattern Rietveld refinements using the programs Fullprof and on integrated intensities taking advantage of the least-squares program AMPhOrAe.

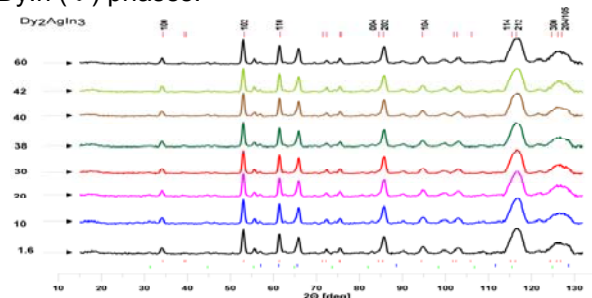


The observed (+) and the calculated (--) diffraction patterns of Dy(Ag,In)₂ at 60 K, modeled after a CaIn₂-type structure analyzed using the 2 stage method. Inset: The diffraction pattern at 2 K. No additional peaks are observed.

The structural parameters of the Dy₂CuIn₃ were refined and the magnetic behavior of the compound between 2 K and 60 K was investigated. No extra magnetic peaks are observed between 60 K and 2 K. The integrated intensities under each Bragg peak remain constant below 60 K. The R_{wp} value of the refined structural parameters is 8.7%.



Profile analysis showing the main Dy₂AgIn₃ (●) phase, along with the Ag_{0.7}In_{0.3} (●), DyIn₃ (●) and DyIn (●) phases.



Diffraction patterns (2θ = 10° - 130°), measured at various temperatures.

Phase at T = 60 K	Structure type -s.g	a [Å]	c [Å]	c/a
Dy ₂ AgIn ₃ (z= 0.5091)	CaIn ₂ P63/mmc	4.7565(2)	7.2896(6)	1.553(4)
DyIn ₃	AuCu ₃ P m -3 m	4.5780(3)		
Ag _{1-x} In _x (x=0.3)	- P6 ₃ /mmc	2.9470(5)	4.7924(5)	1.652(6)

Acknowledgement

This research project has been supported by the European Commission under the 7th Framework Programme through "Research Infrastructures" action of the "Capacities" Programme, contract number CP-CSA_INFRA-2008-1.1.1. Number 226507-NMI

 Neutrons	EXPERIMENTAL REPORT Neutron diffraction studies of tetragonal RCu_2X_2	Proposal: PHY-01-2634 Instrument: E6 Local Contact: A. Hoser
	Principal Proposer: S. Baran, Jagiellonian University, Krakow, Poland Experimental Team: A. Hoser, HZB B. Penc, Jagiellonian University, Krakow, Poland	Date(s) of Experiment 25.09.2009 – 29.09.2009

Date of report: 15.01.2010

Experiment

Six powder samples of ternary intermetallics: $TmCo_2Ge_2$, $TbCu_2Ge_2$, $ErCu_2Ge_2$, $TmCu_2Ge_2$, $TbCu_2Si_2$, and $HoCu_2Si_2$ were investigated by means of neutron diffraction within the temperature range from 1.5 to 15 K on the E6 diffractometer. The incident neutron wavelength was 2.45 Å.

Results

The obtained results indicate that investigated compounds crystallize in the tetragonal $ThCr_2Si_2$ -type crystal structure (space group $I4/mmm$).

The neutron diffraction patterns of all investigated compounds, taken below the Néel temperature, clearly reveal the presence of some additional reflections due to a magnetic ordering. For RCu_2Si_2 ($R = Tb, Ho$) and RCu_2Ge_2 ($R = Tb, Er$) these reflections can be indexed using the propagation vector $\mathbf{k} = [\frac{1}{2}, 0, \frac{1}{2}]$ at 1.5 K. The corresponding magnetic structure can be described as stacked antiferromagnetically ferromagnetic (101) layers. In the $TbCu_2X_2$ ($X = Si, Ge$) compounds the Tb magnetic moment lies along [110] direction. With an increase of temperature a change of the direction from [110] to [010] appears. In $HoCu_2Si_2$ and $ErCu_2Ge_2$ an increasing temperature induces a change of the magnetic structure from a collinear to a modulated one (see Fig. 1).

In $TmCu_2Ge_2$ the magnetic order is described by the propagation vector $\mathbf{k} = [0.117(3), 0.117(3), 0]$. The Tm magnetic moment of $5.0(1) \mu_B$ is parallel to the c-axis.

The $TmCo_2Ge_2$ compound exhibits an antiferromagnetic ordering in the form of a collinear magnetic structure of AFI-type below $T_N = 2.3$ K. The Tm magnetic moment equals $3.33(4) \mu_B$ at $T = 1.5$ K and it is parallel to the a-axis (see Fig. 2).

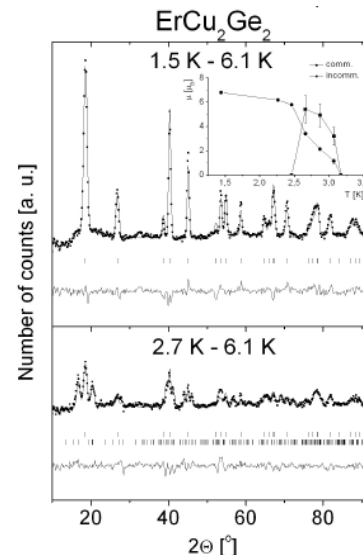


Figure 1. Differential neutron diffraction patterns of $ErCu_2Ge_2$.

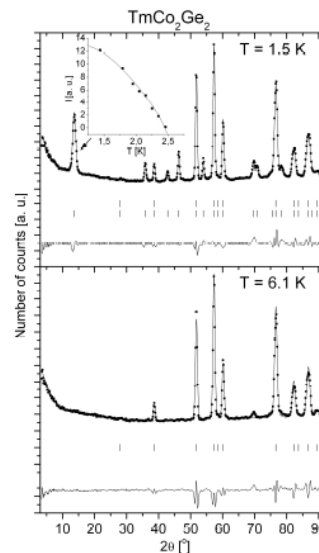


Figure 2. Neutron diffraction patterns of $TmCo_2Ge_2$ collected at 1.5 and 6.1 K.

Acknowledgements

This research project has been supported by the European Commission under the 7th Framework Programme through the Key Action: Strengthening the European Research Infrastructures.

Contract n°: RI-CP-2008-226507 (NMI3).

	EXPERIMENTAL REPORT Magnetic and crystal structure of La_{1/3}Sr_{2/3}FeO_{3-d}: dependence on oxygen content	Proposal: PHY-01-2372 Instrument: E9 Local Contact: Paul Henry
	Principal Proposer: Alexey Kuzmin, Institute of Solid State Physics, Riga, Latvia Experimental Team: Vadim Sikolenko, ETH Zürich and Paul Scherrer Institut Vadim Efimov, Joint Institute for Nuclear Research	Date(s) of Experiment 11.06.2009 - 15.06.2009

Date of report: 23.10.2009

La_{1/3}Sr_{2/3}FeO_{3-d} exhibits charge ordering at T = 210 K probably driven by only magnetic exchange without dominant role of Coulomb interaction. Replacement of La³⁺ in parent compound LaFeO₃ with Sr²⁺ increases the formal Fe valence from 3+ to 3.67. In this solid solution below T ~ 210 K charge disproportionation occurs on the Fe site, 3Fe^{3.67+} → 2Fe³⁺ + Fe⁵⁺, leading to simultaneous charge and spin orderings [1,2,3]. Because of the small Fe-O charge transfer gap, appreciable hole density on oxygen ions leads to an admixture of additional electronic configurations (Fe⁵⁺ → Fe⁴⁺_L → Fe³⁺L²), where _L represents a hole on the oxygen ligand [4]. It is expected that the oxygen character of the doped holes via Fe-O hybridization screens intersite Coulomb interactions significantly. Charge ordering is then driven primarily by the magnetic energy cost of arranging charges to form a metal-centered magnetic domain wall. [1].

In [4] it was suggested that charge ordering in La_{1/3}Sr_{2/3}FeO_{3-d} could be stabilized due to magnetic exchange without of dominant influence from Coulomb interactions. It is also necessary to note, that in [5, 6] there is a discrepancy concerning magnetic moment of Fe ions in different sites as well as crystal symmetry of the samples, which could be due to non-controlled oxygen non-stoichiometry. Our E9 results show that oxygen stoichiometric sample can be refined in the frame of rhombohedral R-3 space group. At low temperature antiferromagnetic ordering of Fe ions have been found. Small oxygen non-stoichiometry leads to drastically changes in structure and increase of distortion (canting of octahedron). The sample with d ~ 0.1 can be refined only in the frame of orthorhombic space group Pbnm. It leads to disappearance of magnetic ordering at low temperature.

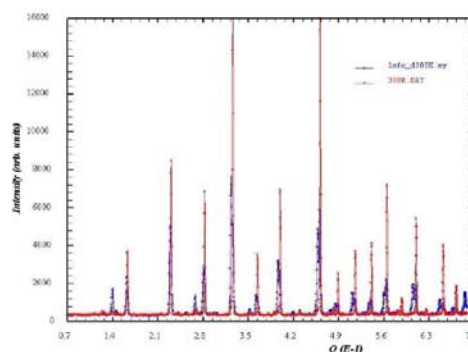


Fig.1. Diffraction pattern, collected at the E9 spectrometer for the stoichiometric sample and oxygen-deficient sample at room temperature.

Acknowledgement

This research project has been supported by the European Commission under the 7th Framework Programme through the Research Infrastructures action of the Capacities Programme

*Contract n° CP-CSA_INFRA-2008-1.1.1
Number 226507-NMI3*

This project has been also partly supported by RFBR, project 08-09-90053-Bel_a.

References

1. T.Mizokawa and F.Fujimori, PRL 80, 1320 (1998)
2. J.Li, S.Park, Y.Matsui, PRL 79, 297 (1997)
3. J.Matsumo et al, Phys.Rev,B 60, 4605 (1999)
4. R.J.McQueeney et al, PRL 98, 126402 (2007)
5. P.Battle et al, J.Sol.St.Chem. 84, 271 (1990)
6. J.B.Yang et al, J.Phys.:Comd.Mat. 15, 5093 (2003)

	EXPERIMENTAL REPORT Study of the mechanism of proton conduction in ceramics	Proposal: ART-01-2465-EF Instrument: E9 Local Contact: Simon Kimber
	Principal Proposer: T. Scherb, HZB F-I1 Experimental Team: S. Kimber, HZB MI1 M. Russina, HZB G-I1 N. Tsapatsaris, HZB G-I1 D. Wallacher, HZB G-I1 G. Schumacher, HZB F-I1 J. Serra, UPV-CSIC	Date(s) of Experiment 03.12.2008 – 08.12.2008

Date of report: 18.08.2009

The tungstates $\text{Ln}_6\text{WO}_{12}$ are proton-conducting materials exhibiting sufficient electronic conductivity to consider them as potential candidates for the separation of hydrogen at high temperature. The $\text{Ln}_6\text{WO}_{12}$ system has three structural classes whose symmetries are dependent on the rare earth ionic radius. These materials crystallize in a disordered pyrochlore or ordered defect fluorite structure and they can be formulated as $\text{Ln}_6\text{WO}_{12}\text{K}_2$ or $\text{A}_4\text{O}_{6.85}\text{K}_{1.15}$ (κ =oxygen vacancies) for a fluorite formulation [1].

Neutron powder diffraction experiments on $\text{Nd}_6\text{WO}_{12}$, sintered at 1150°C were performed at the high resolution powder diffractometer E9 ($\lambda=1.79 \text{ \AA}$). Prior to the diffraction measurements, the specimen was annealed at 350°C for 38 hours. Diffraction measurements were performed at room temperature and 900°C under different atmospheres (high vacuum, $\text{He}+\text{D}_2$ (dry), $\text{He}+\text{D}_2+\text{D}_2\text{O}$, humid atmosphere (D_2O) $p = 0.6$ bar). The humid atmosphere was produced using the DEGAS system connected to a high temperature furnace with a Suprasil quartz tube, which has very low H content, as an insert. The spectrum recorded at room temperature in vacuum is shown in Fig. 1.

Rietveld analysis confirmed the cubic lattice structure with lattice parameter $a=0.54596\text{nm}$ and space group $Fm\bar{3}m$. Superlattice reflections caused by deuterons and changes in the diffraction spectra by D_2O are not visible. The diffraction patterns for all atmospheres look the same and show no cation and oxygen vacancy ordering.

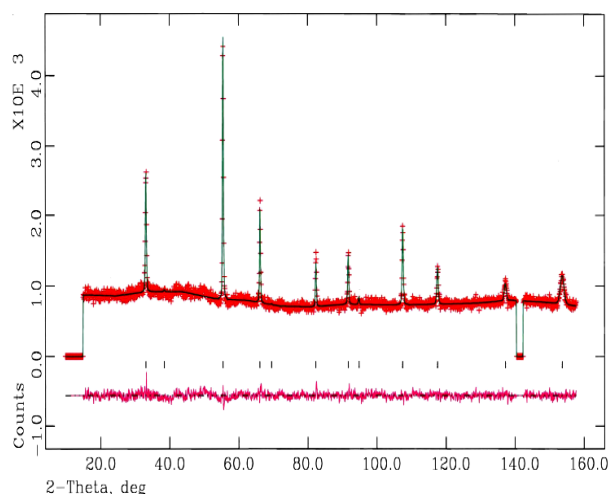


Fig. 1: Neutron diffraction pattern of $\text{Nd}_6\text{WO}_{12}$ recorded at 300 K in vacuum.

Structural parameters and cation site occupancies were obtained by Rietveld analysis (GSAS) of the data using the fluorite structure as model (s.g. $Fm\bar{3}m$) and are plotted in Tab. 1.

Tab. 1: Occupancy of the Wyckoff positions.

Wyckoff position	Element	Occupancy
4a	Nd	0.8615
4a	W	0.1378
8c	O	0.7463

Thus the results allow the suggestion that the amount of incorporated D_2O is too low to be detected.

References:

- [1] Escolástico, S. et al., Chemistry of Materials, 2009.
- [2] McCarthy, G. J. et al., In Proceedings of the 5th Materials Research Symposium, Solid State Chemistry; National Institute of Standards: Washington, D.C., 1972.

This work has been supported by the Helmholtz-Alliance MEM-BRAIN.

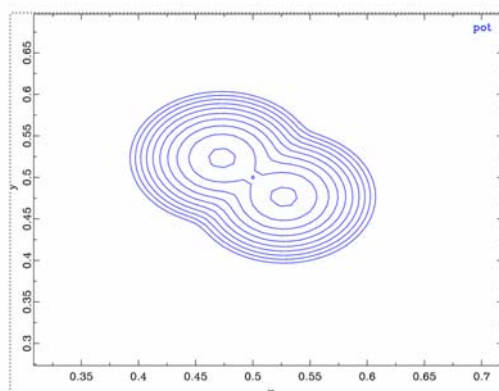
 Neutrons	EXPERIMENTAL REPORT Proton Mobility in Solid Super Proton Conductors	Proposal: CHE-01-2523 Instrument: E9 Local Contact: Michael Tovar
	Principal Proposer: M. Lerch, Institute of Chemistry, TU Berlin Experimental Team: C. A. C. Dreismann, Institute of Chemistry, TU Berlin T. Abdul-Redah, Institute of Chemistry, TU Berlin Michael Tovar, HZB	Date(s) of Experiment 19.03.2009 – 26.03.2009

Date of report: 01.09.2009

Our present research project focuses on the development and optimization of crystalline solid proton conductors as an alternative to the commonly used polymer membranes. We put main emphasis on the fundamental understanding of solid proton conductors, e.g. the correlation between crystal structure and mobility of the ions. Promising candidates for these investigations are $(\text{H}_3\text{O})\text{SbTeO}_6$ and $\text{Rb}_3\text{H}(\text{SO}_4)_2$, both super proton conductors with an outstanding proton conductivity at “low” temperatures.

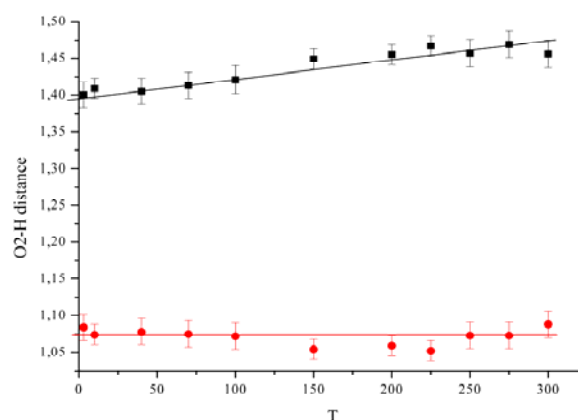
Due to the newest results of our accompanying neutron Compton scattering (NCS) experiments on $\text{Rb}_3\text{H}(\text{SO}_4)_2$ – at the ISIS neutron spallation source, U.K. – in this continuation experiment we decided to concentrate on measurements of $\text{Rb}_3\text{H}(\text{SO}_4)_2$, on $T=10\text{K}$ and $T=70\text{K}$ only. Note that these temperatures are also those of the NCS-results reported in the original PRL [D. Hormouz et al., **PRL** 98, 115502 (2007)]. In the latter paper, the momentum distribution of the protons in a single crystal was reported and the “first direct measurement of the proton 3-dimensional Born-Oppenheimer (BO) potential in any material” was claimed.

In our first experiment (**CHE-01-2203**) on $\text{Rb}_3\text{H}(\text{SO}_4)_2$ we reported diffraction data (at 50 K) providing first experimental evidence that the BO-potential claimed by Hormouz et al is unphysical; see Figure below.



The surprising finding was that the H position appeared **not** to be symmetric between the two O-sites constituting a “symmetric H-bond”, and H appears to occupy one of two sites strongly outside the above O-O axis. Thus our results were in clear contradiction to the claims by Hormouz et al.

Our preliminary data analysis of the new experimental results at $T=10\text{K}$ and $T=70\text{K}$ clearly confirms the results of our previous experiment. Furthermore, we have found that the quality on the data cannot decide beyond any doubt whether the potential shown in Fig 1 has indeed two well-defined minima off the O-O axis or only strongly “elongated”, flat minimum. Nevertheless, using the “split model”, the H-O distances can be extracted from the diffraction data at different temperatures. The next Figure shows the distance of the two possible positions of H from its adjacent two O atoms (H. Boysen). Also these data clearly demonstrate that the O-H-O configuration is not symmetric.



For the above reason, currently we are extending these experiments by using single crystals [experiments in collaboration with H. Boysen and with G. Kearley being presently under progress].

Due to this physical context and its implications to other neutron-scattering fields (see e.g. the above reference), we intent to look into the matter in greatest detail.

	EXPERIMENTAL REPORT Investigation of structural trends in non-stoichiometric Cu-III-VI₂ compounds (III = In, Ca; VI=S, Se)	Proposal: MAT-01-2524 Instrument: E9 Local Contact: Michael Tovar
	Principal Proposer: C. Stephan, HZB Experimental Team: C. Stephan, HZB S. Schorr, Freie Universität Berlin F. Yokaichiya, HZB	Date(s) of Experiment 05.05.2009 – 11.05.2009

Date of report: 09.09.2009

Ternary chalcopyrites like Cu-III-VI₂ (III=In,Ga; VI=S, Se) have recently achieved high interest due to their optical properties for using them as absorber layers in thin film solar cells. They crystallize in the chalcopyrite type crystal structure (s.g. $I\bar{4}2d$) which can be considered as being derived from the cubic zinc-blende type structure by doubling the unit cell along the *c*-axis. The Cu occupies the 4a (0,0,0) position, while In and Ga are occupying the 4b (0,0, 1/2) site.

In general the Cu(In,Ga)Se₂ thin films absorber layers are grown with a Cu-deficiency. With the deviation of stoichiometry the chalcopyrite crystal structure still consists, but lattice parameters and cation site occupancies are changing. The elements Cu⁺ and Ga³⁺ have a similar scattering power for X-rays (same number of electrons). Due to this fact neutron powder diffraction is necessary for differentiating between the cations Cu⁺ and Ga³⁺, because of their different neutron scattering length of Cu and Ga ($b_{Cu}=7.718(4)$ fm, $b_{Ga}=7.288(6)$ fm).

6 CuIn(S,Se)₂ and 11 CuGa(Se,S)₂ samples were studied by neutron powder diffraction. The samples were prepared by solid state reaction of the elements in a sealed evacuated silica tube at 850°C and cooled down fast to room temperature. The chemical composition of all samples was determined by electron microprobe analysis (JEOL JXA-8200).

Neutron powder diffraction experiments were performed at the high resolution powder diffractometer E9 ($\lambda=1.79776$ Å). Structural parameters and cation site occupancies were obtained by Rietfeld analysis (FullProf) of the data using the chalcopyrite structure as model. The average neutron scattering length of the cation sites 4a and 4b ($\bar{b}_{4a}, \bar{b}_{4b}$) were determined from the cation site occupancies resulting from the Rietveld analysis. A decrease of \bar{b}_{4a} in comparison to b_{Cu} in strongly Cu-poor (Cu/In=0.75) CuInSe₂ samples can be interpreted by the generation

of Cu-vacancies ($V_{Cu} \sim 6\%$) and In on 4a site ($In_{Cu}=17\%$; $Cu_{Cu}=77\%$). On the contrary in the Cu-poor CuInS₂ samples only a generation of Cu-vacancies could be observed.

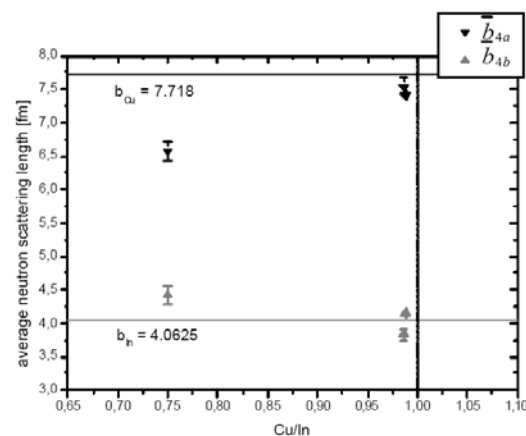


Fig. 1: Average neutron scattering length of the cation sites 4a and 4b of nearly stoichiometric and Cu-poor CuInSe₂

The CuGaSe₂ samples show even in the close-stoichiometric region a generation of Cu-vacancies, observed by a decrease of the average neutron scattering length of the copper site 4a (see table 1). A correlated increase of \bar{b}_{4b} , indexing a Ga_{Cu} antisite formation could not be noticed.

Tab 1: Amount of Cu-vacancies in nearly stoichiometric and strongly Cu-poor CuGaSe₂ samples

Cu/Ga	V_{Cu}
1.02	11 %
0.85	15 %

All analyzed samples showed a decrease of the lattice constants with decreasing Cu/III ratio, caused by the generation of Cu-vacancies. A more detailed data analysis is ongoing. Thus the results allow the suggestion that a real stoichiometric chalcopyrite compound does not exist, if even the close stoichiometric samples contain V_{Cu} . This is an important result for understanding the electronic properties of Cu-III-VI₂ thin film solar cells.

	EXPERIMENTAL REPORT Structural investigation on H₂-sorption sites in new Li containing metal organic frameworks (MOF)	Proposal: PHY-01-2574-EF Instrument: E9 Local Contact: Michael Tovar
	Principal Proposer: Dirk Wallacher, HZB Experimental Team: Dieter Himsl, Erlangen Catalysis Resource Center, Universität Erlangen-Nürnberg Martin Hartmann, Erlangen Catalysis Resource Center, Universität Erlangen-Nürnberg	Date(s) of Experiment 08.06.2009 – 11.06.2009 30.06.2009 – 03.07.2009

Date of report: 09.09.2009

On the quest for solid state materials as hydrogen carriers, porous Metal-Organic Frameworks have been shown to be very suitable candidates for applications in hydrogen storage technology [1]. Very recent theoretical results showed that the incorporation of unsaturated metal sites inside the pores can significantly improve the hydrogen adsorption properties of a given material [2]. Within this field of research the present project is dealing with the hydrogen adsorption properties of microporous metal-organic frameworks (mMOF). The material under study has been a chemically modified analog of MIL-53 [3], which carries a pendant hydroxy-group inside the porous network, thus, enabling further chemical modification of the interior pore surface. In our case this was done via a post-synthetic transformation of the hydroxy-group into a lithiumalkoxide group. This novel material, (2), shows significantly enhanced isosteric heats of adsorption for hydrogen and an increased adsorption capacity [4]. Both materials should show structural flexibility upon external stimuli like temperature or gas phase pressure [5] ("breathing effect, Fig.1).

In the present investigation we liked to focus on the structural properties of the samples as well as the identification of different D₂-sorption sites within the structures. Unfortunately bad scattering properties of the samples, an unforeseen wavelength filter problems allowed only the investigation of sample (1) at 298 K and at 2 different hydrogen fillings: 0 mmol (empty) and 12 mmol (full).

Fig.2 show diffraction patterns of the evacuated sample (1) at 298 K and 77 K. A change from ht- to lt-phase cannot be observed. The patterns

Fig.1:
The structure of MIL-53 can change between the open pored ht-phase and the closed lt-phase.

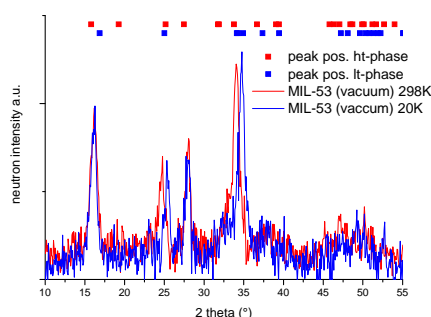


Fig.2:
Diffraction patterns of MIL-53 (1) at 298 K and 77 K.

show that the sample presents a mixture of the two phases in the investigated temperature range. The comparison of the empty and filled material (in fig.3) exhibits remarkable differences in the patterns, but identifying distinct adsorption sites is not possible as long as the underlying host structure is not known. To tackle this point we propose complementary in-situ high resolution XRD measurements.

- [1] R. von Helmolt, U. Eberle, J. Power Sources 2007, 165, 833.
 [2] E. Klontzas, A. Mavrandonakis, E. Tylianakis, G. E. Froudakis, Nano Lett. 2008, 8, 1572.
 [3] T. Loiseau et al., Chem. Eur. J. 2004, 10, 1373.
 [4] D. Himsl, D. Wallacher, M. Hartmann, Angew. Chem. 2009, 48, 4693.
 [5] Y. Liu et al., C. Brown, J. Am. Chem. Soc. 2008, 130, 11813.

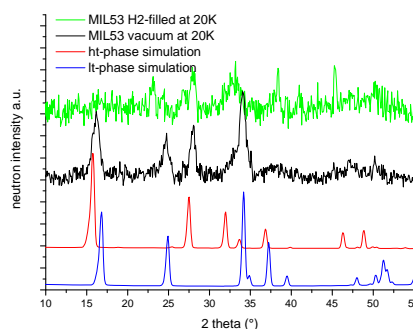


Fig.3:
ND results of filled and empty sample (top). Simulated ht- and lt-phase (bottom). [5]

	EXPERIMENTAL REPORT Resolving the phase field in the materials RbCu_xNi_{1-x}PO₄	Proposal: CHE-01-2593-EF Instrument: E9 Local Contact: P. Henry
	Principal Proposer: Paul Henry, HZB Experimental Team: Paul Henry, HZB	Date(s) of Experiment 18.09.2009 – 23.09.2009

Date of report: 14.01.2010

Introduction and aims

This proposal followed on from CHE-01-2550-EF on E9 looking at mixed transition metal phosphates. In the intervening period between submission of the proposal and the scheduling it had been found that RbCuPO₄ had 5 distinct phases over the T range RT - 550 °C - RT using variable temperature X-ray methods. Preliminary structures had been obtained for all 5 phases that required PND data for corroboration. In addition, it has been found that the monoclinic phase, now ascribed as polymorph II, could be stabilised by fast cooling to ambient conditions in essentially phase pure form. Therefore, the aims of the experiment were to collect data on the 5 phases and to solve the structures. Samples of the partially substituted materials Rb₃Zn₂B(PO₄)₃ (B = Cu and Ni) were also collected as the previous PND experiment had shown that the superstructures were based on TM ordering in crystallographically distinct sites (4 and 5 coordinate) in the ratio 2:1 and, by substitution with non magnetic tetrahedral coordination favouring Zn²⁺, it was hoped to synthesise a material with the potential to host a 1D-spin chain of Cu²⁺.

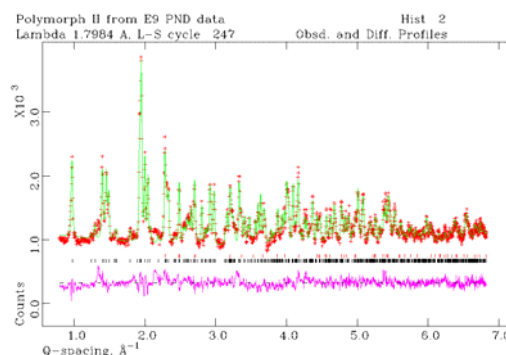
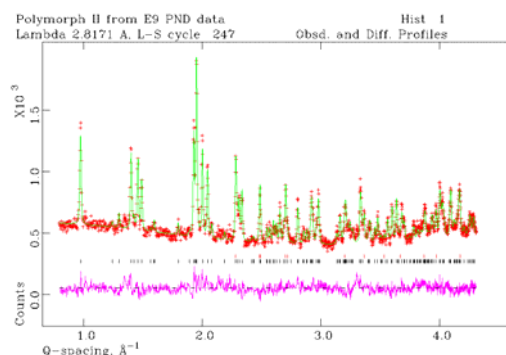
Experiment

Data were collected starting with polymorph I (orthorhombic) at 50, 425, 500, 170 and 475 °C in this order at $\lambda = 1.797 \text{ \AA}$, before the material was quenched to RT so that data could be collected on the pure polymorph II. RT data were also collected on the two partially Zn substituted materials. There was insufficient time to perform an empty furnace run with the silica insert and so all of the VT data sets for RbCuPO₄ have significant amorphous contributions.

Results and further work

Due to the increased background contribution from the silica insert used to contain the samples (as previous experiments have shown that phosphates of this family show markedly different phase behaviour and

transition temperatures when held in vacuum) and the broadening of the diffraction peaks at elevated temperatures, it has not been possible to satisfactorily solve the high temperature structures. It was also found that the scattering from II was much lower than from I and so the possibility of unindexed superstructure peaks remain a possibility. The Rietveld refinement fit for II is given below with the data from $\lambda = 2.8 \text{ \AA}$ as the upper and $\lambda = 1.797 \text{ \AA}$ the lower fit. The partially Zn substituted materials no longer showed the evidence of the superstructure peaks associated with I although data analysis is continuing. On completion, the structures of all these materials will be published with those of CHE-01-2550-EF.



 Neutrons	EXPERIMENTAL REPORT	Proposal: CHE-01-2597 Instrument: E9 Local Contact: M. Tovar
	Neutron diffraction study of different Cu based methanol synthesis catalysts	Date(s) of Experiment 18.08.2009 – 23.08.2009
Principal Proposer: Experimental Team:	Malte Behrens, Fritz-Haber-Institut, Berlin Stefanie Kühn, Fritz-Haber-Institut, Berlin Stefan Kißner, Fritz-Haber-Institut, Berlin Michael Tovar, HZB Dirk Wallacher, HZB	

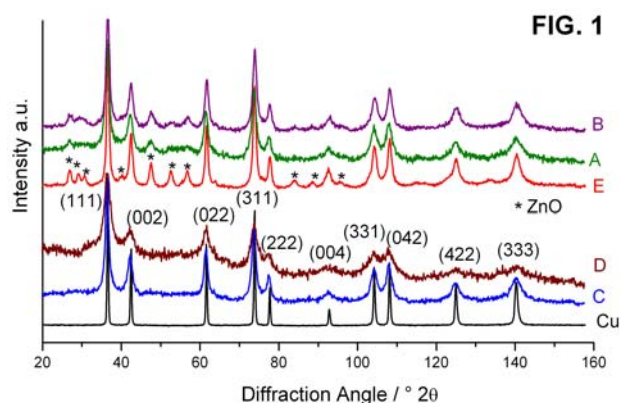
Date of report: 16.12.2009

Nanostructured Cu/ZnO/Al₂O₃ catalysts are industrially employed to produce methanol from syngas (H₂, CO, CO₂). Catalytic activity is governed by the gas accessible Cu surface area and also by intrinsic factors. This intrinsic activity of Cu is related to its defect structure and diffraction methods are well-suited for the analysis of such deviations from the ideal fcc structure of Cu. In particular, neutron diffraction is an excellent tool, as it allows the detection of several higher order reflections of the highly symmetric fcc structure with sufficient intensity at reasonable counting times.

This study aims at finding structure-performance relationships for methanol catalysts and the selection of investigated samples represents a set of Cu-based catalysts with significant differences in microstructure, defect structure and intrinsic activity. Additional to the complex industrial catalyst system (A), several Cu/ZnO/(Al₂O₃) samples prepared from mixed CuZnAl hydroxy-carbonates (B), from amorphous precursors (C) and from a phase-pure hydrotalcite-like precursor (D), a binary Cu/ZnO model system (E) as well as a pure Cu reference (Cu) were investigated. Neutron diffraction patterns of the catalysts were recorded at the E9 beamline ($\lambda = 1.308 \text{ \AA}$) at HZB in inert atmosphere using sealable V-containers.

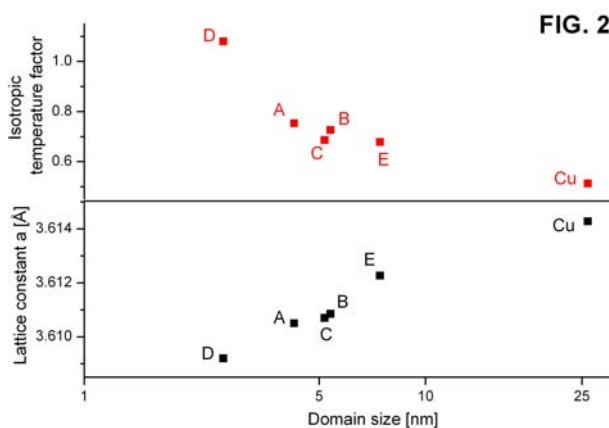
The structural differences among the investigated catalysts concerning e.g. the crystallinity of ZnO and the peak profiles of Cu are already apparent in the raw neutron diffraction patterns (Fig.1).

Structural refinement of the Cu phase using the Rietveld method and determination of the domain sizes from the peak widths could be done on the basis of 10 well-resolved reflections – a number, which is not accessible



by conventional XRD. A contraction of the lattice constant of Cu with decreasing domain size was observed (Fig. 2, bottom).

The isotropic temperature factor of the Cu atoms in the unit cell, which is related to disorder in the Cu phase, could also be refined. It shows an inverse trend with the domain size and indicates that different amounts of disorder or defects are indeed



present in our samples (Fig. 2, top).

These results will be complemented by catalytic data in order to identify structural features, which are indicative of high catalytic performance.

	EXPERIMENTAL REPORT Distribution of functional groups in proton-conducting mesoporous SO₃H-SiO₂ materials	Proposal: MAT-01-2537-EF Instrument: V1 Local Contact: Thomas Hauß
	Principal Proposer: Michael Wark, Leibniz University Hannover Experimental Team: Michael Wark, Leibniz University Hannover Monir Sharifi, Leibniz University Hannover Dirk Wallacher, HZB Thomas Hauß, HZB	Date(s) of Experiment 11.06.2009 – 21.06.2009

Date of report: 18.08.2009

During our stay at BENS in June 2009 we studied the SANS behavior of Si-MCM-41 samples functionalized with SH or SO₃H groups either directly during synthesis (co-condensation) or subsequently by grafting. Confirming results from our first SANS measurements in 2008 we found that the functional groups reduce the intensity of the neutron diffraction peaks due to the electron density introduced in the pores. Furthermore, the diffraction peaks shift to higher scatter lengths. Comparison of grafted SH-propyl and SO₃H-propyl chains now showed that this effect mainly results from the propyl groups since SH- or SO₃H- end groups led only to small differences (Fig. 1).

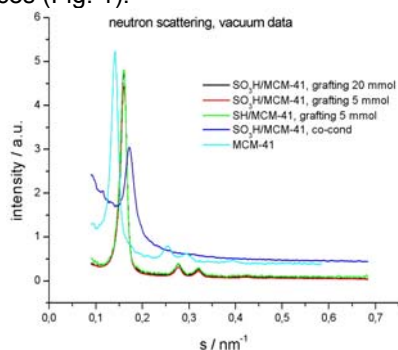


Fig.1: Neutron scattering of differently functionalized mesoporous SiO₂ (MCM-41) samples under vacuum.

Furthermore, the intensity and peak position of the diffraction peaks of grafted samples were almost independent on the amount of silane used for the grafting. Because for samples loaded by co-condensation the peaks shift and decrease in intensity with progressive loading, this indicates that functionalization by grafting is imperfect. This was proven by SANS studies performed during adsorption of a H₂O/D₂O (42:58 vol.-%) mixture. As well as N₂ such mixture leads to a full quenching of the SANS diffraction signals if the pores of a pure Si-MCM-41 are completely filled, because the scatter lengths are similar to that of SiO₂. In case of a grafted SO₃H/MCM-41 the expected decreasing diffraction peak intensity in dependence of the partial pressure of the H₂O/D₂O mixture was found; the strongest decrease taking place around $p/p_0 \approx 0.45$ when the 3 nm wide channels of the MCM-41 are filled by capillary condensation (Fig. 2).

However, in contrast to pure Si-MCM-41 the first diffraction peak does not disappear completely at p/p_0

of almost 1. This indicates that regions with neutron scatter lengths different to that of SiO₂ are present in the sample.

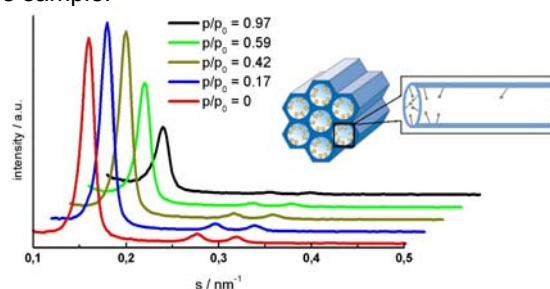


Fig.2: SANS patterns for SO₃H/MCM-41 grafted with 20 mmol mercaptopropylsilane in dependence of pore filling with a H₂O/D₂O mixture.

For a sample functionalized by co-condensation almost no quenching of the neutron diffraction was found (Fig. 3).

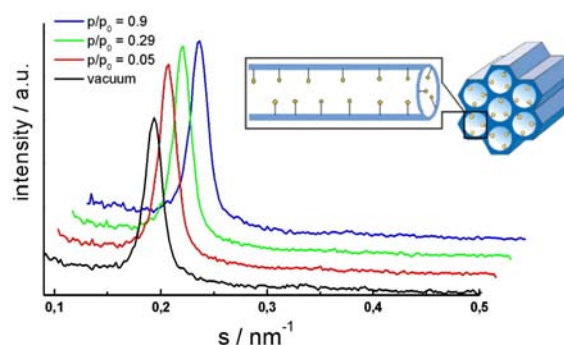


Fig. 3: SANS patterns for SO₃H/MCM-41 synthesized by co-condensation substituting 20% of tetraethylorthosilicate (TEOS) by mercaptopropylsilane in dependence of pore filling with a H₂O/D₂O mixture.

This indicates that here all regions of the pores are altered by the functional groups proving that the loading is much more homogeneous than with grafting by what the functional groups are only anchored at the pore entrances. The more homogeneous distribution of groups after co-condensation explains the higher proton conductivities observed.

The SANS results were included in a talk at the CPM-5 Workshop on Characterization of Porous Materials in New Brunswick, USA (June 2009), at posters presented on the 21st German Zeolite Meeting in March 2009 in Kiel and on a Bunsen-Colloquium held in Hannover in September 2009. A publication is in preparation.

 NEUTRONS	EXPERIMENTAL REPORT		Proposal: PHY-03-632
	Temperature evolution of dynamics of lead nanoparticles		Instrument: V3 Local Contact: M. Russina
Principal Proposer:	Alexander Naberezhnov, Ioffe Phys.-Techn. Institute, RU		Date(s) of Experiment
Experimental Team:	Petr Parshin, Kurchatov Institute, RU Yuri Kibalin, Petersburg Nuclear Physics Institute, RU		30.06.2009 – 07.07.2009

Date of report: 14.01.2010

Lead demonstrates the strong nonlinearity at growth of temperature and large thermal lattice expansion. On the other hand it is shown that the physical properties and structure of confined materials change drastically. In particular in confined sodium nitrite the amplitudes of thermal motions above the ferroelectric phase transition increase in 6-8 times [1]. Our diffraction measurements have indicated an absence of a softening of atomic vibrations due to thermal expansion (Grüneisen effect) in the lead embedded into porous glasses with average pore diameter 7 nm. The characteristic size of nanoparticles was practically constant (~ 15 nm) up to 550 K. We have measured the temperature evolution of vibration density of states (VDOS) of the bulk material and lead within porous glass at RT and at 588 K, i.e. in a vicinity of melting point, where the growth of nanoparticle size was observed in diffraction experiment. For the wavelength 5.5 \AA there is no Bragg scattering neither by lead nor by aluminum, the material of the sample cell, in the available range of the scattering angles. In Fig. 1 the experimental spectra for the bulk at 304 K (curve 1) and at 588 K (curve 2) are presented. It is necessary to underline that the "softening" of VDOS spectrum is absolutely visible. In Fig. 2 the experimental spectra for lead in a restricted geometry are presented, curve 1 – at 304 K, curve 2 – at 588 K. These spectra are the sum of scattering on confined lead, silica matrix and sample environment. The growth of intensity at small energies (250 – 300 channels) is due to scattering on porous glasses. So to compare the results for the bulk and confined materials we have obtained the direct experimental evidence of hardening of phonon spectra in

lead embedded into porous glasses with average pore diameter 5 nm.

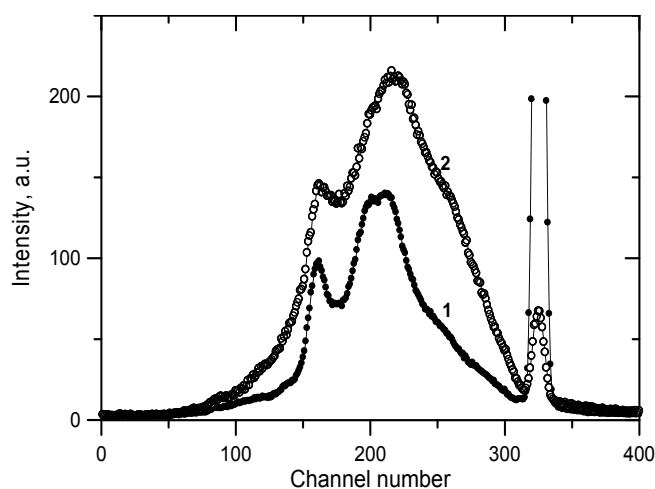


Fig. 1

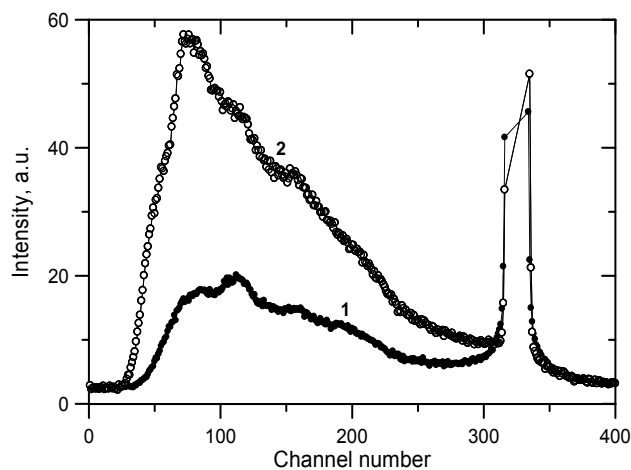


Fig. 2

- 1 A. Naberezhnov, A. Fokin, Yu. Kumzerov, A. Sotnikov, S. Vakhrushev, and B. Dorner, *Eur. Phys. J. E* **12**, s21-s24 (2003)
 2 I.V. Golosovsky, R.G. Delaplane, A.A. Naberezhnov, Y.A. Kumzerov, *Phys. Rev.* **B69**, 132301-1 – 132301-4 (2004)

 HELMHOLTZ ZENTRUM BERLIN für Materialien und Energie NEUTRONS	EXPERIMENTAL REPORT	Proposal: MAT-03-666 Instrument: V3 Local Contact: E. Kemner, M. Russina
	Hydrogen dynamics in liquid LiBH₄	Date(s) of Experiment 13.10.2009 – 22.10.2009
Principal Proposer: Experimental Team:	Arndt Remhof, EMPA Arndt Remhof, EMPA Pascal Martelli, EMPA Dirk Wallacher, HZB	Date of report: 01.02.2010

LiBH₄ is currently discussed as possible future hydrogen storage material. At ambient conditions, it is an ionic crystal, consisting of Li⁺ and BH₄⁻ ions. It melts at 280°C and releases considerable amounts of hydrogen from the liquid phase above 300°C in vacuum. The compound can be stabilized above this temperature by applying external hydrogen pressure. We studied the hydrogen dynamics in liquid LiBH₄ by means of quasi-elastic neutron scattering. Due to the covalent nature of the B-H bond, we expected the hydrogen dynamics to be markedly different than in solid solution metal hydrides.

The experiment was carried out using the cold neutron time-of-flight (TOF) spectrometer "NEAT" (V3). The sample was filled in a double walled Inconel sample container and placed into the high temperature furnace (HTF), provided by the DEGAS lab of the HZB. The HTF was placed onto the sample stage of the V3 instrument and the sample container was connected to the gas loading system, supplying hydrogen (H₂) of 50 bar. Inelastic and quasielastic neutron scattering was carried out at incident wavelengths of 5.1Å and 6Å. During the experiments the temperature of the sample was increased stepwise from room temperature to 450°C. Depending on the chosen wavelength a spectrum was recorded within 6h (5.1Å) or within 18h (6Å). The measured TOF data were reduced and binned to quasielastic spectra in the energy range of $\Delta E = \pm 2$ meV and momentum transfer range of $Q = 0.5 \text{ \AA}^{-1}$ to $Q = 2.5 \text{ \AA}^{-1}$. The QENS spectra were modelled using two components: A Gaussian to describe the elastically scattered neutrons and a Lorentzian-shaped quasielastic contribution, arising from the hydrogen motion. The width of the elastic line was fixed to the one of a vanadium standard sample. In the solid phase, the intensity of the quasielastic contribution increases with increasing Q, while its width is independent of Q for the whole measured Q-range. This observation is indicative of localized hydrogen motion and

confirms earlier reports [1,2]. The liquid phase shows a completely different behaviour as displayed in Figure 1. Here, the quasielastic contribution decreases with increasing Q, indicative of long range translational diffusion, most probably originating from the random walk of the BH₄ units in the liquid.

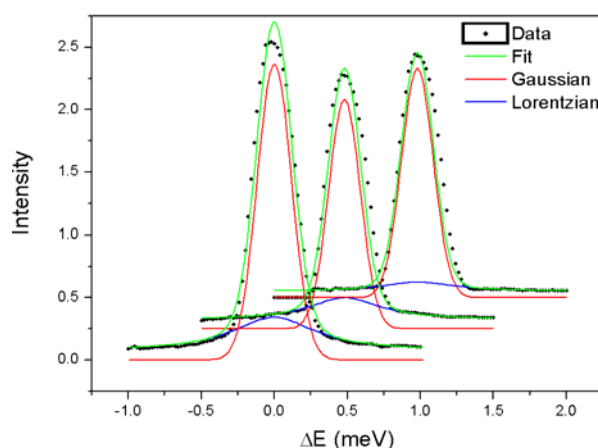


Figure 1: QENS spectra of liquid LiBH₄, measured at $T = 300^\circ\text{C}$, together with the respective two-component fit. The spectra were binned in a range of scattering vectors of $Q = 0.5 \text{ \AA}^{-1}$ to 2.5 \AA^{-1} with $\Delta Q = 0.2 \text{ \AA}^{-1}$. For clarity, the spectra are offset and only the $Q = 0.7 \text{ \AA}^{-1}$, 1.3 \AA^{-1} and 2.1 \AA^{-1} are shown. The liquid state is characterized by a quasielastic contribution that decreases with increasing Q and with a Q-dependent line-width.

Acknowledgements

Financial support from the Swiss National Science Foundation (SNF-Project 200021-119972/1) is gratefully acknowledged. This research project has been supported by the European Commission under the 7th Framework Programme through "Research Infrastructures" action of the "Capacities" Programme, contract number CP-CSA_INFRA-2008-1.1.1. Number 226507-NMI

References:

- [1] A. Remhof et al., *J. Phys. Chem. C*, **2009**, 113 16834.
 [2] A. Remhof et al., *in preparation*.

	EXPERIMENTAL REPORT	Proposal: PHY-03-667
	Influence of conformational disorder on the structure and dynamics of Freon 112	Instrument: V3 Local Contact: E. Kemner
Principal Proposer: Experimental Team:	Muriel Rovira-Esteva, UPC Barcelona, Spain Luis Carlos Pardo, UPC Barcelona, Spain Maria Dolores Ruiz-Martin, UPC Barcelona, Spain	Date(s) of Experiment 22.10.2009 – 29.10.2009

Date of report: 01.02.2010

Orientationally disordered crystals (ODC), or plastic crystals, are molecular materials showing the centers of mass of the molecules ordered in a lattice but rotating more or less freely. Thus translational order still remains but one observes a disorder related to the molecular orientation. The interest in these materials emerges from the fact that the rotator phases, when cooled down at moderate rates, may reach an orientational glassy state in which rotations are frozen and exhibit static orientational disorder. Transitions between these two states involve a true, calorimetric glass-transition [1] offering the possibility to study glass phenomena on long-range ordered system, which are in turn simpler than structural glasses. Detailed comparisons between the dynamics of a material in glass and ODC states [2] show evidence to close proximity in the dynamics of glass and ODC states, where both show strong non-Arrhenius behaviour of the relevant relaxation time. This is a known fingerprint of "fragile" glasses, and indeed Freon 112, 1,1,2,2-tetrachloro-1,2-difluoroethane, $\text{FCI}_2\text{C}-\text{CCl}_2\text{F}$ seems to be the most fragile plastic crystal known so far [3]. Freon 112 displays an ODC phase with bcc symmetry that can be easily super-cooled to even 4 K, being the transition kinetics to the low temperature crystalline ordered stable phase (with an unknown crystal symmetry) extremely slow. The molecules that compose such material display two possible conformations, *trans*- and *gauche*, displaying only the second conformation a dipolar moment, and having a ratio between them that depends at least on temperature. A first calorimetric study on Freon 112, pointed out a series of thermal effects: at 60 K probably related to a secondary relaxation; at 90 K connected to a primary glass transition, and finally at 130 K associated to the freezing of the disorder between the *trans* and *gauche* conformations. The purpose of this experiment was to determine the influence of the conformational disorder on the dynamics of the liquid phase of Freon 112. Measurements of the dynamic scattering function $S(Q, \omega)$ were performed on the NEAT time of flight spectrometer working with a monochromatic neutron beam of $\lambda = 5.5 \text{ \AA}$, which provided an energy resolution of 100 \mu eV , measured at the elastic peak position. Two different thermodynamic states were explored. The first set of measurements was carried out at 300 K, just above the melting point of the sample, and the second one a few degrees below boiling, at 355 K.

The DOS of Freon112 at these temperatures is depicted in Fig. 1, in which significant differences can not be appreciated. Further analyses of the quasielastic part of the spectra are under way.

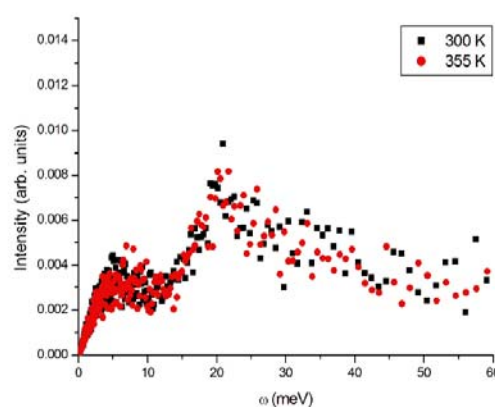


Fig 1. Density of states of Freon 112 at 300 K and a 350 K.

Acknowledgement:

This research project has been supported by the European Commission under the 7th Framework Programme through "Research Infrastructures" action of the "Capacities" Programme, contract number CP-CSA_INFRA-2008-1.1.1. Number 226507-NMI

- [1] Schilling R. J.Phys.: Cond.Matter, 15, S967 (2003); Talon C. et al. PRB 58, 745 (1998) and PRL 88, 115506 (2002)
 [2] Jimenez Ruiz M. et al., PRB 59, 29155 (1999); PRL 83, 2757 (1999) and J.Phys.:Cond.Matter 14, 1509 (2002)
 [3] Angell C.A. et al., J. Chem. Phys. 82,773 (1985); Pardo et al., J. Chem. Phys. 124, 124911 (2006) and J. Non-Cryst. Solids 353, 999 (2007) [4] Kishimoto K., Bul. Soc. Japan 51(6), 1691 (1978)

 HELMHOLTZ ZENTRUM BERLIN für Materialien und Energie NEUTRONS	EXPERIMENTAL REPORT Crystal electric field in PrT₂Ge₂ (T = Ag, Ru) compounds	Proposal: PHY-03-670 Instrument: V3 Local Contact: Z. Izaola
	Principal Proposer: Łukasz Gondek, AGH Univ. of Science and Technology Experimental Team: Joanna Czub, AGH Univ. of Science and Technology Zunbeltz Izaola, HZB	Date(s) of Experiment 19.08.2009 – 23.08.2009

Date of report: 27.09.2009

The proposed experiment aimed at determination of crystal field (CF) levels distribution in group of praseodymium samples of RT₂Ge₂ family. Namely PrNi₂Ge₂ and PrRu₂Ge₂ samples were investigated. The collected inelastic neutron scattering data are especially valuable in order to explain magnetic behaviour of the above mentioned family.

In case of praseodymium-based compounds the CF ground state might be formed by intrinsically non-magnetic singlet. However, if magnetic interactions are of the order of splitting between ground and first excited CF level the long-range magnetic ordering may occur. Thus, performed experiment provided useful information for CF splitting scheme as well as CF parameters values determination.

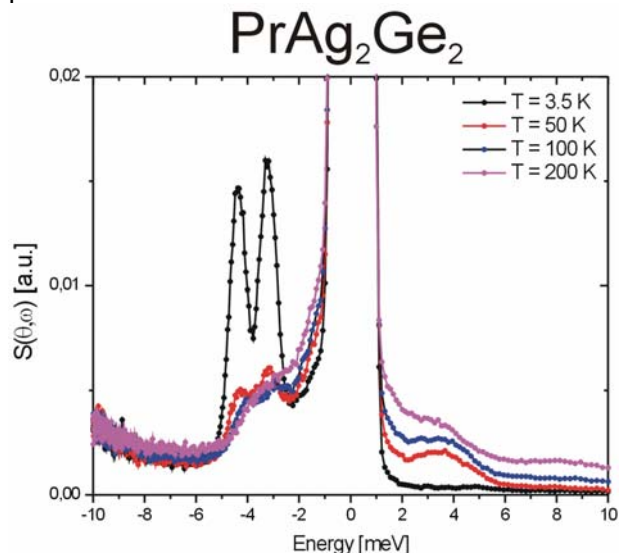


Fig. 1 INS spectra of PrAg₂Ge₂.

The INS spectra of non-magnetic PrAg₂Ge₂ compound are presented in figure 1. At the lowest temperature at least three anomalies are visible. Namely, two distinct peaks at 5.5 and 3 meV are visible. Another, much weaker, anomaly can be noticed at 1.5 meV. It seems, that this anomaly stands for excitation from ground state into the first excited one. It means that ground level singlet is separated from the higher states by energy of at least 1.5 meV

(~17.5 K). Taking into account the paramagnetic Curie temperature of – 3.2 K it is clear, that the strength of magnetic interaction is too weak for forming quasi-doublet of ground and first excited crystal field levels. As a result, no magnetic ordering was noticed in this sample.

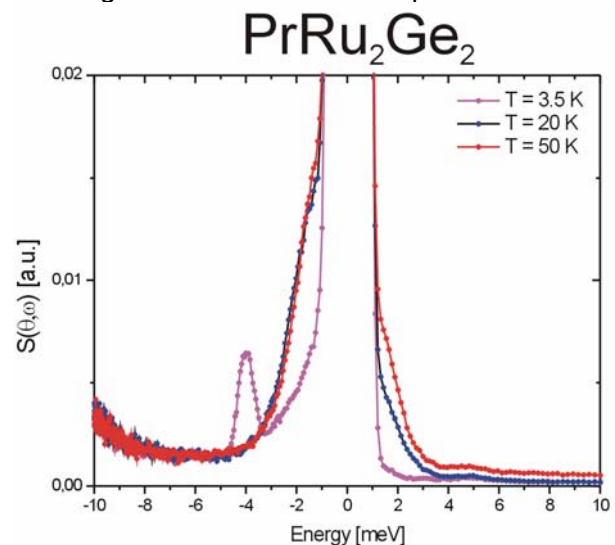


Fig. 2 INS spectra of PrRu₂Ge₂.

Result of studies on magnetically ordered PrRu₂Ge₂ are presented in figure 2. As one can see, there is completely different scheme of crystal field levels below and above the ordering temperature of 14.8 K. This effect can be attributed to molecular magnetic field. Above the ordering temperature the distinct anomaly being at 4 meV (at 3.5 K) is shifted to 1.4 meV (~16 K). Although this splitting is comparable to PrAg₂Ge₂, the sample exhibit magnetic ordering thanks to higher paramagnetic Curie temperature of 15 K.

The NMI3 project is supported by the European Commission through the 7th Framework Programme and it is part of the Research Infrastructures action of the Capacities Programme. (Contract No: 226507).

 HELMHOLTZ ZENTRUM BERLIN für Materialien und Energie NEUTRONS	EXPERIMENTAL REPORT	Proposal: MAT-03-671 Instrument: V3 Local Contact: E. Kemner, M. Russina
	Structure and dynamics of Opal: a combined USANS-QENS experiment	Date(s) of Experiment 11.11.2009 - 20.11.2009
Principal Proposer: Experimental Team:	L.P. Aldridge, ANSTO, Australia P. Thomas, A. Smallwood, A. Ray, UST, Sydney, Australia H.N. Bordallo, E. Kemner, HZB	

Date of report: 15.01.2010

In Australia, the commercial source of precious opal mainly comes from sedimentary environments whereas elsewhere opal is mostly found in volcanic rocks. Australia accounts for as much as 90% of total world precious opal production contributing approximately AU\$1 billion per annum to the economy. Precious opal is associated with play of colour (POC) and opal not exhibiting this POC is often called POTCH Opal. Opal has between 3 and 10% of the sample weight as water trapped in a silica matrix and this water can be supposed to be confined. Hence because of the interest in such an economically important gem whose stability is sometimes thought to be bound up with the water content, and as part of our studies on confined water in clays [1] and cement paste [2] we have compared the confinement of water in three different opals. – Volcanic Opal from Mexico (sample 1), Gem quality Coober Pedy Opal with POC (sample 2), and POTCH Opal from Lightning Ridge (sample 3). These are from the same locations as the Opal studied by USANS, proposal MAT-04-1850.

Using the time-of-flight spectrometer NEAT the powdered OPALS were placed in aluminium sample cans and the incoherent inelastic spectra were measured at a resolution of 98 μeV between 300 and 100 K. Another set of measurements on the same samples were carried out at $\sim 20 \mu\text{eV}$. The resolution spectra from the QENS spectra of vanadium and spectra from empty cans were also measured,

After performing detector efficiency corrections, extracting the Bragg peaks (Fig. 1) and correcting for sample transmission using the programs FITMO and LAMP, preliminary results were obtained for the quasi-elastic part of the spectra, as well information on the vibrational density of states. The QE response vs Q for each sample is similar, however a markedly different half-width at half maximum (HWHM) is observed (Fig. 2). The water in the Volcanic Opal (red line) seems to be less constrained. On the other hand, from the density of States obtained at 300K we clearly observe that the peak at $\sim 6 \text{ meV}$, characteristic of bulk water is extremely reduced

in all samples, suggesting that the water is indeed confined.

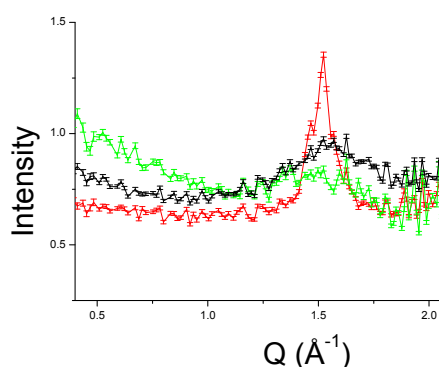


Figure 1: Diffraction pattern of Mexican (Red circle), Lightning Ridge (Black asterisk), and Coober Pedy (Green triangle).

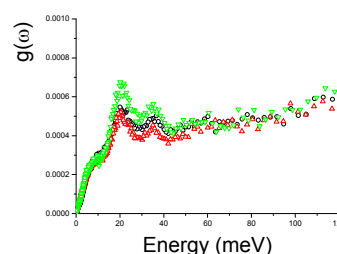


Figure 2: Density of States with samples identified as in Fig 1

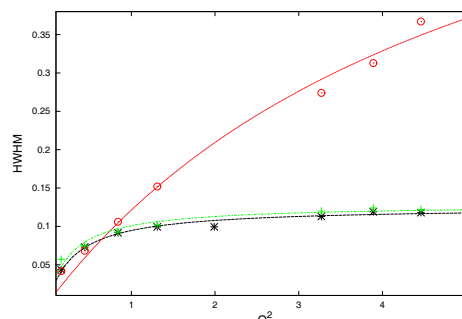


Figure 3: Preliminary fits of the HWHM vs Q^2 at 300K with samples identified as in Fig 1.

[1] H.N. Bordallo, L.P. Aldridge et al J. Phys. Chem C 112(36), 13982 -13991.

[2] H.N. Bordallo, L.P. Aldridge A. Desmedt, J. Phys. Chem. B, 110(36), 17966-76.

	EXPERIMENTAL REPORT	Proposal: CHE-03-643
	Hydroxide ion dynamics in hydrated nanoporous mayenite, Ca₁₂Al₁₄O₃₃	Instrument: V5 Local Contact: S. Wellert
Principal Proposer: Experimental Team:	Camilla Kongshaug, University of Oslo Dirk Wallacher, HZB Niina Jalarvo, University of Oslo	Date(s) of Experiment 03.04.2009 - 09.04.2009

Date of report: 24.01.2010

Solid proton conducting materials are of great interest for various applications, e.g. fuel cells, electrolyzers and hydrogen separation membranes. Understanding the conduction path of hydrogen is important for the utilization of these materials. Until now, the only observed pathway in oxidic materials is migration of the proton from one oxide ion to a neighbouring one. In Ca₁₂Al₁₄O₃₃(OH)₂ we have indications of another type of migration, namely transport of the entire hydroxide ion, where the proton acts as a passenger.

We have studied the migration of hydroxide ions using NSE technique at V5 instrument. The instrumental configuration of 6.5 Å was used and by checking the flipping ratio $I_{up}-I_{down}/I_{up}+I_{down}$ at different angles a suitable Q-range was chosen. Measurements were then taken at average Q-values of 0.4, 1.01, and 1.7 Å⁻¹. Measurements were then performed at temperatures between 500 and 1100 °C, exposure time of each data set being about 24 hours.

The required conditions for this experiment were challenging; extreme temperatures in combination with a vacuum sealed sample container that would not cause depolarization of the beam nor remarkable elastic background. The existing sample holders could not be used, since they could not stand the required high temperatures, or they would cause depolarization of the neutron beam at such temperatures. During the experiment we tested a suprasil quartz tube and a steel container, as well as packing the sample into platinum foil. The steel container appeared to produce too high background signal. Sample packed into platinum foil was more promising; incoherent signal was observed (see figure 1), but the sample was dehydrated at 800 °C during the measurement due to the high vacuum at the furnace. For that reason the sample should be in a container that is sealed.

The quartz container emerges to be more suitable, as we could seal the quartz tube using the DeGas system. Anyhow, some problems were still to be faced with insufficient amount of sample. Finally, amount of the sample was increased, then wrapped into platinum foil and placed into the quartz tube. Subsequently, data was collected at three temperatures 500, 1000 and 1100 °C.

Polarization signal at the three different banks were calculated following the equation

$$\frac{(I_{up}^{sample} - I_{up}^{container}) - (I_{down}^{sample} - I_{down}^{container})}{(I_{up}^{sample} - I_{up}^{container}) + (I_{down}^{sample} - I_{down}^{container})}$$

At Q values of 0.4, 1.01 and 1.7 Å⁻¹ the obtained polarization signals were -2%, -17% and -19% respectively. This indicates spin incoherent signal due to H atom. The background from the quartz tube and platinum was still too dominant and the sample geometry used for the measurements, was also providing problems. Appropriate data analysis was therefore not possible in this case.

We can conclude that we have observed incoherent signal in Ca₁₂Al₁₄O₃₃(OH)₂ indicating H diffusion in the material. For more precise information, a wavelength and appropriate sample container should be used. Design of a suitable sample container is necessary for future experiments.

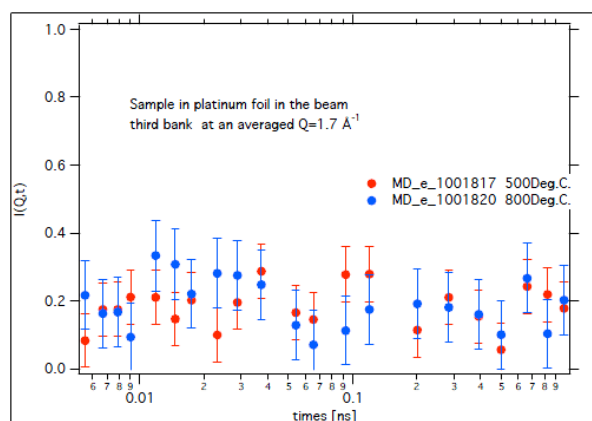


Figure 1. Ca₁₂Al₁₄O₃₃(OH)₂ powder packed into Pt foil at 500 and 800 °C.

 HELMHOLTZ ZENTRUM BERLIN für Materialien und Energie NEUTRONS	EXPERIMENTAL REPORT Influence of conformational disorder on the dynamics of Freon 112	Proposal: CHE-03-676-EF Instrument: V5 Local Contact: S. Wellert
	Principal Proposer: Heloisa N. Bordallo, HZB Experimental Team: Muriel Roviera-Esteva, UPC, Barcelona, Spain Maria Ruiz-Martin, UPC, Barcelona, Spain Luis Pardo, UPC, Barcelona, Spain Heloisa N. Bordallo, HZB	Date(s) of Experiment 22.10.2009 – 01.11.2009

Date of report: 26.01.2010

Orientationally disordered crystals (ODC), or plastic crystals, are molecular materials showing the centers of mass of the molecules ordered in a lattice but rotating more or less freely. Thus translational order still remains but one observes a disorder related to the molecular orientation. The interest in these materials emerges from the fact that the rotator phases, when cooled down at moderate rates, may reach an orientational glassy state in which rotations are frozen and exhibit static orientational disorder. Transitions between these two states involve a true, calorimetric glass-transition [1] offering the possibility to study glass phenomena on long-range ordered system, which are in turn simpler than structural glasses. Detailed comparisons between the dynamics of a material in glass and ODC states [2] show evidence to close proximity in the dynamics of glass and ODC states, where both show strong non-Arrhenius behavior of the relevant relaxation time. This is a known fingerprint of "fragile" glasses, and indeed Freon 112, 1,1,2,2-tetrachloro-1,2-difluoroethane, $\text{FC}_2\text{C}-\text{CCl}_2\text{F}$ seems to be the most fragile plastic crystal known so far [3].

Freon 112 displays an ODC phase with bcc symmetry that can be easily super-cooled to even 4 K, being the transition kinetics to the low temperature crystalline ordered stable phase (with an unknown crystal symmetry) extremely slow. The molecules that compose such material display two possible conformations, *trans*- and *gauche*, displaying only the second conformation a dipolar moment, and having a ratio between them that depends at least on temperature. A first calorimetric

study on Freon 112 [4], pointed out a series of thermal effects: at 60 K probably related to a secondary relaxation; at 90 K connected to a primary glass transition, and finally at 130 K associated to the freezing of the disorder between the *trans* and *gauche* conformations.

Our aim in this study was to determine the influence of the conformational disorder of the molecule on the dynamics of the plastic and glassy phases. Measurements of the intermediate scattering function $S(Q,t)$ were performed on the SPAN neutron spin-echo spectrometer for Q -values in the range $0.3 < Q < 2.5 \text{ \AA}^{-1}$ using an incident neutron wavelength of 5.5 \AA . The data were collected between 100 and 270K and corrected for instrumental resolution by normalizing each scan to the elastic reference scan of the sample obtained at 2K. As depicted in Figure 1, we were able to evidence a very slow motion that is activated at around 100 and persists up to 160K. Further analyses are under way.

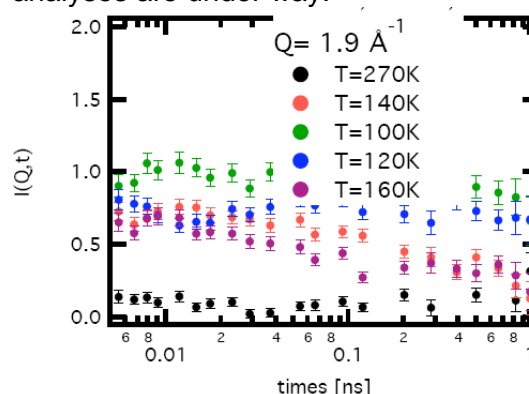


Fig. 1. Q resolved $S(Q,t)$ scans of Freon112 at various temperatures for $Q = 1.9 \text{ \AA}^{-1}$.

[1] Schilling R. J.Phys.: Cond.Matter, 15, S967 (2003); Talon C. et al. PRB 58, 745 (1998) and PRL 88, 115506 (2002)

[2] Jimenez Ruiz M. et al., PRB 59, 29155 (1999); PRL 83, 2757 (1999) and J.Phys.:Cond.Matter 14, 1509 (2002)

[3] Angell C.A. et al., J. Chem. Phys. 82,773 (1985); Pardo et al., J. Chem. Phys. 124, 124911 (2006) and J. Non-Cryst. Solids 353, 999 (2007)

[4] Kishimoto K., Bul. Soc. Japan 51(6), 1691 (1978)

 Neutrons	EXPERIMENTAL REPORT	Proposal: EF
	Study on lead single-crystals	Instrument: V12a Local Contact: W. Treimer
Principal Proposer:	M. Liesegang, S.-O. Seidel, W. Treimer, University of Applied Science	Date(s) of Experiment
Experimental Team:	M. Liesegang, University of Applied Science S.-O. Seidel, University of Applied Science O. Ebrahimi, University of Applied Science N. Karakas, University of Applied Science W. Treimer, University of Applied Science	08.06.2009 – 21.06.2009 30.06.2009 – 13.07.2009

Date of report: 12.01.2010

In this study the mosaic spread σ of nearly mono-crystalline different lead crystals was analyzed to compare σ as a function of orientation and pressure. The raw cylindrical crystals (111, 110 and 100 orientation) had a diameter of 12 mm and a height of 30 mm. Slices were cut with a thickness of 2mm and the intrinsic mosaic spread measured ranging from 0.26 to 1.76 degree with a standard deviation of 2%. Based on these results, different mosaic structures can be realized by deforming the crystal-slices. The process of deformation was supposed to be an irreversible damaging, that influences the crystal structure of crystals concerning defective structures. With these crystals samples, a mosaicity from 0.26 deg. to 2 deg could be produced in order to investigate the phenomenon of magnetic flux-pinning in different distorted crystals.

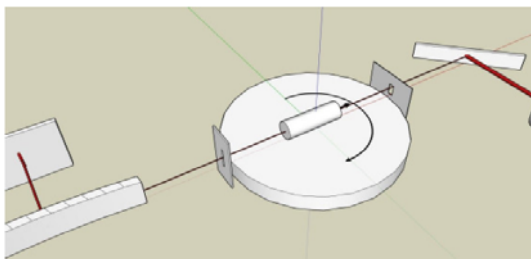


Fig.1: Schematic of measurement at V12.

First the correct orientation of the (hkl) plans had to be determined. Rotating the sample from 0-180° in a double crystal diffractometer one observed minima that corresponds to Bragg planes.

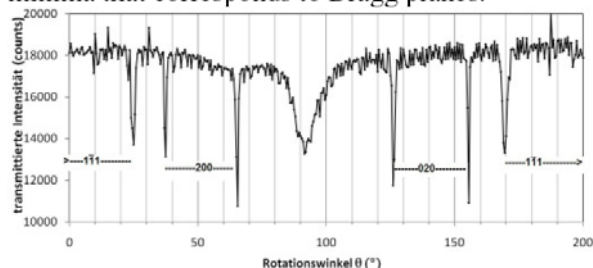


Fig.2: Scattering profile of lead crystal (110). Due to the minima the reflecting crystal-planes were identified and their orientation in the sample.

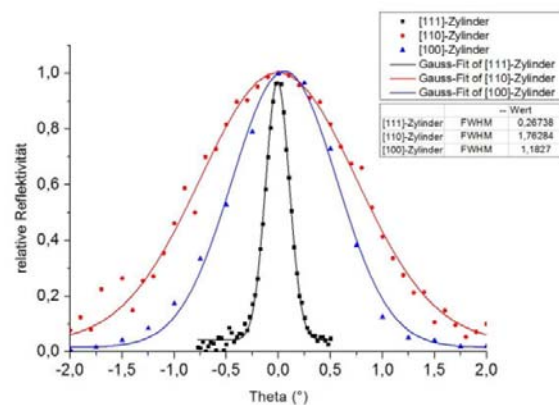


Fig.3: Bragg reflection profiles for three different orientated crystals. Each one has the mosaicity of the non-deformed mode.

From these minima the accurate orientation of the sample with respect to its $\langle 100 \rangle$, $\langle 110 \rangle$ and $\langle 111 \rangle$ could be determined (Fig.1 – Fig.3).

Then one lead slice with the $\langle 111 \rangle$ orientation was deformed with a special designed mechanism and the particular rocking curves measured (Fig.4)

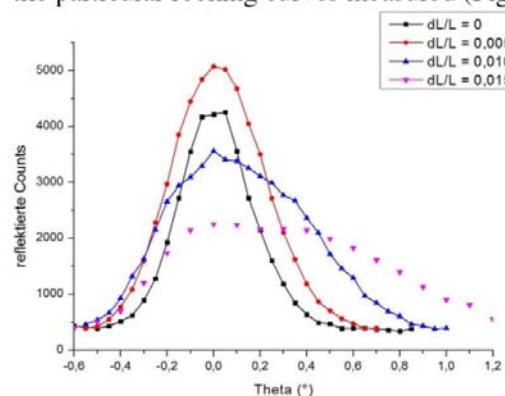


Fig.4: Profile of Bragg reflections from a crystal-slice with the orientation (111) as a function of deformation. Mosaicity of the crystal improved at low deformations, increasing in reflectivity with a maximum of 20% (black and red curve) indicating lower Fresnel- and Schottky-defects.

Some peculiarities were found concerning the dependence of σ on pressure.

	EXPERIMENTAL REPORT Structure and dynamics of Opal: a combined USANS-QENS experiment	Proposal: MAT-04-1850 Instrument: V12a Local Contact: S.-O. Seidel
	Principal Proposer: L. P. Aldridge, ANSTO, Australia Experimental Team: P. Thomas, A. Smallwood, A. Ray, University of Technology, Sydney, Australia H. N. Bordallo, S.-O. Seidel, M. Strobl, HZB C. Rehm, ANSTO, Australia	Date(s) of Experiment 11.11.2009 – 18.11.2009

Date of report: 15.01.2010

Precious opal is associated with play of colour (POC) and opal not exhibiting this POC is often called POTCH Opal. Opal is made up of spheres of silica cemented together with silica. When the spheres are regularly arranged then they diffract light hence the origin of the POC. In the past, SANS has been used to identify the regularity of the arranged spheres and in this study we aimed to determine if USANS can differentiate between the POTCH and POC opal. This was found to be the case.

Four different parcels of opal specimens were selected, 3 sedimentary opals from Australia, and the 4th a volcanic opal; (1) POTCH opal from Lightning Ridge (Australia), (2) POC opal from Coober Pedy (3) Mintabie Both POTCH & POC, and (4) A volcanic opal from Mexico. Three samples (~1*10*10mm) were cut from separate stones from each sample location. The three different samples from Mintabie consisted of one POC and two POTCH and results from these samples are shown here in Figures 1 & 2.

The samples were mounted on a cadmium tray with 8 separate sample holes of 8mm diameter each, drilled into the cadmium and positioned at the same height. The samples were mounted either singly or in 3 layers one on top of the other.

It was found necessary to extend the Q-range towards higher Q by increasing the bending of the analyser crystal at the standard resolution and we were able to record spectra with a Q range between 0.004-0.8 nm⁻¹. Here we show the results for the Mintabie opal (sample 3). Each spectrum was counted for 8 million monitor counts (~4.5 hours). To correct the data the empty hole was counted for the same time. Then the spectra were corrected using procedures available at HZB as follows. First the 2D channels were summed and then a "correction curve" was taken by rotating the analyser and recounting the empty beam. The difference between the peak heights and positions were used to calibrate the detection efficiency and the Q values, respectively. Once the corrections were applied, the curves were normalised and subtracted from the empty beam spectra. The difference between the POC and the POTCH samples is evident. Due to low counting statistics, 5

adjacent Q values were summed and the resulting plots are shown in Figures 1 & 2.

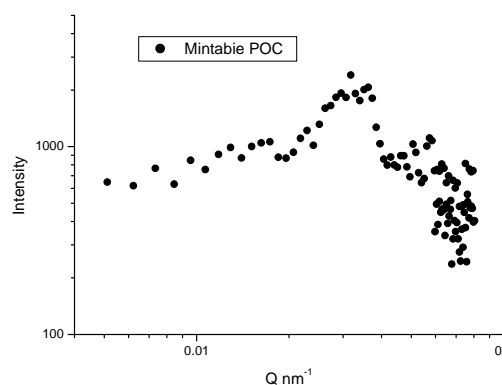


Figure 1: USANS spectra of Mintabie POC..

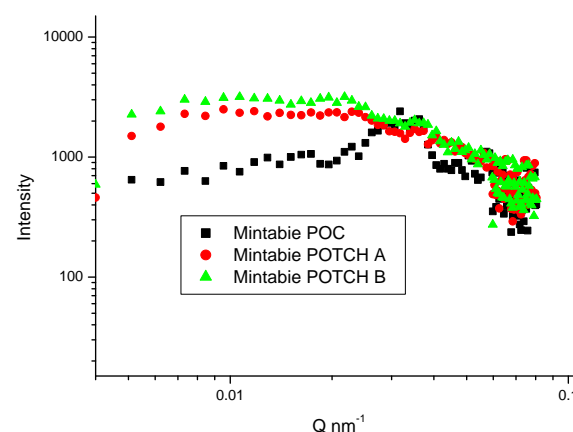


Figure 2: Comparison between USANS Spectra of the Mintabie POC (in black) and POTCH samples (in red and green).

The preliminary analysis of the other 3 opals give similar contrast to the POC and POTCH samples suggesting that USANS can be used to differentiate the gem quality of the OPALS

These results are quite encouraging and a further proposal will be submitted in the near future.

**Radiography of a diffusion process
between D2O and H2O**

Proposal: EF

Instrument: **V19**

Local Contact:
W. Treimer

Principal Proposer: W. Treimer, Beuth Hochschule für Technik & HZB
O. Ebrahimi, S.-O. Seidel, M. Konieczko-Dziadula,
Beuth Hochschule für Technik

Experimental Team: M. Konieczko-Dziadula, O. Ebrahimi, N. Karakas,
S.-O. Seidel, Beuth Hochschule für Technik
W. Treimer, Beuth Hochschule für Technik & HZB

Date(s) of Experiment

23.11.2009 – 23.12.2009

Date of report: 12.01.2010

We report about the imaging of the diffusion process between D2O and H2O using neutron radiography. This method is superior to other techniques, if diffusion cannot be observed directly (with light or other sensors) because of higher attenuation coefficient of the hydrogen isotope H2 compared the deuterium isotope D2 for neutrons. To observe this diffusion process a special cell was constructed as shows Fig.1

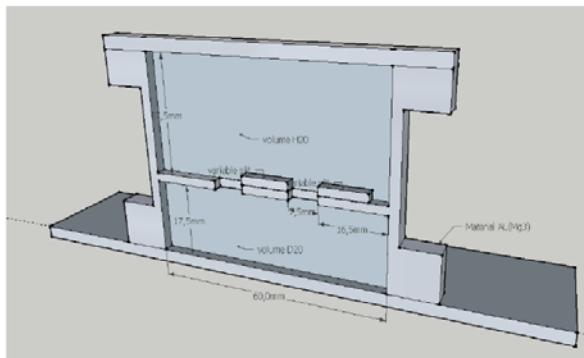


Fig.1 Drawing (slice plane) of the used aluminium diffusion-cell for the experiment

The cell consisted of aluminium having two compartments filled with D2O and H2O in a ratio of 1:1 with defined boundary layer between both fluids and a thickness of 5 mm. H2O was deposited over D2O (both purities = 99.96%). The special feature of this diffusion cell was that it has a manual catch, which separates the two solutions from each other on beginning. The neutron radiography period was performed over more than 17 hours in 3 minutes intervals. Fig.2 shows the first radiography of the sample, the increased absorption of neutrons by distilled hydrogen compared to the deuteriumoxid. After a time the distilled hydrogen mixed up with the deuteriumoxid. The integral intensity over the z-axis of all taken radiograms in one dimension was studied. Fig.3 shows the normalized and from background subtracted distribution of the in-

tensity over the diffusion time, which runs proportional to the diffusion gradient and is caused by the diffusing of H2O in D2O due the increased neutron absorption. We could see an exponential decrease of the Intensity, which is direct proportional to the concentration-profile of H2O and fits with the theory given by

$$\text{the law of Fick: } \frac{\partial c}{\partial t} = \nabla \cdot (D \nabla c)$$

From this one can determine diffusion laws as well as the temporal courses of the diffusion gradient. It shows the significance of neutron radiography concerning research of physical processes, especially where other technics fail to give meaningful informations.

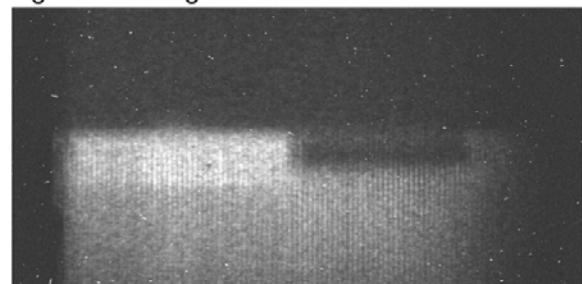


Fig.2 First step of the neutron radiography of the diffusion between heavy water and light water

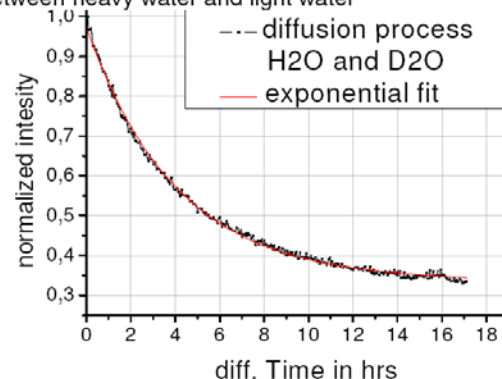


Fig.3 Transmitted intensity within a ROI in Fig.2 as a function of time: Increasing concentration of H2O in D2O decreases the transmitted intensity.

This work was part of the BMBF project 5KN7KF1

Biology & Soft Matter

 Neutrons	EXPERIMENTAL REPORT Neutron Powder Diffraction Studies of L and DL-Cysteine	Proposal: OTH-01-2554-EF Instrument: E9 Local Contact: P. Henry/D.N. Argyriou
	Principal Proposer: Heloisa, N. Bordallo, HZB Experimental Team: Vasily Minkov, Novosibirsk State University Heloisa N. Bordallo, HZB Paul Henry, HZB Dimitri N. Argyriou, HZB	Date(s) of Experiment 03.04.2009 – 07.04.2009

Date of report: 02.12.2009

At ambient temperature, as evidenced by X-ray and neutron diffraction, in L-cysteine the sulfur atoms of the thiol groups are disordered over two positions. The distances between the oxygen and sulfur atoms of the neighboring molecules in the structure are consistent with the hypothesis on the formation of the two types of intermolecular hydrogen bonds, S-H...S and S-H...O [1]. A recent structural study of L-cysteine at 30 K has shown that the sulfur atoms are completely ordered and located at positions corresponding to the formation of the S-H...S hydrogen bonds [2]. Heat capacity measurements on the crystalline orthorhombic polymorph showed a small, 3-5% height, diffuse "jump", or a wide "hump" near 70 K, accompanied by the substantial increase in the thermal relaxation time. Such $C_p(T)$ dependence is typical for a transformation extended over a wide temperature range, responsive to the thermal prehistory of the sample. It was assumed as resulting from non-simultaneous changes in the dynamics and the orientation of the numerous thiol groups in the structure. Besides, the X-rays measurements of the cell parameters and cell volume on cooling suggest a discontinuity in their values over the transition point [3]. On the other hand, for DL-cysteine a first-order phase transition accompanied with the fragmentation of crystals was observed on cooling; where the temperature of the transition strongly depends on the range and cooling rate varying from 250 K to 200 K. The transition is reversible, with a large hysteresis, the reverse transformation on heating being observed at 285 K – 305 K, depending on the heating rate. The crystal structure of the low temperature phase has been solved [4].

The aim of our proposal was to study fully hydrogenated L and DL-cysteine and accurately solve the crystal structure. Such result would allow us to follow the evolution of the hydrogen bonds. Although it is expected that the large incoherent scattering of H results in background scattering that greatly reduces

the signal-to-noise ratio of the neutron powder diffraction data, making it difficult to detect coherent Bragg scattering from the sample, the use of a fully deuterated sample can affect the stability of the crystalline amino acids [5]. Preliminary results obtained from neutron powder diffraction measurements of another sample – DL-serine – were quite encouraging [6]. Figure 1 shows a set of diffraction scans measured with a neutron wavelength of $\lambda = 1.797 \text{ \AA}$ using E9 at 50 K.

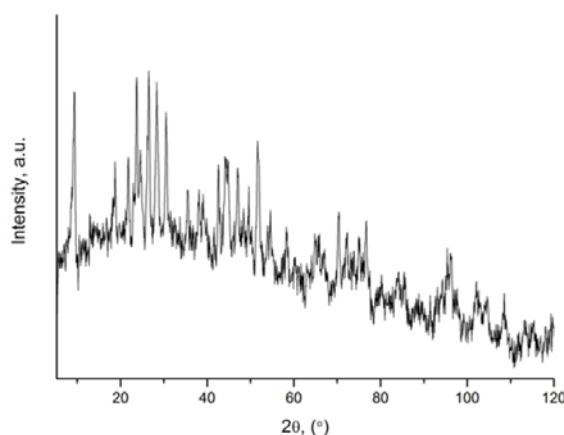


Figure 1. NPD data for DL-cysteine ($C_3H_7NO_2S$) measured on the E9 diffractometer at HZB ($\lambda = 1.797 \text{ \AA}$) at 50 K. The Bragg peaks could be indexed assuming the $P2_1/a$ space group.

Unfortunately due to intrinsic disorder of this particular amino acid a full structural refinement was not possible, and therefore we could not follow the evolution of the hydrogen bonds as originally proposed.

- [1] K.A. Kerr et al, *Acta Cryst. B* **1975**, 31, 2022.
- [2] S.A. Moggach et al, *Acta Cryst. E* **2005**, 61, o2739.
- [3] B.A. Kolesov et al, *J. Phys. Chem. B* **2008**, 112, 12827.
- [4] V.S. Minkov et al, *J. Phys. Chem. B* **2009**, 113, 5262.
- [5] J. de Souza et al, *J. Phys. Chem. B* **2007**, 111, 5034.
- [6] H.N. Bordallo & E.V. Boldyreva, **2008**, PSI Experimental Report.

 Neutrons	EXPERIMENTAL REPORT	Proposal: OTH-01-2555-EF
	Structure of L-Leucine: Symmetry change or Conformational Re-arrangement?	Instrument: E9 Local Contact: Fabiano Yokaichiya
Principal Proposer: Experimental Team:	Heloisa N. Bordallo, HZB Heloisa N. Bordallo, HZB Fabiano Yokaichiya, HZB Paulo T. C. Freire, UFC, Brazil X. Jiao, HZB & China Institute of Atomic Energy	Date(s) of Experiment 30.04.2009 - 04.05.2009

Date of report: 02.12.2009

L-Leucine and L-isoleucine ($C_6H_{13}NO_2$, hereafter LEU and ILE, respectively) are structural isomers, i.e. compounds that have the same molecular formula, similar chemical and physical properties but different structures. ILE possesses a β -branched and LEU a γ -branched side chain strongly hydrophobic formed by four-carbon, the only difference in the position of branching. LEU is considered to be the strongest α -helix forming residual, whereas ILE strongly favours the β -conformation. As both helix and β -conformations are stabilized by hydrophobic contributions, these strongly hydrophobic residues are excellent candidates for being active in the nucleation of secondary structures. Generally, LEU and ILE are attracted to similar hydrophobic side chains, such as valine, tryptophan, and phenylalanine. Moreover, like valine, LEU and ILE have large aliphatic hydrophobic side chains and have the tendency to be located inside of the protein molecule.

At room temperature LEU crystallizes in the monoclinic $P2_1$ space group ($a=9.606(3)$ Å, $b=5.324(7)$, $c=14.666(2)$ and $\beta=86.06^\circ$).¹ By means of differential scanning calorimetric and Raman measurements a phase transition at about 353K has evidenced.² A change of symmetry from the C_2 to the C_s point group through the appearance of new modes at high temperatures was suggested to explain the mechanism of this phase transition. On the other hand, ILE presents polymorphism and crystallizes in the $P2_1$ monoclinic structure ($a=9.57$, $b=5.32$, $c=14.12(3)$ Å $\beta=95.8^\circ$) like LEU, or in the $P2_22_1$ orthorhombic structure ($a=13.89(6)$, $b=20.17(5)$, $c=5.35(3)$ Å).³

The aim of our proposal was to study fully hydrogenated LEU and ILE to observe how the H-bond structure in each structure responds to temperature changes. Figure 1 shows a set of diffraction scans of LEU measured with a neutron wavelength of $\lambda = 1.797$ Å using E9 at 250 K. The NPD patterns between 250 and

120K cannot be indexed assuming the unit cell of the monoclinic $P2_1$ space group previously reported. Assuming a cell in the monoclinic $P2_1$ space group and doubling along the c-axis, as demonstrated by the Figure, allowed indexing the NPD pattern between 120 and 250K. However such approach did fail at 300K and below 120K. Unfortunately the quality of our data at present is not sufficient to determine the detailed crystal structure at lower temperature, and further studies are under way. However, as discussed in the report OTH-01-2560-EF by correlating the structural data to the dynamical response a picture of the driving mechanism of the observed solid-solid phase transition has been obtained.

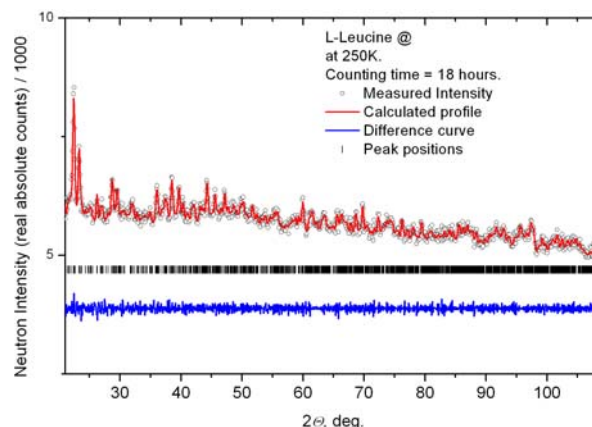


Fig. 1. (a) NPD data for L- Leucine obtained on the E9 diffractometer at HZB at 250K, $K \lambda = 1.797$ Å. The Bragg peaks could be indexed using LeBail fit assuming the $P2_1$ structure with $a = 14.40100(4)$, $b = 5.30461(6)$, $c = 19.14818(6)$ and $\beta = 86.14^\circ$.

- [1] Harding & Howieson, *Acta Crystallogr.* **B32**, 1979, 633. & M. Coll et al, *Acta Crystallogr.* **C42**, 1986, 599
- [2] D. Bougeard, *Ber. Bunsenges. Phys. Chem.*, **87**, 1983, 279. & P. F. Facanha Filho et al, *Brazilian Journal of Physics*, **38**, 2008, 131.
- [3] K. Torii and Y. Iitaka, *Acta Cryst.* **B27**, 1971, 2237. & B. Khawas *Acta Cryst.* **B26**, 1970, 1385.

	EXPERIMENTAL REPORT L-Methionine: Structure and Dynamics of an essential amino acid	Proposal: CHE-01-2591-EF Instrument: E9 Local Contact: P. Henry
	Principal Proposer: Heloisa N. Bordallo, HZB Experimental Team: Jennifer Fischer, Universität Kassel and HZB Heloisa N. Bordallo, HZB	Date(s) of Experiment 30.04.2009 – 04.05.2009

Date of report: 27.01.2010

Methionine is very important in the process of methylation and constitutes a precursor to other amino acids, such as L-cysteine and homocysteine (the latter, being involved in numerous processes of methyl group transfer, plays a fundamental role in the biochemistry of the human body). It has been used as a supportive supplement in immune-deficient patients, and its oxidation has been associated to some of the neurological diseases such as Alzheimer's disease. In crystalline form its hydrogen bonds form single layers and participate in the bond of adjacent layers generating double layers. Although, pronounced changes of the Raman spectra were observed for L- Methionine under pressure, up to date no systematic temperature or pressure study of this crystalline structure has been undertaken. Here we report on such results. Moreover, structural changes in small amino acids are normally followed by changes in the methyl and NH torsion, located at about 30 cm⁻¹ 55 meV in L- Methionine [2], which are usually very difficult to detect by infrared and Raman spectroscopy. Thus information about the density of states using inelastic neutron scattering is essential as a sensitive probe for the H-bonds environment – see Report [CHE-03-660-EF](#).

The crystal structure of L-methionine has been determined by X-ray diffraction methods. L-Methionine crystallizes in the space group P2₁, Z=4, with lattice constants a= 9.498, b= 5.189, c= 15.318 Å, β=97°69'.¹

The aim of our proposal was to study fully hydrogenated L-Methionine to observe how the H-bond structure in each structure responds to temperature changes.

Figure 1 shows a set of diffraction scans measured with a neutron wavelength of λ = 1.797 Å using E9 at 310 and 10 K. All NPD patterns could be indexed assuming the unit cell previously reported.

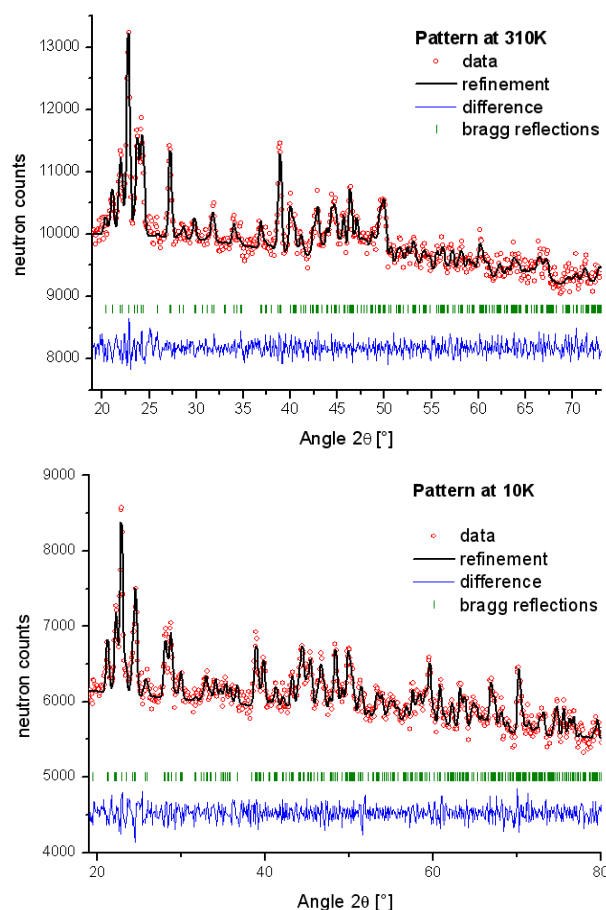


Fig. 1. (a) NPD data for L- Methionine obtained on the E9 diffractometer at HZB at 310 and 10, K λ = 1.797 Å. The Bragg peaks could be indexed using LeBail fit assuming the P 2₁ 2₁ 2₁ structure.

Although a full refinement of the structure was not possible from our data we were able to follow the evolution of the lattice parameters and correlate the structural modifications to observed in the vibrational spectra as reported in [CHE-03-660-EF](#).

[1] Torii & Iitaka, *Acta Crystallogr.* **B29**, 1973, 2799.

 Neutrons	EXPERIMENTAL REPORT	Proposal: PHY-01-2599 Instrument: E9 Local Contact: F. Yokaichiya, M. Tovar
	Influence of conformational disorder on the structure and dynamics of Freon 112	Date(s) of Experiment 20.10.2009 – 27.10.2009
Principal Proposer: Experimental Team:	Muriel Rovira-Esteva, UPC Barcelona, Spain Maria Dolores Ruiz-Martin, UPC Barcelona, Spain Luis Carlos Pardo, UPC Barcelona, Spain	

Date of report: 01.02.2010

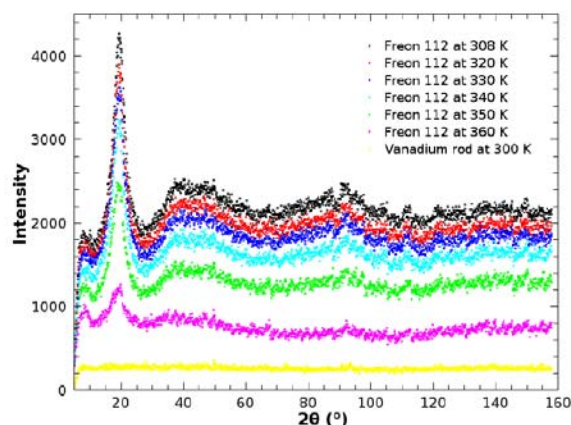
The purpose of the experiment was to analyze in the liquid state the influence of the existence of molecular conformations on the energy landscape as well as on the ability of forming the glass (structural or orientational) state for a simple molecular compound which is a good representative of fragile orientational glasses.

The sample was 1,1,2,2-tetrachloro-1,2-difluoroethane (Freon 112, $\text{FCl}_2\text{C}-\text{CCl}_2\text{F}$) which has two molecular conformers (trans and gauche) and is the most fragile orientational glass known so far. Sample was warmed up above 310 K and then loaded on a cylindrical sample holder which was sealed using indium wire. Then it was measured at 308, 320, 330, 340, 350 and 360 K using a cryofurnace.

Intensity considerations indicated that the sample was evaporating as temperature was raised, so the seal obtained with the aforementioned sample holder and sealing method was not enough for this sample at the work temperatures. That problem became only critical in the last measurement at 360 K. Probably that increase on the evaporation rate within the liquid phase was caused by an abrupt increase in the mobility of the molecules as the boiling temperature was approached.

No changes in the shape of the structure factor for high angles could be observed in the measured temperature range. Since that part of the spectrum is contributed mainly by the intramolecular structure, that disfavours the fact that a variation of the proportion between the trans and gauche conformers is taking place within the liquid phase.

Preliminary analysis suggest that all the variations observed in the first diffraction peak are due to dilatation phenomena and increasing disorder due to temperature effects but not to a change in the short range order of the molecules.



Acknowledgement:

This research project has been supported by the European Commission under the 7th Framework Programme through "Research Infrastructures" action of the "Capacities" Programme, contract number CP-CSA_INFRA-2008-1.1.1. Number 226507-NMI

 Neutrons	EXPERIMENTAL REPORT	Proposal: CHE-01-2602 Instrument: E9 Local Contact: Fabiano Yokaichiya
	Structural analysis of L and DL-Serine	Date(s) of Experiment 10.11.2009 – 18.11.2009
Principal Proposer: Experimental Team:	Boldyreva Elena, Novosibirsk State University Nikolay Tumanov, Novosibirsk State University Heloisa N. Bordallo, HZB Fabiano Yokaichiya, HZB	

Date of report: 09.12.2009

The chemistry of life is chiral. Therefore, stereochemistry is inherent in nearly all biochemical processes, pharmaceutical and agricultural applications, cosmetics and nutrition industries. Although the racemic and enantiomerically pure crystal forms contain the same molecule, their physical properties often differ because many solid-state properties are governed by the crystal structure. A pair L- and DL-serine ($C_3H_7NO_3$) is one of the most striking examples. Serine is prone to form clusters of molecules of the same chirality even in racemic mixtures. In the crystals of DL-serine one can find the chains and the two dimensional arrays of L-serine molecules alternating with chains and layers formed by D-molecules, but their structures are different from those in the crystals of L-serine. Understanding the structure-properties relation in this system is interesting by itself, and because of the biological applications. Serine-serine interactions account for many biochemical processes, in particular – for the functioning of polar clamps and serine zippers in membrane proteins.

Interestingly, the denser structure of L-serine is about 4 times more compressible on cooling at ambient pressure, than that of the DL-serine. The anisotropy of the structural strain in L-serine and in DL-serine both on cooling and with increasing hydrostatic pressure is remarkably different [1].

The aim of our proposal was to study fully hydrogenated L and DL-serine and observe how the H-bond structure in each structure responds to temperature changes. Normally the determination of H positions in biological materials relies on deuteration, often expensive; and as just demonstrated, due to the Ubbelohde effect, an increase in HB lengths may occur inducing changes in the HB interactions [2]. Based on our measurements on November 2008 using HRPT at PS [3] such a problem could be addressed using E9. In the particular case of L or DL-serine although the high incoherent neutron

scattering cross section of H atoms gives rise to a high background the sample is a quite good scatter so the effect can be compensated.

Figure 1 shows a diffraction scan for L-Serine measured with a neutron wavelength of $\lambda = 1.797 \text{ \AA}$ using E9 at 5 K.

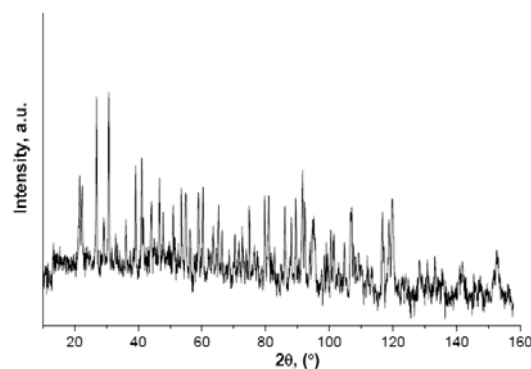


Figure 1. (a) NPD data for L-Serine measured on the E9 diffractometer at HZ Berlin using $\lambda = 1.797 \text{ \AA}$ at 5 K.

Unfortunately due to the different design of E9 (the detector bank consists of 64 ^3He single detector tubes and the diffraction pattern is obtained by step scanning) and HRPT (large position sensitive ^3He detector allowing for simultaneous measurements) a full structural refinement was not possible. We hope that with the new E9 our experiment can be soon realized.

- [1] E. V. Boldyreva et al Chem Phys Lett **2006**, 429, 474 & Z. Kristallogr. **2006**, 221, 150.
- [2] J. de Souza et al, ChemPhysChem. **2009**, online
- [3] H.N. Bordallo & E.V. Boldyreva, PSI Experimental Report, 2008.

	EXPERIMENTAL REPORT The interaction of Ang II with model membranes	Proposal: BIO-01-2535 Instrument: V1 Local Contact: T. Hauß
	Principal Proposer: Julia Preu, Niels Bohr Institute, Copenhagen, DK Experimental Team: Thomas Gutberlet, FZ Jülich Thomas Hauß, HZB	Date(s) of Experiment 14.08.2009 – 23.08.2009

Date of report: 17.12.2009

The renin-angiotensin system plays a critical role in circulatory homeostasis. Part of this system is the peptide hormone Angiotensin II (Ang II), a potent vasoconstrictor that aids in the blood pressure regulation, as well as in body fluid balance maintenance. The octapeptide Ang II derives from the precursor angiotensinogen, through enzymatic reaction catalyzed by renin and the angiotensin converting enzyme (ACE), via Ang I.

On the heart, acting in both endocrine and paracrine fashions Ang II regulates contractility, remodelling, growth, apoptosis, and reduces cell coupling and conduction velocity in cardiac muscles. Ang II has two major receptor subtypes, the Ang II type 1 receptor (AT1 receptor) and the Ang II type 2 receptor (AT2 receptor) and in addition acts on the membrane.

Main aim of the present experiments was to elucidate the concentration-dependent binding of the peptide to model membranes to elucidate the position of the peptide ion the membrane. For the experiments ordered bilayer stacks of chain-deuterated DMPC were deposited on a quartz wafer. Samples were rehydrated by vapour pressure, containing 8, 50 or 100 % D₂O. For samples containing Ang II, the peptide was dissolved in buffer and the lipids were added subsequently.

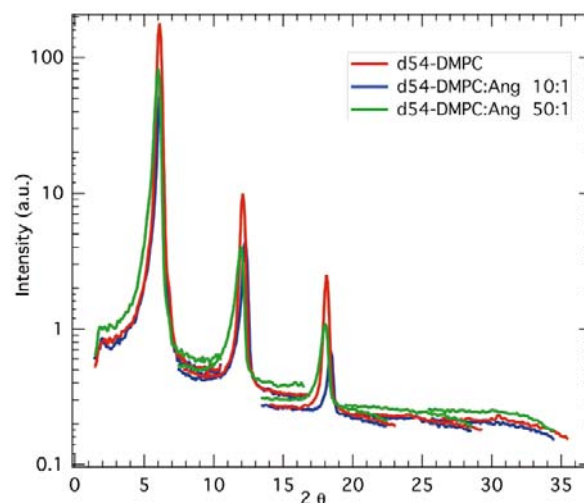
The dispersion was then deposited on a wafer and dried. To ensure a good ordering of the bilayer stacks the samples were preincubated at 40 °C. For pure d54-DMPC samples diffraction peaks up to the 5th order were measured. For the equivalent samples containing peptide Bragg reflections up to the 4th order were detected.

After initial corrections the baseline was subtracted from the data and the area under the peaks was integrated. Subsequent calculation of the structure factors enabled the

calculation of scattering density profiles and the comparison to theoretical models. Subtraction of the profiles of the pure lipid bilayers from the one containing peptide revealed the position of the peptide in the membrane (data not shown).

In accordance with previous SANS measurements it is shown that the peptide is accumulating close to the lipid head groups and not penetrating into the hydrophobic region of the bilayer.

DMPC-54 with increasing concentrations of Ang II in 100 % H₂O at 35 °C



This research project has been supported by the European Commission under the 7th Framework Programme through “Research Infrastructures” action of the “Capacities” Programme, contract number CP-CSA_INFRA-2008-1.1.1. Number 226507-NMI3

	EXPERIMENTAL REPORT Neutron diffraction study of model membranes with complex Stratum corneum-like lipid composition	Proposal: BIO-01-2536 Instrument: V1 Local Contact: A. Buchsteiner, T. Hauß
	Principal Proposer: T. Engelbrecht (Institute of Pharmacy, MLU Halle/Saale) Experimental Team: B. Dobner (Institute of Pharmacy, MLU Halle/Saale) R. Neubert, (Institute of Pharmacy, MLU Halle/Saale) A. Buchsteiner, T. Hauß, HZB	Date(s) of Experiment 13.07.2009 – 23.07.2009

Date of report: 30.11.2009

The mammalian skin is a perfect barrier protecting the body against environmental influences. Developing new transdermal drug delivery systems requires detailed knowledge about the lamellar lipid arrangement in the Stratum corneum (SC). Neutron diffraction studies of SC lipid model membranes containing synthetic ceramides, free fatty acids and cholesterol (CHOL) are an appropriate tool for this purpose. These simplistic mixtures do not mimic the SC, but they offer the possibility to study influences of certain ceramide and lipid species onto the structural lipid assembly in oriented SL lipid model membranes [1].

In our last experiment BIO-01-2536 carried out at V1 of HZB, Berlin, we tried to investigate sophisticated mixtures containing more than four or five components and therefore being more related to the physiological lipid mixture of human SC. Due to problems with synthesis of the deuterated CER[AP] the original plan needed to be modified. The following SC lipid mixture was developed (ratio w/w):

ceramides	free fatty acids	cholesterol	cholesterol sulphate
50%	25%	20%	5%
CER[EOS] 20%	C-16 10%		
CER[NP] 60%	C-18 10%		
CER[AP] 20%	C-20 10%		
	C-22 10%		
	C-24 30%		
	C-26 25%		
	C-18:1 5%		

Mix I contained oleic acid (OA, 5% w/w of the free fatty acid mix) to study a possible influence of this penetration enhancer which can increase the amount of drug penetrating into the skin. Mix II prepared without OA contained 15% w/w of the C-22 fatty acid.

The first remarkable thing was the difficulty of preparing a single-phase system. All model membranes studied showed phase separation,

due to the plurality of ceramide species and free fatty acids being present in the mixture. Nevertheless, we studied the systems using three different D₂O contrasts (100, 80 and 50% D₂O in water for **Mix I**, or 100, 50 and 8% D₂O in water for **Mix II**).

Although CER[EOS] was present in all studied mixtures, no phase with a periodicity of 120 Å (long periodicity phase, LPP) was visible. The existence of the LPP has been often reported in literature for SC lipid mixtures containing the long-chain ω-acyl ceramide [2]. We detected one phase with $d = 38$ Å showing barely a change in peak intensity during varying the D₂O contrast. It seemed that almost no water molecules are incorporated in the lipid head group region. We assume this phase to represent crystalline CER[NP]. Crystalline CHOL was detectable as well as another phase with $d = 42$ Å. Due to the poor lamellar orientation and phase separation, the calculated neutron scattering length density profiles are lacking informative value. We can state that, regarding the study of the structural assembly of SC lipids, the less complex quaternary model membranes are more suitable.

References:

- Schroeter, A., et al., *Evidence of free fatty acid interdigitation in stratum corneum model membranes based on ceramide [AP] by deuterium labelling*. Biochimica Et Biophysica Acta-Biomembranes, 2009. **1788**(10): p. 2194-2203.
- de Jager, M.W., et al., *Modelling the stratum corneum lipid organisation with synthetic lipid mixtures: the importance of synthetic ceramide composition*. Biochimica Et Biophysica Acta-Biomembranes, 2004. **1664**(2): p. 132-140.

	EXPERIMENTAL REPORT Neutron Diffraction Studies of Polymer/Clay Nanocomposites	Proposal: MAT-01-2539 Instrument: V1 Local Contact: T. Hauß
	Principal Proposer: F. K. Katsaros, NCSR "Demokritos" Experimental Team: T. A. Steriotis, NCSR "Demokritos" A. A. Sapalidis, NCSR "Demokritos"	Date(s) of Experiment 03.05.2009 – 15.05.2009

Date of report: 17.12.2009

Polymer-Clay nanocomposites are a new class of materials which attracted great scientific interest since the early 90's. The properties of these materials are influenced by the nanoscale interactions between the polymer chains and the clay particles. In our case polyvinyl alcohol and bentonite nanocomposites membranes were prepared via solution casting.

The neutron membrane diffraction experiments were aiming on the investigation of structural changes (crystallinity, swelling, disordering and migration of clay layers) as a function of the relative humidity of the composites. V1 diffractometer was extremely well suited in this respect, not only due to its geometry but also because of the unique sample environment (in terms of controlled relative humidity) and pertinent know-how available.

The diffraction patterns obtained from lamellar and in-plane sample positions revealed that there is a specific orientation of bentonite plates, parallel to the film surface. This conclusion is in agreement with the results obtained from XRD measurements and gas permeability technique.

Experiments conducted on samples prepared with polymers having different molecular masses and degree of hydrolysis revealed that the crystallization behaviour of polyvinyl alcohol changes. The observed neutron diffraction patterns indicate that the crystal of polyvinyl alcohol becomes bigger due to interactions between hydroxyl groups of clay and polymer. The hydroxyl groups of PVA are responsible for the formation of the crystal's unit cell dimensions.

The observation that polyvinyl alcohol's crystal changes were in agreement with

differential scanning calorimetry (dsc) experiments.

The use of D₂O as a vapor for equilibrating the samples prior measurement induced the contrast of the polymer while reducing the effect of bentonite in the diffraction patterns.

By using the contrast variation technique we were able to distinguish between patterns obtained from the polymer crystal and by clay particles.

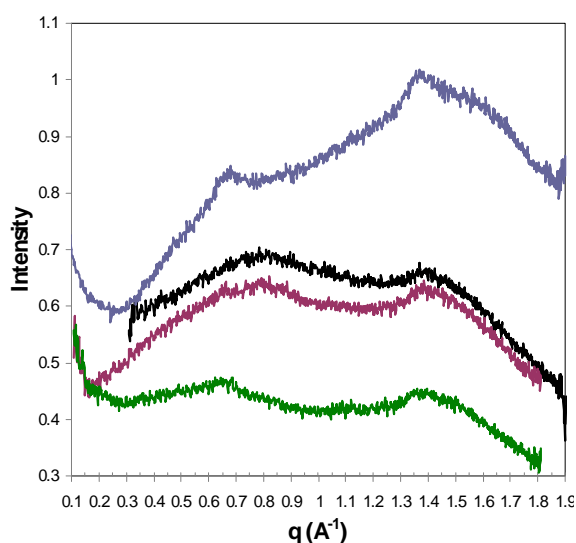


Fig. Diffraction patterns for samples with 20% w/w Bentonite content and different molecular masses.

Acknowledgements

This research project has been supported by the European Commission under the 7th Framework Programme through "Research Infrastructures" action of the "Capacities" Programme, contract number CP-CSA_INFRA-2008-1.1.1. Number 226507-NMI3

 Neutrons	EXPERIMENTAL REPORT	Proposal: BIO-01-2656-LT
	Interaction of a γ-secretase inhibitor with β-amyloid and lipid membranes	Instrument: V1 Local Contact: Th. Hauß
Principal Proposer: Experimental Team:	Thomas Hauß, TU-Darmstadt, HZB Norbert A. Dencher, TU-Darmstadt Boris Schmidt, TU-Darmstadt Alexandra Buchsteiner, HZB	Date(s) of Experiment 30.03.2009-09.04.2009 27.04.2009-05.05.2009 12.10.2009-26.10.2009

Date of report: 24.02.2010

Recently, new strategies were developed to find a therapeutic approach to Alzheimer's disease [1,2,3]. The targets of the new approaches are enzymes responsible for the cleavage or modification of the amyloid precursor protein (APP) into the neurotoxic peptides β -amyloid with 40 to 43 amino acids. In the group of Prof. Schmidt, TU-Darmstadt newly designed inhibitors and modulators for β -secretase were successfully tested in cultured cells and in mice [1,2]. The cleavage site of β -secretase is in the hydrophobic core of the cell membrane, for that reason the inhibitor of β -secretase is lipophilic.

We investigated the interaction of a newly synthesised and specifically deuterated β secretase inhibitor, a carprofen derivative, with lipid membranes. The experiments in the first half of 2009 established a suitable protocol for the preparation of biological highly relevant membrane models consisting of POPC, sphingomyelin, and cholesterol. This lipid mixture exhibits a change in lattice spacing, indicating a phase transition, at temperatures between 10°C and 40°C, with and without the inhibitor. The neutron diffraction experiments in October established the localization of the deuterated inhibitor in the membrane lipids. Fig.1 depicts the preliminary results as difference in the scattering length density profile. The difference is calculated from samples of membrane lipids mixed with the protonated or selectively deuterated inhibitor carprofen, respectively, at two different contrast points (8% D₂O, 20% D₂O in the aqueous atmosphere) at 15°C. The maxima in the difference density profile at $z = \pm 2.5$ nm are attributed to the location of the deuterated label. The tentative interpretation is, that the inhibitor with its deuterated segment resides in the head-group region of the lipid membrane

close to the phosphate group of the lipids.

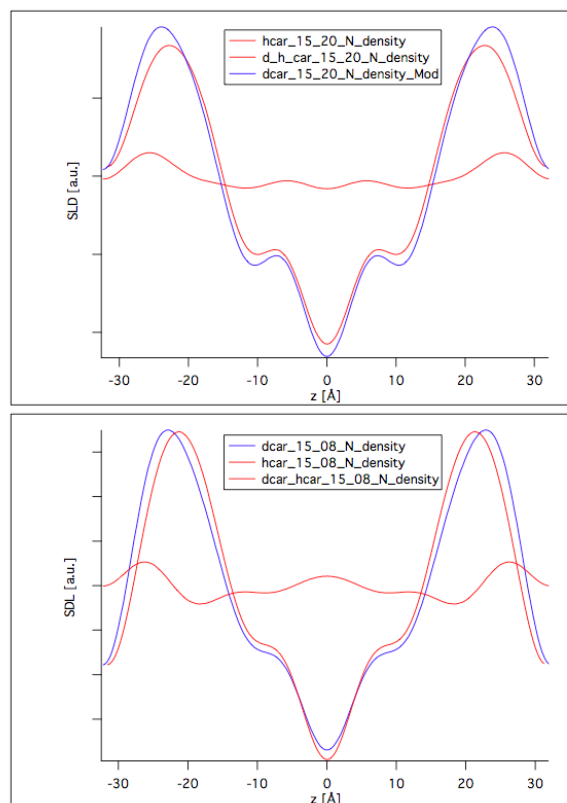


Fig 1) Neutron scattering length density (SLD) profiles at 20% D₂O (top) and 8% D₂O (bottom) with protonated (red) and deuterated (blue) carprofen and the difference at 15°C.

- [1] Rajendran et al., Efficient inhibition of the Alzheimer's disease β -secretase by membrane targeting, *Science* **320**, 520 (2008)
- [2] Kukar et al., Substrate-targeting γ -secretase modulators, *Nature* **453**, 925 (2008)
- [3] Schilling et al., Glutaminyl cyclase inhibition attenuates pyroglutamate. A and Alzheimer's disease-like pathology, *Nature Medicine* **14**, 1106 (2008)

	EXPERIMENTAL REPORT Quaternary stratum corneum model membranes with or without penetration enhancers and the impact of pH	Proposal: BIO-01-2657 Instrument: V1 Local Contact: T. Hauß A. Buchsteiner
	Principal Proposer: T. Engelbrecht, MLU - Halle/Saale Experimental Team: B. Dobner, MLU - Halle/Saale R. Neubert, MLU - Halle/Saale A. Buchsteiner, HZB T. Hauß, HZB	Date(s) of Experiment 16.11.2009 – 29.11.2009

Date of report: 19.03.2010

Neutron scattering was shown to be an appropriate tool for structural investigation of oriented stratum corneum (SC) model membranes [1, 2]. It is possible to study these systems in a detailed way, focusing on bilayer nanostructure and lipid arrangement. Especially simplistic models, which consist of only few synthetic SC lipids combined in a certain ratio, offer the possibility to investigate the influence of lipid head group architecture on the lipid arrangement.

In our last experiment BIO-01-2657 carried out at V1 of HZB, Berlin, the scheduled experiment needed to be changed since problems in synthesis of the specifically deuterated CER[EOS] had occurred. Therefore, we decided to start with a quaternary system already investigated before and added penetration enhancers, in this case oleic acid, and isopropyl myristate. The following SC lipid mixtures were investigated (ratio w/w):

1. CER[AP]/ palmitic acid/ cholesterol/ cholesterol sulphate (55/ 25/ 15/ 5) with **oleic acid 10%**
2. Same system as in 1, but additionally treated with alkaline buffer solution (pH 9.6)
3. CER[EOS]/ CER[AP]/ behenic acid/ cholesterol (23/ 10/ 33/ 33) with **oleic acid 5%** or
4. Same system as in 3, **+isopropyl myristate 5% instead of oleic acid.**

For all samples studied, the diffraction patterns were recorded at three different D₂O contrasts with fixed relative humidity (r.h.) of either 58 %, or 98 %. The detection of up to five or six diffraction orders allowed the calculation of the neutron scattering length density profiles for interpretation of the nanoscaled bilayer architecture. The first remarkable thing was the strong improvement of sample quality in terms of mosaicity and phase separation after alkaline buffer treatment. While the scan of sample 1 revealed poor lamellar lipid assembly and phase-separated cholesterol (fig. 1a), the rocking scan of sample 2 showed complete

cholesterol incorporation and increased peak intensity (fig. 1b).

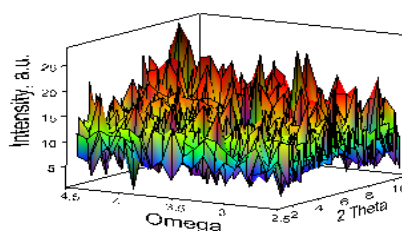


Fig.1a

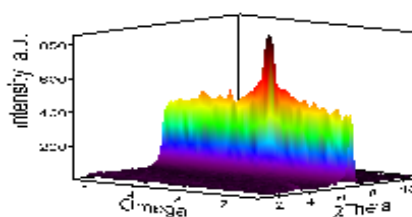


Fig. 1b

Seemingly, the pH has strong influence on the lipid assembly of the SC model membranes. Until now, this relation was insufficiently considered for our sample preparation, but we plan further studies addressing this issue. Furthermore, stronger hydration of sample 1 was observed when comparing the lamellar *d*-spacings at 58 % r.h. (44.6 Å), and 98 % r.h. (46.9 Å) with the ones for sample 2 (45.4 Å for 58 % r.h. and 46.13 Å for 98 % r.h.). The reason might be the improved hydration of ionized lipid compounds due to buffer treatment. Presence of penetration enhancers in sample 3 and 4 induced no changes of the *d*-spacings (48.3 Å with and without penetration enhancer); the evaluation of the Fourier profiles is in progress.

References:

- [1] A. Schroeter, D. Kessner, M.A. Kiselev, T. Hauss, S. Dante and R.H.H. Neubert, *Biophysical Journal* 97 (2009) 1104-1114.
- [2] A. Schroeter, M.A. Kiselev, T. Hauss, S. Dante and R.H.H. Neubert, *Biochimica Et Biophysica Acta-Biomembranes* 1788 (2009) 2194-2203.

Principal Proposer: Chris Garvey, ANSTO, Australia
Experimental Team: Gary Bryant, RMIT University, Melbourne, Australia
Thomas Lenne, Australian National University, Canberra, Australia
A. Buchsteiner, Markus Strobl, HZB

Date(s) of Experiment

09.11.2009 - 16.11.2009

Date of report: 26/01/10

This study focuses on the interaction between sugar molecules and lipid bilayers and the mechanism by which such small molecules may protect membranes against deleterious phase transitions (Figure 1).

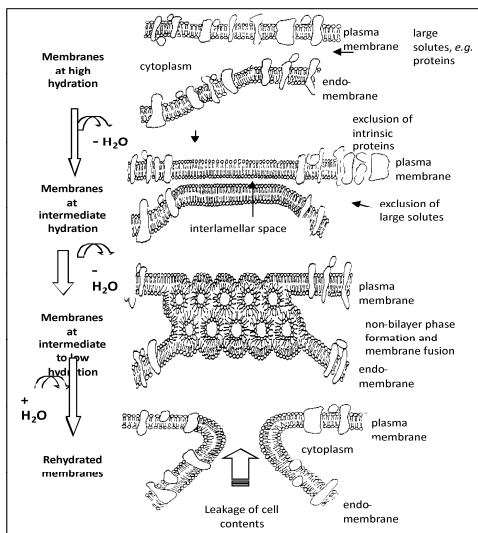


Figure 1 Proposed mechanism of membrane disruption by non-lamellar phase transitions.

There are two main explanations for the membrane stabilising effects of small sugar molecules:

1. The hydration forces explanation relies on a short-range repulsive interaction due to the hydration of lipid head groups. The removal of the solvent brings membranes into close contact and the short range hydration interaction induces a lateral compressive stress in the membrane. This compressive stress is responsible for transitions from the lamella liquid phase. These transitions are associated with changes in the correct functioning of the cell membrane [1].
2. An alternative explanation, the water replacement hypothesis involves a very specific interaction between sugars and the

lipid head group, and close proximity of the sugar molecule to the lipid head group. This explanation is commonly invoked to explain the “anomalous” cryoprotectant properties of trehalose [2 and references therein].

The localisation of sugar molecules with respect to the lipid head groups, and the concentration profile of sugar between lipid bilayers should provide insight into the validity of these two models.

Membrane diffraction measurements at 3 different contrasts were made on aligned membranes of 1,2-dioleoyl-sn-glycero-3-phosphocholine (DOPC) containing 3 different amounts of sugar at 57 % relative humidity. Measurements in 100% D₂O humidity are shown in Figure 2.

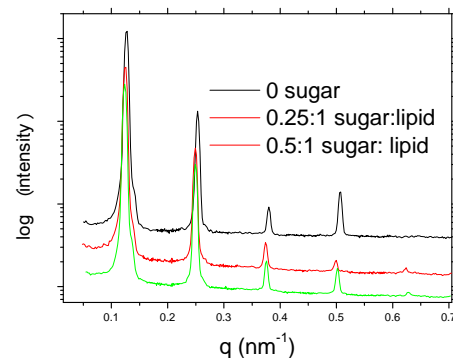


Figure 2 Membrane diffraction measurements on aligned DOPC bilayers with different sugar (deuterated glucose): lipid ratios.

Inclusion of sugar causes a swelling of the bilayers at a particular humidity. Currently the scattering length density of bilayers including sugar is being reconstructed from the scattering data.

[1] Bryant, G.; Koster, K. L. *Colloids Surf., B* 2004, **35**, 73.

[2] Peregira, C.S. et al. *Biophys. J.*, 2004, **86**, 2273.

	EXPERIMENTAL REPORT	Proposal: OTH-01-2560-EF
	Study of the Vibrational and Structural Properties of L-leucine and L-isoleucine	Instrument: V3 Local Contact: E. Kemner
Principal Proposer: Experimental Team:	Heloisa N. Bordallo, HZB Heloisa N. Bordallo, HZB Paulo T. C. Freire, UFC, Brazil	Date(s) of Experiment 27.04.2009 – 04.05.2009

Date of report: 03.12.2009

L-Leucine and L-isoleucine ($C_6H_{13}NO_2$, hereafter LEU and ILE) are structural isomers, i.e. they possess the same molecular formula, similar chemical and physical properties but different structures. LEU is the strongest α -helix forming protein residue, whereas ILE strongly favors the β -conformation. As both helix and β -conformations are stabilized by hydrophobic contributions, these hydrophobic residues are excellent candidates for being active in the nucleation of secondary structures.

At 300K LEU crystallizes in the monoclinic $P2_1$ space group¹, while ILE shows polymorphism. Like LEU, ILE crystallizes either in the $P2_1$ or in the $P2_122$ structure.² Differential scanning calorimetric and Raman measurements evidenced a phase transition (PT) at about 353K in LEU.³ No PT is reported for ILE.

The aim of our proposal was to study the dynamical response of LEU and ILE in a wide frequency (time) range to understand how the structural changes will affect their hydrogen dynamics. In particular, inelastic neutron scattering (INS) provides a most suitable probe for studies of vibrational dynamics for given solids. The measured scattering function $S(Q, \omega)$, where Q is the magnitude of the scattering wave vector and ω is the energy transfer, will express different contributions depending on the observed time (energy resolution) range. This function can be decomposed into 3 parts: elastic (E), quasi-elastic (QE) and inelastic (IN). The E component originates from neutrons without change in energy, while IN is related to vibrational modes. QE scattering, which is a broadening of the elastic peak, describes the dynamical nature of the molecular motion. In this particular study $S(Q, \omega)$ will be dominated by the incoherent cross section of the H atom.

The low-frequency vibrational contribution to the specific heat of LEU and ILE was determined from $S_{Elastic}(Q, \omega \sim 0)$. The evolution of the mean square displacement, $\langle u^2 \rangle$ vs T , was assessed by evaluating $[S_{Elastic}(Q, \omega \sim 0)(T)/S_{Elastic}(Q, \omega \sim 0)(T \sim 20K)]$, as shown in

Fig.1. Then, assuming that the Debye model is applicable, the data were fitted in terms of the following expression:⁴

$$\langle u^2 \rangle = \frac{3\hbar^2 T}{mk_B \theta_D^2} \left[\Phi\left(\frac{\theta_D}{T}\right) + \frac{1}{4} \left(\frac{\theta_D}{T}\right)^4 \right],$$

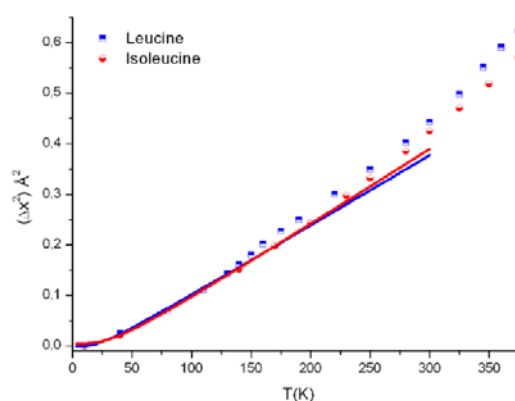


Fig. 1. $\langle u^2 \rangle$ of LEU and ILE from elastic neutron scattering measurements using V3 with a resolution $\Delta E = 98 \mu\text{eV}$. The lines are the calculated $\langle u^2 \rangle$ as described in the text.

This very first scrutiny of the data shows a dynamical transition at about 250K for ILE, most likely related to a crossover of the molecular fluctuations between harmonic and non-harmonic dynamical regimes. For LEU the deviation from the Debye behavior around 150K may be connect to a low temperature PT as evidenced by NPD data. See report OTH-01-2555-EF. Further analyses are under way.

- [1] Harding & Howieson, *Acta Crystallogr.* **B32**, 1979, 633. & M. Coll et al, *Acta Crystallogr.* **C42**, 1986, 599
- [2] K. Torii and Y. Iitaka, *Acta Cryst.* **B27**, 1971, 2237. & B. Khawas *Acta Cryst.* **B26**, 1970, 1385.
- [3] D. Bougeard, *Ber. Bunsenges. Phys. Chem.*, **87**, 1983, 279. & P. F. Facanha Filho et al, *Brazilian Journal of Physics*, **38**, 2008, 131.
- [4] B.T.M. Willis and A.W. Pryor, Cambridge University Press, Cambridge, 1975

	EXPERIMENTAL REPORT Dynamical transition in a large globular protein: macroscopic properties and glass transition	Proposal: PHY-03-555 Instrument: V3 Local Contact: M. Russina, E. Kemner
	Principal Proposer: A.V. Sokolova, ANSTO, Australia Experimental Team: G.J. Kearley, ANSTO, Australia E.P. Gilbert, ANSTO, Australia E. Kemner, HZB M. Russina, HZB	Date(s) of Experiment 05.07.2008 – 14.07.2008

Date of report: 09.12.2009

The Report consists of data, analysis and conclusions published in the article:

"Dynamical transition in a large globular protein: macroscopic properties and glass transition"

Biochimica et Biophysica Acta, 2009, 1804 (2010) 34–40

C.S. Kealley^{a,b}, A.V. Sokolova^b, G.J. Kearley^b, E. Kemner^c, M. Russina^c, A. Faraone^d, W.A. Hamilton^b, E.P. Gilbert^b

^a*Institute for Nanoscale Technology, University of Technology, Sydney, PO Box 123, Broadway, NSW, 2007, Australia*

^b*Bragg Institute, Australian Nuclear Science and Technology Organisation, PMB 1, Menai, NSW, 2234, Australia*

^c*Department Methods and Instruments, Helmholtz-Zentrum, Berlin, Glienicker Str. 100, D-14109, Berlin*

^d*Department of Materials Science and Engineering, University of Maryland, College Park, MD 20742, and NIST Center for Neutron Research, NIST, Gaithersburg, MD 20899, USA*

We find evidence of a transition analogous to those found in smaller proteins, when investigated as a function of temperature, at the so-called dynamical transition. In contrast, the glass transition seems to be unrelated. Small proteins are good model systems for the much larger proteins because the relaxation characteristics are rather similar despite the change in scale. For dry samples, which do not show the dynamical transition, the dynamics of the methyl group is probably the most important contribution to the QENS spectra, however a simple rotational model is not able to explain the data. Our results indicate that the dynamics that occurs above the transition temperature is unrelated to that at lower temperatures and that the transition is not simply related to the relaxation rate falling within the spectral window of the spectrometer.

Abstract

Hydrated soy-proteins display different macroscopic properties below and above approximately 25% moisture. This is relevant to the food industry in terms of processing and handling. Quasi-elastic neutron spectroscopy of a large globular soy-protein, glycinin, reveals that a similar moisture-content dependence exists for the microscopic dynamics as well.

 HELMHOLTZ ZENTRUM BERLIN für Materialien und Energie NEUTRONS	EXPERIMENTAL REPORT Study of the mechanism of proton conduction in ceramics	Proposal: ART-03-614-EF Instrument: V3 Local Contact: M. Russina
	Principal Proposer: T. Scherb, HZB, F-I1 Experimental Team: M. Russina, HZB, G-I1 Z. Izaola, HZB, G-I1 N. Tsapatsaris, HZB, G-I1 D. Wallacher, HZB, G-I1 G. Schumacher, HZB, F-I1 J. Serra, UPV-CSIC	Date(s) of Experiment 02.12.2008 – 06.12.2008

Date of report: 18.08.2009

The tungstates $\text{Ln}_6\text{WO}_{12}$ are proton-conducting materials exhibiting sufficient electronic conductivity to consider them as potential candidates for the separation of hydrogen at high temperature. The $\text{Ln}_6\text{WO}_{12}$ system has three structural classes whose symmetries are dependent on the rare earth ionic radius. These materials crystallize in a disordered pyrochlore or ordered defect fluorite structure and they can be formulated as $\text{Ln}_6\text{WO}_{12}\text{K}_2$ or $\text{A}_4\text{O}_{6.85}\text{K}_{1.15}$ (κ =oxygen vacancies) for a fluorite formulation [1].

Quasi-elastic neutron scattering (QENS) measurements on $\text{Nd}_6\text{WO}_{12}$, sintered at 1150°C were performed at the Time-of-Flight-Spectrometer V3 (NEAT). Prior to the QENS measurements, the specimen was annealed at 350°C for 38 hours in order to remove incorporated water.

We intended to get information on the diffusion process of hydrogen in the lattice. Therefore QENS measurements were performed at 600°C and 900°C under different atmospheres (high vacuum, H_2 (dry), $\text{H}_2+\text{H}_2\text{O}$, humid atmosphere (H_2O) $p = 0.6$ bar). The humid atmosphere was produced using the DEGAS system connected to a high temperature furnace with a Suprasil quartz tube, which has very low H content, as an insert.

Within the experimental uncertainty the QENS measurements performed at 600°C and 900°C under different atmospheres show the same spectra for all atmospheres (see Fig. 1). This indicates that the water uptake in the specimen is not high enough to be detected by QENS.

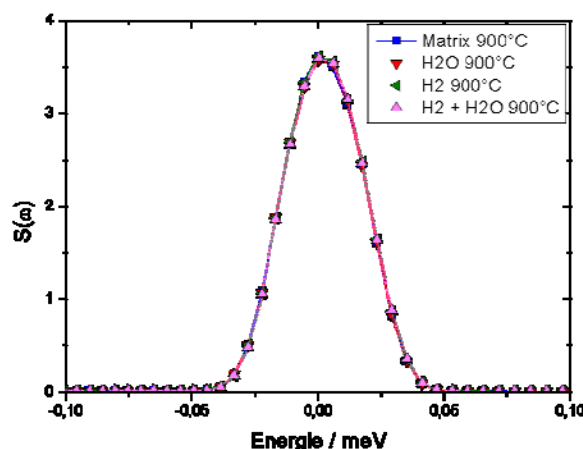


Fig. 1: QENS-spectrum measured on $\text{Nd}_6\text{WO}_{12}$ at 900°C under different atmospheres (vacuum (Matrix), H_2 , H_2O , $\text{H}_2+\text{H}_2\text{O}$).

References:

[1] Escolástico, S. et al., Chemistry of Materials, 2009.

This work has been supported by the Helmholtz-Alliance MEM-BRAIN.

	EXPERIMENTAL REPORT Study of the low frequency dynamics of the psychrophile enzyme alpha-amylase in bioprotectant mixtures	Proposal: PHY-03-630 Instrument: V3 Local Contact: M. Russina
	Principal Proposer: Salvatore Magazù, University of Messina, Italy Experimental Team: Salvatore Magazù, University of Messina, Italy Federica Migliardo, University of Messina, Italy Margarita Russina, HZB Nikolaos Tsapatsaris, HZB	Date(s) of Experiment 17.06.2009 – 21.06.2009

Date of report: 16.12.2009

The objective of the measurements was to use NEAT to study the low frequency dynamics and to evaluate the relaxational vs. vibrational contribution for the ternary systems composed by protein/ bioprotectant/water mixtures. This study is to be collocated in the research activity performed in the framework of the UNESCO-L'Oréal Fellowship for Young Women in Life Sciences 2008.

The characterization of molecular mechanisms underlying the numerous functions of trehalose is very important for the understanding and exploitation of the potentialities of the disaccharide. Many of the mechanisms are cryptic, but it is clear that they involve interactions that derive from the unique properties of the water molecules. It has been recently demonstrated by QENS and NSE experiments performed on NEAT and V5 SPAN that trehalose diffusion in solution is slower than its homologous, maltose and sucrose. Furthermore it is clearly pointed out that the dynamics of disaccharides and water is strongly coupled, with a higher coupling strength in the case of trehalose water solution.

The mechanism of protein stabilization by glassy solvents is not entirely clear, and the stabilizer effective for a given protein is often discovered empirically. Low frequency Raman spectroscopy has been used as an effective tool to directly evaluate the ability of different solvents to suppress the conformational fluctuations that can lead to both protein activity and denaturation. Low frequency Raman spectra show two contributions, one vibrational and the other relaxational. Taking into account low-frequency Raman data, Sokolov et al. have found a correlation between the degree of bioprotection and the relaxational to the vibrational contributions. It has been observed that the relaxational to the vibrational contribution is the highest in

solid lysozyme:glycerol sample at low T, decreases in lysozyme:trehalose sample and is the lowest in the dry state, i.e., with no solvent surrounding the protein.

The experiment has been performed by using the NEAT spectrometer to study the low frequency dynamics and to evaluate the Boson peak behaviour for the ternary protein/bioprotectant/water systems.

The data obtained by NEAT will allow to improve the knowledge about the Boson peak features of proteins in the presence of bioprotectant systems.

The experiment has been performed on NEAT without any difficulty and with the competent and kind assistance and help of Margarita Russina and Nikolaos Tsapatsaris.

Acknowledgement for Support by the European Commission

We gratefully acknowledge the European support for our experiments at BER II.

This research project has been supported by the European Commission under the 7th Framework Programme through "Research Infrastructures" action of the "Capacities" Programme, contract number CP-CSA_INFRA-2008-1.1.1. Number 226507-NMI3

 HELMHOLTZ ZENTRUM BERLIN für Materialien und Energie NEUTRONS	EXPERIMENTAL REPORT	Proposal: BIO-03-648-EF
	Lipid Lateral Diffusion in Phase Separated Multilamellar Systems	Instrument: V3 Local Contact: E. Kemner
Principal Proposer: Kasten Vogtt, HZB Experimental Team: Marie-Claire Bellissent-Funel, HZB Ewout Kemner, HZB Margarita Russina, HZB	Date(s) of Experiment 08.07.2009 – 13.07.2009	

Date of report: 14.01.2010

The phase separation and diffusion of lipids is of special interest for biological research, because lipid bilayers act as cellular boundary surface in nearly all biological organisms. Especially in eukaryotes lipid vesicular structures exhibit a broad functionality and are strongly involved in cellular events like endocytosis and exocytosis. The concept of “lipid rafts”, i.e. the lateral partition of a lamellar lipid mixture into small microdomains upon phase separation, plays an important role in the understanding of these processes on molecular level (1). Hence, the structure and dynamics of such microdomains are of crucial interest for a thorough physico-chemical characterization of related biological processes.

A ternary lipid mixture known to exhibit phase separation on microscopic scale (2) was examined using quasi elastic neutron scattering (QENS) at two different temperatures (283 and 323 K). At the higher temperature the system resides in a single liquid phase, while at lower temperature two liquid phases are present. The mixture consisted of dioleoylphosphatidylcholine, dipalmitoylphosphatidylcholine and cholesterol. The microdomains are expected to be enriched in cholesterol, which leads to a higher density of these objects (3). Measurements were undertaken to study the influence of the phase transition – and in particular the effect of the cholesterol enrichment – on the (local) dynamics.

For the two temperatures the Q-dependence of the scattered intensity $I(Q)$ is considerably different: The broadening of the quasi elastic peak with increasing Q is more pronounced at the higher temperature (see Fig. 1).

In a first analysis a fit of the data using a single Lorentzian yielded an agreeable match. However, standard plots of the respective line widths vs. Q and Q^2 yielded no linear correlation, suggesting the presence of a more complex motion composition. Therefore a more elaborated motion model has to be applied.

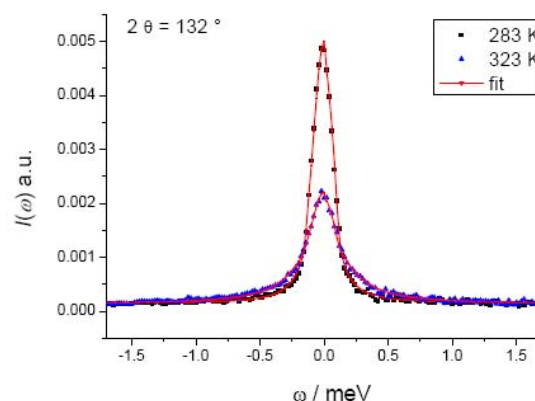


Fig. 1: QENS-intensity $I(\omega)$ at 283 and 323 K as well as the respective fits.

References:

1. Simons, K. and Toomre, D., *Nat. Rev. Mol. Cell Biol.*, **2000**, *1*, 31-39
2. Veatch, S. L.; Soubias, O. Sarah L. Keller, S. L. and Gawrisch, K., *Proc. Natl. Acad. Sci. U. S. A.*, **2007**, *104*, 1650-1655
3. Binder, W. H.; Barragan, D. & Menger, F. M., *Angew. Chemie*, **2003**, *115*, 5980-6007

 HELMHOLTZ ZENTRUM BERLIN für Materialien und Energie NEUTRONS	EXPERIMENTAL REPORT	Proposal: CHE-03-660-EF
	L-Methionine: Structure and Dynamics of an essential amino acid	Instrument: V3 Local Contact: E. Kemner
Principal Proposer: Heloisa N. Bordallo, HZB Experimental Team: Jennifer Fischer, Universität Kassel and HZB Heloisa N. Bordallo, HZB	Date(s) of Experiment 08.08.2009 – 12.08.2009	

Date of report: 26.01.2010

Gaining an understanding of the organic solid state is one of the big questions to be solved in chemistry [1], and on the experimental side, incoherent inelastic neutron scattering (IINS) provides a suitable probe for studies of H-vibrational dynamics for given solids; and subtle volume changes that arise from changes in packing density due to the decrease in intermolecular distances in the H-bond network can give rise to visible changes in the energy spectra. Among molecular organic crystals, those of amino acids attract special attention – as biomimetics, as solid drugs, as materials for molecular electronics, as systems important for geo- and cosmochemistry. Amino acids constitute molecular systems where Van der Waals interactions and H-bonds play important roles in the stability of the crystalline structure. Methionine is an essential amino acid very important in the process of methylation and constitutes a precursor to other amino acids, such as L-cysteine and homocysteine (the latter, being involved in numerous processes of methyl group transfer, plays a fundamental role in the biochemistry of the human body). Although, pronounced changes of the Raman spectra were observed for L- Methionine under pressure, and indications of a phase transition were reported by means of specific heat in a powder sample at ~ 305K [2], up to date no systematic temperature study of this crystalline structure has been undertaken.

Using the time-of-flight spectrometer NEAT we got hold of valuable information on the dynamics of L- Methionine. NEAT is an appropriate instrument simply because we can combine the high incoherent cross section of H (thus good signal/background ratio) with the energy range covered by the instrument (one can obtain information from both the collective and local motions).

As depicted in Fig. 1, by analyzing the dynamical susceptibility contribution ($\chi''(E)$), obtained using NEAT, we were able to correlated the transition observed by means of

specific heat to distinctive lattice modes observed in the low frequency region of the spectra.

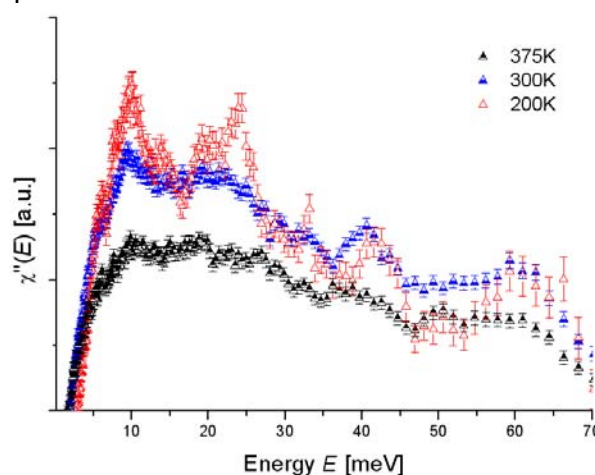


Fig. 1. Dynamical susceptibility $\chi''(E)$ of the H-atoms in L-methionine at 300 and 200K.

Moreover it should be noted that excitations due to harmonic vibrations should have a susceptibility that fits into the same master curve, but in L-Methionine a re-distribution of the intensity of the bands is noticeable between 375 and 200K. These changes in the spectra can be interpreted as resulting from rapid jumps between equivalent torsion positions of the carbon and oxygen atoms in L-Methionine, as was observed for the NH_3 group in glycine [3], L-alanine [4] and in acetanilide [5]. Based on this observation, we can conclude that conformational changes take place in L-Methionine.

[1] S.A. Moggach *et al* Crystallography Reviews **14**, 143 (2008).

[2] J.O. Hutchens, A.G. Cole, and J. W. Stout, The Journal of Biological Chemistry, **239**, 591 (1964)

[3] H.N. Bordallo *et al*, J. Phys. Chem. B **112**, 8748 (2008).

[4] M. Barthès *et al* J. Phys. Chem. A **106** 5230 (2002).

[5] R.L. Hayward *et al* J. Chem. Phys. **102** 5525 (1995)

 HELMHOLTZ ZENTRUM BERLIN für Materialien und Energie NEUTRONS	EXPERIMENTAL REPORT Distinct Dynamics of Water Molecules in Hydrated Pores (2)	Proposal: CHE-03-668 Instrument: V3 Local Contact: M. Russina
	Principal Proposer: Natalia Pérez-Hernández, CSIC, Sevilla, Spain Experimental Team: Juergen Eckert, University of California, USA Nikolaos Tsapatsaris, HZB	Date(s) of Experiment 21.09.2009 – 27.09.2009

Date of report: 17.12.2009

Our research focuses on the description of water dynamics in confined environments. The present series of measurements constitutes a continuation of a previous experiment (CHE-03-596), in which we performed temperature-dependent time of flight quasi-elastic neutron scattering experiments on a sample of hydrated organic pores of narrow diameter. In those pores, motions of water appear to be fairly restricted.

A new sample containing wider pores with confined water was measured under the same conditions as in the previous experiment with the aim to obtain a complete set of data for a comparative study of motion of water in pores with different sizes, and, at the same time, facilitate the interpretation of previous results.

We therefore carried out QENS experiments on NEAT with a incident neutron wavelength of 5.5 Å, as well as a second configuration with neutrons of wavelength of 7.5 Å for higher resolution. We utilized approximately 215 mg of our sample and measured at 100, 170, 200, 230, 260, 270, 280, 290, 300 and finally at 340K. Water is known to leave the pores at around this highest temperature, so that this last measurement should be useful in monitoring if significantly different dynamics of water can be identified when compared to the case where most of the water remains inside the pores.

We encountered some “technical” problems as the computer froze on several occasions during the night, which led to the loss of valuable experimental time and data. Because of the problems we were unable to complete the planned measurements. We have been compensated in part by our local contact at the HZB carrying out some (but not all) of the missing measurements, and hope to receive some more time in the future in order to complete the present study.

Data are currently being processed using the “FITMO” software, to which remote access has been provided. This is an extremely slow and cumbersome procedure, and we would like to suggest that a portable version of FITMO is provided to users to be installed on computers in their home institution. Our preliminary results reveal a stronger signal than that in last year’s experiment, which arises in part from using a larger amount of sample used (~ 40% more), but also from the fact that the water is less confined in and thus more mobile in the present case.

Nonetheless, the relative amount of quasi-elastic scattering is very small compared to that of the elastic peak as a whole, so that it is rather difficult to get the software to properly account for this, and hence obtain significant results. From the analysis of the Q-dependence and the dependence of the signal on resolution and temperature, we hope to extract rotational as well as translational diffusion constants in the near future. We also expect to be able to relate the water mobility to the sizes of the respective confining pores by comparing the two sets of experiments.

This research project has been supported by the European Commission under the 7th Framework Programme through “Research Infrastructures” action of the “Capacities” Programme, contract number CP-CSA_INFRA-2008-1.1.1. Number 226507-NMI3

	EXPERIMENTAL REPORT Study of dynamic properties of reconstituted myelin sheath	Proposal: BIO-03-669 Instrument: V3 Local Contact: E. Kemner
	Principal Proposer: J. Peters, Université Joseph Fourier, Grenoble, FR Experimental Team: F. Natali, CNR-OGG, Grenoble, FR W. Knoll, ILL, Grenoble, FR P. Kursula, Oulu University, FL	Date(s) of Experiment 14.12.2009 – 21.12.2009

Date of report: 10.01.2010

The project concerns myelin, the lipid-rich, multilamellar membrane discontinuously wrapped around nerve axons, which increases the efficiency of saltatory impulse conduction. The molecular components of the myelin sheath interact tightly with each other and molecules on the axonal surface to drive myelination, to keep both myelin and the axon intact, and to transduce signals from myelin to the axon and *vice versa*.

Despite the presence of myelin-specific proteins, little is known about the dynamics of these proteins and their influence on myelin stability. The purpose of the proposal is to provide information on the dynamical properties of the myelin membrane.

We did elastic and quasi-elastic neutron scattering measurements at 230 and 300 K of four samples made of oriented lipids (a mixture of DOPS and DOPC), with and without myelin proteins (MBP, P2 and MBP+P2). Data were also collected on Vanadium and the empty cell for correction purposes. All measurements were done at two orientations with respect to the neutron beam, corresponding to the momentum transfer parallel and perpendicular to lipid membrane surface.

The two temperatures correspond to values below and above a phase transition from a gel to liquid phase, occurring around 265 K for this kind of lipids. On NEAT we have chosen an energy resolution of 220 μeV (~ 3 ps time window). These studies are complementary to former investigations on the same samples on IN5 (ILL) with a 15 μeV resolution and on Osiris (ISIS) with a 100 μeV resolution. Each time window gives access to different types of motions, ranging from local vibrations to large translations.

Difficulties were encountered with respect to the sample transportation, because they had to be sent from the UK (experiment scheduled on

OSIRIS from 2nd to 8th December 2009) in dry-ice to the HZB. Unfortunately, the logistics' company spent 5 days for the transport, without any prevention for keeping the sample box at -80 °C as demanded, and all dry-ice was evaporated. A short test of all samples on V1 and on NEAT at 100 μeV (to check OSIRIS results reproducibility) showed, however, that the samples probably survived.

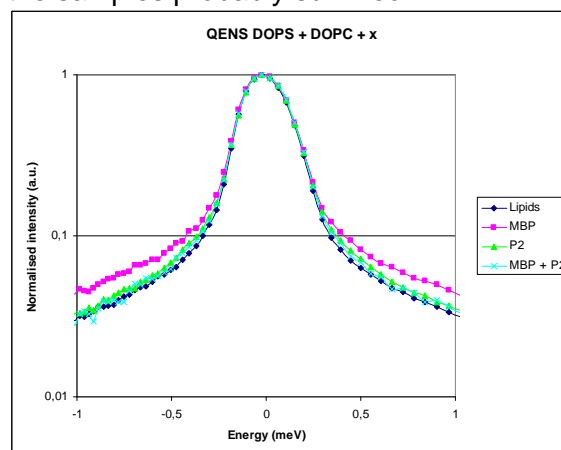


Fig. 1: QENS data of all four samples at 45 deg and 300 K.

Figure 1 show first results of quasi-elastic neutron scattering (QENS) for all four samples at 300 K and summed over all Q-values. Obviously the proteins rend the lipids stiffer and MBP has much more effects than P2. These results confirm previous results on other instruments (IN5 and Osiris), but show also differences due to the different time window.

A detailed analysis of the QENS data is now under progress to permit conclusions about the type of motions within the time window.

Acknowledgement:

This research project has been supported by the European Commission under the 7th Framework Programme through "Research Infrastructures" action of the "Capacities" Programme, contract number CP-CSA_INFRA-2008-1.1.1. Number 226507-NMI

	EXPERIMENTAL REPORT Bicontinuous phases based on sugar surfactant: Structure and influence of the co-surfactant	Proposal: CHE-04-1817 Instrument: V4 Local Contact: S. Prevost
	Principal Proposer: T. Hellweg, Universität Bayreuth Experimental Team: K. v. Nessen, Universität Bayreuth S. Wellert, HZB	Date(s) of Experiment 11.12.2009 – 15.12.2009

Date of report: 12.01.2010

The aim of the proposed experiment was twofold. In the first part the influence of alcohol used as tuning parameter for the curvature of the amphiphilic film in bicontinuous structures was studied and the structure of lamellar phases in binary surfactant-water systems was characterized. The second part was dedicated to the investigation of micro- and macrogel properties.

Figure 1 shows examples of SANS spectra measured in the bicontinuous region of the quaternary phase system Cyclohexane-D₂O-C₈₋₁₀G_{1,4}-alcohol. The inset shows the

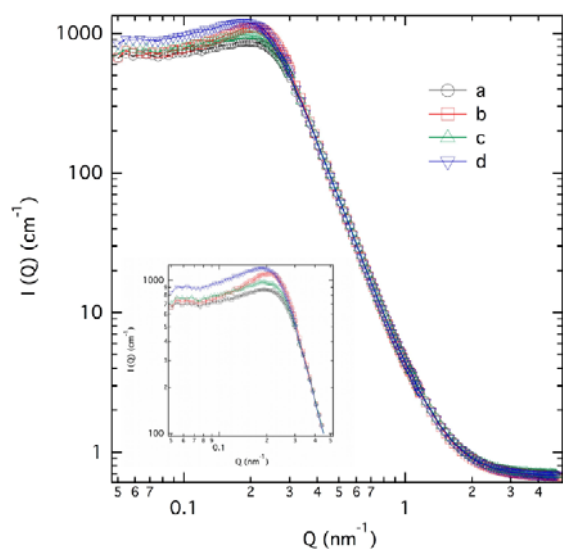


Figure 1: SANS spectra of bicontinuous microemulsions composed of cyclohexane, D₂O, C₈₋₁₀G_{1,4} and different alcohols as tuning parameters for the curvature of the amphiphilic film. The inset shows the region of around the broad structure factor maximum

region of the structure factor maximum. The measurements were varied out at three sample-detector distances of 1m, 4m and 16m at a wavelength of 4.5Å. The samples were prepared in bulk contrast.

A quantitative analysis of these curves using the Teubner-Strey approach will give insight on the influence of the alcohol. These results will then contribute to the analysis of a NSE experiment exploring the dynamics in the reported systems. Additionally, lamellar phase structures from binary mixtures of D₂O and C₁₂E₅, C₁₂E₆ and mixtures of both surfactants were studied. In combination with a previously performed NSE experiment these data will contribute to the understanding of dynamics inside concentrated and diluted lamellar phases.

The second part of the experiment was related to the structure of micro- and macrogels below, at and above the phase transition temperature.

In contrast to microgel-systems where the phase transition is fast and well characterized using various methods less results are available for macrogels which show a slow relaxation up to a few days.

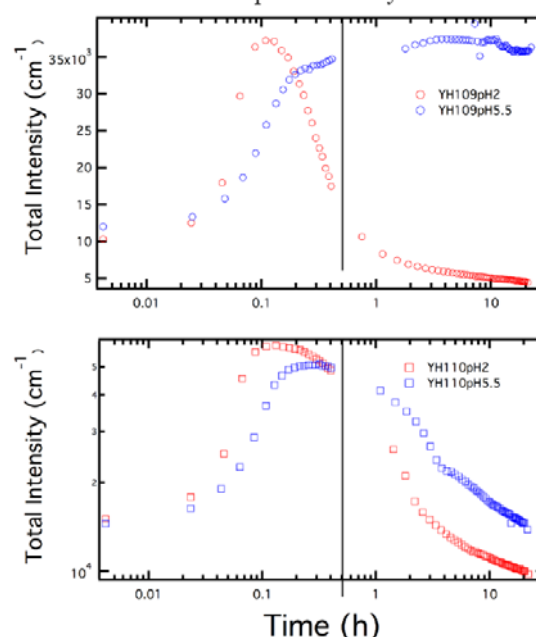


Figure 2: Total detector intensity in absolute scale for the relaxation kinetics of macrogel samples at 38° C of two compositions and each composition at 2 pH-values.

We monitored the relaxation kinetics in a temperature jump experiment with four macrogel samples of different composition at 2 pH values at a sample-detector distance of 8m and a wavelength of 4.5Å. Figure 2 shows the total detector intensity in absolute scale for these samples. They were placed in the thermostated sample holder and monitored for 20h. The black line marks the time when the sample reached a constant temperature. Up to this time a fast intensity increase was observed followed either by a plateau phase or a steep decrease which turned over into a slow part after the first 2-3 hours.

The temporal evolution of the scattering curves obtained for the macrogels will give more insights in the relaxation of such macroscopic gels. Additionally a comparison with the case of microgels will be possible.

 <p>HELMHOLTZ ZENTRUM BERLIN für Materialien und Energie</p> <p>NEUTRONS</p>	<p>EXPERIMENTAL REPORT</p> <p>Investigation of Preparation Techniques of Polyelectrolyte Multilayer</p>	<p>Proposal: BIO-04-1450-EF</p> <p>Instrument: V6</p> <p>Local Contact: R. Köhler</p>
<p>Principal Proposer: Experimental Team:</p>	<p>Ralf Köhler, MPI, Potsdam Marta Kolasinska, MPI, Potsdam Rumen Krastev, NMI at the University of Tübingen Thomas Gutberlet, ETH Zürich & PSI, CH Piotr Warszynski, Polish Academy of Sciences, Krakow, Poland</p>	<p>Date(s) of Experiment</p> <p>23.03.2007 -26.03.2007 07.05.2007 – 08.05.2007</p>

Date of report: 5. Jan 2010

Polyelectrolytes (PE) are macromolecules possessing ionic groups along the chain. PEM are films built up by subsequent adsorption of PEs of opposite charge onto a solid substrate. The structure of PEM is determined by the combination of long-range Coulombic forces, intrachain van der Waals interactions, and steric hindrance, resulting in a variety of specific features, which makes PEM a complex subject to study.

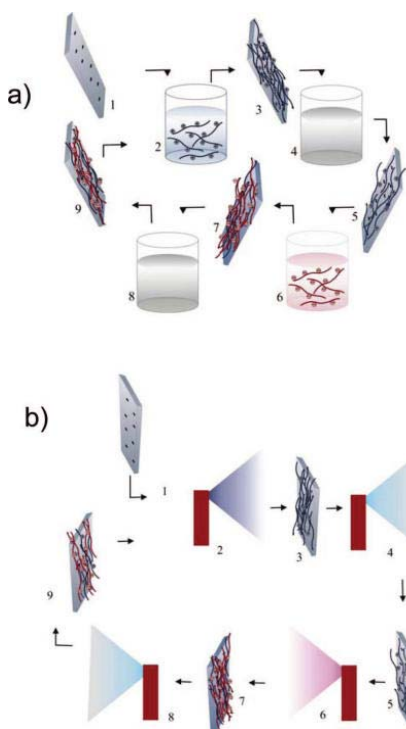


Figure 1: Scheme of preparation techniques for PEM Dipping (a), Spraying (b)

We investigate the properties of PEM prepared using the technique of PE deposition from solution (dipping) or supplying the solutions to the surface by spraying (figure 1). For sample characterisation neutron reflectometry and X-ray reflectometry studies were performed in PSI Villigen (CH), and HMI Berlin.

We found that sprayed films are thinner and rougher than PEMs having the same number of layers, i.e., having the same number of deposition cycles, prepared by dipping.

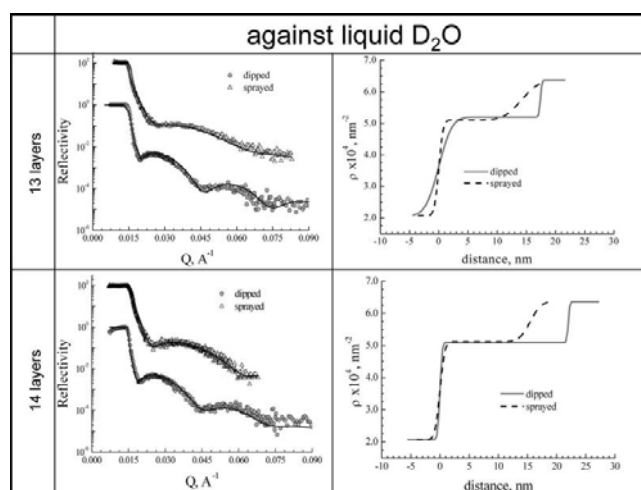


Figure 2: Neutron reflectometry data and fits; SLD profiles of PAH/PSS multilayer against D₂O, dipped sample (straight line), sprayed sample (dashed line)

Sprayed samples are also less stable to variable external conditions. Having the great advantage of a really short time of preparation, they cannot provide same features common for dipped PEMs such as stability or uniformity. Our study shows that the preparation method strongly influences structure and properties of the PEM. This might be one reason for the broad variations in PEM behaviour.

Reference:

Marta Kolasinska, Rumen Krastev, Thomas Gutberlet, and Piotr Warszynski, Layer-by-Layer Deposition of Polyelectrolytes. Dipping versus Spraying, *Langmuir* 2009 25 1224

 HELMHOLTZ ZENTRUM BERLIN für Materialien und Energie NEUTRONS	EXPERIMENTAL REPORT Type of growth and water content of polyelectrolyte multilayers	Proposal: CHE-04-1736 Instrument: V6 Local Contact: R. Steitz
	Principal Proposer: S. Dodoo, TU Berlin Experimental Team: S. Dodoo, TU Berlin R. v. Klitzing, TU Berlin R. Steitz, HZB	Date(s) of Experiment 30.06.2009 – 07.07.2009

Date of report: 09.10.2009

The sequential adsorption of oppositely charged polyelectrolytes onto a charged surface from aqueous solutions can lead to the build up of polyelectrolyte multilayers (PEM) [1,2]. Depending on the preparation conditions, the multilayer could grow linearly, exponentially or become unstable with increasing adsorption step [3]. The conditions which determine the type of growth of the multilayer build-up will be discussed in this report. Previously we reported that the total water content of the polyelectrolyte multilayers is the sum of the “void water” and the “free water”. In this report we present the effect of the type of salt and ionic strength on the total water content of the polyelectrolyte multilayers. Samples: Si/PEI/(PSS/PDADMAC100%)₆ and Si/PEI/(PSS/DADMAC75%-co-NMVA25%)₆ with different concentrations of NaF, NaCl and NaBr salts. The samples were measured against vacuum after H₂O, vacuum after D₂O, H₂O liquid and D₂O liquid. The type of growth depending on type of ion, ionic strength and degree of charge density of the polycation can be seen in Table 1. Linear growth PEM is the type of growth where the thicknesses of consecutive double layers are the same with increasing adsorption step. Exponential growth of PEM is where the thicknesses of consecutive double layers increases with increasing adsorption step. During the exponential growth, some of the polycation are adsorbed at the surface and some diffuse into the PEM matrix because they are mobile. Upon adsorption of the polyanions, the polycations which are already in the matrix diffuse to the surface to form complexes with the polyanions in addition to the complexes form as a result of surface charge reversal. The unstable PEM formation is the situation where some of the intrinsically compensated complexes formed during the adsorption step shortly after their formation collapse into the aqueous solution. In Fig. 1 it can be seen that the water content of the PEM increases with

increasing ionic strength for the respective salts [4].

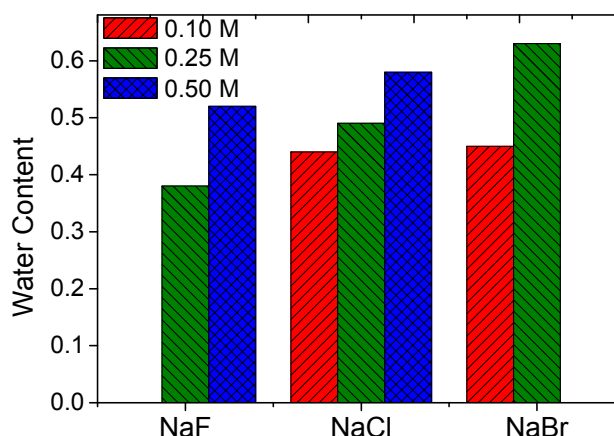


Fig.1 Neutron reflectivity result of water content of PEM against type of salt for (PSS/PDADMAC100%)₆.

Table1. Type of growth of PEM in relation to the type of salt and degree of charge of polycation i.e., PDADMAC100% or PDADMAC75% charged.

Type of growth	NaF		NaCl		NaBr	
	100%	75%	100%	75%	100%	75%
Linear	0.25M 218 Å		0.25M 275 Å		0.1M 230 Å	0.1M 210 Å
Exponential				0.25M 322 Å	0.25M 498 Å	
Unstable		0.25M 97 Å				0.25M 99 Å

Reference:

- [1] G. Decher et al., *Thin Solid Films* 210/211 (1992) 831
- [2] G. Decher, *Science* 277 (1997) 1232
- [3] J. E. Wong et al., *Langmuir* 25 August 2009
- [4] S. Dodoo, R. Steitz, R. v. Klitzing in preparation

Principal Proposer:
Experimental Team:

Claus Czeslik, TU Dortmund
Florian Evers, Metin Tolan, TU Dortmund
Ralf Köhler; Roland Steitz, HZB
Claus Czeslik, Christian Reichart, TU Dortmund

Date(s) of Experiment

04.05.2009 – 11.05.2009

Date of report: 19.08.2009

It is well-known that a poly(acrylic acid) (PAA) brush becomes almost completely protein resistant, when the ionic strength of the protein solution is increased to about 500 mM at pH = 7. However, we have observed recently by fluorescence spectroscopy that this salt effect is inverted at pH = 2 [1]. Here, the degree of insulin adsorption is strongly increasing, when salt is added to the protein solution. In order to understand the mechanism underlying this new protein binding property of a PAA brush, we have performed neutron reflectivity experiments (Fig. 1).

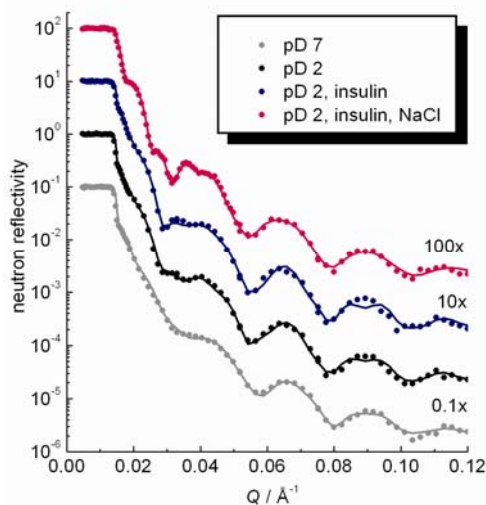


Fig. 1. Neutron reflectivities of a planar PAA brush that covers a silicon wafer. Solution conditions are given in the legend. Solid lines are fits based on layer models.

The obtained neutron reflectivities have been analyzed by fitting calculated curves. Calculations were based on layer models for the interfacial structures. The corresponding scattering length density (SLD) profiles are shown in Fig. 2 and 3.

At both pD-values, insulin adsorbs at a PAA brush. The SLD profiles indicate a deep penetration and interaction between insulin and the PAA chains. At pD = 7, the well-known salt effect could be reproduced: In the presence of 500 mM NaCl, insulin is rejected from the PAA brush (Fig. 2). In contrast, a massive deposition of insulin at a PAA brush is

found at pD = 2, when NaCl is added to the insulin solution (Fig. 3), in excellent agreement with earlier fluorescence data [1].

From the SLD profiles at pD = 2, it is suggested that the salt-induced adsorption of insulin is partially controlled by protein-protein interactions, since significant amount of insulin is located at $z = 650 - 850 \text{ \AA}$, where the PAA density is essentially zero.

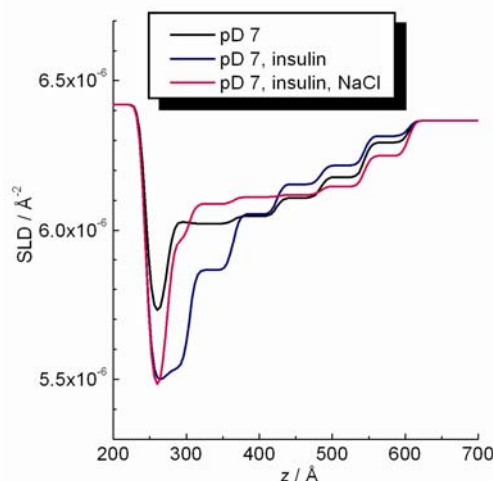


Fig. 2. Scattering length density profiles of a planar PAA brush with and without immobilized insulin. At pD = 7, adding NaCl to the insulin solution leads to a desorption of insulin from the brush.

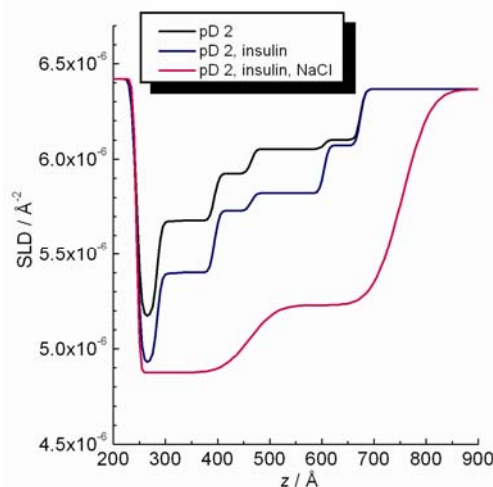


Fig. 3. Scattering length density profiles of a planar PAA brush with and without immobilized insulin. At pD = 2, adding NaCl to the insulin solution leads to a massive adsorption of insulin.

[1] C. Reichart, C. Czeslik, Langmuir **25** (2009) 1047-1053.

 HELMHOLTZ ZENTRUM BERLIN für Materialien und Energie NEUTRONS	EXPERIMENTAL REPORT	Proposal: CHE-04-1744 Instrument: V6 Local Contact: A. Teichert
	Surfactants at the metal-oil interface	Date(s) of Experiment 06.07.2009 – 13.07.2009
Principal Proposer: Experimental Team:	Ali Zarbakhsh, QM UCL, UK Mario Campana, QM UCL, UK Roland Steitz, HZB Anke Teichert, HZB	

Date of report: 15.03.2010

The lubrication of surfaces by oils is a key aspect of many academic and industrial problems with significant financial implications. Although lubrication has been exploited for many centuries, the details of the underlying physics and chemistry are still to be resolved. There are three broad regimes of friction/lubrication depending upon the applied load: from (i) the hydrodynamic regime, where a reasonable layer of oil can survive between the moving surfaces to (ii) the boundary regime where the high load pushes most oil out leaving a molecularly thin film between the surfaces and (iii) an intermediate ‘mixed’ regime. In many commercial applications, additives (boundary lubricants) can be added to the oil to maintain and enhance the oil monolayer adsorbed on surfaces, which are believed to act by adsorption to the metal surfaces. The physisorption or chemisorption of long chain polar organic molecules on metal surfaces are considered to form a thin film between the moving metal surfaces which can result in a reduction in the coefficient of friction. A simple example of these additives could be fatty acids adsorbed from non-polar hydrocarbon oils onto a metal surface. Other additives are also included in these systems for example to prevent oxidation and dispersal of particulates. In many cases these are also surface active agents. This area of science is growing in importance because of: Advances in engine technology combined with lower emission requirements; the demand for fuel efficiency and improved friction reduction; and the desire for a longer oil change interval. Hence understanding the role and the adsorption isotherms for lubricant additives at the oil-metal interface is essential. The measurements outlined below would help to achieve these goals to improve design and establish a more efficient formulation.

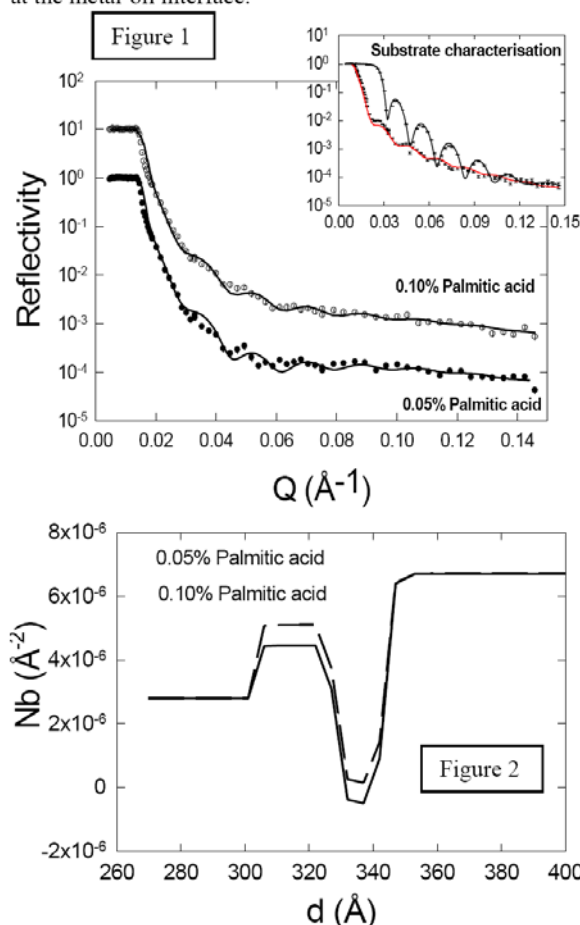
A series of reflectivity measurements were carried out on the V6 reflectometer to help to understand the underlying physics and chemistry involved at the metal-oil interface. A series of well defined sputtered metal Fe/oxide (Fe_2O_3) substrates were used. The bare substrate was first characterised. Reflectivity profiles were then measured using the polarized neutron beam to determine the adsorption isotherm for Palmitic acid ($\text{CH}_3(\text{CH}_2)_{14}\text{COOH}$) at the oxide/oil (deuterated hexadecane) interface. We observed that the spin down reflectivity profiles were the most sensitive to the adsorption profile of the fatty acid. A series of profiles was measured for concentration of the Palmitic acid from 0.05% to 0.10 %.

The spin up and spin down reflectivity data for the characterisation of the Fe sputtered layer on a Si

substrate is shown in Figure 1 (insert). The solid lines are the fit to the data (layer thickness of $d_{\text{Fe}} = 304 \pm 4 \text{ \AA}$ and $d_{\text{Fe}_2\text{O}_3} = 24 \pm 2 \text{ \AA}$).

The reflectivity profiles (spin down contrast) for 0.05% and 0.10% Palmitic acid adsorbed from Hexadecane oil ($6.80 \times 10^{-6} \text{ \AA}^{-2}$) on the metal surface are shown in Figure 1. The fits to the data are shown by the solid lines. The scattering length density profiles for these fits are given in Figure 2.

The data indicate a penetration of Palmitic acid into the oxide layer upto 25% for 0.10% concentration. We also deduce an adsorbed layer of 16Å of the Palmitic acid corresponding to a fully stretched Palmitic acid molecule at the metal-oil interface.



Acknowledgement:

This research project has been supported by the European Commission under the 7th Framework Programme through ‘‘Research Infrastructures’’ action of the ‘‘Capacities’’ Programme, contract number CP-CSA_INFRA-2008-1.1.1. Number 226507-NMI

 HELMHOLTZ ZENTRUM BERLIN für Materialien und Energie NEUTRONS	EXPERIMENTAL REPORT		Proposal: BIO-04-1805-EF
	A Model Interface for Artificial Implants		Instrument: V6 Local Contact: R. Steitz
Principal Proposer:	Martin Kreuzer, Ruprecht-Karls-Universität Heidelberg	Date(s) of Experiment	
Experimental Team:	Reiner Dahint, Ruprecht-Karls-Universität Heidelberg Roland Steitz, HZB	15.06.2009 -21.06.2009	

Date of report: 08.01.2010

In natural joints the two surfaces of the joint are separated by a liquid phase, the synovial fluid, which mainly contains hyaluronic acid (HA). Many studies emphasize the importance of HA for joint lubrication. Furthermore surface-active lipids, which cover the contact areas of natural joints, are considered to play an important role in the reduction of friction. For a detailed understanding of the relevant processes on the molecular scale, more information on the interface cartilage/synovial fluid under load is needed.

As the shear set-up was unavailable at the time we decided to study the response lipid covered interfaces to elevated pressure by neutron reflectometry instead. The lipid coatings were realized by spin coating from a solution of DMPC lipids in chloroform. This produces well-defined lipid multilayers and would be a beneficial method of preparing lipid-coated implants, if the multilayer remained stable on the substrate. In a first round of experiments we measured the lipid multilayer against a solution of pure D₂O (Figure 1).

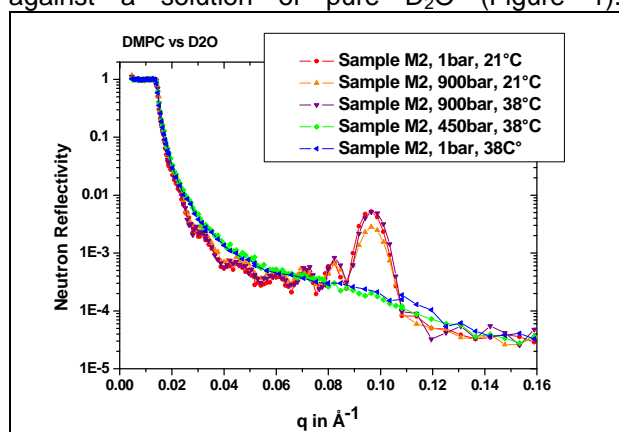


Figure 1: Neutron Reflectivity of a DMPC multilayer against D₂O.

The Bragg peak at $q=0.096 \text{ \AA}^{-1}$ (Figure 1, red curve) corresponds to a repeat distance of the lipid multilayer of 65 Å. After increasing the pressure to 900 bar the Bragg peak position remains stable, while its amplitude is reduced by 50% (Figure 1, orange curve). After rising the temperature to 38°C, the intensity of the Bragg peak returns to its initial value (Figure 1, purple curve). Upon crossing the phase transition from the gel- to the fluid-like L_α-phase (700 bar at 38°C) by decreasing pressure to

450 bar, a detachment of most of the lipid lamellae is observed: only one double layer remains on the substrate (Figure 1, green curve). Further pressure decrease to 1 bar does not change the reflectivity anymore (Figure 1, blue curve). Measurements with a second sample led to a similar result.

In an independent experiment a freshly prepared lipid multilayer was measured against a solution of 3 mg/mL HA in D₂O (Figure 2). Below the phase transition, i.e. in the gel state, we observed identical effects as with the multilayer against pure D₂O.

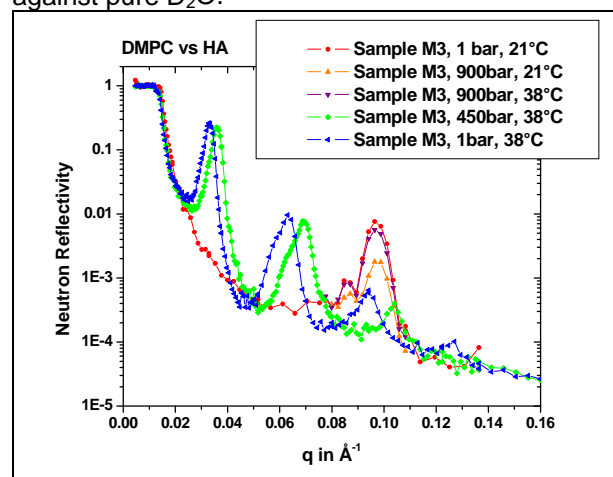


Figure 2: Neutron Reflectivity of a DMPC multilayer against a solution of HA in D₂O.

Above the bulk phase transition, however, the lipid multilayer remained on the substrate, but now an immense swelling occurred: Only after about 3 days at 38°C and 450 bar, the system reached a stable configuration (Figure 2, green curve). The first Bragg peak at $q=0.036 \text{ \AA}^{-1}$ corresponds to a repeat distance of 175 Å. Upon pressure decrease to 1 bar the multilayer swelled even further, with a repeat distance of 191 Å reached after 7 days (Figure 2, blue curve). A detailed analysis of the data is currently under way.

This research project has been supported by the German Ministry for Education and Science (BMBF) through Contract n°: 05KN7VH1.

 HELMHOLTZ ZENTRUM BERLIN für Materialien und Energie NEUTRONS	EXPERIMENTAL REPORT		Proposal: PHY-04-1806-EF
	Continuation 2: Water at a Hydrophobic Substrate and the Effect of Pressure		Instrument: V6 Local Contact: R. Steitz
Principal Proposer: Experimental Team:	Roland Steitz, HZB Reiner Dahint, Ruprecht-Karls-Universität Heidelberg Martin Kreuzer, Ruprecht-Karls-Universität Heidelberg		Date(s) of Experiment 20.07.2009 – 26.07.2009

Date of report: 15.01.2010

Recent studies of the interface of water against hydrophobic surfaces by neutron and X-ray reflectometry have revealed a depletion of water in a thin boundary layer next to the substrate. [1,2] These findings can be explained in the general context of drying transitions where the depletion of water is seen as a (weak) dewetting of the hydrophobic wall in contact with the bulk aqueous phase. [3]

In that context neutron reflectivity experiments performed on the interface of heavy water (D_2O) against thin films of perdeuterated polystyrene (dPS) spin-coated onto silicon blocks have revealed a non-vanishing scattering contrast at the polymer-water interface, although the two materials (dPS and D_2O) have closely similar scattering length densities. [4] The source of that non-vanishing contrast was identified as a depletion of water in the boundary layer against the hydrophobic surface. The observed depletion layer had a thickness of 26 Å with a water density of 90% of bulk water density, corresponding to a depletion length, d_2 , of about 2.6Å. The depletion length represents the thickness of an equivalent vacuum layer and is a convenient measure for comparing results from different experiments and theoretical predictions. In fact, the value $d_2 \approx 2.6\text{Å}$ observed for the dPS- D_2O interface is in excellent agreement with the depletion length of 2.56Å derived by molecular dynamics (MD) simulations on the interface of an alkane slab in water.

The latter study also investigated pressure effects on the depletion length and predicts a decrease in d_2 from 2.56Å to 1.89Å as the pressure is increased from ambient (1bar) to a hydrostatic pressure of 1000bar at a constant sample temperature of 300K. [5]

In the experiment we report here we set out to test the predicted pressure dependence of d_2 by performing neutron reflectivity measurements on the dPS- D_2O interface as a function of applied hydrostatic pressure up to 1000bar. We measured two samples each at 1 and

1000bar and observed a pressure-induced increase in d_2 by 0.5Å for the first sample and a decrease by 0.8Å for the second sample.

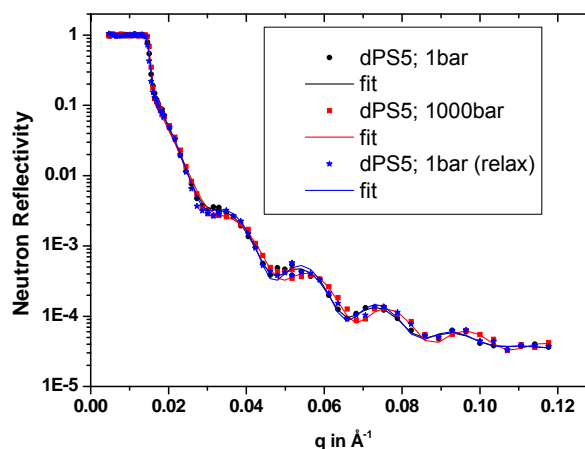


Figure 1: Neutron Reflectivity of the second sample (dPS5), measured against a D_2O fronting of varied hydrostatic pressure. Note, that there is a reversible right-shift of the Kiessig fringes at 1000bar.

The observed increments in d_2 were therefore contrary to prediction for the first sample, but were as predicted for the second sample. The depletion length at 1 bar were 3.6Å and 3.9Å, respectively, for the two samples and were at 1000bar 4.1Å and 3.1Å. We attribute these high values to a contamination of the dPS- D_2O interface by (nondeuterated) organic substances.

It was possible to implement the Heidelberg high pressure cell and achieving full functionality of the experimental setup. A detailed analysis of the data is currently under way.

Literature

- [1] Schwendel et al., Langmuir 2003, 19 2284
- [2] Torben et al., Phys. Rev. Lett. 2003, 086101
- [3] Lum et al., J. Phys. Chem. B 1999, 103, 4570
- [4] Steitz et al., Langmuir 2003, 19, 2409
- [5] Mamatkulov et al., Langmuir 2004, 20, 4756

 NEUTRONS	EXPERIMENTAL REPORT Polyelectrolyte Multilayer under Mechanical Stress	Proposal: PHY-04-1891-LT Instrument: V6 Local Contact: R. Köhler
	Principal Proposer: Ralf Köhler, MPI, Potsdam Experimental Team: Johannes Früh, MPI, Potsdam Rumen Krastev, NMI at the University of Tübingen	Date(s) of Experiment 22.08.2008 – 24.08.2008 03.11.2008 – 11.11.2008 04.08.2009 – 11.08.2009

Date of report: 10.Jan.2010

Polyelectrolyte Multilayers (PEM) are films of organic polyions of opposite charge which were subsequently adsorbed onto solid substrates. This material exhibits due to its complex internal interactions (long-range Coulombic and van der Waals forces and short-range hydrogen bonding) a highly tuneable spectrum of physico-chemical properties.

Although PEMs were in focus of investigations for more than one decade the knowledge about their internal structure is still limited. We want to learn about their structural behaviour on macroscopic and microscopic scale by testing PEM mechanically. Therefore the PEM films made from PSS and PDADMAC¹ were exposed to uniaxial stress with a special homemade device, and were measured with X-ray (XRR) and neutron reflectometry (NR).

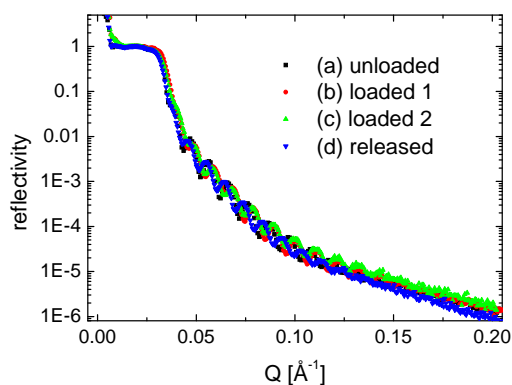


Figure 1: X-ray reflectivity curves of pristine PEM (a), at ca 0.25% strain (b), at ca 0.5% strain (c), and released (d).

XRR shows that the thickness of PEM film shrinks depending on the extent of applied stress. Elastic and plastic mode of deformation can be observed. After release of plastically deformed PEM, the film thickness increases drastically and appears very rough compared with the original state. Whereas the thickness decrease during deformation is in the order of the error bars (5%), the detected thickness increase after relaxation is distinct (10±5) %.

The NR measurements were performed at the V6 instrument in HZB using a 2d-detector. The PEM samples featured a superstructure i.e. every 6th layer was made from fully deuterated material (dPSS) instead of hydrogenated PSS. This way Bragg peaks are visible in addition to the Kiessig fringes in the reflectivity curves.

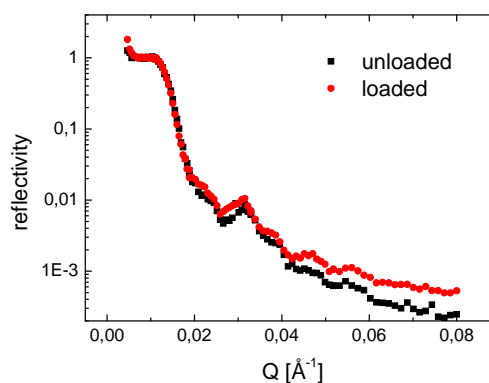


Figure 2: NR data of unloaded and loaded PEM: Variations of Bragg-Peak and Kiessig fringes.

Probably due to smaller deformations obtained in these measurements, NR data do not show the same clear behaviour as X-ray does.

The diffuse scattering data exhibit variations for loaded and unloaded PEM but the proprietary data format of the 2d-detector did not allow for full data treatment up to now.

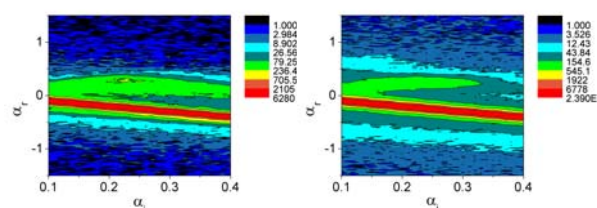


Figure 3: Specular and off-specular data of unloaded (left) and loaded PEM film (right).

 HELMHOLTZ ZENTRUM BERLIN für Materialien und Energie NEUTRONS	EXPERIMENTAL REPORT Interfacial Behaviour of Ionic Liquids	Proposal: PHY-04-1892-LT Instrument: V6 Local Contact: R. Köhler
	Principal Proposer: Ralf Köhler, MPI, Potsdam Experimental Team: Rumen Krastev, NMI at the University of Tübingen Benilde Saramago, IST Lisbon, Portugal	Date(s) of Experiment 08.06.2009 – 10.06.2009 01.11.2009 – 05.11.2009

Date of report: 12.01.2010

Although Ionic Liquids (IL) are known since almost 100 years their interesting intrinsic properties as room temperature liquid salts are intensely studied only recently.

The strong internal interactions of these ionic liquids cause a low vapour pressure. This and the molecular asymmetry of at least one of the compounds, with an ionic and a non-polar part, make them interesting candidates for solvents, lubricants, and catalysts. The physico-chemical behaviour of the organic ions can be tuned chemically e.g. by addition or reduction of aliphatic (hydrocarbon) chains or the use of different (e.g. multivalent charged) ions.

We are interested in the interfacial behaviour of these liquids. Especially the wetting behaviour of solid substrates and a possible structuring of the ions towards the solid/liquid and liquid/gas interfaces stand in focus of our investigations.

First experiments with Atomic Force Microscopy (AFM), X-ray (XRR), and neutron reflectometry (NR) were performed. They showed the possibility to establish homogeneous IL films on silver and gold coated silicon and glass substrates.

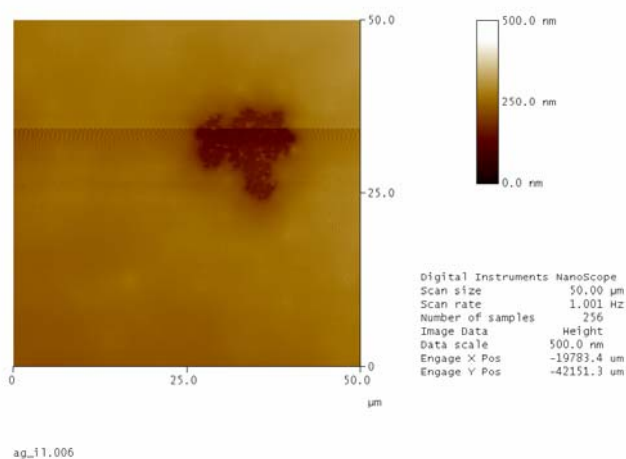


Figure 1: AFM image of a defect in wetting IL film

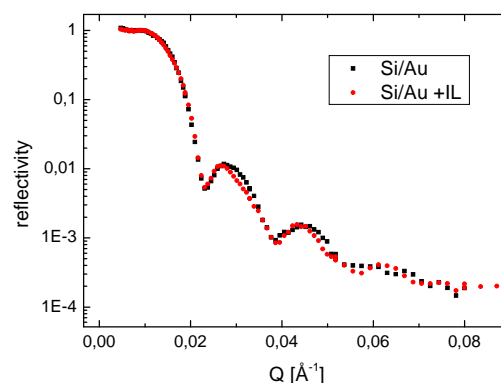


Figure 2: Neutron reflectometry wetting IL layer on silicone/gold substrate

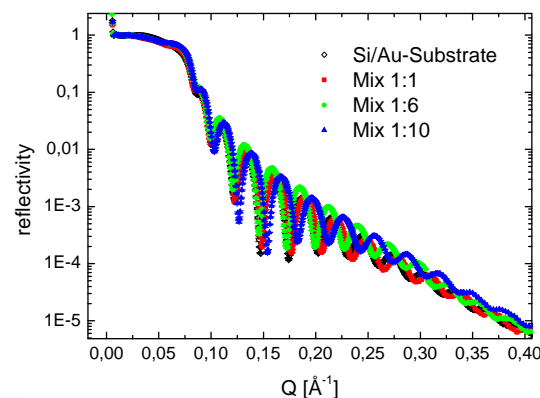


Figure 3: X-ray reflectometry data of IL films of different thickness adsorbed on Si/Au substrate

The film thickness can be adjusted by spin-coating of IL solutions (ethanol) with variable IL concentrations onto the substrates. Hereby the film thickness and the concentration of the IL solution do not depend linearly. This inconsistency gives evidence for an internal structuring of the IL films. The contradictory thickness data require a careful fitting with multilayer models.

 HELMHOLTZ ZENTRUM BERLIN für Materialien und Energie NEUTRONS	EXPERIMENTAL REPORT Lipid-coated surfaces exposed to joint fluid, effects of temperature and joint fluid composition	Proposal: BIO-04-1893-EF Instrument: V6 Local Contact: R. Steitz
	Principal Proposer: Martin Kreuzer, Ruprecht-Karls-Universität Heidelberg Experimental Team: Reiner Dahint, Ruprecht-Karls-Universität Heidelberg Roland Steitz, HZB Matthias Reinhardt, HZB	Date(s) of Experiment 07.12.2009 - 15.12.2009

Date of report: 15.01.2010

In natural joints the two surfaces of the joint are covered with lipids and separated by a liquid phase, the synovial fluid, which mainly contains hyaluronic acid (HA). For a detailed understanding of the relevant processes on the molecular scale, more information on the interface lipid-synovial fluid under load is needed. As the shear set-up was unavailable at the time we decided to study the response lipid covered interfaces to elevated temperatures and solutions by neutron reflectometry instead. The lipid coatings were realized by spin coating from a solution of DMPC lipids in chloroform. This produces well-defined lipid multilayers and would be a beneficial method of preparing lipid-coated implants, if the multilayer remained stable on the substrate.

In a first round of experiments we measured the lipid multilayer against a solution of pure D₂O with increasing temperature steps. We repeated the measurement with five differently prepared multilayers: multilayer I was spin coated with a 5mg/mL lipid solution, II and III with a 10mg/mL solution, IV with a 10mg/mL solution on a 130Å interlayer of titanium and the V consisted of a cast film. All spin coated multilayers detached from the Si-substrate between 24°C and 26°C. On the contrary, the cast film remained stable up to the highest experimental temperature of 40°C.

In an independent experiment a freshly prepared lipid multilayer, VI, was measured against a solution of 3mg/mL HA in D₂O (Figure 2). The sample was measured shortly after incubating at 21°C (Figure 1, green curve), 8 days after incubating (Figure 2, magenta curve) and subsequently after increasing to 38°C (Figure 1, purple curve). The lipid multilayer remained stable on the substrate, but an immense swelling occurred.

A further experiment with a freshly prepared sample, VII, measured against a solution of HA and 1M NaCl in D₂O did not show a swelling behavior (Figure 2). On the opposite, there was only very little change in film structure with time and temperature. The added NaCl screens the electrostatic charges of the system. Hence, we conclude that the pronounced swelling of the

multilayer observed in the presence of HA without NaCl is driven by electrostatic interactions between the negatively charged HA molecules and the zwitterionic lipids. A detailed analysis of the data is currently under way.

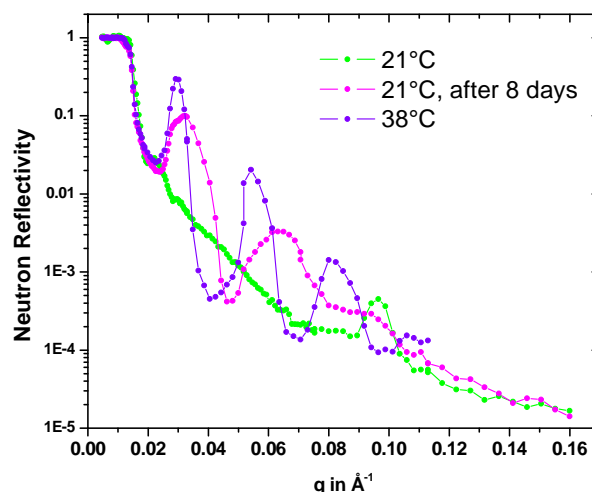


Figure 1: Reflectivity of a DMPC multilayer, VI, against a solution of HA in D₂O.

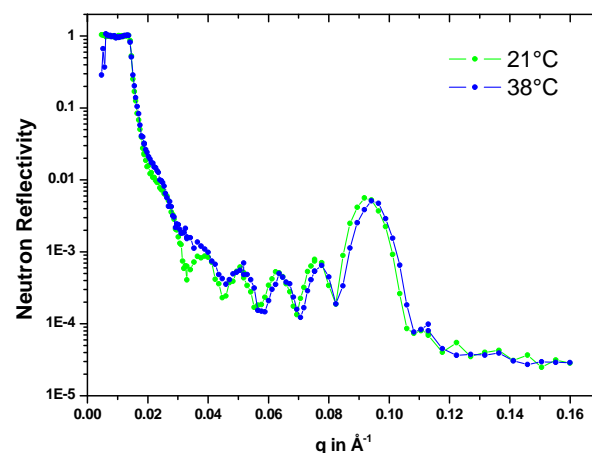


Figure 2: Reflectivity of a DMPC multilayer, VII, against a solution of HA and 1M NaCl in D₂O.

This research project has been supported by the German Ministry for Education and Science (BMBF) through Contract n°: 05KN7VH1.

Principal Proposer: T. Hellweg, Universität Bayreuth
Experimental Team: S. Wellert, HZB
R. Stehle, Universität Bayreuth

Date(s) of Experiment

28.09.2009 – 04.10.2009

Date of report: 11.01.2010

Due to their commercial availability bion-inspired amphiphilic molecules are of great interest for the formulation of environmentally compatible complex fluids of low health risk. In many desired applications, especially in cleaning and cosmetics, solid surfaces play an essential role. The aim of the reported experiment was to explore the near surface interfacial region of a sugar surfactant based bicontinuous microemulsion wetting planar solid surfaces of different wettability.

The reflectometry measurements were performed using a bicontinuous sample of the water-cyclohexane- $C_{8-10}G_{1,4}$ -pentanol phase system. Samples were prepared at three oil/water+oil ratios α of 0.1, 0.5 and 0.9 in bulk and in the case of $\alpha=0.5$ also in film contrast. Additionally, a H_2O/D_2O mixture, providing the total reflection and a reduced signal from the structure factor maximum from the bulk phase was used in the case of $\alpha=0.5$.

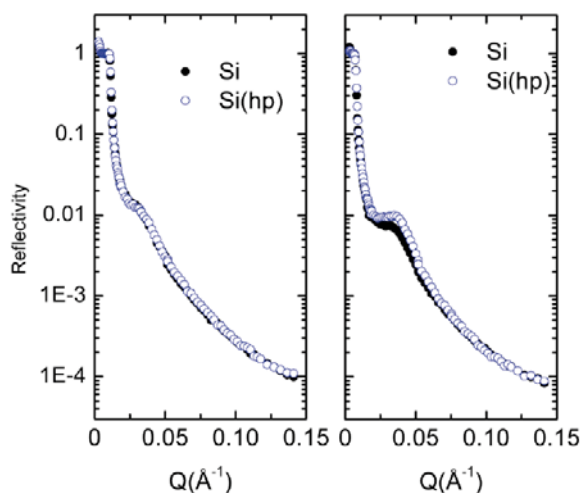


Figure 1: Left: Reflectivity curves measured with a sample of $\alpha=0.1$ in bulk contrast at a hydrophilic surface (Si) and a hydrophobic surface (Si(hp)). Right: Reflectivity curves at $\alpha=0.5$ at an intermediate contrast providing the total reflection edge and a reduced structure factor peak. From the difference between the reflectivity curves in the right side image information about the near surface structure will be obtained.

Figure 1 shows reflectivity curves for two bicontinuous samples of $\alpha=0.1$ (left image) and $\alpha=0.5$ (right image) wetting a hydrophilic surface (Si) and a hydrophobic surface (Si(hp)). While there is no difference between the curves in the left image the curves measured with the sample of $\alpha=0.5$ show different behaviour around the structure factor signal at. The difference between the

curves provides information about the near surface ordering in the case of the hydrophobic surface.

Figure 2 shows scattering maps obtained for these two samples. Images a) and b) are the results for the sample with $\alpha=0.1$ at the hydrophilic and -phobic surface.

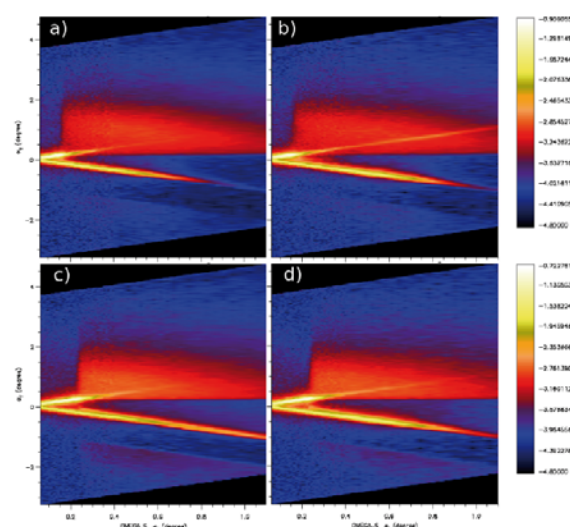


Figure 2: Scattering maps from a bicontinuous sample of $\alpha=0.1$ at the hydrophilic (a) and the hydrophobic surface (b) and a sample of $\alpha=0.5$ at the same surfaces (c) and d). Additional contributions to the diffuse scattering are observed at the hydrophobic surface for both samples.

Images c) and d) show scattering maps for the case of $\alpha=0.5$ at the same surfaces. For both samples in the pattern an additional feature occurs in the diffuse scattering at the hydrophobic surface while in the case of the hydrophilic surface only a broad diffuse signal from the bulk structure is observable. This clearly indicates a different near surface structure for the two kinds of surface.

From a further analysis of the reflectivity curves and the scattering maps quantitative information about the coupling of the complex fluids on the surface will be obtained. A continuation of this experiment will clarify if the reported observations are a general property of sugar surfactant based systems. Furthermore, an additional reference (oxide) layer at the used Si-blocks will have to be used to investigate the first molecular layer at the surfaces to discover the reason for the different near surface structure.

 EXPERIMENTAL REPORT		Proposal: CHE-04-1900 Instrument: V6 Local Contact: R. Steitz
Inhibition of insulin adsorption and aggregation at hydrophobic interfaces		
Principal Proposer: Experimental Team:	Claus Czeslik, Fakultät Chemie, TU Dortmund Florian Evers, Metin Tolan, Fakultät Physik, TU Dortmund Roland Steitz, Martin Kreuzer, HZB Claus Czeslik, Fakultät Chemie, TU Dortmund	Date(s) of Experiment 13.10.2009 - 19.10.2009

Date of report: 06.01.2010

Insulin can form amyloid fibrils at hydrophobic interfaces, which represents a severe issue in handling insulin solutions. Adding cosolvents to a protein solution has significant effects on the structure of adsorbates formed by the protein. For example, we have found that the presence of glycerol decreases the interfacial affinity of the protein RNase [1]. Glycerol stabilizes the native folded structure of a protein and strengthens its hydration shell. Thus, interfacial interactions based on hydrophobic interactions and/or conformational changes are disfavoured. On the other hand, there is a series of molecules that are known to inhibit the growth of protein amyloid fibrils, such as resveratrol (Fig. 1), which is a red wine compound.

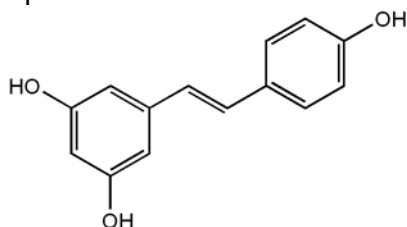


Fig. 1. Resveratrol, a red wine compound, can inhibit the formation of protein amyloid fibrils.

In this project, we have analyzed how the cosolvents glycerol and resveratrol modify the structure of an insulin adsorbate at a hydrophobic interface. If insulin would form aggregates at this interface that resemble short amyloid structures, then resveratrol can be expected to have a pronounced effect. In contrast, if the insulin adsorbate is characterized by an amorphous structure, the presence of glycerol will simply reduce the adsorbed amount by decreasing the packing density of adsorbed protein molecules.

Silicon wafers were spin-coated with a thin film of perdeuterated poly(styrene) (dPS) to generate a hydrophobic surface. Insulin solutions (pD = 7), containing various concentrations of glycerol and resveratrol, were brought into contact with these wafers. The insulin adsorbates, which have formed

under these conditions, were analyzed by neutron reflectometry using the instrument V6. In Fig. 2, typical neutron reflectivity curves are shown. Preliminary data analysis has been performed using the Parratt32 software (vers. 1.6).

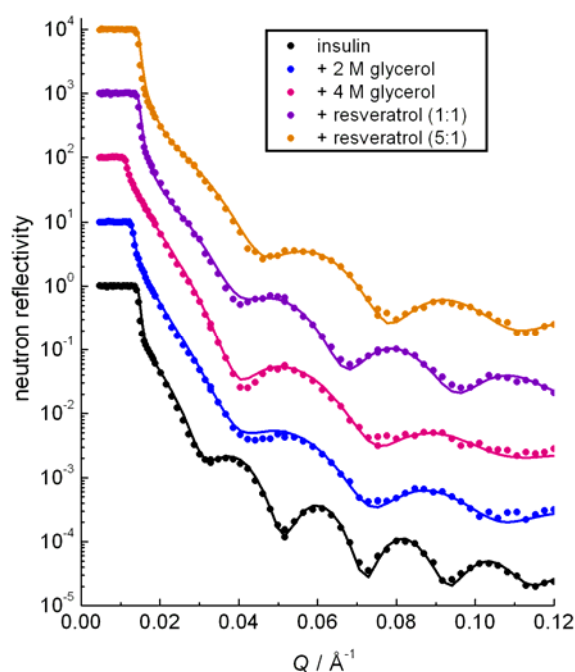


Fig. 2. Typical neutron reflectivity curves as obtained in the performed experiments (symbols). Silicon wafers were coated with a thin film of perdeuterated poly(styrene). Insulin has been adsorbed at this hydrophobic interface in the absence and the presence of glycerol and resveratrol, as indicated in the legend. The data have been analyzed by fitting simple layer models for the interfacial structures (solid lines).

The analysis of the neutron reflectivity data suggests that the adsorption of insulin at a dPS surface is strongly reduced in the presence of glycerol. However, the addition of resveratrol induces a very little effect only. Thus, one might conclude that an insulin adsorbate at a hydrophobic dPS surface has a rather amorphous structure.

[1] J. Koo, T. Gutberlet, C. Czeslik, *J. Phys. Chem. B* **112** (2008) 6292-6295.

 HELMHOLTZ ZENTRUM BERLIN für Materialien und Energie NEUTRONS	EXPERIMENTAL REPORT	Proposal: BIO-04-1882
	Water transport in giant algal cells by neutron radiography	Instrument: V7 Local Contact: N. Kardjilov
Principal Proposer: Experimental Team:	Chris Garvey, ANSTO, Australia Markus Strobl, HZB	Date(s) of Experiment 15.11.2009 - 17.11.2009

Date of report: 27.01.2010

Charophytes are the green algal most closely related to modern vascular plants. As members of the order Charophyceae with a well-defined geometry and large size, *Chara australis* is a useful and interesting model system to study water transport in plant cells (Figure 1). They are also an important opportunity to study the important group of trans-membrane water transporter channels, the aquaporins.

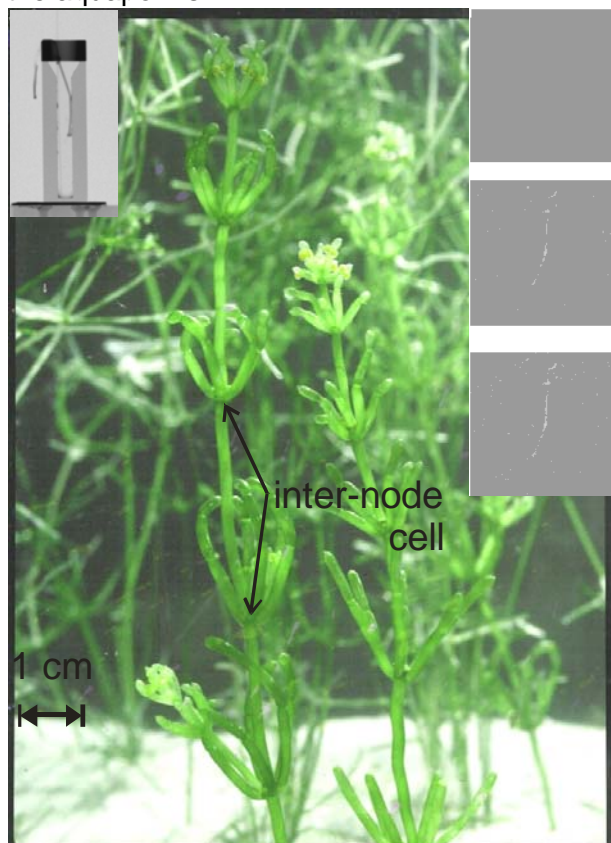


Figure 1

Chara australis cells showing the scale of the internode cells used for this experiment. The LHS inset shows the sample cell, and the RHS inset an example of data.

The *Chara* cell is simple – it consists of a thin cell wall and membrane surrounding the cylindrical cell cytoplasm. In this way the geometry (surface to volume ratio) of the cell is well defined. The experimental cell is shown in the left hand inset of Figure 1. A single

internode cell consisting of 1H water cell cytoplasm was placed in a quartz cuvette. The field of view of the measurement was minimised to minimise the read out time on the neutron detector. Heavy water was injected into the cuvette with the *Chara* cell at the start of the experiment, and images taken during the time course, during which ¹H and D exchange across the membrane, the image of the cell was lost. Using the procedure we were able to obtain a time resolution of approximately 3 seconds per frame. A schematic of the measurement is shown in Figure 2.

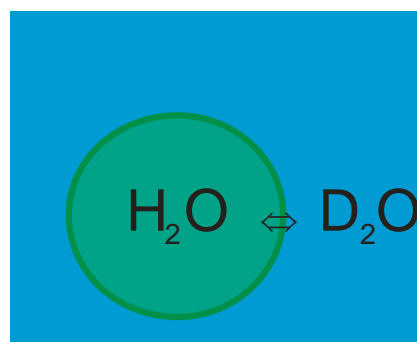


Figure 2 Schematic of the experiment.

Chara australis (green) are immersed in D₂O. As the difference between H:D (contrast) is lost between outside and inside the cell the image of the cell disappears

The RHS inset of Figure 1 shows three frames, 3 seconds apart, normalised to the first image (top). The images reflect changes from the fully hydrogenated cell.

Further analysis of the data is to aim at making quantitative observation on the transport of water across the cell membrane. The dimensions of the cell are known, so the ratio of H:D in the water of the cell cytoplasm is related to the adsorption coefficient and the cross-section of the cell.

Principal Proposer: Johannes Körner and Karl Kratz, GKSS Centre for Biomaterial Development
 Experimental Team: Sven-Oliver Seidel, University of Applied Science
 Johannes Körner, GKSS Centre for Biomaterial Development
 Wolfgang Treimer, University of Applied Science

Date(s) of Experiment

14.05.2009 – 22.05.2009

Date of report: 14.12.2009

Ultra small angle neutron scattering (USANS) was tested as a method to analyse the inner structure of a deposit from electro spun polymer fibres (Fig 1). It should have shown whether single polymer chains in the fibres have a certain orientation or not.

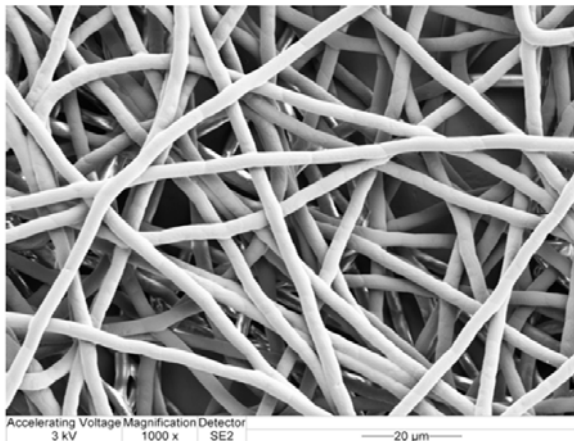


Fig. 1: polymer fibres from PPDO

Therefore a sample of random orientated polymer fibres was tentatively analysed with the ultra small angle neutron scattering. Fig. 2 shows the behaviour from a non- and a stretched sample. The stretched sample should be a simulation of an orientated fibre sample which is needed for a closer look to the inner structure of the polymer chains. There are no significant differences visible between the stretched and the non stretched sample. It is possible that the stretched sample includes random orientated fibres, too. However, the measurement should be repeated with parallel deposited fibres to see. The influence of the sample thickness was also investigated and is shown in Fig 3. As expected and clearly visible is the dependence with increasing of numbers of layers. Both of the diagrams in Fig.3 show the variation, only the scaling is different.

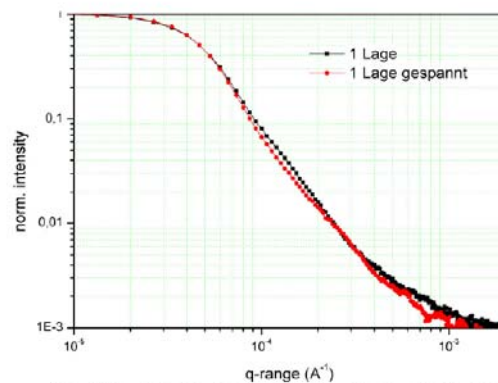


Fig. 2: q-range from a non- and a stretched sample

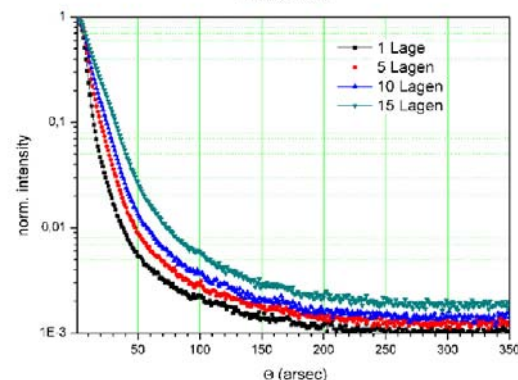
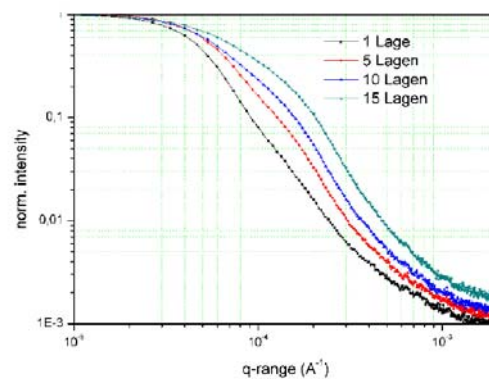


Fig. 3: q-range and scattering dependence on the numbers of sample layers

Material Science

	EXPERIMENTAL REPORT Determination of load-affected through-thickness residual stresses in welded aluminium alloys	Proposal: MAT-01-2428 Instrument: E3 Local Contact: R. C. Wimpory
	Principal Proposer: Th. Nitschke-Pagel, TU Braunschweig Experimental Team: Th. Nitschke-Pagel, TU Braunschweig R. C. Wimpory, HZB	Date(s) of Experiment 25.03.2009 – 06.04.2009

Date of report: 15.01.2010

Residual stresses induced by welding processes may affect significantly the fatigue strength properties of cyclically loaded welded constructions if they are more or less constant during the whole lifetime. However it is well known from general investigations, that initial residual stresses may be reduced during the first load cycles due to plastic overloads or even due to accumulated plastic deformations which are occurring with an increasing number of load cycles. The relaxation behaviour depends on the material properties, the amount of the initial residual stresses and the intensity of the load in combination with the number of load cycles. As the numerical evaluation of the relaxation behaviour is not easily to handle because this requires the difficult and extensive calculation of the initial residual stresses, the notch geometry and the microstructural composition investigations with regard to the residual stress relaxation are performed usually experimentally using X-ray diffraction which allows the systematic determination of the residual stresses around a weld seam after different loads and numbers of load cycles. However the results can not be evaluated explicitly in each case because the information is usually limited on the surface.

In order to enable a more reliable description and evaluation of the relaxation behaviour of the welding residual stresses neutron diffraction experiments were carried out in combination with XRD-measurements. Different soft and age-hardened aluminium alloys (AlMg4.5Mn, AlMgSi1Mn, AlZn4.5Mg1, AlZn5Mg3Cu) were observed after welding and after cyclic loading with different loads.

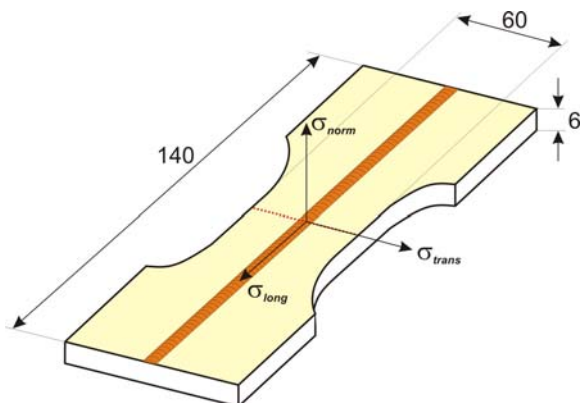


Figure 1: Shape of the used samples

Experimental Setup of the E3 diffractometer was used to determine the through thickness residual stress distributions in specimens with longitudinal butt welds. The residual stresses were measured using a volume of 8 mm³ which combines a sufficient resolution with an acceptable exposure time. Surface residual stresses were measured by means of X-ray diffraction using CuK_α-radiation. Fig 1 shows schematically the shape of the used samples with the longitudinal butt weld. Residual stresses were measured along the red-dotted line in the centre of the sample and the coordinate system. The measurements were performed in the as-welded state and after loads with upper stresses of 88 MPa and 176 MPa and 10⁴ load cycles.

The three measured components of the initial residual stresses in an average depth of 2.4 mm after welding are representatively shown Fig 2 for

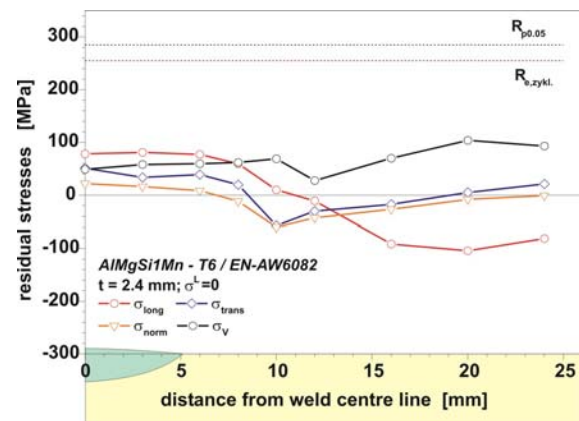


Figure 2: Residual stress distributions 2.4 mm below the surface in the as-welded state.

the age-hardened alloy AlMgSi1Mn. Significant tensile residual stresses are found in loading direction (σ_{long}) with a uniform distribution in the weld seam and the zone adjacent to the weld. With increasing distance to the weld seam the residual stresses in loading direction change into the compressive range to fulfil the equilibrium conditions. The residual stress components transverse to the weld (σ_{trans}) and in thickness direction (σ_{norm}) show a similar distribution with lower maximum values. Consequently the resulting v'Mises stress distribution shows a relative constant

level in the investigated area. The most interesting longitudinal residual stress profiles are distributed uniformly across the plate thickness and the distributions agree very good with the profile determined at the surface by XRD (fig.3).

Tensile residual stresses with an amount between 50 and 100 MPa can be found in the weld seam and in the adjacent heat affected zone. With increasing distance to the weld toe the residual stresses change into the compressive range. This distribution of the longitudinal residual stresses was the expected one due to the constraint conditions of the weld seam. The total amount of the tensile residual stresses is significantly lower than the yield strength ($R_{p0.05}$) respectively than the cyclic yield strength ($R_{e,zykl.}$).

Fig.4 shows the residual profiles in loaded specimens after 10^4 load cycles under a tensional loading with a load amplitude of 40 MPa (mean stress 48 MPa) and 80 MPa (mean stress 97 MPa). The lower load obviously does not influence significantly the residual stress distribution. The resulting v'Mises stress (including the load stress) shows a level between 160 and 235 MPa in the zone around the weld seam. In a larger distance to the weld the v'Mises stress decreases significantly. The higher load leads to a strong residual stress relaxation. All residual stress components are distributed uniformly with values close to zero. Therefore the resulting v'Mises stresses are predominantly affected by the load stresses and show a uniform level of approximately 190 MPa.

The results of the presented experiments have shown that the residual stresses around welds in aluminium alloys are distributed relatively uniformly across the plate thickness. This result is of course not representative for each plate thickness but for the investigated thickness. This means, that the residual stresses which can be determined at the surface are as well a good representative Indicator for the residual stress in deeper layers. On the other side the experiments have shown that the reliability of the results obtained with neutron diffraction is high although the experiences with

XRD have shown, that the diffraction conditions especially in the weld material are difficult due to coarse grain in aluminium alloys. Therefore valuable measurements can be performed with neutron diffraction in combination with a good spatial resolution and an acceptable exposure time. Yielding due to cyclic loading leads to a reduction of

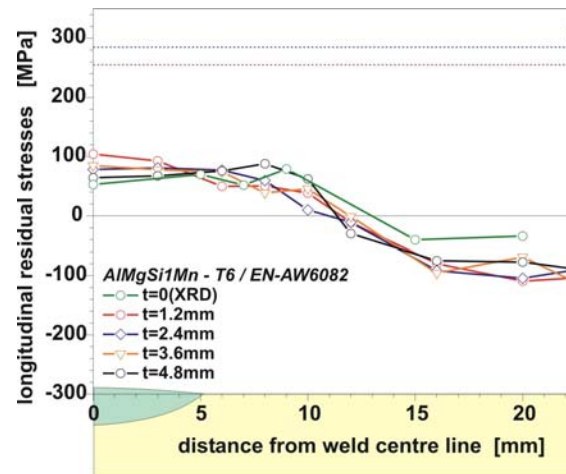


Figure 3: Longitudinal residual stress distributions in different depths in comparison the surface values (XRD).

the residual stress peaks with the consequence, that the residual stress distributions more uniformly in different depths. The results of the experiments are very helpful to confirm the parallel measurements by means of XRD and enable a better understanding and at least an evaluation of the residual stress relaxation behaviour of welded aluminium alloys.

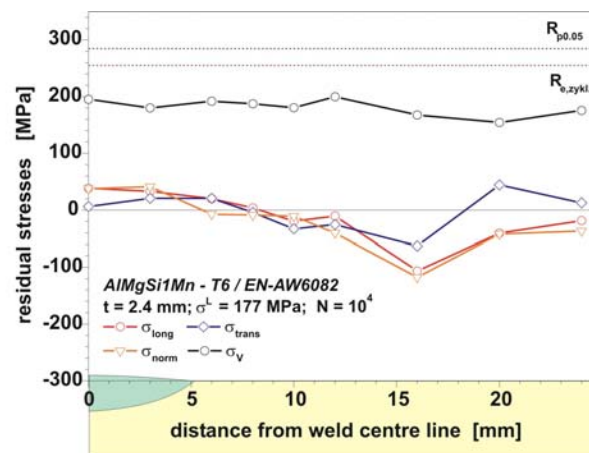
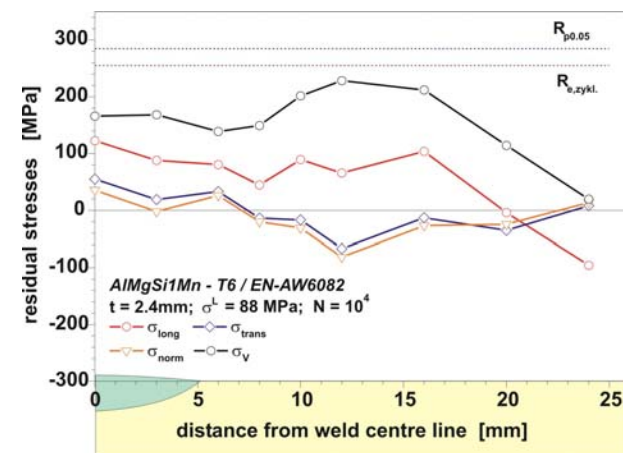


Figure 4: Residual stress distributions 2.4 mm below the surface after cyclic loading ($R = 0.1$) with load amplitude of 40 MPa (left) and 80 MPa (right).

	EXPERIMENTAL REPORT	Proposal: MAT-01-2430
	Residual stresses in diamond reinforced MMC under mechanical load	Instrument: E3 Local Contact: Robert Wimpory
Principal Proposer: Experimental Team:	Michael Schöbel, TU Wien Johannes Jonke, TU Wien Patrik Dobron, TU Wien Nikolaus Eder, TU Wien	Date(s) of Experiment 16.06.2009 – 21.06.2009

Date of report: 07.12.2009

Motivation

Metal matrix composites are developed for heat sink applications. Diamonds are used as reinforcement because of their best known thermal conductivity. The low reactivity of diamond with the metal matrix is problematic and has to be improved by heat treatments. Differences in interface reactivity at the diamond (hkl) surfaces can be expected.

Experiment

Tensile tests at room temperature were made during increasing external load measuring the strains in situ in the diamond particles. Several diamond peaks were acquired in load direction with a big gauge volume (6x6x2) mm³ to increase particle statistics. Lattice strains were determined relative to the unloaded condition. The test rig from Stress Spec, FRM2, Garching was used for the experiment. Neutron diffraction was made during several load steps until fracture. The tensile test was performed in the elastic regime only due to the low yield strain of the composites.

Results

A stress strain diagram of an Al/CD/60p MMC is shown in figure 1. The diamond strain in 10h heat treated MMC increase at 100 MPa until fracture at 200 MPa. Low load transfer into the diamonds can be observed in the 3h heat treated Al/CD/60p until fracture at 160 MPa.

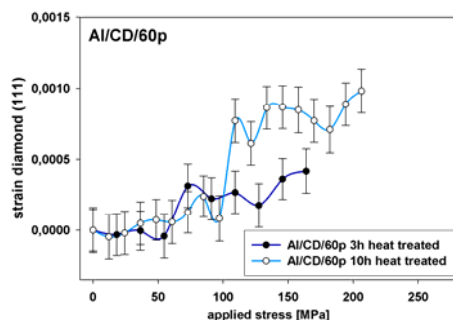


Figure 1: Diamond lattice strains in Al/CD/60p after 3h and 10h heat treatment.

The stress strain correlation for the AgSi11/CD/60p system is shown in figure 2. In the JR1 diamond particles strain increases from starting point continuously to fracture at 220 MPa. The MBD4 system show low particle strains up to fracture at 270 MPa.

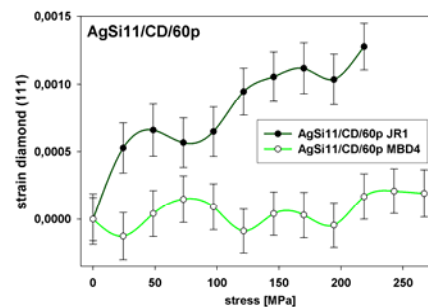


Figure 2: Diamond lattice strains in AgSi11/CD/60p with two different diamond particle types (JR1/MBD4).

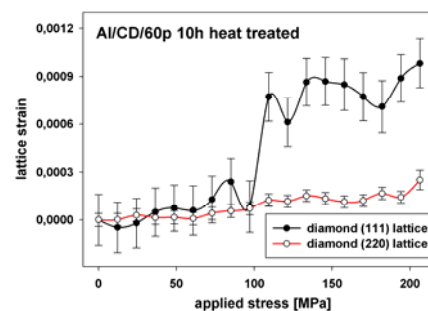


Figure 3: The Al/CD/60p ht 10h with different strains in diamond (111) lattice compared to (220).

Higher load transfer can be observed in the diamond (111) lattice compared to the (220) lattice in Al/CD/60p 10h.

Conclusions

The increasing bonding strength by carbide forming heat treatments of Al/CD MMC was proven by higher load transfer into the particles. In AgSi11/CD/60p the low quality JR1 diamonds show stronger interface bonding strength than the MBD4 reinforced system. Different lattice strains in different (hkl) planes could be observed and their origin from bonding strength variations has to be clarified.

Acknowledgement

First of all I thank to Ludger Weber, EPFL Lausanne for cooperation and sample preparation. Especially I would like to thank Michael Hofmann lending us the tensile test rig from Stress Spec, FRM2 making the experiment possible. Last but not least I thank Robert Wimpory for his kind support on E3 setting up the experiment.

This research project has been supported by the European Commission under the 7th Framework Programme through "Research Infrastructures" action of the "Capacities" Programme, contract number CP-CSA_INFRA-2008-1.1.1. Number 226507-NMI

	EXPERIMENTAL REPORT Residual stress states in case hardened discs for the validation of simulation results	Proposal: MAT-01-2496 Instrument: E3 Local Contact: R. C. Wimpory
	Principal Proposer: Jeremy Epp, Universität Bremen Experimental Team: Thomas Hirsch, Universität Bremen Robert C. Wimpory, HZB Jeremy Epp, Universität Bremen	Date(s) of Experiment 09.06.2009 – 16.06.2009 19.07.2009 – 21.07.2009

Date of report: 10.12.2009

In the present study, the residual stress state of a low pressure case hardened and quenched disc from steel grade AISI 5210 (EN 20MnCr5) has been investigated by means of neutron and laboratory X-ray diffraction methods. These discs served as a simplified model for gear components. The measured results were compared to simulation results.

The case hardening was accomplished by low pressure carburization. Each batch consisted of eight disks hanging in a single layer. Carburization was carried out at 940 °C in a C₂H₂-atmosphere. The batch was gas quenched with 10 bar nitrogen after holding for 20 minutes at 840 °C. The case hardening depth was adjusted to 0.8 mm. The microstructure after quenching consisted of martensite and retained austenite in the carburized layer and martensite/bainite and retained austenite in the core.

For the X-ray diffraction measurements of the surface layer (up to 1.5 mm in depth) measurements of residual stress tensors were realized as the microstructure in the surface layer is composed of two phases (martensite and austenite). Moreover, in this type of material a triaxial residual stress state with $\sigma_{33} \neq 0$ should be considered. For this, equations predicting changes of stress free lattice spacings as a function of the carbon content have been used.

For comparison, simulations of the case hardening process were made. For these simulations the commercial FEM-software package Sysweld® was used. Heterogeneities in the heat transfer coefficients were used because of the gas quenching oriented from top to bottom. Values were between 500 and 700 W/m²K distributed as shown in Figure 1.

Neutron diffraction measurements were evaluated using d_0 from cube measurements and with d_0 calculated from a condition of axial force balance in the whole cross section. The results calculated with d_0 from a condition of a force balance are about 50 MPa than those calculated with d_0 from the cubes.

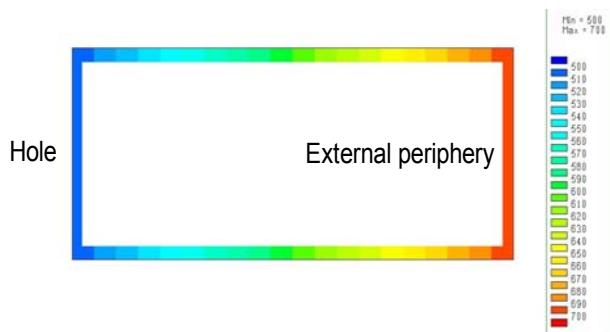


Figure 1: Distribution of the heat transfer coefficients on the half disc

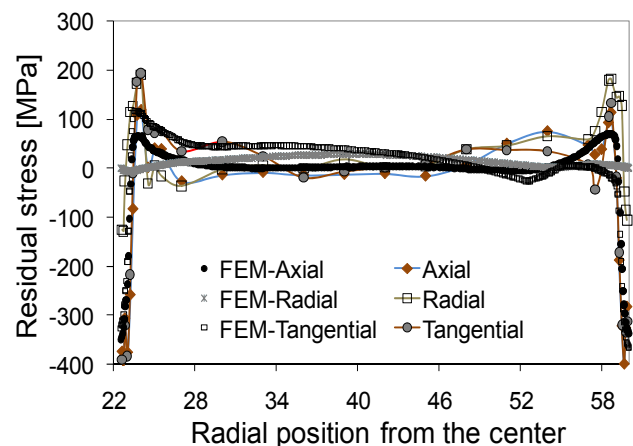


Figure 2: Residual stress distribution measured along the radius compared to simulation results

The comparison of the experimental results (obtained with d_0 from the force balance criterion) with the simulation is given in figure 2. Simulation and experimental results show a satisfying overall agreement in the residual stress distribution but discrepancies are still present. In order to improve the simulation results, 3-dimensional simulations with enhanced streaming simulation of the gas quenching process will be employed.

Principal Proposer: Adele Carradò, IPCMS, Strasbourg, France
Experimental Team: Heinz Palkowski, TU Clausthal, Clausthal-Zellerfeld
Robert C. Wimpory, HZB

Date(s) of Experiment

06.07.2009 – 12.07.2009

Date of report: 14.07.2009

Seamless precision tubes are produced by extrusion and brought to final dimension by successive drawing through a die. The geometry of the tubes is not uniform (ovality, eccentricity) after the extrusion process. Drawing reduces these variations. However, this means a non-uniform flow of material not only in the axial, but also in the hoop direction while passing through the die. Amongst others, this may result in varying residual stresses which influence the performance of the tube. Finite element calculations have been performed to describe the material flow and to calculate the resulting residual stress field. The aim of this experiment was to provide experimental data to validate the calculations. The tube investigated was produced by extrusion, drawn twice in a cold drawing process and stress annealed before being cold drawn under controlled laboratory conditions to its final dimension under variation of **eccentricity**. The orientation of the tube was kept the same for all drawing steps. This procedure was applied in order to allow connecting geometry factors with stress. The geometry of the tube was measured before and after drawing. The parameters for fabrication of the investigated tube are given in the table below (**Table 1**). Tube 5 is a tube drawn without plug to a final outer diameter of 40 mm.

circumference. For each point measured, 9 to 11 scans (900 s) had been done over wall thickness. Gauge volume had been selected to $2 \times 2 \times 2 \text{ mm}^3$. The elastic constants used were 116 GPa for the Young's modulus and 0.36 for the Poisson ratio.

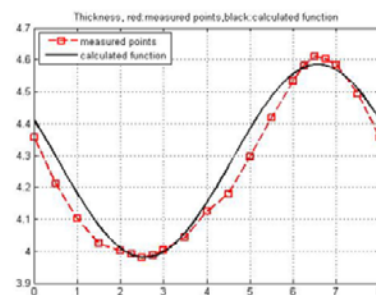


Figure 2: Measured and approximated (by sin-function) wall thickness for tube 5 over circumference.

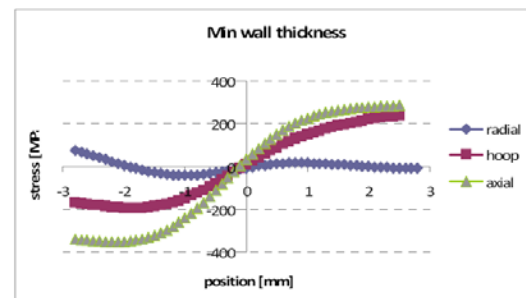


Figure 3: Profile of residual stress in minimum wall thickness (position "-3" internal surface of the tube)

Outer Ø (mm)		Av. thickness (mm)		Δ thickness (mm) Δt	Ovality O (%)		Eccentricity E (%)	
d _{A0}	d _{A1}	t _{ave0}	t _{ave1}		Before	After	Before	After
48.0	40.0	4.2	4.37	0.8	0.54	< .05	9.5	5.4

Table 1: Geometrical data of tube investigated.

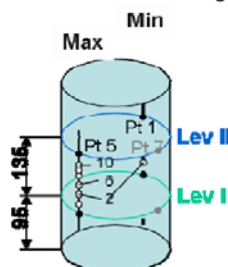


Figure 1: Measured points from tube 5

Residual strain measurements over circumference and thickness were performed by triaxial-method at E3. The family plane {311} with $2\theta=86^\circ$ was used with a wavelength of $\lambda = 0.14865 \text{ nm}$. 11 points in the maximum and minimum thickness were measured in radial, hoop and axial directions. **Fig. 1** gives a sketch from their position on tube 5 and **Fig 2** shows measured and calculated wall thickness of tube 5 over

Following **Fig. 3** it is to be seen that the radial stress component has the expected small level ($< 100 \text{ MPa}$) changing from tension on the inside to low compression to the outside. The hoop component changes from compression at the inner surface (-200 MPa), increasing pressure level to centre and then strongly changing to tension to the outside (200 MPa). The axial component shows the strongest change in stress over thickness starting on the inside with strong compression (-400 MPa) and with broad plateau (approx. 300 MPa). The positions directly at the surfaces were corrected by boundary effects. The comparison between thickest and thinnest wall (max. and min.) shows no significant difference without a small shifting in the position of zero stress.

Acknowledgement

This research project has been supported by the European Commission under the 7th Framework Programme through "Research Infrastructures" action of the "Capacities" Programme, contract number CP-CSA_INFRA-2008-1.1.1. Number 226507-NMI

	EXPERIMENTAL REPORT Residual stresses in butt joint and lap joint aluminium alloys welded by friction stir technique	Proposal: MAT-01-2500 Instrument: E3 Local Contact: R. C. Wimpory
	Principal Proposer: Vittorio Calbucci, Univ. Politecnica delle Marche, IT Experimental Team: Vittorio Calbucci, Univ. Politecnica delle Marche, IT Adrian Manescu, Univ. Politecnica delle Marche, IT Robert C. Wimpory, HZB Vittorio Calbucci, Univ. Politecnica delle Marche, IT	Date(s) of Experiment 11.05.2009 – 16.05.2009

Date of report: 31.01.2010

With the aim to determine the residual stresses behaviour in different aluminium alloy welded specimens, obtained by using the friction stir welding technique, neutron diffraction measurements at the E3 instrument were carried out on three different samples. The specimens were made of Al6056, Al2139 and Al2098 in butt joint configuration, and only Al2024 for the lap joint configuration. The difference between the samples was not only in the constitutive material but also in the welding process parameters, like the rotation pin speed and the welding velocity. The geometry of the samples in butt joint configuration and the considered directions for the measurements are shown in fig.1.

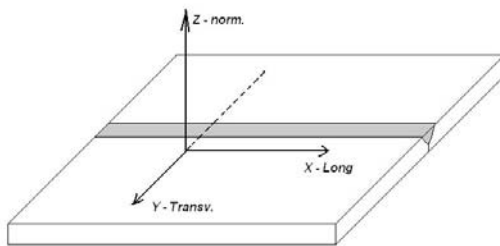


Fig.1 - Geometry of the samples measured direction in the butt joint sample.

All the measurements have been performed using a beam wavelength of 1.57 Å and a gauge volume of 1.5x1.5x1.5 mm³, selecting the primary and secondary slit of 1.5mm. Concerning the d₀ value, assuming the plain stress condition, we determine in each of the three samples, the value of d₀ in every considered point, using the condition:

$$d_0 = ((1-\nu) d_z + \nu (d_x + d_y)) / (1 + \nu)$$

In all the specimens we investigated many points placed in a line transversal to the welding direction. In each of them the transversal (Y direction in fig.1) and longitudinal (X-direction in fig.1) stresses were calculated. Due to the presence of big grains in the inner structure of the sample, we could not perform the measurements for the Al2098 sample.

The obtained residual stresses results are reported in the following graphs.

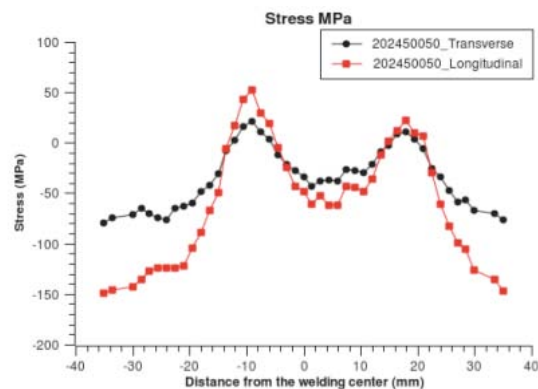


Fig.2 Residual stress in the Al2024 specimen. The 0 value in the abscissa axis represents the center of the welding.

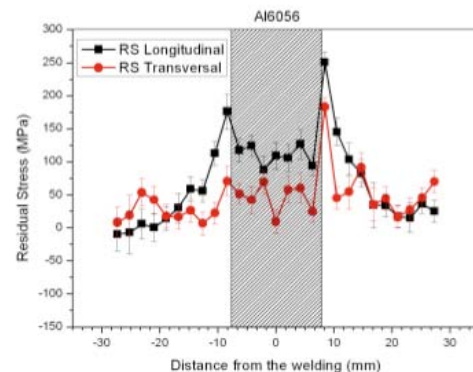


Fig.3 Residual stress in the Al6056 specimen

The results obtained for the analysed specimens are in good agreement with the FEM simulation results and exhibit a quite symmetrical trend of the stresses with respect to the welding line.

Acknowledgement:

This research project has been supported by the European Commission under the 7th Framework Programme through "Research Infrastructures" action of the "Capacities" Programme, contract number CP-CSA_INFRA-2008-1.1.1. Number 226507-NMI

	EXPERIMENTAL REPORT Residual Stress Analysis of Drawn 1045 Steel Bars	Proposal: MAT-01-2501 Instrument: E3 Local Contact: R. C. Wimpory
	Principal Proposer: A. da S. Rocha, UFRGS, Porto Alegre, Brazil Experimental Team: A. da S. Rocha, UFRGS, Porto Alegre, Brazil R. Nunes, UFRGS, Porto Alegre, Brazil T. Hirsch, IWT – Uni Bremen R. C. Wimpory, HZB	Date(s) of Experiment 13.07.2009 – 19.07.2009

Date of report: 10.08.2009

1 Introduction

In this work a combined straightening and bar drawing process to produce AISI 1045 round bars from coils of a hot-rolled material are investigated. The generation of residual stresses is seen as one of the main causes of distortion of these bars. Furthermore residual stresses are also responsible for a possible distortion in any further manufacturing step of this material as e.g. induction hardening. In this manufacturing route under investigation, the steel rods are first pre-straightened, shot-blasted, drawn, cut and final straightened with crossed rolls. The near surface results of X-ray diffraction analyses and hole drilling method are compared with the neutron diffraction analysis to receive a complete view of the residual stress states in the bars. These results support an undergoing Ph. D. thesis executed in cooperation between UFRGS-Brazil and IWT-Germany.

2 Experimental Description

The processed material is an AISI 1045 steel for which the chemical composition is given in table 1. The combined process starts with the as hot rolled material with a nominal diameter of 21.64 mm. The final products are round bars with nominal dimensions of 20.25 mm of diameter and 6 m of length. Samples were taken after each step of the process, as follows:

- Horizontal and vertical pre-straightening (1st step);
- Sand blasting (2nd step);
- Drawing (3rd step);
- Cutting, simultaneous polishing and straightening with crossed rolls (4th step).

Table 1: Chemical analysis of the material.

Element	C	Si	Mn	P	S	Cr
%	0.4	0.2	0.7	<0.01	<0.02	0.19
Element	Mo	Ni	Cu	Nb	Al	Fe
%	0.0	0.19	0.09	<0.01	<0.01	rest

The samples were marked with 0° line to keep the reference of the bars as they pass the processing line. In such manner it is possible to correlate positions over samples surface to a reference in the machines. This reference is crucial to correlate residual stresses with the applied strains during the process. The drawing die geometry and the angle of the crossed rolls in the final straightening are the main parameters that affect the distortion behaviour [Nak01]. A priority was given to obtain data from these both manufacturing steps. A gauge volume of 2 x 2 x 2 mm has been used to optimize the use of the beam time. For the determination of the reference *d0* value a cube of size 3 x 3 x 3 mm was prepared and measured at the actual measurement set-up used in the experiment. The following 3 samples have been measured in the experiment: a sample drawn with a

die angle of 20°, a sample drawn with a die angle of 15° and a sample which was drawn with a die angle of 15° and finally simultaneously straightened and polished.

3 Results

The following two figures present results from the sample drawn with the die angle of 20°. Figure 1 gives the residual stresses in a cross section of the bar. If the *d0*-value is taken as a mean value of all measurements high tensile residual stresses of 400 to 500 MPa in axial and hoop direction are measured near the surface. In the center of the bar the axial residual stresses decrease to compressive stresses of 500 MPa. Hoop stresses decrease to zero. Two measurements have been executed for the hoop and radial residual stresses in the center of the bar. The two values correlate which each other indicating a good reproducibility of the individual measurements. Radial stresses remain quite low over the whole cross section. This behaviour of drawn bars is well known [Bue58, Bue65]. Residual axial stresses at the surface measured by X-Ray diffraction analysis agree fairly well with the values given in figure 1.

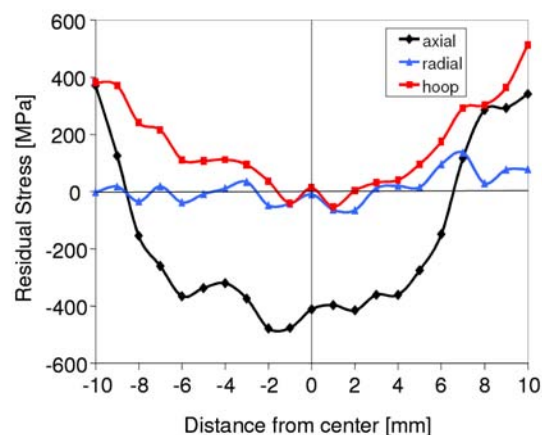


Figure 1: Axial, hoop and radial residual stresses plotted against the distance from the central axis of the bar (drawn with a die angle of 20°)

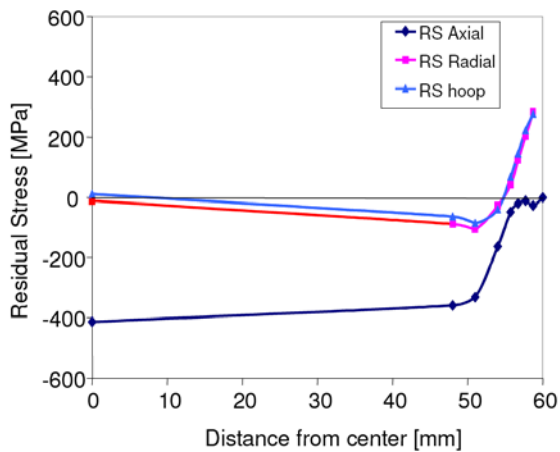


Figure 2: Axial, hoop and radial residual stresses plotted against the distance from the central plane of the bar (drawn with a die angle of 20°)

Figure gives an image of the significant change of the residual stress state near the end of the bar. The values of the middle plane of the bar are taken from figure 1. The axial residual stresses approach a zero value as required from mechanics. The decrease of the axial residual stresses at the end of the cylindrical bar rearranges hoop and radial residual stresses to high tensile values. It is assumed that this behaviour will contribute to distortions of the bar during the following surface heat treatment.

4 Consequences

The results will be published in the near future. The next experiments will be extended to other steps of the shaft manufacturing route including induction hardening of the cylinders.

5 References

[Bue58] Bühler, H., Altmeyer, G.: Der Einfluss des Nachziehens und des Richtens auf die Eigenspannungen in Stahldrähten, Stahl und Eisen, 7 (1958), S. 1822-1827

[Bue65] Bühler, H., Lehmann, T., Schmitt, F. J.: Untersuchungen über die dimensionsanalytische Berechnung von Eigenspannungen in gezogenen Stäben, Archiv für das Eisenhüttenwesen, 36 (1965), S. 29 – 34

[Nak01] Akikazu Nakagiri, Takaaki Yamano, Masazumi Konaka, Motoo Asakawa, Wataru Sasaki and Kazunari Yoshida. Behavior of residual stress and drawing stress in conical-type die and circle-type die drawing by FEM simulation and experiment. Wire Journal International 34 no8 August 2001 p. 73

Principal Proposer: Robert C. Wimpory, HZB
Experimental Team: Robert C. Wimpory, HZB

Date(s) of Experiment

07.04.2009-09.04.2009
20.04.2009-26.04.2009

Date of report: 18.01.2010

Within Task Group 4 (TG4) of the European Network on Neutron Techniques standardization for Structural Integrity (NeT) [1], residual stress determinations by neutron diffraction were determined on a 3-pass slot weld made from AISI 316 austenitic stainless steel as part of a round robin exercise (dimensions 18x150x194 mm³). By following a pre-defined protocol, residual stress distributions were evaluated in the plate. A 3x3x3mm³ gauge volume was used with a continuous omega motion of +/- 5 degrees in order to smooth out grain size effects. For the residual stress determination a large number of measurement locations have been suggested. Variations of the stress free reference parameter in the fusion zone and the heat-affected zone were taken into account from coupons that were taken one of the welded specimens.

Figures 1 and 2 show the results for a line 2mm and 9mm below the surface of the weld plate directly through the weld and underneath the weld respectively. Figure 3 shows the repeatability of the experimental measurement along a line through thickness.

The residual stress determinations will provide an important basis for understanding the nature of cyclic hardening in multipass austenitic stainless steel. It is considered that the modest increase in the number of weld passes will still allow the modelling community to give full appreciation to the geometry of the problem in performing full 3-dimensional analyses of the welding process.

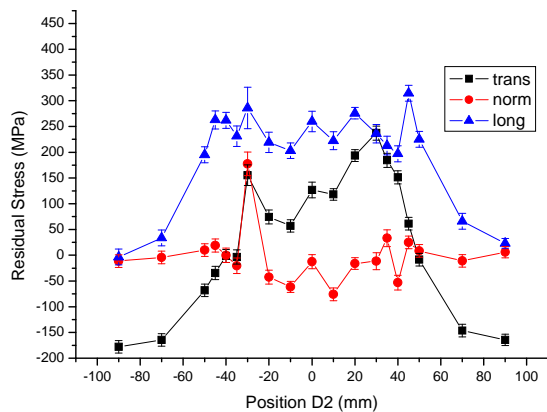


Figure 1. Weld transverse, longitudinal and normal 2mm below the surface of the plate.

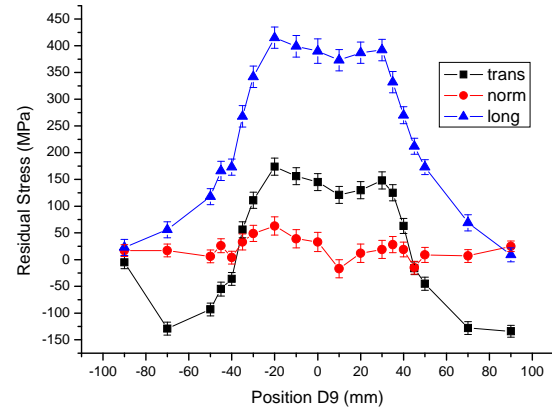


Figure 2. Weld transverse, longitudinal and normal 9mm below the surface of the plate.

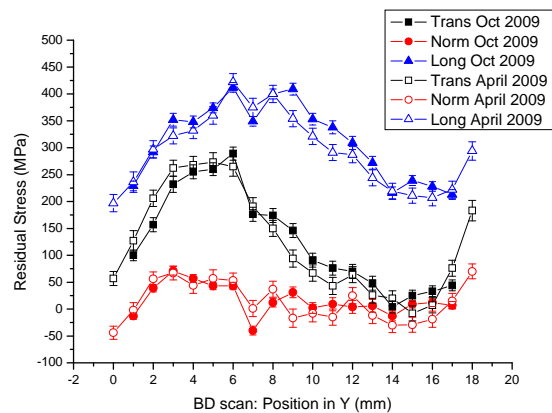


Figure 3. Weld transverse, longitudinal and normal along a line through thickness

References

[1] Ohms, C., Martins, R.V., Uca, O., Youtsos, A.G., Bouchard, P.J., Smith, M., Keavey, M., Bate, S.K., Gilles, P., Wimpory, R.C., Edwards, L., The European Network on Neutron Techniques Standardization for Structural Integrity - NeT. In: Proceedings of PVP2008 ASME Pressure Vessels and Piping Division Conference July 27-31, 2008, Chicago, Illinois, USA, 2008.

	EXPERIMENTAL REPORT Structure determination of unpolished Ni-Mn-Ga magnetic shape memory alloy single crystals	Proposal: MAT-01-2673-EF Instrument: E3 Local Contact: R. C. Wimpory
	Principal Proposer: Markus Chmielus, HZB Experimental Team: Markus Chmielus, HZB Rainer Schneider, HZB Robert C. Wimpory, HZB Peter Müllner, Boise State University	Date(s) of Experiment 18.11.2009 - 25.11.2009

Date of report: 19.01.2009

Spark eroding, which is commonly employed to cut samples out of magnetic shape-memory alloy single crystals, produces a rough surface layer. Directly after cutting, the single crystals exhibited a high twinning stress of 10 to 15 MPa measured at Boise State University, ID, USA. After removal of a surface layer through electropolishing, the twinning stress reduced significantly and stress-strain curves became serrated (see fig. 1, inset for serrated flow).

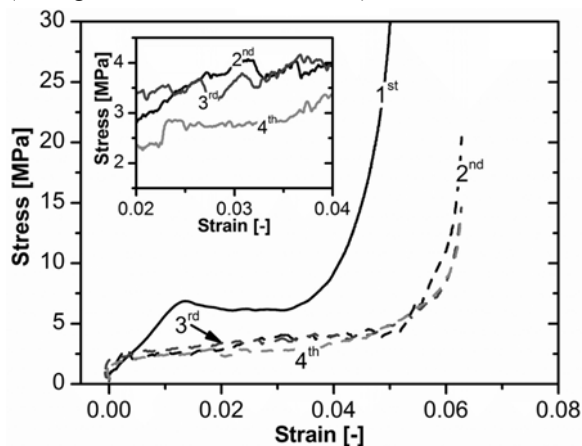


Figure 1: Example for twinning stress reduction of a polished sample due to repeated mechanical deformation. Average twinning stresses decreased from around 12 MPa to 1.5 MPa after four compressions. Inset shows serrated flow of stress-strain curve.

So far, the reduction of twinning stress was attributed to the removal of the defective surface layer. In this work, it is shown that different surface treatments in combination with repeated mechanical deformation experiments significantly reduced the twinning stress, regardless of whether electro polishing is used or not. The reduction of the twinning stress is due to softening that takes place as a mechanical training effect, which occurs with mechanical testing. In addition, the stress-strain curves of samples, which were subjected to different surface treatments, differed in so far as the curves of electropolished samples showed serrated flow while the curves of unpolished samples and those of mechanically polished samples were smooth. Furthermore the unpolished samples displayed significant hardening at higher strain. By subsequent mechanical polishing, this hardening reduced to nearly zero and the average twinning stress decreased another 30-50% to 1.6 MPa and below. For these samples, the

twinning stress stayed at a very low level until twinning was complete.

Initially, structural information was not available for the mechanically tested samples. Therefore, one day of the proposal time was used to determine the lattice parameters and martensite structure of two tested samples. Figure 2 shows an exemplary $hk0$ plane of one sample that showed 8.8% strain (less than 14M, but more than 10M martensite).

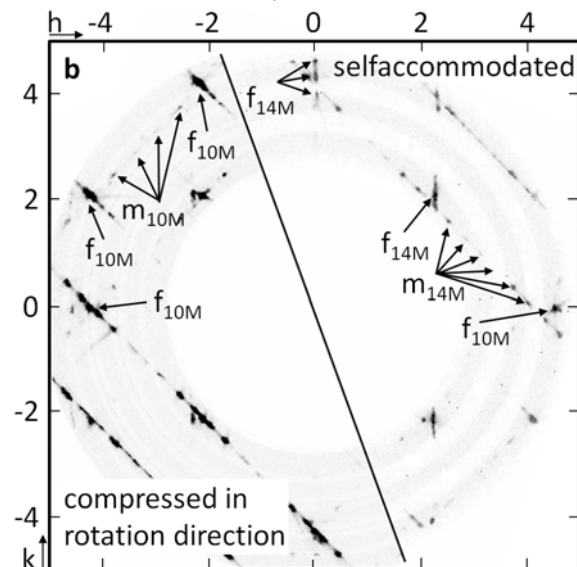


Figure 2: The $hk0$ planes of a sample showing 8.8% strain in a selfaccommodated and compressed state.

Figure 2 shows the $hk0$ plane of sample B3 (b) in the self-accommodated state (top right) and the compressed state (bottom left) state. The number of modulation reflections indicate a mixture of 10M and 14M martensites of sample B3 (6 modulation reflections top right part, 4 in bottom left part, b). Examples for modulation and fundamental reflections are marked with subscript 'm' and 'f'. The 8.8% stress induced strain is a results of the mixture of 10M and 14M martensite. Further results and in depth discussion will be published [1].

References:

- [1] M. Chmielus, K. Rolfs, R. Wimpory, W. Reimers, P. Müllner, R. Schneider, "Effects of surface roughness and training on the twinning stress of Ni□Mn□Ga magnetic shape□memory alloys", to be submitted

	EXPERIMENTAL REPORT In-situ observation of twin structure change during loading and unloading of Ni₂MnGa Magnetic Shape Memory Alloys in a magnetic field	Proposal: MAT-01-2673-EF Instrument: E3 Local Contact: R. C. Wimpory
	Principal Proposer: Markus Chmielus, HZB Experimental Team: Markus Chmielus, HZB Rainer Schneider, HZB Robert C. Wimpory, HZB Peter Müllner, Boise State University	Date(s) of Experiment 18.11.2009 - 25.11.2009

Date of report: 19.01.2009

MSMA with twinned martensite tend to deform in response to an external magnetic field reversibly (elastic), irreversibly (plastic), or as a combination of both. In 1996, the first results of the magnetoplastic effect and MFIS for a Ni₂MnGa Heusler alloy were published [1]. Since then, the interest in MSMA has grown, and large MFIS of around 10% in a rotating magnetic field were published in 2002 [2].

In this experiment, the twinning process via the variation of twin variant volume fraction during mechanical loading with an applied magnetic bias field were observed as well as the orientation and volume fraction of the twins at different loading stages. The original twin configuration (prior to deformation) can be restored (after deformation) with a magnetic bias field [3]. For these experiments, a special sample holder was designed and built. This sample holder contained removable magnets that create an applied magnetic field of about 0.7 T, which is sufficient for magnetic-field-induced twin boundary motion. Additionally, the sample holder allows the compressive deformation of the sample and the measurement of the strain (see Fig. 1). It can be seen in the exemplarily shown *hk0* planes in fig. 2 that not only the volume fraction of the martensite variant is changing according to the deformation state, but also that the martensite modulation is only

occurring in the plane perpendicular to the compression direction. In the left column (fig. 2, sample short in *z*-direction), the modulation is only visible in the plane perpendicular to the *z*-direction, while in the right column (sample short in *y*-direction) the martensite modulation is only visible in the plane perpendicular to the *y*-axis. In the intermediate state, modulations are visible in both planes. After this, the sample was also deformed to an intermediate state in *x*- and then *z*-direction (not shown here), which resulted in modulations around the *y*- and *x*-axis, and around all three axis, respectively.



Figure 1: Sample compression stage with possibility of applying a magnetic field of 0.7 T and measuring deformations with an accuracy of 0.01 mm without applying torsion on the sample.

References:

- [1] K. Ullakko et al., Appl Phys Lett, 69(13), 1966-1968 (1996)
- [2] A. Sozinov, Appl Phys Lett, 80(10), 1746-1748 (2002)
- [3] M. Chmielus et al., ICOMAT 2008 Conference Proceedings, TMS, accepted

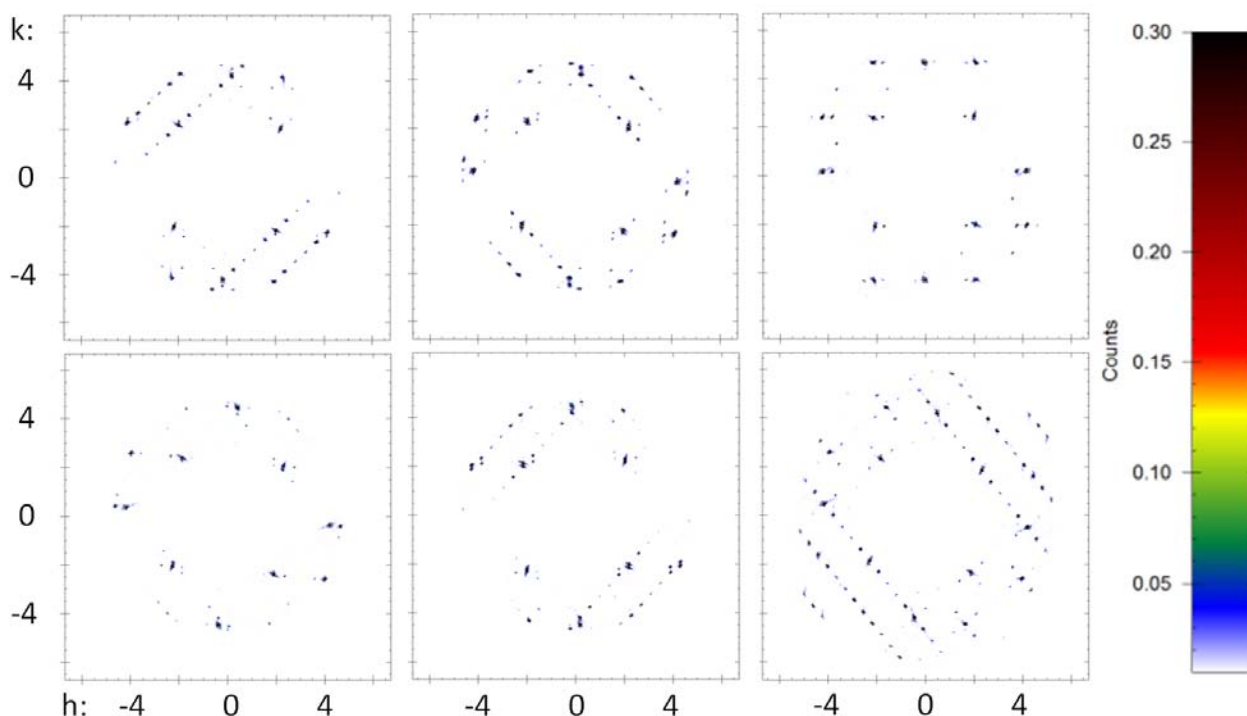


Figure 2: *hk0* planes of different deformation states and different diffraction planes of a 10M Ni-Mn-Ga single crystal. The top row are the *hk0* planes measured while rotating around the *z*-axis, the bottom row while rotating around the *y*-axis; the left column while short in *z*-direction, the right while long in *z*-direction and the middle column in an intermediate state.

Principal Proposer: Majid Farajian-Sohi, TU Braunschweig
Experimental Team: Majid Farajian-Sohi, TU Braunschweig
Robert C. Wimpory, HZB

Date(s) of Experiment

25.11.2009 – 29.11.2009
07.12.2009 – 13.12.2009

Date of report: 20.01.2010

Based on the X-ray diffraction technique, the residual stress measurements had been accomplished by a middle point free 8 axis diffractometer at the institute of joining and welding in the University of Braunschweig. By this technique the residual stress can be measured at the surface layer with a depth of 20 μ but surface residual stress profile is not representative for the whole residual stress field and in order to achieve fatigue resistant welded structures, it is necessary to gain a better understanding of the whole residual stress field and its behaviour under mechanical loadings.

In series of experiments at the Helmholtz Centre Berlin the initial residual stress field in welded P460NL, S960QL and S1100QL steel specimens were measured. The neutron strain scanner instrument E3 at the Helmholtz Centre Berlin uses a double focussing Si (400) monochromator, the resultant wavelength of the neutrons is 0.1486nm. For the sample the {211} ferritic peak was used for all measurements, resulting in a scattering angle of approximately 78.8 degrees in 2theta. A gauge volume of 2 x 2 x 2 mm³ was used and this was kept as far away as possible from the surface in case of potential surface effects.

The specimens were positioned to permit determination of stresses in the three orthogonal directions of the welds. These directions were assumed to be the principal stress directions being coincident with the direction of welding (longitudinal), transverse and normal to the welding. Specimen alignment in all movement directions was done by neutron intensity scanning and alignment with a theodolite. The reference diffraction angles were obtained from comb specimens which were made by electrical discharge machining. For these reference measurements, the same instrument set-up was used as for the actual stress determinations in the plate, including the size of the gauge volume.

The welding residual stress distributions in transverse and longitudinal directions are presented in figures 1a and b. The distribution profile on the surface consists of residual stress measurement on 15 specimens by means of x-ray diffraction. The mean value is shown in black and the scatter bands are drawn with dashed lines.

The in-depth neutron diffraction measurements in figure 1 represents also the transverse and longitudinal residual stresses at a distance of 1.7, 3 and 4.3mm from the surface. In the transverse direction the peak in the weld seam disappears, penetrating into the material and compressive residual stresses appears. The compressive residual stresses in the vicinity of the weld toe on the surface on the other hand changes sign and become tensile in deeper layers of the sample. In the longitudinal

direction the tensile peak in the weld seam changes its sign to negative values in deeper layers. In contrast the longitudinal peaks in the vicinity of weld toe not only remains through thickness but also increase in value to 600-700MPa compared with 300-400MPa on the surface.

Further investigation of the residual stress field and its behaviour in depths of up to 1 or 2 mm is required to explain the drastic disappearance of transverse residual stress peaks in deeper layers. A technique suitable for such measurements could be synchrotron diffractometry.

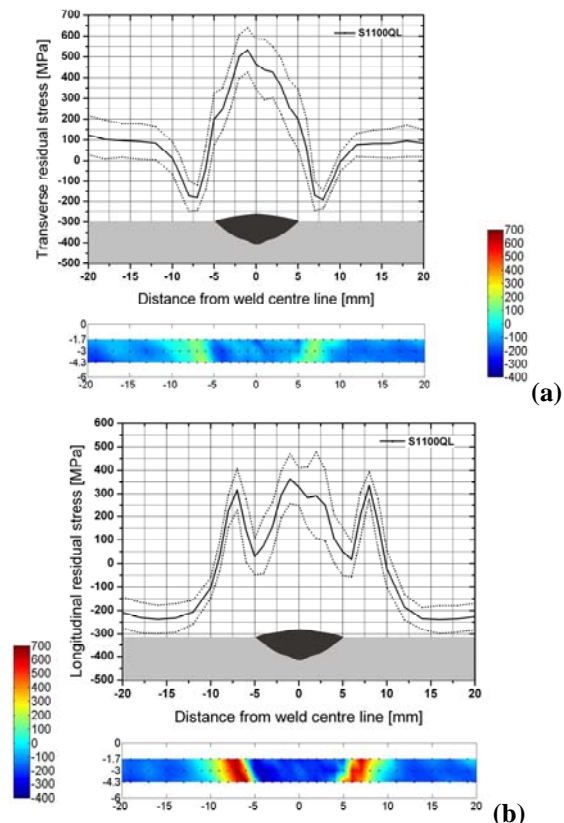


Figure 1. Residual stress distribution in S1100QL specimens; a) Transverse, b) Longitudinal

The results of the performed experiments at Helmholtz centre Berlin are part of a paper titled: "Relaxation and Stability of Welding Residual Stresses in High Strength Steel under Mechanical Loading" by M. Farajian-Sohi, Robert C. Wimpory and Th. Nitschke-Pagel. The paper is finished and will be submitted to the Journal of Science and Technology of Welding and Joining by the end of January 2010.

	EXPERIMENTAL REPORT	Proposal: MAT-01-2678
	Minimisation of spurious strains in neutron strain scanning at the surface	Instrument: E3 Local Contact: R. C. Wimpory
Principal Proposer: Experimental Team:	M. Hofmann, TU München, FRM II R. C. Wimpory, HZB M. Hofmann, TU München, FRM II J. Gibmeier, TU Karlsruhe	Date(s) of Experiment 21.09.2009 – 28.09.2009

Date of report: 03.02.2010

Two nominal identical ferritic steel samples (dimensions 50 mmx50 mm x10 mm) were investigated at the residual stress instrument E3 to study the stress profile induced by shot peening.

These samples have been used to benchmark the capabilities of neutron diffraction measurements of steep stress gradients close to surfaces as it is well known that neutron diffraction experiments to determine residual stresses are critical at the surface. Pseudo peak shifts arise when the gauge volume is not completely filled by material and, hence, the centre of the gauge volume does not coincide with the centre of the irradiated material. These aberration peak shifts can be of the same order as the peak shifts related to residual strains [1].

In this experiment we used the advantageous setup of E3 which allows surface measurements with a properly adjusted Si-monochromator [2]. This was checked during the experiment using a stress free specimen as a d0 reference and calibration sample. A nominal gauge volume size of 1x10x1 mm³ was used and the slits were brought as close as possible to the sample surface (< 20 mm) to avoid peak clipping effects and blurring of the gauge volume. The measurements were performed in the centre position of the specimens through the complete thickness of the samples. Close to the surface the step size was 0.1 mm. The step size was increased to 0.2 mm after the gauge volume was fully immersed in the sample.

Figure 1 shows the resulting stress profile (stress direction s_{xx}) after adjusting the translator (motor) position to the correct centroid position of the gauge volume in the sample. Comparison of the results to averaged stress values obtained from a round robin campaign using layer removal and X-Ray diffraction [3] shows excellent agreement. The stresses close to the surface (< 200 μm) are at

the same level of around ~ 650 MPa as determined by X-Ray diffraction. Going deeper into the sample it was not possible to pick up the steep stress gradient at about ~ 250 -300 μm due to the averaging effect of the relative large gauge volume used in the neutron diffraction experiment. Work is currently underway to deconvolute the overlapping gauge volume information. Below about 1 mm of the surface we find a stress balancing tensile stress of about 80 MPa which is constant across the inside of the sample.

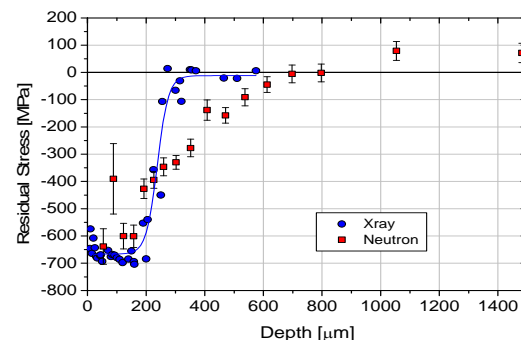


Figure 1. Residual stress profile of a shot peened ferritic steel sample as determined by neutron diffraction on E3 (red symbols). For comparison the averaged results from a round robin campaign using X-Ray diffraction [3] is also given (blue).

[1] P.J. Webster, G. Mills, X.D. Wang, W.P.Kang and T.M. Holden, *J. Neutron Research* **3** (1995) pp. 223, 1995

[2] R.C. Wimpory, NET-Meeting 2008, Petten, Netherlands

[3] J. Gibmeier, J. Lu and B. Scholtes, *Mat. Sci. Forum* **404-407** (2002) 659

Principal Proposer: Catrin M. Davies, Imperial College London
Experimental Team: Catrin M. Davies, Imperial College London
Robert C. Wimpory, HZB

Date(s) of Experiment

14.12.2009 – 22.12.2009

Date of report: 10.01.2010

The aim of the experiment is to examine the influence of welding parameters, including the weld tool traversal speed, v , and rotation speed, ω , on the residual stress distributions in butt welded AA2024 aluminium alloy plates joined by the friction stir welding (FSW) process. Four plates with a controlled range of ω and v , details of which are given in Table 1 were measured across the weld line at the welds mid length and thickness in three mutually orthogonal directions.

Table 1 : Details of the plates' welding speeds

Plate Name	v (mm/min)	ω (rpm)
FSW2	150	750
FSW3	350	750
FSW5	150	1200
FSW7	150	475

A gauge volume on $2 \times 2 \times 2 \text{ mm}^3$ was used. Since the manufacture of a reference comb is destructive, plane stress assumptions have been employed and hence the strain free lattice parameter, unique to each position, is chosen that give zero stress in the through thickness direction. This assumption has been justified through preliminary finite element studies.

Note from Table 1 that the value of ω is common between plates FSW2 and FSW3 and v is common between plates FSW2, FSW5 and FSW7 to enable the relative influences of ω and v to be determined in addition to the ratio of both velocities, $v/\omega r$ where r is the tool radius. The longitudinal stresses exhibited in plate FSW7 are higher than that of FSW5 within the weld region which extends approx. $\pm 10 \text{ mm}$ from the weld centreline, this is due to the higher energy input per unit length of material in plate FSW7.

The results shown in Figure 1 confirms that over doubling v results in a reduction of approx. 40 MPa in the peak stress, due to the reduced heat input per unit length of weld. The 60% increase in ω between plates 2 and 3, shown in Fig. 2, results in a peak increase of approx. 25 MPa. The widths of the high tensile zones are consistent in each case. The peak stress occur approx 10 mm from the weld centre i.e. in the heat affected zone (HAZ).

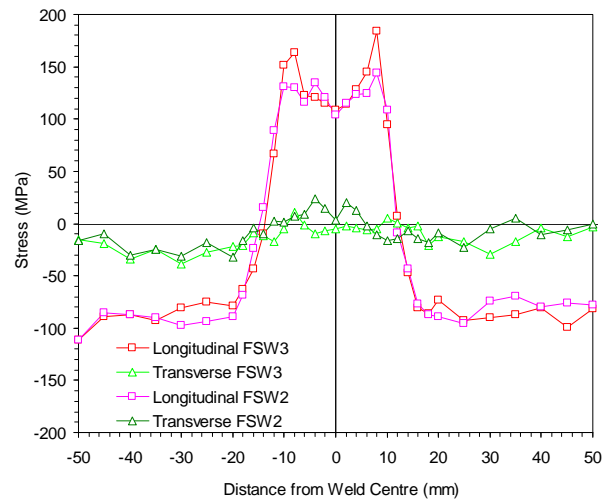


Figure 1: Influence of tool traversal speeds on the residual stress distributions

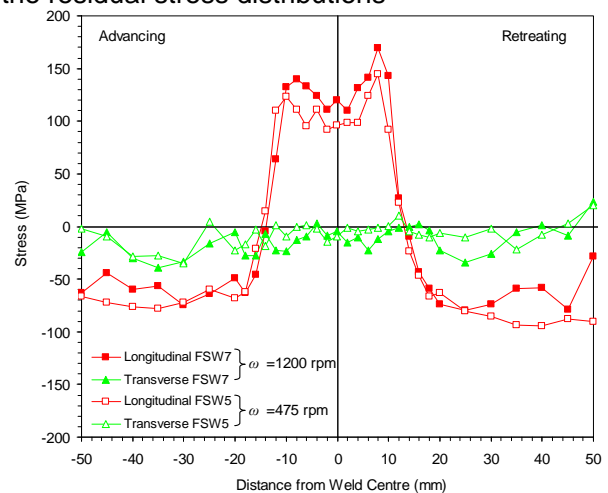


Figure 2: Influence of tool rotational speeds on the residual stress distributions

Metallographic studies will reveal the microstructural changes that have taken place on both the advancing and retreating side, that have influenced the residual stress distributions observed. The results are to be used to develop and validate finite element simulations of the FSW processes, which can then be used to examine a wide range of welding conditions.

Acknowledgement:

This research project has been supported by the European Commission under the 7th Framework Programme through "Research Infrastructures" action of the "Capacities" Programme, contract number CP-CSA_INFRA-2008-1.1.1. Number 226507-NMI3.

	EXPERIMENTAL REPORT Influence of residual stress and precipitation on the lattice parameter of aluminium alloy Jominy end quench samples	Proposal: MAT-01-2680 Instrument: E3 Local Contact: R. C. Wimpory
	Principal Proposer: J.S. Robinson, University of Limerick, Ireland Experimental Team: J.S. Robinson, University of Limerick, Ireland R. C. Wimpory, HZB	Date(s) of Experiment 12.10.2009 – 20.10.2009

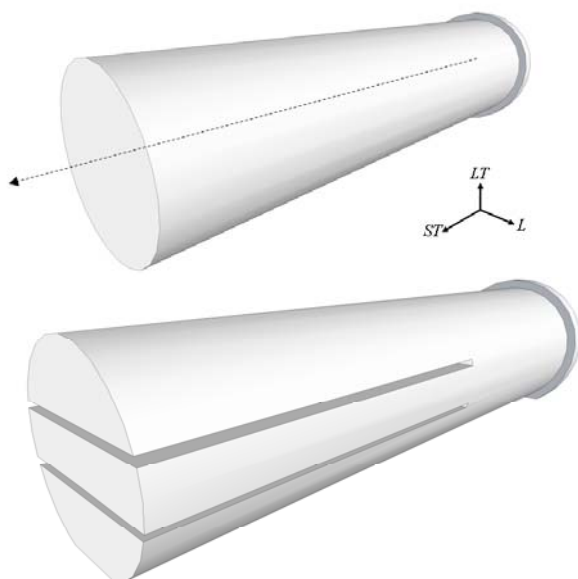
Date of report: 29.01.2010

Eleven aluminium alloy Jominy end quench samples were examined on the E3 instrument at the HZB between the 12th and the 20th of October 2009. The alloys examined were 7449, 5083, 2014A, 7075, high purity Aluminium and a special 7475 "calibration" sample.

The lattice parameter variation along the long axis of the samples in three orthogonal directions was measured, (see figure below). The {311} aluminium matrix peak was used for all measurements. A gauge volume of approximately $3 \times 3 \times 3 \text{ mm}^3$ was used for all measurements as it was found this volume gave an acceptable diffraction peak in a reasonable length of time (~800-1400 seconds).

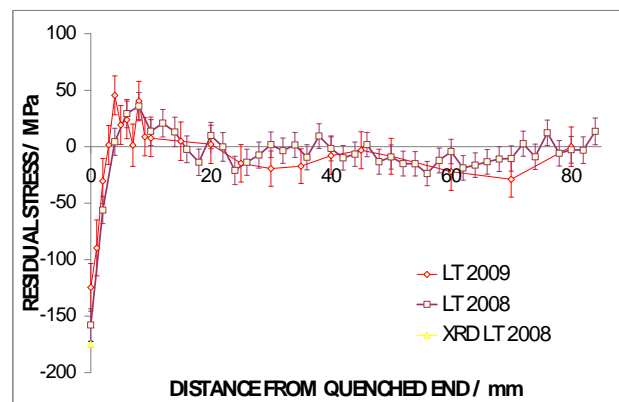
Two Jominy end quench samples had been manufactured from each alloy and one of these had been cut as shown in the figure below to act as a dzero sample. This will enable the decoupling of the influence of cooling rate induced precipitation and actual residual stress on the lattice parameter.

7449 (J4)



All measurements were analysed and converted to strains and stresses at the HZB during the 7 days of beam time. There were no problems with hardware or software and the experiment was successful. It is anticipated these data will be incorporated into a journal papers to be submitted in 2010.

Some preliminary results are shown below and compared to a x-ray residual stress measurement made on the exposed end face. The agreement is good for this alloy (7449) because it is not quench sensitive but when the 7075 alloy is examined it is expected to show poor agreement and will require the influence of precipitation to be accounted for which is now possible with the data collected on E3.



Acknowledgement

This research project has been supported by the European Commission under the 7th Framework Programme through "Research Infrastructures" action of the "Capacities" Programme, contract number CP-CSA_INFRA-2008-1.1.1. Number 226507-NMI.

	EXPERIMENTAL REPORT Measurement of axial residual stresses in a section of a bi-metallic piping weld	Proposal: MAT-01-2682 Instrument: E3 Local Contact: R. C. Wimpory
	Principal Proposer: Carsten Ohms, JRC Petten, NL Experimental Team: Carsten Ohms, JRC Petten, NL Robert C. Wimpory, HZB	Date(s) of Experiment 16.08.2009 - 23.08.2009

Date of report: 29.01.2010

In the context of the projects ADIMEW and NESC III [1,2] residual stresses had been investigated in a bi-metallic piping weld of substantial dimensions by neutron diffraction at the HFR in Petten, NL, and by numerical analysis executed at different laboratories. The specimen under investigation here was representative of a nuclear application. The background then was also to use residual stress data as input in a failure analysis. While the previous measurements then gave a relative idea of the strains/stresses in the circumferential direction because of a favourable (100)-texture in this direction, the measurements in the piping axial and radial directions were of substantially less quality due to grain size effects and a less favourable texture. Unfortunately the axial stresses would have been most interesting as input for the failure analysis. Because of the significant need of material for the materials characterization programmes within the ADIMEW and NESC-III projects not even a small piece of material could be retained for further investigations. This companion specimen from the project that was not completely identical to the original specimen, but nevertheless quite similar, has been detected from which slices could be extracted for new residual stress measurements. These slices are sufficiently large to retain a substantial portion of the axial stresses. It is thus the purpose of the proposed experiment to investigate the residual stresses mainly in the piping axial direction with a much higher resolution than possible with the original specimen.

The specimen investigated was a 6 mm slice from a bi-metallic, ferritic to austenitic steel, piping weld with 52 mm wall thickness. The slice is about 200 mm long, which is the dimension in the axial direction; thus the axial welding stresses are expected to be retained in this specimen. In the circumferential direction only 6 mm thickness are retained; therefore no circumferential stresses are expected to be present. Fig. 1 depicts a macrograph of the specimen. In addition to the specimen itself there were reference coupons for determination of the variation of the reference parameter.



Figure 1 Macrograph of bi-metallic piping weld for investigations.

The specimen was measured with emphasis on the axial stresses with a relatively high density of measurement locations, in particular near the internal interfaces. A sampling volume of 2x2x2 mm was used using the 211 hkl reflection for the ferritic part of the weld and the 311 hkl reflection for the austenite part of the weld. The feature for specimen rocking at E3 was particularly important for dealing with grain size issues in the fusion zones and the austenitic steel.

Data analysis is still on going but some preliminary results can be shown here. The graph in figure 1 shows the residual stress along the well interface in the axial direction. The distribution was force balanced (+38MPa) which was within the typical uncertainty of 40 MPa. 0mm represents the top of the weld.

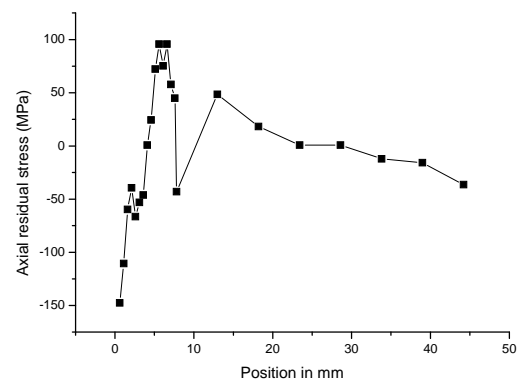


Figure 2. Axial Residual stress along Fe/weld interface

References: N. Taylor, C. Faigy, P. Gilles, (eds.), "Assessment of Dissimilar Weld Integrity: Final Report of the NESC-III Project", European Commission, Directorate General Joint Research Centre, Institute for Energy, Petten, The Netherlands, EUR 22510 EN, ISSN 1018-5593, European Communities, Luxembourg, 2006
 C. Ohms et al. "ADIMEW - Assessment of aged piping DIssimilar MEtal Weld integrity, Contract FIKS-CT-2000-00047, Work Package 3, Deliverable D3.1-a: Report on Residual Stress Measurements", Project report, Nov 2003

Acknowledgment:

This research project has been supported by the European Commission under the 7th Framework Programme through "Research Infrastructures" action of the "Capacities" Programme, contract number CP-CSA_INFRA-2008-1.1.1. Number 226507-NMI

	EXPERIMENTAL REPORT Influence of shifting Mn/Ga-ratio on martensite structure in Ni-Mn-Ga alloyed with 0.6% Cobalt	Proposal: MAT-01-2811-EF Instrument: E3 Local Contact: R. C. Wimpory
	Principal Proposer: Katharina Rolfs, HZB Experimental Team: Katharina Rolfs, HZB	Date(s) of Experiment 09.11.2009 – 17.11.2009

Date of report: 18.01.2010

Magnetic Shape-Memory Alloys (MSMAs) can potentially substitute giant magnetostrictive materials as well as piezoelectrical ceramics in actuating devices due to their large magnetic-field-induced strains. One of the most promising materials in this field is Ni-Mn-Ga. However applications are still limited by the relatively low structural phase transition from the martensite to the austenite and the high brittleness impedes long-term application. To improve those properties, Ni-Mn-Ga has been alloyed with cobalt.

For the experiment a single crystalline rod with a length of 80mm and a diameter of 16mm and the nominal composition $\text{Ni}_{49.2}\text{Co}_{0.8}\text{Mn}_{28.4}\text{Ga}_{21.6}$ was grown by the Bridgman like technique called SLARE [1]. Due to a segregation during the growth process, the composition changes along the growth axis. To determine the influence of the composition on the structure, 7 samples were cut out of different positions of the crystal rod and their structures were measured at room temperature. Therefore the (6 x 5 x 4) mm samples were orientated and the hk0- and h0k-plane were measured by 180° omega scans in a 2 theta range of 47-90°.

Independent from the deviation in the composition (see Table 1), all samples showed a tetragonal modulated structure (called 5M structure) at room temperature (see Fig.1).

Mn/Ga	a [Å]	b [Å]	c [Å]	V [Å ³]
1.067	5.934	5.934	5.588	195.78
1.072	5.953	5.953	5.578	197.99
1.112	5.953	5.953	5.576	197.57
1.139	5.953	5.953	5.576	197.57
1.188	5.953	5.953	5.580	197.74
1.199	5.986	5.986	5.576	199.80

Table 1: Mn/Ga – ratio and the determined cell parameter and volumes of the cut out 6 x 5 x 4 mm Ni-Cio-Mn-Ga - samples

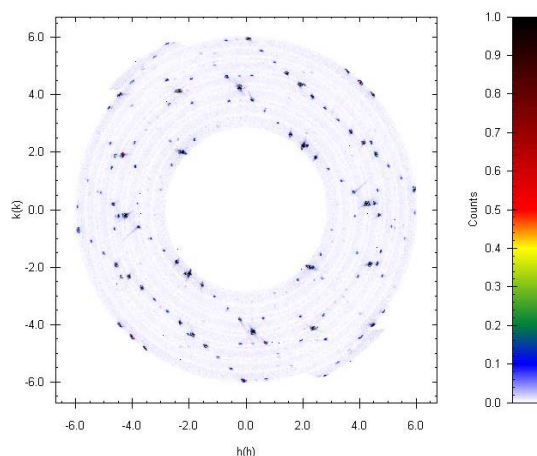


Figure 1: hk0-plane of Ni-Co-Mn-Ga with a Mn/Ga – ratio of 1.067.

By determining the lattice parameters of the samples it was observed, that the long lattice parameters a and b slightly increase with increasing Mn/Ga – ratio, while the short axis c lightly decreases with the increasing amount of manganese. As a result, the cell volume of Ni-Co-Mn-Ga increases with an increasing Mn/Ga – ratio. This can be explained by the increasing Mn – content, which has a bigger radius than gallium and therefore leads to a bigger unit cell size.

The author appreciates the support of this work by grants of the Deutsche Forschungsgemeinschaft (SPP1239, grant No. Schn 1106/1).

[1] A.Mecklenburg, S.Fiechter, H.-P-Nabein, R.Schneider, DE102004018664A1 (2005).

	EXPERIMENTAL REPORT Gas solid synthesis of LiBD₄ by borane absorption of LiD	Proposal: MAT-01-2630 Instrument: E6 Local Contact: Andreas Hoser
	Principal Proposer: Arndt Remhof, EMPA Experimental Team: Arndt Remhof, EMPA Oliver Friedrichs, EMPA Dirk Wallacher, HZB	Date(s) of Experiment 15.09.2009 – 23.09.2009

Date of report: 27.10.2009

LiBH₄ with a gravimetric hydrogen density of 18.4 mass% represents a promising material for hydrogen storage applications [1]. Previously we demonstrated a solvent free synthesis, by starting the LiBH₄ formation from the elements or from the reaction of binary boron compounds such as LiB or AlB₂ with LiH in applied H atmosphere. Thereby neutron powder diffraction (NPD) served as a valuable tool to understand the reaction mechanism [2-5]. Recently we have shown the synthesis of LiBH₄ by solid gas reaction between LiH and B₂H₆ at 120°C and ambient pressures [6]. The reaction is supposed to follow $2\text{LiH} + \text{B}_2\text{H}_6 \rightarrow 2\text{LiBH}_4$. Details of the reaction, the role of intermediates and unwanted by-products such as Li₂B₁₂H₁₂ are still unknown.

In the present experiment we examined the reaction of LiD with B₂D₆ by in-situ neutron diffraction. The borane was provided from an internal source, as depicted in Figure 1. Thereby, a custom made stainless steel sample container, developed by the HZB's DEGAS laboratory was utilized.

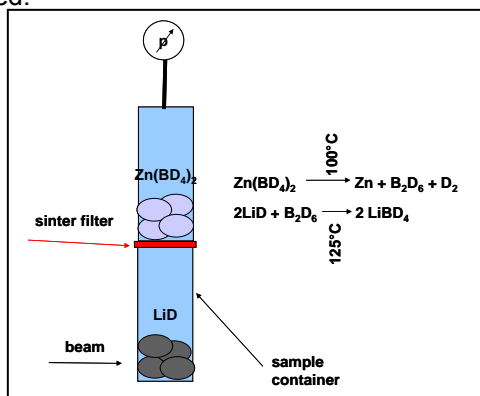


Fig. 1: Experimental set-up

The borane emission is accomplished by using solid LiZn₂(BH₄)₅ as borane source. By heating the source to 100°C the borane is rapidly released according to the following reaction: $\text{Zn}(\text{BH}_4)_2 \rightarrow \text{Zn} + \text{B}_2\text{H}_6 \uparrow + \text{H}_2 \uparrow$. During the experiment, the diffraction pattern of the LiD containing part of the container was recorded consecutively. We first heated the sample container to 100°C. Already at this temperature, the diborane released from the source reacts with LiD to form LiBD₄, as the corresponding Bragg reflections can clearly be identified. However, the reaction stops after several hours and only a small amount of LiBD₄ has

formed. Then the temperature was increased stepwise to 200°C. The reaction continues until about 50% of the LiD has been converted to LiBD₄. We attribute this incomplete reaction to the formation of a LiBD₄ passivation layer around the grains, acting as a barrier for the borane.

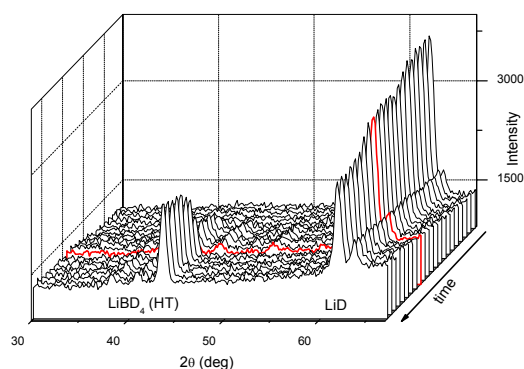


Figure 2: In situ recorded neutron powder diffractograms. The red measurement marks the moment the temperature was increased.

The measurement clearly shows that the reaction follows the proposed route: LiBD₄ forms from LiD and B₂H₆ in a gas solid reaction at moderate temperatures and pressures. No intermediate products were observed.

References:

- [1] A. Züttel, et al., Scripta Mat., **56** 823 (2007); and references therein.
- [2] O. Friedrichs et al., Acta Mater. **56** 949 (2008)
- [3] A. Remhof, et al., Phys. Chem. Chem. Phys. **38** 5859 (2008) and BENSC Exp. Report MAT-01-2169-EF.
- [4] O. Friedrichs et al., Phys. Chem. Chem. Phys. **11** 1515 (2009).
- [5] A. Remhof et al., J. Alloys Compd. **484** 654 (2009) and BENSC Exp. Report MAT-01-2395.
- [6] O. Friedrichs et al., Chemistry Europ. J., **15** 5531 (2009).

Acknowledgement

This research project has been supported by the European Commission under the 7th Framework Programme through "Research Infrastructures" action of the "Capacities" Programme, contract number CP-CSA_INFRA-2008-1.1.1. Number 226507-NMI

	EXPERIMENTAL REPORT Residual strain-stress in anisotropic cold-rolled Zr-alloy	Proposal: MAT-01-2504 Instrument: E7 Local Contact: R. C. Wimpory
	Principal Proposer: V. Sumin, JINR, Russia Experimental Team: R. C. Wimpory, HZB V. Sumin, JINR, Russia A. Venter, NECSA, RSA	Date(s) of Experiment 12.05.2009 – 19.05.2009

Date of report: 25.01.2010

We continue to gather experimental data about strains in high textured Zr-rod (see report MAT-01-2266, 2008).

To use the geometric mean approach [1] we need carry out strain measurements of Zr-rod in the some part of the cylindrical samples. We choose the $5 \times 5 \times 5 \text{ mm}^3$ in center of 10 mm cylinders in diameter. For this purpose the gauge volume on E3 spectrometer was restricted by $5 \times 5 \times 5 \text{ mm}^3$. In last measurements the samples were inside the neutron beam with dimensions $11 \times 11 \text{ mm}^2$ which is greater than sample sizes.

Zr-alloys with strong texture need this method. As estimated earlier, Zr-samples have cylindrical symmetry of texture. The determination of strain tensor requires measuring only azimuthal dependence of $d_{hkl} - d_{hkl}(\gamma)$. Measurements were performed on E7 spectrometer

Two studied samples have had difference in preceding handling: one (number 0) was only cold worked, another (number 1) underwent annealing at 600 °C after cold working. Measurements were carried out by revolving the sample in the plane of diffraction vector with the step of 10 degrees. Range of displacement came to 90 degrees: from the position where diffraction vector and axis of texture are parallel (0°) to the position where they are perpendicular.

Annealed Zr1 and cold worked Zr0 samples showed quite different behavior in $d_{hkl}(\gamma)$ for all studied planes. See, for example, (100) and (101) (Fig. 1,2). Data differ from previous data, MAT-01-2266,2008.

[1] S.Matthies, H.G.Priesmeyer and M.R.Daymond. Appl. Cryst. (2001) v.34, pp.585-601

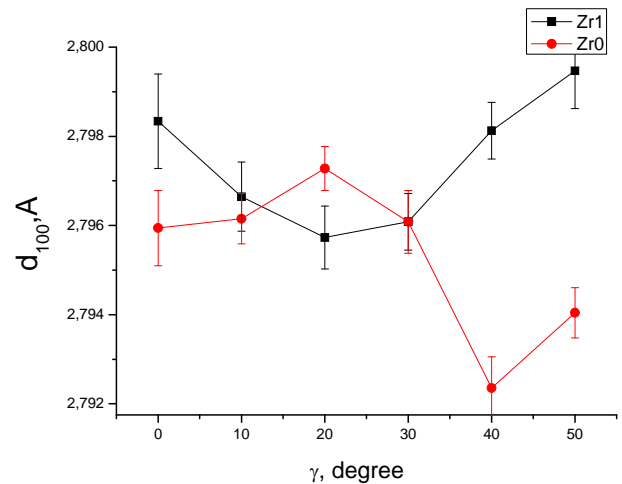


Fig.1 $d_{hkl}(\gamma)$ dependence for (100) plane

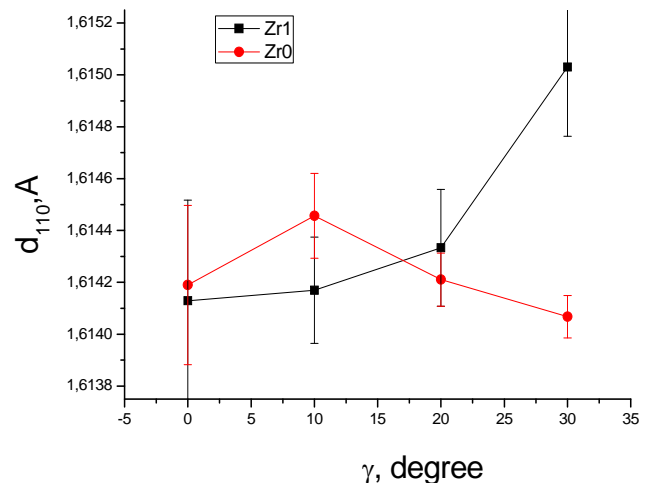


Fig.2 $d_{hkl}(\gamma)$ dependence for (110) plane

	EXPERIMENTAL REPORT Microscopic change of carbon aerogel EDLC electrodes during charging	Proposal: MAT-01-2658 Instrument: V1 Local Contact: Th. Hauß A. Buchsteiner
	Principal Proposer: Volker Lormann, ZAE Bayern Experimental Team: Gudrun Reichenauer, ZAE Bayern Matthias Wiener, ZAE Bayern Christian Scherdel, ZAE Bayern Thomas Hauß, HZB Alexandra Buchsteiner, HZB	Date(s) of Experiment 26.10.2009 – 29.10.2009

Date of report: 02.03.2010

The power density of electrochemical double layer capacitors (EDLC's) is limited by the electrical resistance at the interface between capacitor and current collector as well as by the accessibility of ions to the microscopic electrolyte/electrode interface. The latter is governed by constraints on the microscopic scale such as the mouth of the micropores (diameter < 2nm).

Charge separation can induce structural relaxation as a result of the change of interfacial energy upon formation of the electrochemical double layer. The objective of the proposed experiment was to extract information on the accessibility and microscopic changes upon charging of EDLC's. The measurements were performed in a cell equipped with glass windows and aluminium current collectors. Aluminium is used as current collectors, because it is nearly transparent for the neutrons. The test cell (Fig. 1) was later on filled with 1M KCl electrolyte solution in a mixture of H₂O and D₂O with an effective coherent scattering length density of zero ("zero matched" water); the initially planned electrolyte (1M H₂SO₄) could not be used since it is corrosive in contact with aluminium.

The scattering curve of the carbon electrode shows a pronounced shoulder between 0.1 and 0.5 nm⁻¹ (Fig.2 a)). Unfortunately only a minor part of the shoulder is actually due to scattering from the carbon micropores; it is the latter contribution that would reflect the changes with relaxation processes. Analyzing the empty beam in detail, we found that this signal changes with time so that it seems impossible to correct the signal of the test cell with carbon electrode reliably for the blank cell containing large contributions of empty beam scattering.

When adding "zero matched" water to the test cell with the carbon electrode we found that the contribution due to the incoherent scattering background of the "zero matched" water is very high and thus masks the coherent scattering of the micropore signal. Part of this high incoherent contribution can be reduced by minimizing the water filled space between the carbon and the aluminum electrodes and by increasing the density of the carbon electrode in the synthesis step.

Fig.2 b shows the scattering curves of the EDLC electrode filled with 1M KCl electrolyte at different voltages applied.

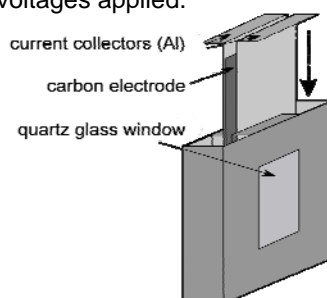


Fig. 1: Scheme of electrochemical test cell.

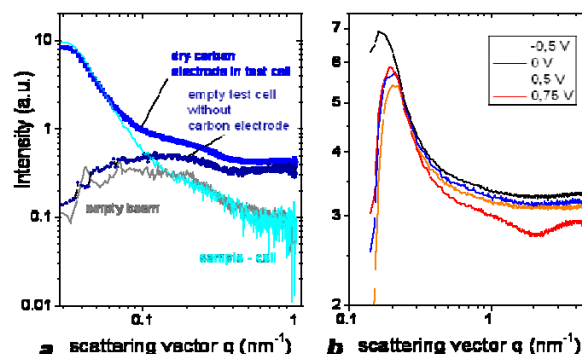


Fig. 2: Double log plot of the scattering intensity / vs. the scattering vector q . (a) empty beam, test cell without carbon, carbon electrode only and carbon electrode in test cell with „zero matched“ water. (b) Scattering for differently charged EDLC electrodes.

Again, no pronounced micropore signal is visible. However, a systematic change in the scattering pattern with the voltage applied is evident, that in part is due to the ions being separated in the charged state and located at the carbon / pore interface. However, due to the shoulder in the empty beam and test cell scattering a detailed evaluation of the scattering curves is not possible.

The measurements performed should therefore be repeated on another beam line (e.g. V7) that provides a stable and q-independent background signal; for future experiments based on the measurements performed an optimized test cell and carbon electrode can be provided

The experiment PHY-01-2659 was cancelled due to the shortage of beam time and a low S/N-ratio. The released experimental time was used for detailed investigations with respect to MAT-01-2658 instead.

 HELMHOLTZ ZENTRUM BERLIN für Materialien und Energie NEUTRONS	EXPERIMENTAL REPORT	Proposal: MAT-04-1645 Instrument: V4 Local Contact: U. Keiderling
	Characterization of ODS nanoparticles in Fe-Cr model alloys	Date(s) of Experiment 26.11.-29.11.2009 27.01.-28.01.2010
Principal Proposer: Experimental Team:	A. Ulbricht, Forschungszentrum Dresden- Rossendorf A. Ulbricht, FZD C. Heintze, FZD U. Keiderling, HZB	

Date of report: 12.02.2010

Ferritic-martensitic chromium steels are candidate materials for future application in both Gen-IV fission and fusion technology. In order to improve irradiation-creep properties and to reduce detrimental helium effects oxide-dispersion strengthened (ODS) variants of these steels are of prime interest. This experiment is aimed at supporting a combined modelling and experimental approach towards a physical understanding of the effect of the ODS nanoparticles on relevant properties.

Binary Fe-9%Cr alloys containing 0.3 and 0.6% Y_2O_3 were investigated by SANS along with an ODS-free variant. The measurements were carried out at V4 with a wavelength of 0.6 nm, two sample-detector distances of 1 and 4 m with corresponding collimation length, covering a scattering vector of about 0.2 to 3 nm^{-1} . The samples were placed in a magnetic field of 1.03 T. Data calibration was done using a water standard. Data reduction was carried out using the BerSANS software package.

The measured total (magnetic and nuclear) scattering cross sections of the Fe-9%Cr alloys without and with 0.6% ODS nanoparticles are shown in Fig. 1(a). The SANS data for the 0.3% ODS alloy are located between these two curves (not plotted here). The difference scattering curve, i.e. the scattering intensity caused by the ODS nanoparticles, are shown in Fig. 1(b). The calculated size distribution of the ODS nanoparticles are given in Fig. 1(c). This size distribution fits the experimental data well (see Fig. 1(b) line).

The quality of the ODS material produced by means of a special procedure of powder metallurgy was checked. We found nanoparticles with radii between 2.5 and about 10 nm. The mean size is 4.5 nm in radius. Therefore, the attribute "nano" is justified.

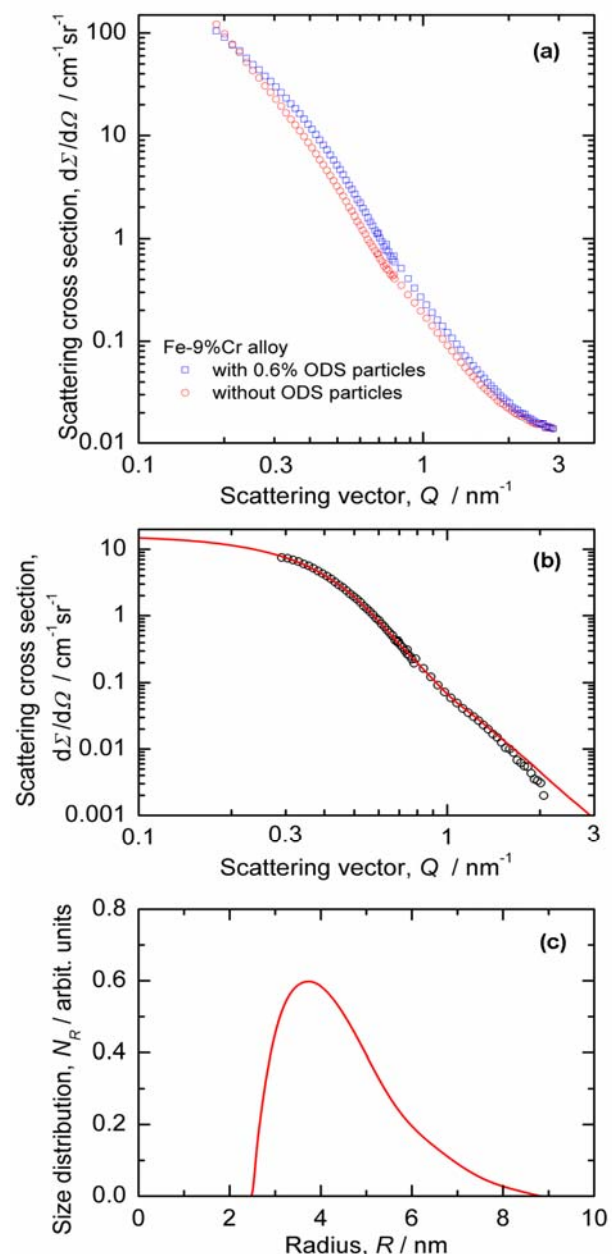


Fig. 1: (a) Measured SANS intensities of Fe-9%Cr model alloys with 0.6% and without ODS nanoparticles, (b) difference scattering curve (symbols) and data fit (line), (c) calculated size distribution, number density per radius interval, N_R , of ODS nanoparticles.

 HELMHOLTZ ZENTRUM BERLIN für Materialien und Energie NEUTRONS	EXPERIMENTAL REPORT	Proposal: MAT-04-1655 Instrument: V4 Local Contact: U. Keiderling
	Stability of carbides in Co-Re-base alloy at high temperatures	Date(s) of Experiment 08.12.2009 – 11.12.2009
Principal Proposer: Experimental Team:	P. Strunz, NPI Řež P. Strunz, NPI Řež U. Keiderling, HZB D. Mukherji, TU Braunschweig	

Date of report: 05.02.2010

A desire to increase temperature and thereby also the efficiency of combustion in gas turbines is a driving force behind new high temperature materials development for application at temperatures at 1200°C and above. Co-Re based alloys, which are being developed at TU Braunschweig (German patent application no. 10 2009 037 622.4 Aug2009), are candidates for a new generation of high temperature alloys. Presence of various strengthening phases in Co-Re alloys and their evolution on exposure at high temperatures is not yet fully mapped.

During the time of V4 detector repair and waiting for the beamtime (1.5 year from the submission), we performed a couple of neutron diffraction experiments and other investigations on Co-Re alloys which led us to a modification of the experimental program. Instead of an originally planned ex-situ experiment, we decided to perform in-situ measurement at HT. The previous neutron scattering experiments on Co-Re alloys did not answer question concerning formation of fine lamellar $Cr_{23}C_6$ carbides in type Co-17Re-23Cr-2.6C alloy (L1), particularly if they form during cooling from solution temperature or at the HT and in which sequence with the large blocky $Cr_{23}C_6$ -type carbides. In-situ solutioning at 1450°C followed by temperature decrease and hold at and below 1200°C was suggested to shed more light on this issue.

The sample of Co-Re alloy (L1 type) was heated up to 1450°C in order to solutionize all the carbides. It was followed by step-by-step temperature decrease which should reveal, at which temperature the formation of carbides occurs.

It was observed that the integrated intensity of SANS signal at 4 m sample-to-detector distance (SDD) decreases on heating to 1450°C, particularly at temperatures above 1000°C. It indicates dissolution of the original population of lamellar carbides. This is finished at 1260°C. However, the integrated intensity does not revert back on cooling for the

intensity measured at 4 m SDD. At 16 m SDD, only a small increase in the integral intensity is visible around 1050°C (Fig. 1).

It indicates that some irreversible transformation occurred at high temperatures. This behaviour can be caused by $Cr_{23}C_6$ transformation to sigma phase. Another explanation would be that the carbides growth to large sizes very quickly during the cooling and give thus instantly practically no scattering at SDD=4m.

A detailed evaluation of the SANS data (measurement performed in December 2009) is currently being carried out. The final microstructure has to be investigated also by electron microscopy for better understanding, after the samples are allowed to be transported (radiation protection).

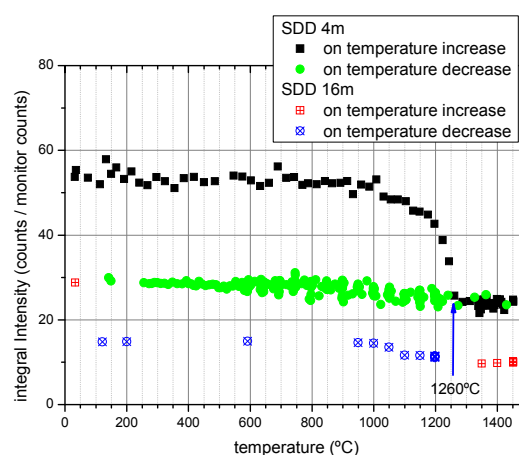


Fig. 1: Integral intensities scattered to small angles, predominantly by the lamellar $Cr_{23}C_6$ -type carbides.

Acknowledgement:

This research project has been supported by the European Commission under the 7th Framework Programme through "Research Infrastructures" action of the "Capacities" Programme, contract number CP-CSA_INFRA-2008-1.1.1. Number 226507-NMI

 HELMHOLTZ ZENTRUM BERLIN für Materialien und Energie NEUTRONS	EXPERIMENTAL REPORT Research of water balance in PEM fuel cells		Proposal: MAT-04-1588-LT Instrument: V7 Local Contact: I. Manke
	Principal Proposer: T. Arlt, I. Manke, HZB Experimental Team: N. Kardjilov, T. Arlt, HZB P. Krüger, R. Kuhn, ZSW Ulm A. Schröder, FZ Jülich T. Sanders, ISEA		

Date of report: 15.01.2010

Introduction

Water management is one of the key factors for the performance and durability of low temperature PEM fuel cells. For an optimized operation it is necessary to detect and differentiate water in the membrane, in the gas diffusion layer and excess water in the flow field channels. The water content of each layer influences the performance in different ways: drying and flooding as the two extreme conditions have to be avoided.

Experiment and results

In this experiment, we have prepared a fuel cell with two different gas diffusion layers (GDL) at the cathode side. One GDL was new (right side in fig.1); the other one had been aged in an acid solution to simulate the conditions in a running cell (left side in fig.1). During the aging process, the hydrophilic behavior of the GDLs gets lost. That means that the adhesion of the upcoming water increases. The advantage is the setup of the cell, containing the two GDLs to run them in the same cell at the same time. This effect could be verified in this experiment. Fig.1 shows that the left part of the cell contains more water in the channels, attributed to the aged GDL material.

Higher water contents means sooner flooding of the channels. As shown in fig.2, this will lead to a lower current density at that place. Additional to

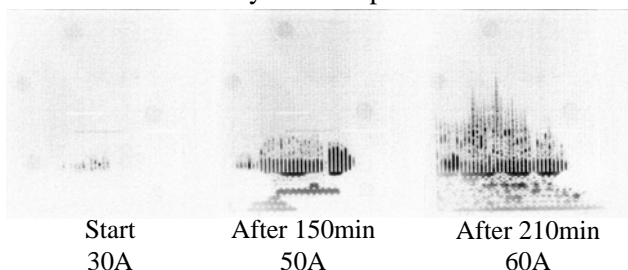


Fig.1: Temporal development of the water management in a PEM fuel cell by means of in-situ neutron radiography

earlier measurement sessions [1], we observed the temporal development of water in the whole active area under various operation conditions.

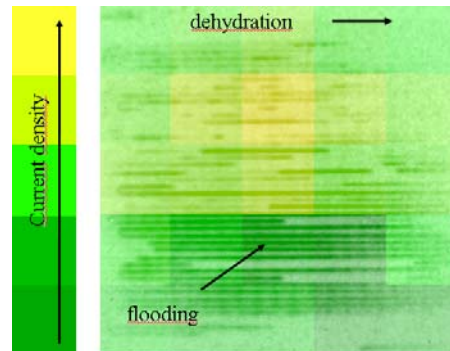


Fig.2: Areas with low/lots of water cause lower current densities compared to areas with a moderate water distribution

Furthermore, we have investigated the development of water under the ribs of the flow fields. This is some kind difficult because of the low water volumes. To solve this problem, we had created a mask as shown in fig.3. This allows hiding the dominant water in the channels. Analyses are going on.

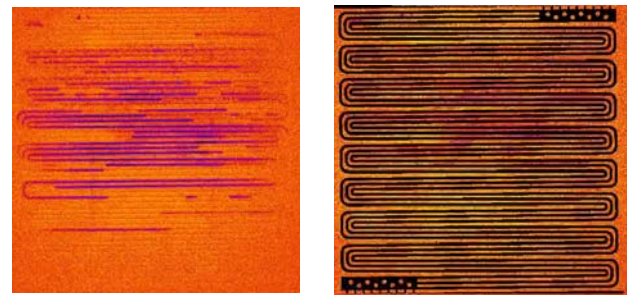


Fig.3: Masking out the channels for better analyses of water volumes under the ribs.

References

- [1] I.Manke et al., *Characterization of water exchange and two-phase flow in porous gas diffusion materials by hydrogen-deuterium contrast neutron radiography* **APL** 92, 244101 (2008)
- [2] I. Manke et al., *Quasi-in situ neutron tomography on polymer electrolyte membrane fuel cell stacks* **APL** 90, 184101 (2007)

Principal Proposer: L. Josic, PSI, NUM, NIAG, Switzerland
 Experimental Team: N. Kardjilov, HZB
 A. Hilger, HZB
 M. Dawson, HZB
 M. Tamaki, TAMAKI Memorial Institute, Japan
 E. Lehmann, PSI, NUM, NIAG, Switzerland

Date(s) of Experiment

24.11.2008 – 30.11.2008

Date of report: 24.02.2009

Energy selective neutron imaging has been performed at cold neutron imaging beam line CONRAD (V7 instrument) of HZB. Samples of different structures and purposes were investigated in order to understand their scattering behavior in transmission mode with high spatial resolution.

Powders, powder mixtures and polycrystals of different materials were scanned in the broad energy range to investigate scattering cross sections and sample structures. In the Fig. 1. examples of Fe and Cu are shown together with theoretical evaluations and experimental data from the cold neutron imaging beam line ICON (PSI, CH). It can be seen that experimental data agree well in first order with theoretical predictions and deviations indicate textures in materials (the absence or suppression of the first Bragg edge). The objective of this investigation was to confirm scattering cross sections of different materials for the application in the quantitative radiography and tomography.

In welded materials energy selective neutron imaging at specific neutron energies can detect structural changes in details (Fig. 2). Measured images do not show any similarities to any other available imaging technique (e.g. optical). The objective of this part of the experiment was to investigate structural changes in industrial materials during manufacturing processes.

In the third part of the experiment the mosaicities of several single graphite monocrystals were measured. The objective of this investigation was a development of the energy selective option for the polychromatic neutron beam. It was shown that the mosaicity is conveniently given by the Gaussian function of the neutron transmission trough the crystal as a function of the angle θ which corresponds to the neutron wavelength λ ($\lambda=2d\sin\theta$, d-the distance between planes in the crystal). The minimum of the Gaussian function θ_c is the rotation angle of the crystal in respect to the initial polychromatic neutron beam direction for which the corresponding wavelength λ_c is the most attenuated by the crystal. Using at least two crystals and changing the value θ_c of each crystal enables an extraction of the wanted wavelength λ (Fig 3).

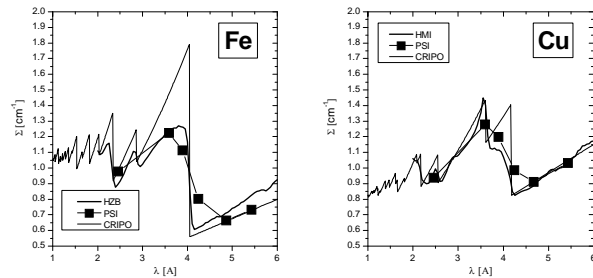


Fig 1. Comparison of the experimental data (HMI, PSI) with theoretically evaluated data (CRIPO) for Fe and Cu. The presence of textures is shown.

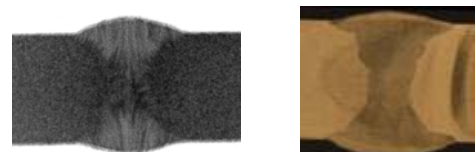


Fig 2. Left: Neutron image of X-type of weld at a single energy. Right: Optical image of the same weld. The difference in the images is clearly shown.

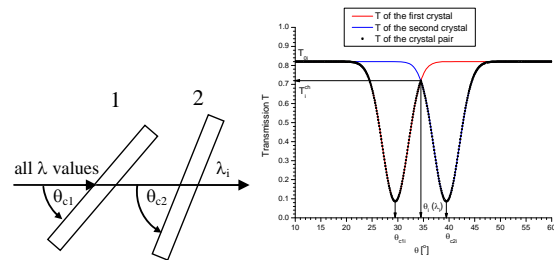


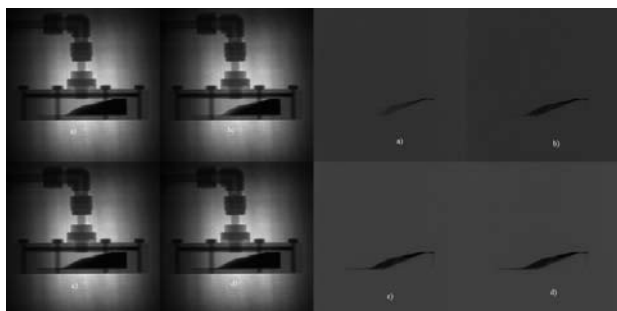
Fig 3. The principle of the extraction of the wanted wavelength λ_i from the initial polychromatic neutron beam. Transmissions of single crystals are given by their mosaicities (red and blue lines). The resulting transmission of the crystal pair is shown with open symbols.

This research project has been supported by the European Commission under the 6th Framework Programme through the Key Action: Strengthening the European Research Infrastructures. Contract n^o: RII3-CT-2003-505925 (NMI 3).

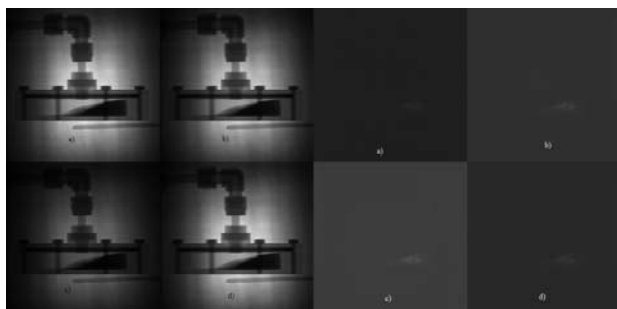
	EXPERIMENTAL REPORT	Proposal: MAT-04-1689
	Hydrogen absorption/desorption in La Ni_{4.6} Al_{0.4} based disc-like storage tank	Instrument: V7 Local Contact: N. Kardjilov
Principal Proposer:	Nivas Babu Selvaraj, AGH University, Krakow, Poland	Date(s) of Experiment
Experimental Team:	Łukasz Gondek, AGH University, Krakow, Poland Nikolay Kardjilov, HZB	12.07.2009 – 17.07.2009

Date of report: 12.12.2009

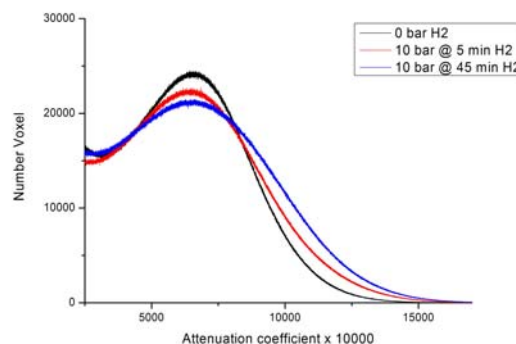
The hydrogen absorption experiment was done at 5 bar, the distribution of particles inside the tank was not flat, in this case an interesting behaviour of the reaction was observed, the particles at surface were hydrided initially and suddenly, but the interior particles were hydrided in a slow rate. The other observation is that the hydrogen penetration depth is less where the particle layer thickness is more and vice versa, and the hydrogen penetration is proportional to the time ie as time goes more interior particle are exposed to hydrogen. This intern is contradict with the existing models which says hydrogen is distributed uniformly inside the tank. The NRG pictures taken after 1hour, 3 hours, 6 hours and 9 hours are shown below. Also the propagation of reaction is more understood by dividing the NRG before reaction and at different time, it is shown as reaction profile.



The neutron radiography picture (left) and reaction profile (right) taken during hydrogen absorption at 5 bar a) after 1hour, b) after 3 hours, c) after 6 hours and d) after 9 hours.



The neutron radiography picture (left) and reaction profile taken during hydrogen desorption a) after 15minutes, b) after 30m, c) after 1 hours and d) after 2hours



Comparison of hystograms at 0 and 10 bars.

After analyzing absorption/desorption at 5 bar and 10 bar The following conclusions were made.

- 1) The performance of the tank depends mainly on
 - a) The amount of metal hydrides (MH) filled (packing fraction).
 - b) Distribution of particle inside the tank.
- 2) The hydrogen penetration depth depends on the thickness of the MH layer, more the thickness less the penetration depth.
- 3) The reaction rate increases with pressure, and temperature (in the range 300-360K).
- 4) Contradict to the existing models we observed that distribution of hydrogen inside the tank has a spatial dependence. From the absorption/desorption at higher pressure and temperature we expect more interesting results.

Acknowledgement:

This research project has been supported by the European Commission under the 7th Framework Programme through the 'Research Infrastructures' action of the 'capacities' Programme, Contract n°: CP-CSA_INFRA-2008-1.1.1 Number 226507-NMI3".

 NEUTRONS	EXPERIMENTAL REPORT	Proposal: MAT-04-1781
	In-situ Stress and Structure Changes Using Portable Tensile Testing System and Large Chamber SEM	Instrument: V7 Local Contact: N. Kardjilov
Principal Proposer: D. Penunadu, University of Tennessee Experimental Team: N. Kardjilov, HZB R. Woracek, University of Tennessee M. Dawson, A. Hilger, HZB	Date(s) of Experiment 17.11.2009-23.11.2009	

Date of report: 16.02.2010

Introduction

Within collaboration (KV090409) between the University of Tennessee and the Helmholtz Center Berlin (HZB), the CONRAD instrument at HZB was used to obtain the location and stress induced shifts of the Bragg Edge for BCC Fe [110] for a steel sample under plane stress conditions.

Mechanical loading corresponding to multi-axial condition was applied in-situ while neutron transmission measurements were recorded. These experiments can be seen as a first step of strategically developing an in-situ method of measuring elastic (and plastic) strain and stress in engineering materials, providing a large view area (in the order of several centimeters) with a spatial resolution below one hundred micrometers, utilizing energy selective neutron imaging. Results obtained with a Large Chamber SEM help with data interpretation (structure and texture evolution).

The neutron attenuation coefficient for polycrystalline materials decreases suddenly for well-defined neutron wavelengths where the conditions for Bragg scattering are no more fulfilled – the so-called Bragg edges. The position of the Bragg-cut-off can be related to the correspondent d_{hkl} spacing.

Experiment and results

An automated mechanical loading system has been developed by the proposers especially for the purpose of this experimental series. The loading system (Fig. 1) has a capability of 50kN axial force and 12Nm torque, while the sample can also be rotated 360 degrees under load.

The global strain was related to local strains obtained by neutron transmission and results show a correct trend (Fig. 2, straight lines). However, strong binning of 100 pixels by 100 pixels corresponding to a size of 2.7mm x 2.7mm was necessary to obtain good signal-to-noise ration, and can be improved by increasing the count time, increase in flux, and

improved energy resolution, which will be the goal within this collaboration between UTK and HZB.

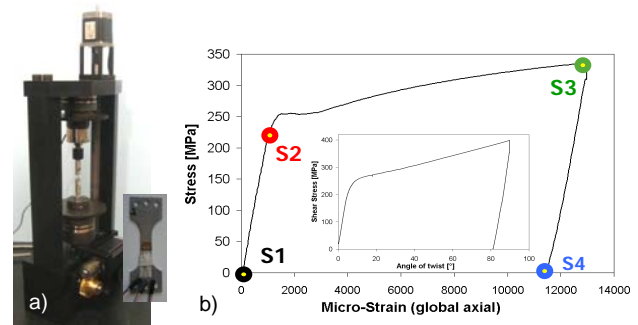


Fig. 1: a) Portable Loading system (and specimen with rosette gauge) b) recorded Stress-Strain of tensile test (inset: Torsion)

If a correction is done for expected uncertainties of the monochromatic option (which needs to be further investigated in future experiments), the measured strain matches the expected values (f.e. 300 microstrain for S2) very close (Fig.2, dotted lines).

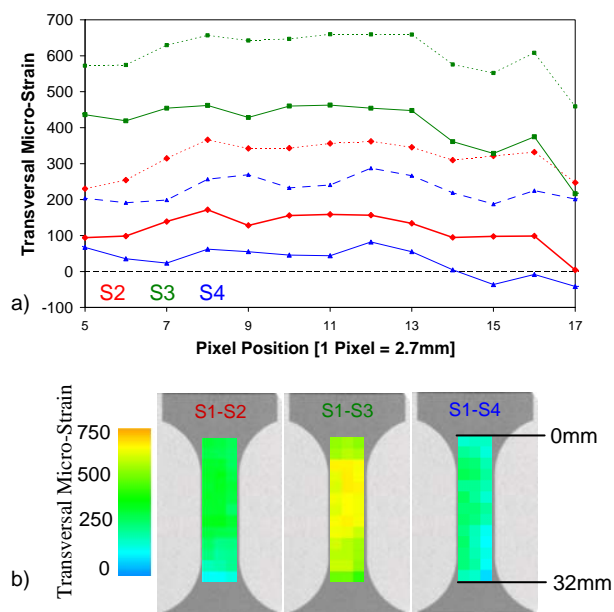


Fig. 2: Transversal strain obtained by Bragg Edge Imaging a) along specimen height b) spatially resolved

	EXPERIMENTAL REPORT	Proposal: MAT-04-1863-EF
	Influence of magneto-mechanical cycling on the initialization and growth of crack in Ni₂MnGa magnetic shape-memory single crystal specimens	Instrument: V7 Local Contact: A. Hilger
Principal Proposer: Experimental Team:	Markus Chmielus, HZB Markus Chmielus, HZB, Rainer Schneider, HZB Andreas Paulke, HZB, André Hilger, HZB Peter Müllner, HZB	Date(s) of Experiment 02.11.2009 - 04.11.2009

Date of report: 21.01.2010

Magnetic shape memory alloys (MSMA) with twinned martensite tend to deform in response to an external magnetic field reversibly (elastic), irreversibly (plastic), or as a combination of both. In 1996, the first results of the magnetoplastic effect and MFIS for a Ni₂MnGa Heusler alloy were published [1]. Since then, the interest in MSMA has grown, and large MFIS of around 10% in a rotating magnetic field were published in 2002 [2]. In a previous study [1], magnetic-field-induced strain (MFIS) had been measured for a Ni-Mn-Ga single crystal in a rotating magnetic field of 0.97 T for a total of 100 million cycles. After a maximum MFIS of 2.1 % at 0.6 million cycles was reached, the MFIS decreased slowly and stayed nearly constant for the final 30 million cycles. After the test was stopped, cracks were found on the surface of the sample and were examined using x-ray micro computer tomography [2].

Due to these findings, we started systematic tests, which include x-ray tomography measurements at different stages in the life of Ni-Mn-Ga single crystal sample. In this study, the initial condition of samples with a new Ni-Mn-Ga composition (Ni_{49.7}Mn_{29.3}Ga_{21.0}) compared to samples in the last proposal were studied. Because of problems during the growth process of the single crystal ingot, only five slices with each two samples instead of ten slices with each five samples could be cut from the ingot.

Figure 1 shows exemplarily some of the defects in the samples studied with x-ray tomography. While pores were present in all samples (visible especially in figure 1a and 1c), cracks were only found in two samples. Figure 1a shows a surface crack or scratch that reaches approximately 100 µm into the sample. Two large cracks reaching over the entire depth of a sample and reaching approximately 1 mm into the width of the sample, where they nearly combine (figure 1b).

Since these samples are magneto-mechanically soft, they will be tested and magneto-mechanically cycled in a rotating magnetic field for 0.5 million cycles. Thereafter, the samples will be examined again and the size and number of cracks will be compared with the here given results to identify crack initialization points and crack growth. It was shown here that x-ray tomography is the non-destructive method of choice to identify pores and cracks in 10 µm range and larger for Ni-Mn-Ga single crystals.

References:

[1] M. Chmielus et al., Training, constraints, and high-cycle magneto-mechanical properties of Ni-Mn-Ga magnetic shape-memory alloys, Eur. Phys. J. Special Topics 158, 79-85 (2008).

[2] M. Chmielus et al., magneto-mechanical properties and Fracture Of a mechanically constrained Ni-Mn-Ga Single Crystal after extended magnetic cycling, ICOMAT 2008 Conference Proceedings, TMS, accepted

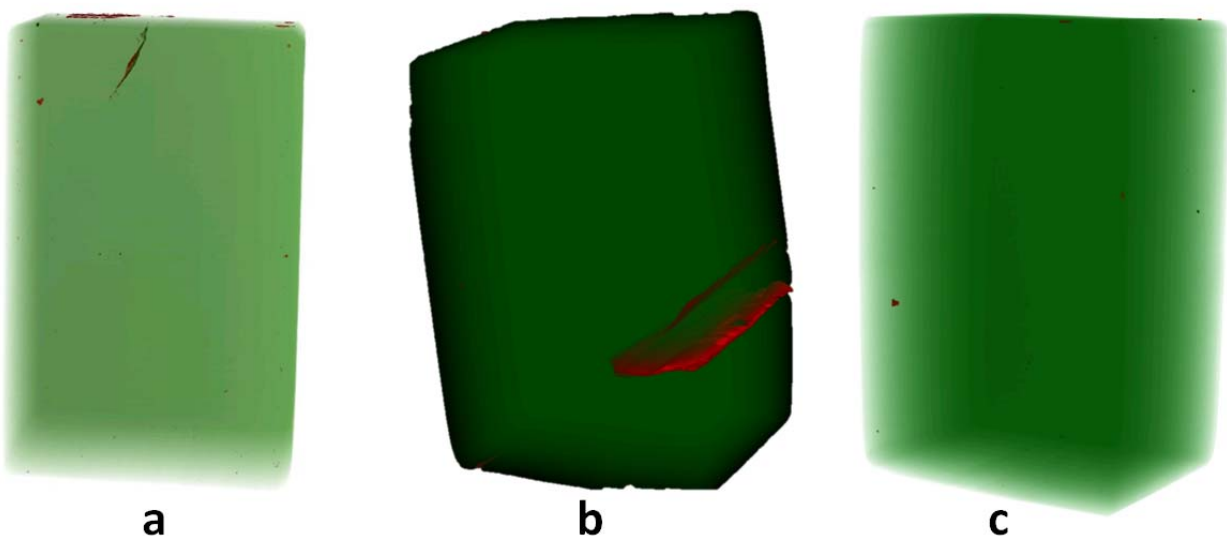


Figure 1: Exemplarily three dimensional reconstructions of defects found in three samples of the new grown Ni_{49.7}Mn_{29.3}Ga_{21.0} single crystal ingot. Pores and surface cracks can be identified in (a), two large cracks that reach in a sample and are close to combine are shown in (b), and a small pore is shown in (c). All samples shown here have dimensions of approximately 6 x 4 x 3 mm³.

 NEUTRONS	EXPERIMENTAL REPORT	Proposal: OTH-04-1871-EF
	Visualisation of magnetic domains by dark-field neutron imaging	Instrument: V7 Local Contact: N. Kardjilov
Principal Proposer: M. Strobl, Uni Heidelberg and HZB Experimental Team: I. Manke, HZB, A. Hilger, HZB N. Kardjilov, HZB, M. Dawson, HZB	Date(s) of Experiment 28.09.2009 – 02.10.2009	

Date of report: 12.01.2010

It could be shown already in the 1990ies that a very high angular sensitivity of an instrument like a double crystal diffractometer can be used to image magnetic domain walls with neutrons [1]. However, only recently a grating interferometer could be introduced, which allows such investigations on reasonable time scales and which can be implemented in conventional imaging instruments [2]. A corresponding device has been made available at the cold neutron imaging instrument CONRAD (V7) and has been used for differential phase contrast and dark-field neutron imaging investigations [3]. The current measurements aimed to test the ability and feasibility of investigations on magnetic domains in bulk ferromagnetic samples with the available grating interferometer device.

The formation of image contrast in the grating interferometer is based on the spin-dependent refraction of neutrons at Bloch walls [4], which for an unpolarized neutron beam results in an ultra-small angle scattering-like angular broadening of the beam and hence provides dark-field contrast [3], if a Bloch wall is close to parallel to the incident beam (Fig. 1).

First measurements have been performed with a SiFe plate with a well defined domain structure geometry (Fig. 2 left), which could be revealed with corresponding measurements at the Paul-Scherrer-Institute (CH) before [2]. First measurements have been performed with a monochromatic beam achieved by the double-crystal monochromator available at CONRAD. Subsequent measurements have been performed with a more relaxed wavelength resolution and correspondingly higher neutron flux by utilizing an energy-selector. It could be proved that more moderate wavelength resolution is sufficient for the corresponding measurements. The results presented by Ch. Grünzweig et al. [2] could be reproduced at CONRAD.

Further subsequent measurements addressing the magnetic domains in bulk SiFe

crystals of different geometry seem to have been successful as well, however, the data is still being analyzed.

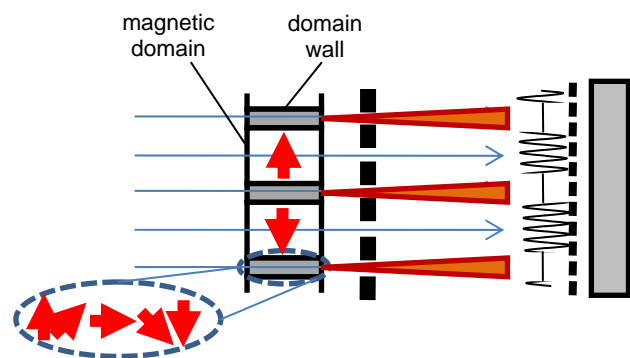


Fig. 1 Schematic representation of the contrast formation by magnetic domain walls in a grating interferometer set-up for neutron imaging.

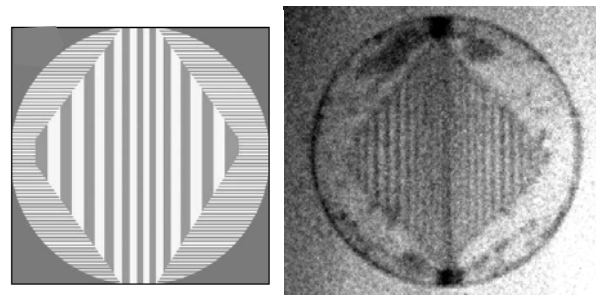


Fig. 2 Schematic representation of the magnetic domains in the investigated SiFe plate (left side) and the corresponding dark-field image visualizing domain walls

References

- [1] K.M. Podurets et al., Zh. Tekh. Fiz. 67 (1997)
- [2] Ch. Grünzweig et al., APL **93**, 112504 (2008)
- [3] M. Strobl et al., PRL 101, 123902 (2008)
- [4] J. Peters et al., Phys. Rev. B **64** 214415 (2001)

 HELMHOLTZ ZENTRUM BERLIN für Materialien und Energie NEUTRONS	EXPERIMENTAL REPORT CO₂-deposition-evacuation in spherical particles for correlations with thermal conductivity models	Proposal: PHY-04-1874 Instrument: V7 Local Contact: N. Kardjilov
	Principal Proposer: Matthias Geisler, Bavarian Centre for Applied Energy Research Experimental Team: Gudrun Reichenauer, Bavarian Centre for Applied Energy Research Nikolay Kardjilov, HZB Martin Dawson, HZB	Date(s) of Experiment 30.10.2009 – 01.11.2009

Date of report: 03.12.2009

Radiography measurements were performed at CONRAD (V7) to investigate the CO₂-deposition within a sample consisting of a bed of ~1µm sized solid glass spheres that is exposed to a temperature gradient at cryogenic temperatures. The quantitative CO₂-distribution is needed to obtain more information about the characteristic deposition of a filling gas within a cryogenic thermal insulation. In advance, measurements of the thermal conductivity were performed with respect to the total amount of deposited CO₂ within the sample [2008 Geisler]. This measurement technique is limited to measure the total effect of the deposited gas on the thermal conductivity, but does not provide information on the mass distribution.

As neutron radiography is expected to be sensitive to the CO₂-distribution, a special sample holder was designed which enforces the identical temperature gradient (77 K to 293 K) as in the already performed thermal conductivity measurements (see Fig.1).

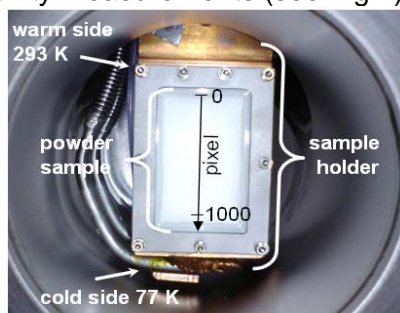


Fig.1: The experimental setup consists of the sample holder for a vacuum chamber with feed throughs for LN₂, CO₂ and electrics. The black arrow represents the evaluated zone.

In parallel, thermal conductivity models were developed describing two opponent cases for the same amount of CO₂ in the system. Homogeneous deposition results in a moderate increase of the thermal conductivity compared to the evacuated system. Point contact deposition yields in an increase of

almost one order of magnitude of the thermal conductivity. The differentiation between both extremes is only possible when knowing the CO₂-distribution.

By these radiographies we obtained the distribution of the deposited CO₂ (see Fig.2). The attenuation of the neutron flux reveals that all CO₂ deposits preferably at and close to the cold wall. The effect correlates directly to the total amount of CO₂ injected into the sample. We are now able to correlate these results with the thermal conductivity measurements.

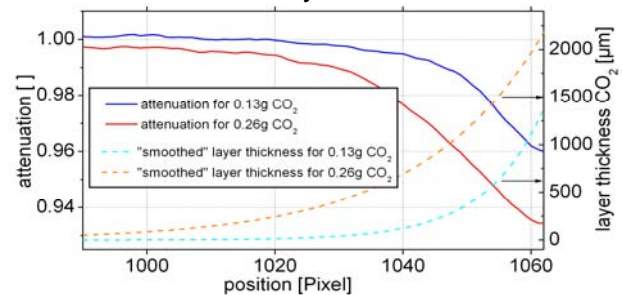


Fig.2: Evaluation of the radiographies show the normalized attenuation caused by deposited CO₂ (for two amounts of CO₂) within the sample along the vertical middle axis of the sample. The evaluated zone is at the cold side of the sample holder. In addition the calculated layer thickness of CO₂ is depicted.

These investigations are essential for all cryogenic thermal insulation materials which are usually mechanically evacuated using vacuum pumps to minimize the gas conduction. The usage of deposition evacuation is an elegant way of creating a low enough vacuum gas pressure.

[2008 Geisler] Geisler M., Ebert H.-P., International Journal of Thermophysics, "Thermal characterisation and effect of deposited CO₂ on a cryogenic insulation system based on a spherical powder", (submitted on 17 September 2008).

Note: The primal experiment PHY-01-2659 was cancelled due to the shortage of time and a low S/N-ratio. The released experimental time was used for detailed investigations concerning MAT-01-2658 instead.

	EXPERIMENTAL REPORT Use of Neutron Tomography to Study the Effects of Microporosity in Binary Aluminum Alloy Castings	Proposal: MAT-04-1885 Instrument: V7 Local Contact: N. Kardjilov
	Principal Proposer: D. Penunadu, University of Tennessee, USA Experimental Team: N. Kardjilov, HZB J. Bunn, University of Tennessee, USA M. Dawson, HZB A. Hilger, HZB	Date(s) of Experiment 23.05.2009 – 24.05.2009

Date of report: 26.01.2010

Introduction

Porosity effects in castings have been well studied in the past. Existing knowledge and related theory does not take into account the critical aspect of dissolution of hydrogen into the liquid aluminum melt. Hydrogen readily dissolves into liquid aluminum from the surrounding air, but hydrogen is no longer held in solution once it solidifies leading to an increase in porosity and related casting defects. Hydrogen could also introduce other adverse effects such as hydrogen embrittlement. Measurement of the hydrogen in the aluminum has shown that even in a case with low or no porosity the hydrogen is still trapped in the sample.

The goal of this research is to determine the presence of hydrogen in samples with known bulk hydrogen content in melt stage. Two plate samples were prepared. One sample contained high hydrogen content (sample C) in the liquid melt, and the other was degassed to reduce the amount of dissolved hydrogen to as little as possible (sample B). The exact bulk hydrogen content for the plate samples is not known, but a large difference is expected to exist between the two. The set of samples was formed by using a simple plate mold which is cooled in one direction only. This one dimensional cooling causes a porosity gradient from the cooled end of the sample. The aluminum used in all the samples in our study is a binary alloy with 88%Al-12%Si.

Experiment and results

The CONRAD instrument was used at HZB for all imaging experiments. A standard tomography was first performed. It consisted of a series of 500 projections over 360°. The pixel size of the radiographs was 40µm. A long exposure time was needed in the experiments to ensure a large signal to noise ratio since aluminum has such a small neutron cross section.

The standard tomography shows much higher porosity in sample C than in sample B. This is expected since sample C has larger hydrogen content. Many highly attenuating spots are seen in the samples. They are observed in both sample B and C. They are more frequent and much brighter in sample C. These spots are shown in Figure 1 below. There was also a very large spot in sample C. This is shown in Figure 1c.

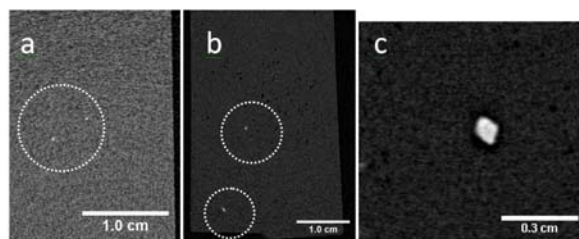


Fig. 1 Reconstructed slices of a) sample B and b,c) sample C. The spots are circled for emphasis.

Energy selective radiographs were also taken for the plate samples. The image in Figure 3 is taken with 4.6 Å wavelength neutrons. The effect of the one dimensional cooling is easily discernable from the image. The dark areas are areas of preferred orientation, and the effect of evolved texture in the sample can be seen clearly.

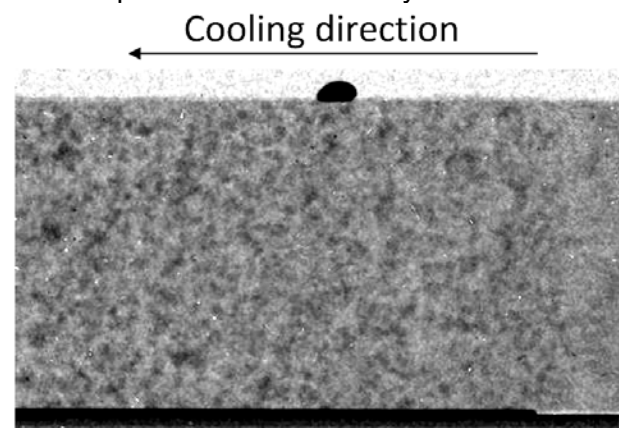


Figure 2. Radiograph of sample C taken at 4.6Å.

Cultural Heritage

	EXPERIMENTAL REPORT Report on use of μ-ct scans for research under GEO-04-1870 and GEO-04-1774	Proposal: GEO-04-1870 GEO-04-1774 Instrument: V7/μ-ct Local Contact: N. Kardjilov
Principal Proposer: Experimental Team:	Ch. Neumann, P. Giere, HU Berlin Th. Lehmann, Senckenberg Forschungsinstitut und Naturkundemuseum Frankfurt N. Kardjilov, HZB A. Hilger, HZB A. Paulke, HZB	Date(s) of Experiment 20.08.2008 – 11.12.2009

Date of report: 15.01.2010

a. "Ethmoid exposure in Tenrecidae"

Micro-ct scans were used to elucidate the previously unclear bone formations in the orbital mosaic of Malagassy tenrecs. One macerated juvenile specimen of *Tenrec ecaudatus* of the mammal collection in the Museum für Naturkunde Berlin showed signs of growing replacement bone other than the Orbitosphenoid and Alisphenoid in the orbital mosaic, the combination of bones that makes up the side wall of the mammalian skull in the orbito-temporal region. The bone in question had previously erroneously been identified as palatine (Muller 1934, Neerl J Zool 1: 118-259) or frontal (Cox 2006, J Zool 269: 514-526) but its true nature as a replacement bone was only suspected by examination of an ontogenetic series of this species and was confirmed in 2009 using the virtual x-ray cross sections provided by the micro-ct facility of the Helmholtz Zentrum Berlin. This result was presented at the annual meeting of the "Deutsche Gesellschaft für Säugetierkunde" (German Society of Mammalogy) as part of an oral presentation (P. Giere: "Ethmoid exposure in the mammalian skull", cf. Fig. 1). The abstract was published at Giere, P. 2009. Ethmoid exposure in the mammalian skull. Mammalian Biology 74S: 11.

b. "Aardvark ontogeny"

In a related project, the ontogeny of another member of the recently formed taxon of Afrotheria, the aardvarks (*Orycteropus afer*) was studied and first results introducing a morphological age class system for this species employing among other characters tooth eruption patterns and vertebral counts. In this project, micro-ct scans performed at the Helmholtz Zentrum Berlin enabled the acquisition of otherwise inaccessible information of a rare aardvark embryo housed in the Embryological Collection of the Museum für Naturkunde Berlin. The initial results were presented in an oral presentation at the annual meeting of the "Deutsche Gesellschaft für Säugetierkunde", September 13-17, 2009, in Dresden. The abstract of this talk can be found at Lehmann, T. 2009. Notes on the ontogeny of the aardvark (*Orycteropus afer*). Mammalian Biology 74S: 17.

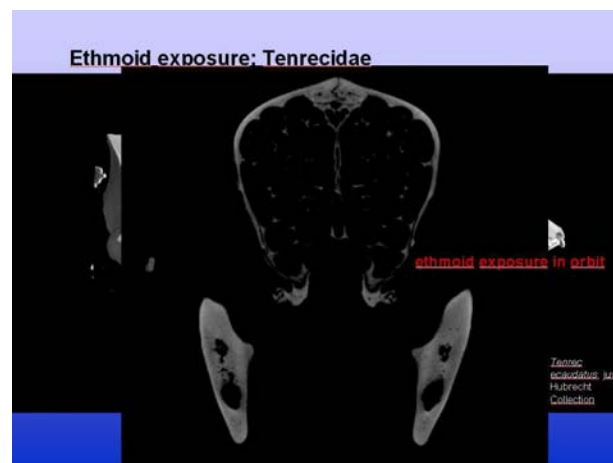


Fig. 1. Reconstruction (left) and cross sections (right) of a *Tenrec ecaudatus* skull produced at the Helmholtz Zentrum Berlin (reproduced from slides of "Giere, P. 2009. Ethmoid exposure in the mammalian skull" talk on the annual meeting of the "Deutsche Gesellschaft für Säugetierkunde", Dresden, 13-17 September 2009).

	EXPERIMENTAL REPORT Archaeometric characterization by Neutron Tomography of recovered underwater items	Proposal: ART-04-1877 Instrument: V7 Local Contact: N. Kardjilov
	Principal Proposer: Roberto Triolo, Università di Palermo, Italy Experimental Team: Roberto Triolo, Università di Palermo, Italy Irene Ruffo, ITC "L. Sturzo", Bagheria, Italy F. Wieder, M. Dawson, N. Kardjilov, HZB	Date(s) of Experiment 17.08.2009 – 23.08.2009

Date of report: 01.01.2010

Conservation of Cultural Heritage is extremely important not only from the cultural point of view, but also from a practical one. We must feel the duty to pass on to our descendants the cultural heritage left to us by our ancestors. Neutron Imaging is very important in dealing with investigation and conservation of Cultural Heritage finds. For example, a typical case might be finds from shipwrecks, including parts of the ship itself. Objects of a variety of different materials might be hidden from heavy and thick layers of calcareous concretions, to the point that could be impossible to gain the necessary information without seriously damaging the find.

An example is shown in figure 1, dealing with a find recovered from a sunken ship (presumably IV - V century A.D.) near Sicily coast. In a) is shown a picture of the find, in b) the central slice of a Neutron Tomography Image and in c) the extracted image of the original item surrounded by a thick (about 4 cm) layer of carbonates. The sample looks like to be a fork (could it be a hairpin?) and is clearly visible in the NT slice. Only the high penetrability of the neutron beam has allowed the investigation of the find.

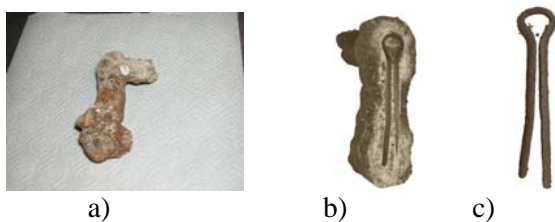


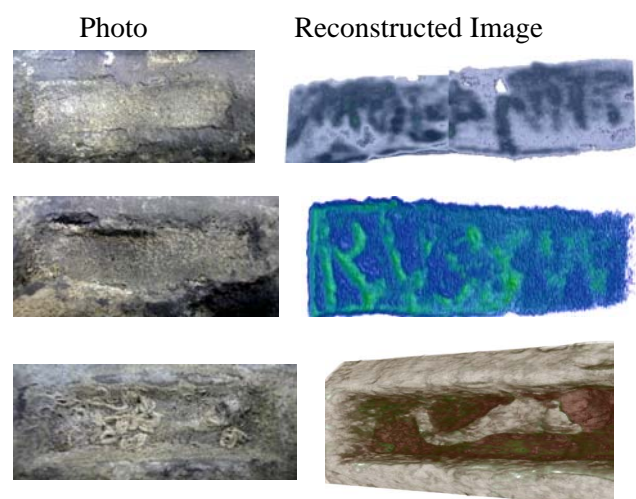
Figure 1 Neutron Imaging of a find from a sunken ship

Figure 2 shows 2 finds run together. The top and the bottom samples are actually portions of different original finds. On the left is shown a photo of the two finds together, while on the right are shown the enlarged extracted images of the top sample and of the bottom sample obtained by NT.



Figure 2 Extracted Images of two finds

An interesting example of application of the unique penetrability properties of neutrons is given by the following figures. The find, was a lead block recovered from a ship sunk not too far from the Sicilian city of Syracuse. Selected portions of the block contained information hidden by corrosion products and calcareous concretions. Words and a dolphin image could be recovered by properly treating the NT data.



Acknowledgment of Support:

This research project has been supported by the European Commission under the 7th Framework Programme through "Research Infrastructures" action of the "Capacities" Programme, contract number CP-CSA_INFRA-2008-1.1.1. Number 226507-NMI3 and by the Soprintendenza del Mare of the Sicilian Regional Government

	EXPERIMENTAL REPORT Neutron Tomography study of pottery fragments from Vörs- Máriaasszonysziget: 5600 BC - 300 AD	Proposal: ART-04-1686 Instrument: V7 Local Contact: N. Kardjilov
	Principal Proposer: Dirk Visser, FAME, RID, TU-Delft, NL Experimental Team: Dirk Visser, FAME, RID, TU-Delft, NL Nikolay Kardjilov, HZB	Date(s) of Experiment 30.10.2008 – 02.11.2008

Date of report: 09.03.2009

The present study focuses on potentials of 3D neutron imaging in the pottery matrix. Samples of coarse grain temper (organic and inorganic, i.e., chaff, grog (broken pottery) and rock fragments will be studied to investigate possibilities of non-destructive analysis of the interiors of pottery samples. The objects for this study are provided by the Hungarian National Museum excavated from Vörs-Máriaasszonysziget, a site which has special importance in the spreading of the "Neolithic package", i.e., notions on productive economy, pottery-making and other Neolithic crafts in the Central parts of Europe.

We concentrated during the experiment on 4 pottery objects of the Starcevo - I culture, Early Neolithic, 5600 – 5400 BC. These pottery shards are characterized by a serial texture with mainly quartz and feldspars as non-plastic constituents. They contain also vegetal temper (probably chaff).

We have taken during the experiment 2 sets of neutron tomography data on the 4 Starcevo Period I samples, with L/D = 200 and a neutron flux of 2×10^7 n / cm² s.

For the first set we used low resolution set up with a ⁶Li / ZnS.Ag, 200 μm thickness, recording times of 20 seconds. For the second high-resolution set a Gd₂O₂S:Tb scintillator of 10 μm thick was used. The detection time was 3 x 20 sec per image. The detector pixel size was 30 μm.

Neutron computer tomography images were reconstructed with Octopus and analyzed with VG-Studio Max software.

The histograms of the attenuation coefficients (cm⁻¹) were obtained. They showed a more or less Gaussian profile. The maxima are shifted per object and are slightly different for each individual scintillator. The range lies between 0.40 – 0.90 cm⁻¹ (Gadox) and 0.42 – 1.02 cm⁻¹ (⁶Li). The tomographic reconstructions show voids in each sample which are related to the

volumes occupied by the organic material (chaff). The volume percentages lie between 0.3 – 2.5 %.

Finally we recorded also X-ray tomography data sets for 21 Vörs-Máriaasszonysziget objects of 6 different time periods using the in house X-ray set up (100KeV). Comparative results have been obtained. In certain cases one can recognize in the void imprint the plant material.



Fig.1 Neutron tomographic reconstruction of Starcevo sample 4, using a Gadox scintillator. The transparency of the bulk material has been reduced to visualize the voids in the pottery shard.

*This research project has been supported by the European Commission under the 6th Framework Programme through the Key Action: Strengthening the European Research Infrastructures.
Contract n°: RII3-CT-2003-505925 (NMI 3).*

Part II

List of Publications

Theses	171
Publications	172
Author Index	187

Theses 2009
Examina

PhD theses

2008 (supplement)

<i>Molisso, A.</i> PVA modified hydrogels: study of phase behaviour in the presence of polymers and simple salts Chemistry Department, University of Naples, Italy (2008)	V12a IHP: 1212
--	-------------------

2009

<i>Buchter, F.</i> Insights into the Structure and Dynamics of Tetrahydroborates Universite de Fribourg (Suisse) (2009)	E6 NMI3: 1355
<i>Le, M. D.</i> Magnetism and Quadrupolar Order in f-electron Systems University of London (2009)	V2 NMI3: 1163 NMI3: 1237 NMI3: 1286

Publications 2009
BENSC Experiments and BENSC Authors

2006 (supplement)

<p><i>Christianson, A.D.; et al</i> Novel coexistence of superconductivity with two distinct magnetic orders Physical Review Letters 95 (2006) 217002</p>	E4
<p><i>Strobl, M.; Treimer, W.; Hilger, A.</i> The new V12a diffractometer at HMI and neutron computerized tomography Europhysics Conference Abstract Volume 30A, p 621, ISBN 2-914771-32-0 (2006) 30A (2006), 621 -</p>	V12a
<p><i>Treimer, W.; Strobl, M.; Kardjilov, N.; Hilger, A.; Manke, I.</i> A double monochromator device for the CONRAD radiography instrument at HMI and ap-plications Europhysics Conference Abstract Volume 30A, p 621, 448, ISBN 2-914771-32-0 (2006) 30A (2006), 621 -</p>	V7

2007 (supplement)

<p><i>Jalarvo, N.; Aliouane, N.; Bordallo, H.N.; Milne, C.J.; Veira, J.R.; Argyriou, D.N.</i> Rotational motion of the water molecules in the superconductor Na_{0.28}CoO₂·yH₂O European Physical Journal-Special Topics 141 (2007), 69 - 72</p>	V3
<p><i>Rule, K.C.; Ehlers, G.; Stewart, J.R.; Cornelius, A.L.; Deen, P.P.; Qiu, Y.; Wiebe, C.R.; Janik, J.A.; Zhou, H.D.; Antonio, D.; Woytko, B.W.; Ruff, J.P.; Dabkowska, H.A.; Gaulin, B.D; Gardner, J.S.</i> Polarized inelastic neutron scattering of the partially ordered Tb₂Sn₂O₇ Physical Review B: Condensed Matter 76 (2007), 212405 -</p>	V2
<p><i>Strobl, M.; Treimer, W.; Ritzoulis, C.; Wagh, A.G.; Abbas, S.; Manke, I.</i> The new V12 ultra-small-angle neutron scattering and tomography instrument at the Hahn-Meitner Institut Journal of Applied Crystallography 40 (2007), s463 - s465</p>	V12a

2008 (supplement)

<p><i>Davies, C.M.; Wimpory, R.C.; Dye, D.; Nikbin, K.M.</i> The effects of plate dimensions on residual stresses in welded thin steel plates ASME Conference Proceedings 2009 (2008) 1221 - 1229</p>	
<p><i>Kamarad, J.; Mihalik, M.; Sechovsky, V.; Arnold, Z.</i> Miniature uniaxial pressure cels for magnetic measurements High Pressure Research 28 (2008), 633 - 636</p>	E4 IHP: 1357
<p><i>Kleinert, K.; Reimelt, M.</i> Ein komplexer Malprozeß mit ikonographischen Konsequenzen. Zur Bildgenese des Werkes "Wie die Alten sungen, so pfeifen die Jungen" von Jan Steen in der Gemäldegalerie Jahrbuch der Berliner Museen 2008 (2008)</p>	B8

<i>Kleinert, K.; Laurenze-Landsberg, C.</i> Zur Bildgenese von Rembrandts Gemälde ‚Simson und Delila‘ Jahrbuch der Berliner Museen 2008 (2008), 147 - 155	B8
<i>Remhof, A.; Friedrichs, O.; Buchter, F.; Mauron, Ph.; Züttel, A.; Wallacher, D.</i> Solid-state synthesis of LiBD4 observed by in situ neutron diffraction Physical Chemistry Chemical Physics 10 (2008), 5859 - 5862	E6 NMI3: 1314
<i>Thiedmann, R.; Fleischer, F.; Hartnig, Ch.; Schmidt, V.; Lehnert W.;</i> Stochastic 3D Modeling of the GDL Structure in PEMFCs Based on Thin Section Detection Journal of The Electrochemical Society 155 (2008), B391 -	V7
2009	
<i>Akhtar, N.; Qureshi, A.; Scholta, J.; Hartnig, Ch.; Messerschmidt, M.; Lehnert, W.;</i> Investigation of water droplet kinetics and optimization of channel geometry for PEM fuel cell cathodes International Journal of Hydrogen Energy 34 (2009) 3104 Proposal-Nr: MAT-04-1588-LT	V7
<i>Aliouane, N.; Schmalzl, K.; Senff, D.; Maljuk, A.; Prokes, K.; Braden, M.; Argyriou, D.N.</i> Flop of Electric Polarization Driven by the Flop of the Mn Spin Cycloid in Multiferroic TbMnO3 Physical Review Letters 102 (2009) 207205	E4
<i>Argyriou, D.N.; Bordallo, H.N.</i> Decisions on the European Spallation Source Nature Materials 8 (2009) 440 - 440	
<i>Atkin, R.; De Fina, L.M.; Keiderling, U.; Warr, G.G.</i> Structure and Self Assembly of Pluronic Amphiphiles in Ethylammonium Nitrate and at the Silica Surface Journal of Physical Chemistry B 113 (2009) 12201 - 12213	V4
<i>Balanda, M.; Penc, B.; Baran, S.; Jaworska-Golab, T.; Arulraj, A.; Szytula, A.</i> Magnetic Properties of TbNi_{1-x}AuxIn Compounds Acta Physica Polonica A 115 (2009) 174 - 177	E6 NMI3: 1348
<i>Baran, S.; Hoser, A.; Kaczorowski, D.; Kiefer, K.; Penc, B.; Szytula, A.</i> Low temperature magnetic order in HoFe₂Ge₂ Solid State Communications 149 (2009) 1261 - 1263	E6 NMI3: 1392
<i>Baran, S.; Kaczorowski, D.; Arulraj, A.; Penc, B.; Szytula, A.</i> Frustrated magnetic structure of TmAgGe Journal of Magnetism and Magnetic Materials 321 (2009) 3256 - 3261	E6 NMI3: 1393
<i>Baranov, N.V.; Proshkin, A.V.; Czternasty, C.; Meissner, M.; Podlesnyak, A.; Podgornykh, S.M.</i> Butterflylike specific heat, magnetocaloric effect, and itinerant metamagnetism in (Er,Y)Co₂ compounds Physical Review B: Condensed Matter 79 (2009) 184420	
<i>Behne, D.; Alber, D.; Kyriakopoulos, A.</i> Effects of long-term selenium yeast supplementation on selenium status studied in the rat Journal of Trace Elements in Medicine and Biology 23 (2009) 258 - 264	NAA

<p><i>Behne, D.; Alber, D.; Kyriakopoulos, A.</i> Selenium distribution in tissues and monitor materials after long-term selenium supplementation investigated by neutron activation analysis <i>Journal of Radioanalytical and Nuclear Chemistry</i> 281 (2009) 31 - 34</p>	NAA
<p><i>Bertelsmann, H.; Behne, D.; Kyriakopoulos, A.</i> Studies with Regard to the Apoptosis of Testicular Germ Cells in Rats Fed a Diet Enriched with Polyunsaturated Fatty Acids <i>Natural Compounds and their Role in Apoptotic Cell Signaling Pathways</i> 1171 (2009) 372 - 376</p>	NAA
<p><i>Bird, M.D.; Bai, H.Y.; Bole, S.; Chen, J.P.; Dixon, I.R.; Ehmler, H.; Gavrilin, A.V.; Painter, T.A.; Smeibidl, P.; Toth, J.; Weijers, H.; Xu, T.; Zhai, Y.H.</i> The NHMFL Hybrid Magnet Projects <i>IEEE Transactions on Nuclear Science</i> 19 (2009) 1612 - 1616</p>	
<p><i>Bleckmann, M.; Buchsteiner, A.; Stuesser, N.; Gofryk, K.; Kaczorowski, D.; Suellow, S.</i> Antiferromagnetic structure of UPd₂Sb <i>Physica B - condensed matter</i> 404 (2009) 3011 - 3013</p>	E6
<p><i>Bobrovskii, V.; Kazantsev, V.; Mirmelstein, A.; Mushnikov, N.; Proskurnina, N.; Voronin, V.; Pomjakushina, E.; Conder, K.; Podlesnyak, A.</i> Spontaneous and field-induced magnetic transitions in YBaCo₂O_{5.5} <i>Journal of Magnetism and Magnetic Materials</i> 321 (2009) 429 - 437</p>	
<p><i>Bolisetty, S.; Schneider, C.; Polzer, F.; Ballauff, M.; Li, W.; Zhang, A.; Schluter, A.D.</i> Formation of Stable Mesoglobules by a Thermosensitive Dendronized Polymer <i>Macromolecules</i> 42 (2009) 7122 - 7128</p>	
<p><i>Bonisch, S.P.; Namaschk, B.; Wulf, F.; Kleisch, T.; Dube, S.</i> PSD Read-out Electronics Development for the New Exed Experiment at the Helmholtz-Zentrum Berlin (HZB) <i>2008 IEEE Nuclear Science Symposium and Medical Imaging Conference (2008 NSS/MIC), Vols 1-9</i> (2009) 1266 - 1270</p>	
<p><i>Bordallo, H.N.; Aldridge, L.P.; Fouquet, P.; Pardo, L.C.; Unruh, T.; Wuttke, J. Yokaichiya, F.</i> Hindered Water Motions in Hardened Cement Pastes Investigated over Broad Time and Length Scales <i>ACS Applied Materials & Interfaces</i> 1 (2009) 2154 - 2162</p>	
<p><i>Buchsteiner, A.; Stuesser, N.</i> Optimizations in angular dispersive neutron powder diffraction using divergent beam geometries <i>Nuclear Instruments and Methods in Physics Research Section A</i> 598 (2009) 534 - 541</p>	E6
<p><i>Canfield, P.C.; Bud'ko, S.L.; Ni, N.; Kreyssig, A.; Goldman, A.I.; McQueeney, R.J.; Torikachvili, M.S.; Argyriou, D.N.; Luke, G.; Yu, W.</i> Structural, magnetic and superconducting phase transitions in CaFe₂As₂ under ambient and applied pressure <i>Physica C</i> 469 (2009) 404 - 412</p>	
<p><i>Carretta, S.; Guidi, T.; Santini, P.; Amoretti, G.; Pieper, O.; Lake, B.; van Slageren, J.; El Hallak, F.; Wernsdorfer, W.; Mutka, H.; Russina, M.; Milios, C.J.; Brechin, E.K.</i> Neutron spectroscopy and magnetic relaxation of the Mn-6 nanomagnets <i>Polyhedron</i> 28 (2009) 1940 - 1944</p>	V3

<p><i>Chatterji, T.; Hansen, T.C.; Brunelli, M.; Henry, P.F.</i> Negative thermal expansion of ReO₃ in the extended temperature range Applied Physics Letters 94 (2009) 241902</p>	
<p><i>Chen, J.S.; Kohler, R.; Gutberlet, T.; Mohwald, H.; Krastev, R</i> Asymmetric lipid bilayer sandwiched in polyelectrolyte multilayer films through layer-by-layer assembly Soft Matter 5 (2009) 228 - 233</p>	V6
<p><i>Chernenko, V.A.; Chmielus, M.; Mullner, P.</i> Large magnetic-field-induced strains in Ni-Mn-Ga nonmodulated martensite Applied Physics Letters 95 (2009) 104103</p>	
<p><i>Chernenko, V.A.; Oikawa, K.; Chmielus, M.; Besseghini, S.; Villa, E.; Albertini, F.; Righi, L.; Paoluzi, A.; Mullner, P.; Kainuma, R.; Ishida, K.</i> Properties of Co-alloyed Ni-Fe-Ga Ferromagnetic Shape Memory Alloys Journal of Materials Engineering and Performance 18 (2009) 548 - 553</p>	
<p><i>Chmielus, M.; Zhang, X.X.; Witherspoon, C.; Dunand, D.C.; Mullner, P.</i> Giant magnetic-field-induced strains in polycrystalline Ni-Mn-Ga foams Nature Materials 8 (2009) 863 - 866</p>	
<p><i>da Silva, J. H.; Lima Jr, J.A.; Freire, P.T.C.; Lemos, V.; Mendes Filho, J.; Melo, F.E.A.; Pizani, P.S.; Fischer, J.; Klemke, B.; Kemner, E.; Bordallo, H.N.</i> Raman spectroscopy and inelastic neutron scattering study of crystalline L-valine Journal of Physics: Condensed Matter 21 (2009), 415404</p>	V3
<p><i>Danilyan, G.V.; Granz, P.; Krakhotin, V.A.; Mezei, F.; Novitsky, V.V.; Pavlov, V.S.; Russina, M.; Shatalov, P.B.; Wilpert, T.</i> Rotational effect of fissile nucleus in binary fission of U-235 induced by cold polarized neutrons Physics Letters B 679 (2009) 25 - 29</p>	V13
<p><i>Darul, J.; Nowicki, W.</i> Preparation and neutron diffraction study of polycrystalline Cu-Zn-Fe materials Radiation Physics and Chemistry 78 (2009) S109 - S111</p>	E9 NMI3: 1345
<p><i>de Souza, J.M.; Freire, P.T.C.; Argyriou, D.N.; Stride, J.A.; Barthès, M.; Kalceff, W.; Bordallo, H.N.</i> Raman and Neutron Scattering Study of Hydrogen Bonds in Partially Deuterated L-Alanine: Evidence of a Solid-Solid Phase Transition' ChemPhysChem 10 (2009), 3337 - 3343</p>	E9/V3
<p><i>Dyadkin, V.A.; Grigoriev, S.V.; Moskvina, E.V.; Maleyev, S.V.; Menzel, D.; Schoenes, J.; Eckerlebe, H.</i> Critical scattering in the helimagnets Fe_{1-x}CoxSi Physica B - condensed matter 404 (2009) 2520 - 2523</p>	
<p><i>Estrela-Lopis, I.; Leporatti, S.; Clemens, D.; Donath, E.</i> Polyelectrolyte multilayer hollow capsules studied by small-angle neutron scattering (SANS) Soft Matter 5 (2009) 214 - 219</p>	V4
<p><i>Evers, F.; Steitz, R.; Tolan, M.; Czeslik, C.</i> Analysis of Hofmeister Effects on the Density Profile of Protein Adsorbates: A Neutron Reflectivity Study Journal of Physical Chemistry B 113 (2009) 8462 - 8465</p>	V6

<p><i>Feyerherm, R.; Dudzik, E.; Wolter, A.U.B.; Valencia, S.; Prokhnenko, O.; Maljuk, A.; Landsgesell, S.; Aliouane, N.; Bouchenoire, L.; Brown, S.; Argyriou, D.N.</i></p> <p>Magnetic-field induced effects on the electric polarization in RMnO₃(R=Dy,Gd) Physical Review B: Condensed Matter 79 (2009) 134426</p>	
<p><i>Fokin, A.; Kumzerov, Y.; Koroleva, E.; Naberezhnov, A.; Smirnov, O.; Tovar, M.; Vakhrushev, S.; Glazman, M.</i></p> <p>Ferroelectric phase transitions in sodium nitrite nanocomposites Journal of Electroceramics 22 (2009) 270 - 275</p>	E9
<p><i>Fouquet, P.; Farago, B.; Andersen, K.H.; Bentley, P.M.; Pastrello, G.; Sutton, I.; Thaveron, E.; Thomas, F.; E. Moskvina E.; Pappas C.</i></p> <p>Design and Experimental Tests of a Novel Neutron Spin Analyzer for Wide Angle Spin Echo Spectrometers Review of Scientific Instruments 80 (2009) 095105</p>	V5
<p><i>Friedrichs, O.; Kim, J. W.; Remhof, A.; Buchter, F.; Borgschulte, A.; Wallacher, D.; Cho, Y. W.; Fichtner, M.; Oh, K. H.; Züttel, A.</i></p> <p>The effect of Al on the hydrogen sorption mechanism of LiBH₄ Physical Chemistry Chemical Physics 11 (2009) 1515 - 1520</p>	E6 IHP: 1355
<p><i>Garlea, V.O.; Zheludev, A.; Habicht, K.; Meissner, M.; Grenier, B.; Regnault, L.P.; Ressouche, E.</i></p> <p>Dimensional crossover in a spin-liquid-to-helium magnet quantum phase transition Physical Review B: Condensed Matter 79 (2009) 60404</p>	V2
<p><i>Gil, G.O.; Prevost, S.; Losik, M.; Hermes, F.; Schlaad, H.; Hellweg, T.</i></p> <p>Polypeptide hybrid copolymers as selective micellar nanocarriers in nonaqueous media Colloid and Polymer Science 287 (2009) 1295 - 1304</p>	V4
<p><i>Goldman, A.I.; Kreyssig, A.; Prokes, K.; Pratt, D.K.; Argyriou, D.N.; Lynn, J.W.; Nandi, S.; Kimber, S.A.J.; Chen, Y.; Lee, Y.B.; Samolyuk, G.; Leao, J.B.; Poulton, S.J.; Bud'ko, S.L.; Ni, N.; Canfield, P.C.; Harmon, B.N.; McQueeney, R.J.</i></p> <p>Lattice collapse and quenching of magnetism in CaFe₂As₂ under pressure: A single-crystal neutron and x-ray diffraction investigation Physical Review B: Condensed Matter 79 (2009) 24513</p>	E4
<p><i>Gonçalves, R.O.; Freire P.T.C.; Bordallo, H.N.; Lima Jr., J.A.; Melo, F.E.A.; Mendes Filho, J.; Argyriou, D.N.; Lima, R.J.C.</i></p> <p>High-pressure Raman spectra of deuterated L-alanine crystal Journal of Raman Spectroscopy 40 (2009), 958 - 963</p>	E9/V3
<p><i>Gonçalves, R.O.; Freire P.T.C.; Bordallo, H.N.; Lima Jr, J. A.; Melo, F.E.A.; Mendes Filho, J.; Argyriou, D.N.; Lima, R.J.C.</i></p> <p>High-pressure Raman spectra of deuterated L-alanine crystal Journal of Raman Spectroscopy 40 (2009), 958 - 963</p>	E9
<p><i>Gondek, L.; Czub, J.; Szytula, A.; Izaola, Z.; Kemner, E.</i></p> <p>Crystal field in RPdIn (R=Ce, Pr, Nd) compounds Solid State Communications 149 (2009) 1596 - 1599</p>	V3 NMI3: 1395 NMI3: 1349
<p><i>Gontrani, L.; Russina, O.; Lo Celso, F.; Caminiti, R.; Annat, G.; Triolo, A.</i></p> <p>Liquid Structure of Trihexyltetradecylphosphonium Chloride at Ambient Temperature: An X-ray Scattering and Simulation Study Journal of Physical Chemistry B 113 (2009) 9235 - 9240</p>	
<p><i>Gontrani, L.; Russina, O.; Lo Celso, F.; Caminiti, R.; Annat, G.; Triolo, A.</i></p> <p>Liquid Structure of Trihexyltetradecylphosphonium Chloride at Ambient Temperature: An X-ray Scattering and Simulation Study Journal of Physical Chemistry B 113 (2009), 9235 - 9240</p>	

<p><i>Gourdon, O.; Izaola, Z.; Elcoro, L.; Petricek, V.; Miller, G.J.</i> Structure Determination of Two Modulated gamma-Brass Structures in the Zn-Pd System through a (3+1)-Dimensional Space Description <i>Inorganic Chemistry</i> 48 (2009), 9715 - 9722</p>	
<p><i>Grigoriev, S.V.; Dyadkin, V.A.; Moskvina, E.V.; Lamago, D.; Wolf, T.; Eckerlebe, H.; Maleyev, S.V.</i> Helical spin structure of Mn_{1-y}FeySi under a magnetic field: Small angle neutron diffraction study <i>Physical Review B: Condensed Matter</i> 79 (2009), 144417 -</p>	
<p><i>Gruener, S.; Hofmann, T.; Wallacher, D.; Kityk, A.V.; Huber, P.</i> Capillary rise of water in hydrophilic nanopores <i>Physical Review E</i> 79 (2009), 067301 -</p>	
<p><i>Habel, D.; Gorke, O.; Tovar, M.; Willinger, M.; Ziemann, M.; Schwarz, O.; Schomacker, R.; Schubert, H.</i> Microstraining in titania-, alumina- and silica-supported V₂O₅-catalysts <i>Journal of the European Ceramic Society</i> 29 (2009), 1093 - 1099</p>	E9
<p><i>Harriger, L.W.; Schneidewind, A.; Li, S.; Zhao, J.; Li, Z.; Lu, W.; Dong, X.; Zhou, F.; Zhao, Z.; Hu, J.; Dai, P.</i> Transition from Three-Dimensional Anisotropic Spin Excitations to Two-Dimensional Spin Excitations by Electron Doping the FeAs-Based BaFe_{1.96}Ni_{0.04}As₂ Superconductor <i>Physical Review Letters</i> 103 (2009), 087005 -</p>	
<p><i>Hartnig, C.; Manke, I.; Kuhn, R.; Kleinau, S.; Goebbels, J.; Banhart, J.</i> High-resolution in-plane investigation of the water evolution and transport in PEM fuel cells <i>Journal of Power Sources</i> 188 (2009), 468 - 474</p>	
<p><i>Hartnig, C.; Manke, I.; Schloesser, J.; Kruger, P.; Kuhn, R.; Riesemeier, H.; Wippermann, K.; Banhart, J.</i> High resolution synchrotron X-ray investigation of carbon dioxide evolution in operating direct methanol fuel cells <i>Electrochemistry Communications</i> 11 (2009), 1559 - 1562</p>	
<p><i>Henry, P.F.; Weller, M.T.; Wilson, C.C.</i> Neutron powder diffraction in materials with incoherent scattering: an illustration of Rietveld refinement quality from nondeuterated gypsum <i>Journal of Applied Crystallography</i> 42 (2009), 1176 - 1188</p>	
<p><i>Himsl, D.; Wallacher, D.; Hartmann, M.</i> Improving the Hydrogen-Adsorption Properties of a Hydroxy-Modified MIL-53(Al) Structural Analogue by Lithium Doping <i>Angewandte Chemie International Edition Engl.</i> 48 (2009), 4639 - 4642</p>	
<p><i>Hofmann, M.; Wimpory, R.C.</i> NET TG1: Residual stress analysis on a single bead weld on a steel plate using neutron diffraction at the new engineering instrument 'STRESS-SPEC' <i>International Journal of Pressure Vessels and Piping</i> 86 (2009), 122 - 125</p>	
<p><i>Inosov, D.S.; Evtushinsky, D.V.; Koitzsch, A.; Zabolotnyy, V.B.; Borisenko, S.V.; Kordyuk, A.A.; Frontzek, M.; Loewenhaupt, M.; Loser, W.; Mazilu, I.; Bitterlich, H.; Behr, G.; Hoffmann, J.-U.; Follath, R.; Buchner, B.</i> Electronic Structure and Nesting-Driven Enhancement of the RKKY Interaction at the Magnetic Ordering Propagation Vector in Gd₂PdSi₃ and Tb₂PdSi₃ <i>Physical Review Letters</i> 102 (2009), 46401 -</p>	E2
<p><i>Jardin, R.; Griveau, J.-C.; Prokes, K.; Heathman, S.; Colineau, E.; Kolomyiets, O.; Normile, P.; Wastin, F.; Rebizant, J.</i> Pressure effects and magnetic structure in U₄PdGa₁₂ <i>Physical Review B: Condensed Matter</i> 79 (2009), 014409 -</p>	E2/E4

<p><i>Jauch, W.; Reehuis, M.</i> Electron density distribution in hexagonal cobalt: A gamma-ray diffraction study Physical Review B: Condensed Matter 80 (2009), 125126 -</p>	
<p><i>Jeworrek, C.; Hollmann, O.; Steitz, R.; Winter, R.; Czeslik, C.</i> Interaction of IAPP and Insulin with Model Interfaces Studied Using Neutron Reflectometry Biophysical Journal 96 (2009), 1115 - 1123</p>	V6
<p><i>Jung, D.; Paradiso, M.; Wallacher, D.; Brandt, A.; Hartmann, M.</i> Formation of cross-linked chloroperoxidase aggregates in the pores of mesocellular foams: Characterization by SANS and catalytic properties ChemSusChem 2 (2009), 161 - 164</p>	V4
<p><i>Kardjilov, N.; Hilger, A.; Manke, I.; Strobl, M.; Dawson, M.; Banhart, J.</i> New trends in neutron imaging Nuclear Instruments and Methods in Physics Research Section A 605 (2009), 13 - 15</p>	V7
<p><i>Kartini, E.; Nakamura, M.; Arai, M.; Inamura, Y.; Taylor, J.W.; Russina, M.</i> Universal dynamics behavior in superionic conducting glasses Solid State Ionics 180 (2009), 506 - 509</p>	V3
<p><i>Kealley, C.S.; Sokolova, A.V.; Kearley, G.J.; Kemner, E.; Russina, M.; Faraone, A.; Hamilton, W.A.; Gilbert, E.P.</i> Dynamical transition in a large globular protein: Macroscopic properties and glass transition Biochimica et Biophysica Acta: Biomembranes 1804 (2009), 34 - 40</p>	V3
<p><i>Kharlamova, M.V.; Arulraj, A.</i> Phase transition in nanostructured LaMnO₃ Journal of Experimental and Theoretical Physics Letters 89 (2009), 301 - 305</p>	E6
<p><i>Kimber, S.A.J.; Kreyssig, A.; Zhang, Y.Z.; Jeschke, H.O.; Valenti, R.; Yokaichiya, F.; Colombier, E.; Yan, J.; Hansen, T.C.; Chatterji, T.; McQueeney, R.J.; Canfield, P.C.; Goldman, A.I.; Argyriou, D.N.</i> Similarities between structural distortions under pressure and chemical doping in superconducting BaFe₂As₂ Nature Materials 8 (2009), 471 - 475</p>	
<p><i>Kimber, S.A.J.; Rodgers, J.A.; Wu, H.; Murray, C.A.; Argyriou, D.N.; Fitch, A.N.; Khomskii, D.I.; Attfield, J.P.</i> Metal-Insulator Transition and Orbital Order in PbRuO₃ Physical Review Letters 102 (2009), 46409 -</p>	E6
<p><i>Kiselev, M.A.; Ermakova, E.V.; Fillippova, S.N.; Surgucheva, N.A.; Dante, S.; Hauss, T.; Gal'chenko, V.F.</i> Structural organization of the phospholipid constituent of cell membranes from Streptomyces hygrosopicus, as determined from neutron diffraction data [Article in Russian] Biofisika Cell Biophysics 54(4):668-74 54 (2009), 668 - 674</p>	V1
<p><i>Kleinert, K.; Denker, A.; Schröder-Smeibidl, B.; Laurenze-Landsberg, C.; Reimelt, M.</i> Zur Bildgenese von Jan Steens Werk "Wie die Alten sungen so zwitschern die Jungen" in der Gemäldegalerie Berlin Jahrestagung Archäometrie und Denkmalpflege 2009, Metalla Sonderheft 2, ISSN 0947-6229, 258-260 (2009)</p>	B8
<p><i>Knafo, W.; Meingast, C.; Boris, A.V.; Popovich, P.; Kovaleva, N.N.; Yordanov, P.; Maljuk, A.; Kremer, R.K.; Lohneysen, H.V.; Keimer, B.</i> Ferromagnetism and lattice distortions in the perovskite YTiO₃ Physical Review B: Condensed Matter 79 (2009), 54431 -</p>	

<p><i>Köbler, U; Hoser, A; Thomas, C</i> Dimensionality crossover upon magnetic saturation in Fe, Ni and Co Journal of Magnetism and Magnetic Materials 321 (2009), 1202 - 1208</p>	V2/E6
<p><i>Kofu, M.; Ueda, H.; Nojiri, H.; Oshima, Y.; Zenmoto, T.; Rule, K.C.; Gerischer, S.; Lake, B.; Batista, C.D.; Ueda, Y.; Lee, S.H.</i> Magnetic-Field Induced Phase Transitions in a Weakly Coupled s=1/2 Quantum Spin Dimer System Ba₃Cr₂O₈ Physical Review Letters 102 (2009), 177204 -</p>	V2
<p><i>Köhler, R.; Donch, I.; Ott, P.; Laschewsky, A.; Fery, A.; Krastev, R.</i> Neutron Reflectometry Study of Swelling of Polyelectrolyte Multilayers in Water Vapors: Influence of Charge Density of the Polycation Langmuir 25 (2009), 11576 - 11585</p>	V6
<p><i>Kovaleva, N.N.; Boris, A.V.; Capogna, L.; Gavartin, J.L.; Popovich, P.; Yordanov, P.; Maljuk, A.; Stoneham, A.M.; Keimer, B.</i> Dipole-active optical phonons in YTiO₃: Ellipsometry study and lattice-dynamics calculations Physical Review B: Condensed Matter 79 (2009), 45114 -</p>	
<p><i>Kravtsov, E.; Nefedov, A.; Nowak, G.; Zhernenkov, K.; Zabel, H.; Hjorvarsson, B.; Liebig, A.; Hoser, A.; McIntyre, G.J.; Paolasini, L.; Remhof, A.</i> Fine-tuning of the spin-density-wave state in Cr/V heterostructures via hydrogen uptake Journal of Physics: Condensed Matter 21 (2009), 336004 -</p>	
<p><i>Krist, T.</i> Trevor Hicks and solid state neutron optics Journal of Physics: Condensed Matter 21 (2009), 124208 -</p>	
<p><i>Kuhbacher, M.; Bartel, J.; Hoppe, B.; Alber, D.; Bukalis, G.; Brauer, A.U.; Behne, D.; Kyriakopoulos, A</i> The brain selenoproteome: priorities in the hierarchy and different levels of selenium homeostasis in the brain of selenium-deficient rats Journal of Neurochemistry 110 (2009), 133 - 142</p>	NAA
<p><i>Landsgesell, S.; Maljuk, A.; Hansen, T.C.; Prokhnenko, O.; Aliouane, N.; Argyriou, D.N.</i> Structural tuning of magnetism in the orthorhombic perovskite Nd_{1-x}Y_xMnO₃: Evidence for magnetic phase separation Physical Review B: Condensed Matter 80 (2009), 14412 -</p>	E9
<p><i>Lazzara, G.; Milioto, S.; Gradzielski, M.; Prevost, S.</i> Small Angle Neutron Scattering, X-ray Diffraction, Differential Scanning Calorimetry, and Thermogravimetry Studies to Characterize the Properties of Clay Nanocomposites Journal of Physical Chemistry C 113 (2009), 12213 - 12219</p>	V4 NMI3: 1384
<p><i>Lehmann, S.; Fuertes Marrón, D.; Tovar, M.; Tomm, Y.; Wolf, C.; Schorr, S.; Schedel-Niedrig, T.; Arushanov, E.; Lux-Steiner, M.Ch.</i> A structural study on the CuGaSe₂-related copper-poor materials CuGa₃Se₅ and CuGa₅Se₈: thin-film vs. bulk material Physical Status Solidi A 206 (2009), 1009 - 1012</p>	E9
<p><i>Lelievre-Berna, E.; Bentley, P.; Bourgeat-Lami, E.; Thomas, M.; Pappas, C.; Kischnik, R.; Moskvin, E.</i> Spherical neutron polarimetry applied to spin-echo and time-of-flight spectroscopy Physica B - condensed matter 404 (2009), 2624 - 2628</p>	V5
<p><i>Maljuk, A.; Tsurkan, V.; Zestrea, V.; Zaharko, O.; Cervellino, A.; Loidl, A.; Argyriou, D.N.</i> Floating-zone growth of large high-quality CoAl₂O₄ single crystals Journal of Crystal Growth 311 (2009), 3997 - 4000</p>	

<p><i>Manke, I.; Kardjilov, N.; Hilger, A.; Strobl, M.; Dawson, M.; Banhart, J.</i> Polarized neutron imaging at the CONRAD instrument at Helmholtz Centre Berlin Nuclear Instruments and Methods in Physics Research Section A 605 (2009), 26 - 29</p>	V7
<p><i>Mascotto, S.; Wallacher, D.; Brandt, A.; Hauss, T.; Thommes, M.; Zickler, G.A.; Funari, S.S.; Timmann, A.; Smarsly, B.M.</i> Analysis of Microporosity in Ordered Mesoporous Hierarchically Structured Silica by Combining Physisorption With in Situ Small-Angle Scattering (SAXS and SANS) Langmuir 25 (2009), 12670 - 12681</p>	V1
<p><i>Matsushima, U.; Herppich, W.B.; Kardjilov, N.; Graf, W.; Hilger, A.; Manke, I.</i> Estimation of water flow velocity in small plants using cold neutron imaging with D2O tracer Nuclear Instruments and Methods in Physics Research Section A 605 (2009), 146 - 149</p>	V7
<p><i>Matsushima, U.; Kardjilov, N.; Hilger, A.; Manke, I.; Shono, H.; Herppich, W.B.</i> Visualization of water usage and photosynthetic activity of street trees exposed to 2ppm of SO2 - A combined evaluation by cold neutron and chlorophyll fluorescence imaging Nuclear Instruments and Methods in Physics Research Section A 605 (2009), 185 - 187</p>	V7
<p><i>Mengarelli, V.; Auvray, L.; Zeghal, M.</i> Phase behaviour and structure of stable complexes of oppositely charged polyelectrolytes EPL-Europhysics Letters 85 (2009), 456 -</p>	V4 IHP: 1155
<p><i>Mezei, F.; Russina, M.; Chen, G.; Frauenfelder, H.; Fenimore, P.W.; Falus, P.; Farago, B.</i> Dynamic transition and glassy behaviour in hydrated proteins Journal of Physics: Conference Series 177 (2009), 012011/1 - 2</p>	V3
<p><i>Mihalik, M.; Kitazawa, H.; Divis, M.; Sechovsky, V.</i> Magnetism in PrPdSn and NdPdSn studied on single crystals International Journal of Materials Research 100 (2009), 1190 - 1192</p>	
<p><i>Mihalik, M.; Matej, Z.; Divis, M.; Sechovsky, V.</i> Polymorphism of PrIr2Si2 - In situ XRPD experiments and theoretical calculations Intermetallics 17 (2009), 927 - 929</p>	
<p><i>Milani, S.; Berti, D.; Dante, S.; Hauss, T.; Baglioni, P.</i> Intercalation of Single-Strand Oligonucleotides between Nucleolipid Anionic Membranes: A Neutron Diffraction Study Langmuir (2009), 4084 - 4092</p>	V1
<p><i>Milano-Brusco, J.; Prevost, S.; Lugo, D.; Gradzielski, M.; Schomacker, R.</i> Catalytic hydrogenation of dimethyl itaconate in non-ionic microemulsions: influence of the size of micelle New Journal of Chemistry 33 (2009), 1726 - 1735</p>	V4
<p><i>Mitsuda, S.; Nakajima, T.; Yamano, M.; Takahashi, K.; Yamazaki, H.; Masuda, K.; Kaneko, Y.; Terada, N.; Prokes, K.; Kiefer, K.</i> Electric polarization memory effect in a magnetoelectric multiferroic CuFe1-xGaxO2 Physica B - condensed matter 404 (2009), 2532 - 2534</p>	E4
<p><i>Mori, T.; Shishido, T.; Nakajima, K.; Kiefer, K.; Siemensmeyer, K.</i> Magnetic properties of the thulium layered compound (Tm2AlB6)-B-11: An AIB2-type analogue Journal of Applied Physics 105 (2009), 07E124-1 - 07E124-3</p>	

<p><i>Morris, D.J.P.; Roger, M.; Gutmann, M.J.; Goff, J.P.; Tennant, D.A.; Prabhakaran, D.; Boothroyd, A.T.; Dudzik, E.; Feyerherm, R.; Hoffmann, J.U.; Kiefer, K.</i></p> <p>Crystal-to-stripe reordering of sodium ions in Na_xCoO_2 ($x \geq 0.75$)</p> <p>Physical Review B: Condensed Matter 79 (2009), 100103 -</p>	E2
<p><i>Morris, D.J.P.; Tennant, D.A.; Grigera, S.A.; Klemke, B.; Castelnovo, C.; Moessner, R.; Czternasty, C.; Meissner, M.; Rule, K.C.; Hoffmann J-U.; Kiefer, K.; Gerischer, S.; Slobinsky, D.; Perry, R.S.</i></p> <p>Dirac Strings and Magnetic Monopoles in Spin Ice $\text{Dy}_2\text{Ti}_2\text{O}_7$</p> <p>Science 326 (2009), 411 - 414</p>	E2
<p><i>Mufti, N; Blake, G.R.; Nugroho, A.A.; Palstra, T.T.M.</i></p> <p>Magnetic field induced ferroelectric to relaxor crossover in $\text{Tb}_{1-x}\text{Ca}_x\text{MnO}_3$</p> <p>Journal of Physics: Condensed Matter 21 (2009), 452203 -</p>	E4 IHP: 1343
<p><i>Muhlbauer, S.; Pfleiderer, C.; Boni, P.; Forgan, E.M.; Brandt, E.H.; Wiedenmann, A.; Keiderling, U.</i></p> <p>Intrinsic bulk vortex dynamics revealed by time resolved small angle neutron scattering</p> <p>Physica B - condensed matter 404 (2009), 3231 - 3234</p>	V4
<p><i>Muhlbauer, S.; Pfleiderer, C.; Boni, P.; Laver, M.; Forgan, E.M.; Fort, D.; Keiderling, U.; Behr, G.</i></p> <p>Morphology of the Superconducting Vortex Lattice in Ultrapure Niobium</p> <p>Physical Review Letters 102 (2009), 136408 -</p>	V4
<p><i>Nakajima, T.; Mitsuda, S.; Takahashi, K.; Yamano, M.; Masuda, K.; Yamazaki, H.; Prokes, K.; Kiefer, K.; Gerischer, S.; Terada, N.; Kitazawa, H.; Matsuda, M.; Kakurai, K.; Kimura, H.; Noda, Y.; Soda, M.; Matsuura, M.; Hirota, K.</i></p> <p>Comprehensive study on ferroelectricity induced by a proper-screw-type magnetic ordering in multiferroic CuFeO_2: Nonmagnetic impurity effect on magnetic and ferroelectric order</p> <p>Physical Review B: Condensed Matter 79 (2009), 214423 -</p>	E4
<p><i>Niazi, A.; Bud'ko, S.L.; Schlagel, D.L.; Yan, J.Q.; Lograsso, T.A.; Kreyssig, A.; Das, S.; Nandi, S.; Goldman, A.I.; Honecker, A.; McCallum, R.W.; Reehuis, M.; Pieper, O.; Lake, B.; Johnston, D.C.</i></p> <p>Single-crystal growth, crystallography, magnetic susceptibility, heat capacity, and thermal expansion of the antiferromagnetic $\text{S}=1$ chain compound CaV_2O_4</p> <p>Physical Review B: Condensed Matter 79 (2009), 104432 -</p>	E5
<p><i>Nowicki, W.</i></p> <p>Synthesis, structure and magnetic properties of Fe-doped tetragonal $\text{Li}_{0.95}\text{Mn}_{2.05}\text{O}_4$</p> <p>Zeitschrift für Kristallographie (2009), 415 - 420</p>	E9 NMI3: 1257
<p><i>Ohms, C.; Wimpory, R.C.; Katsareas, D.E.; Youtsos, A.G.</i></p> <p>NET TG1: Residual stress assessment by neutron diffraction and finite element modeling on a single bead weld on a steel plate</p> <p>International Journal of Pressure Vessels and Piping 86 (2009), 63 - 72</p>	
<p><i>Orts-Gil, G.; Prévost, S.; Losik, M.; Hermes, F.; Schlaad, H.; Hellweg, Th.</i></p> <p>Polypeptide hybrid copolymers as selective micellar nanocarriers in nonaqueous media</p> <p>Colloid and Polymer Science 287 (2009), 1295 - 1304</p>	V4

<p><i>Painter, T.A.; Bird, M.D.; Dixon, I.R.; Ehmler, H.; Heinrich, J.; Smeibidl, P.; Xu, T.; Zhai, Y.H.</i> Series-Connected Hybrid Magnetic Shielding Conceptual Design for the Helmholtz Centre Berlin for Materials and Energy IEEE Transactions on Applied Superconductivity 19 (2009), 1600 - 1603</p>	
<p><i>Pappas, C.; Lelievre-Berna, E.; Falus, P.; Bentley, P.M.; Moskvina, E.; Grigoriev, S.; Fouquet, P.; Farago, B.</i> Chiral Paramagnetic Skyrmion-like Phase in MnSi Physical Review Letters 102 (2009), 197202 -</p>	
<p><i>Pappas, C.; Lelievre-Berna, E.; Falus, P.; Farago, B.; Bentley, P.; Moskvina, E.; Krist, T.; Grigoriev, S.</i> Challenges in neutron spin echo spectroscopy Physica B - condensed matter 404 (2009), 2578 - 2581</p>	V5
<p><i>Pickup, R.M.; Cywinski, R.; Pappas, C.; Farago, B.; Fouquet, P.</i> Generalized Spin-Glass Relaxation Physical Review Letters 102 (2009), 97202 -</p>	
<p><i>Pieper, J.; Buchsteiner, A.; Dencher, N.A.; Lechner, R.E.; Hauß, T.</i> Light-induced modulation of protein dynamics during the photocycle of bacteriorhodopsin. Photochemistry and Photobiology 85 (2009), 590 - 597</p>	V3
<p><i>Pieper, O.; Lake, B.; Daoud-Aladine, A.; Reehuis, M.; Prokes, K.; Klemke, B.; Kiefer, K.; Yan, J.Q.; Niazi, A.; Johnston, D.C.; Honecker, A.</i> Magnetic structure and interactions in the quasi-one-dimensional antiferromagnet CaV₂O₄ Physical Review B: Condensed Matter 79 (2009), 180409 -</p>	E4/E5
<p><i>Pleshchev, V.G.; Selezneva, N.V.; Maksimov, V.I.; Korolev, A.V.; Podlesnyak, A.V.; Baranov, N.V.</i> Specific features of the structure, magnetic properties, and heat capacity of intercalated compounds Cr (x) TiSe₂ Physics of the Solid State 51 (2009), 933 - 939</p>	
<p><i>Pooke, D.M.; Chamritski, V.; Fee, M.; Gibson, S.; King, B.T.; Tallon, J.L.; Meissner, M.; Feyerherm, R.; Olsen, S.R.; Kennedy, S.J.; Robinson, R.A.</i> HTS 5 Tesla Synchrotron and Neutron Beamline Magnets IEEE Transactions on applied superconductivity 19 (2009), 1372 - 1375</p>	
<p><i>Pratt, D.K.; Zhao, Y.; Kimber, S.A.J.; Hiess, A.; Argyriou, D.N.; Broholm, C.; Kreyssig, A.; Nandi, S.; Bud'ko, S.L.; Ni, N.; Canfield, P.C.; McQueeney, R.J.; Goldman, A.I.</i> Suppression of antiferromagnetic spin fluctuations in the collapsed phase of CaFe₂As₂ Physical Review B: Condensed Matter 79 (2009), 060510 -</p>	
<p><i>Prevost, S.; Gradzielski, M.</i> SANS investigation of the microstructures in catanionic mixtures of SDS/DTAC and the effect of various added salts Journal of Colloid and Interface Science 337 (2009), 472 - 484</p>	V4
<p><i>Prokes, K.</i> The effect of uniaxial pressure on the antiferromagnetic structure of UNiAl studied using single-crystal neutron diffraction Journal of Physics: Condensed Matter 21 (2009), 236009 -</p>	E2
<p><i>Prokes, K.; Bruck, E.; Sechovsky, V.</i> Antiferromagnetic structure in UNiAl at dilution temperatures Physica B - condensed matter 404 (2009), 3025 - 3027</p>	E4/E6
<p><i>Prokes, K.; Gukasov, A.</i> Magnetization densities in URhSi studied by polarized neutron diffraction Physical Review B: Condensed Matter 79 (2009), 24406 -</p>	E2

<p><i>Prokes, K.; Lander, G.H.; Bernhoeft, N.</i> Anomalous shift of magnetic diffuse scattering studied by neutron diffraction <i>Journal of Physics: Condensed Matter</i> 21 (2009), 285402 -</p>	E4
<p><i>Prokes, K.; Mydosh, J.A.</i> On the ground-state magnetic structure in Er₂Ni₂Pb <i>European Physical Journal B</i> 67 (2009), 1 - 6</p>	E6
<p><i>Prokes, K.; Mydosh, J.A.</i> Field-induced ferromagnetic structure in Er₂Ni₂Pb <i>Journal of Physics: Condensed Matter</i> 21 (2009), 216005 -</p>	E6
<p><i>Prokes, K.; Sechovsky, V.; Syshchenko, O.</i> Magnetic structure of Er₆Ni₂Sn <i>Journal of Alloys and Compounds</i> 467 (2009), 48 - 53</p>	E6
<p><i>Raekers, M.; Kuepper, K.; Bartkowski, S.; Prinz, M.; Postnikov, A.V.; Potzger, K.; Zhou, S.; Arulraj, A.; Stusser, N.; Uecker, R.; Yang, W.L.; Neumann, M.</i> Electronic and magnetic structure of RScO₃ (R=Sm,Gd,Dy) from x-ray spectroscopies and first-principles calculations <i>Physical Review B: Condensed Matter</i> 79 (2009), 125114 -</p>	E6
<p><i>Remhof, A.; Friedrichs, O.; Buchter, F.; Mauron, Ph.; Kim, J.W.; Oh, K.H.; Buchsteiner, A.; Wallacher, D.; Züttel, A.</i> Hydrogen cycling behavior of LiBD₄/Al studied by in situ neutron diffraction <i>Journal of Alloys and Compounds</i> 484 (2009), 654 - 659</p>	E6 IHP: 1355
<p><i>Repper, J.; Hofmann, M.; Krempaszy, C.; Wimpory, R.C.; Petry, W.; Werner, E.</i> Microstrain accumulation in multiphase superalloys <i>Powder Diffraction</i> 24 (2009), S65 - S67</p>	
<p><i>Rolfs, K.; Mecklenburg, A.; Guldbakke, J.-M.; Wimpory, R.C.; Raatz, A.; Hesselbach, J.; Schneider, R.</i> Crystal quality boosts responsiveness of magnetic shape memory single crystals <i>Journal of Magnetism and Magnetic Materials</i> 321 (2009), 1063 - 1067</p>	E3
<p><i>Rule, K.C.; Ehlers, G.; Gardner, J.S.; Qiu, Y.; Moskvina, E.; Kiefer, K.; Gerischer, S.</i> Neutron scattering investigations of the partially ordered pyrochlore Tb₂Sn₂O₇ <i>Journal of Physics: Condensed Matter</i> 21 (2009), 486005 -</p>	V5
<p><i>Russina, M.; Mezei, F.</i> First implementation of Repetition Rate Multiplication in neutron spectroscopy <i>Nuclear Instruments and Methods in Physics Research Section A</i> 604 (2009), 624 - 631</p>	V3
<p><i>Russina, O.; Beiner, M.; Pappas, C.; Russina, M.; Arrighi, V.; Unruh, T.; Mullan, C.L.; Hardacre, C.; Triolo, A.</i> Temperature Dependence of the Primary Relaxation in 1-Hexyl-3-methylimidazolium bis((trifluoromethyl)sulfonyl)imide <i>Journal of Physical Chemistry B</i> 113 (2009), 8469 - 8474</p>	V5 NMI3: 1295
<p><i>Saensunon, B.; Stewart, G.A.; Gubbens, P.C.M.; Hutchison, W.D.; Buchsteiner, A.</i> The crystal field interaction at the rare earth site in ErNiAl₄ <i>Journal of Physics: Condensed Matter</i> 21 (2009), 124215 -</p>	

<p>Sazonov, A.P.; Troyanchuk, I.O.; Gamari-Seale, H.; Sikolenko, V.V.; Stefanopoulos, K.L.; Nicolaides, G.K.; Atanassova, Y.K. Neutron diffraction study and magnetic properties of La_{1-x}BaxCoO₃ (x = 0.2 and 0.3) Journal of Physics: Condensed Matter 21 (2009), 156004 -</p>	E9 IHP: 1243
<p>Schorr, S.; Tovar, M.; Hoebler, H.-J.; Schock, H.-W. Structure and phase relations in the 2(CuInS₂) - Cu₂ZnSnS₄ solid solution system Thin Solid Films 517 (2009), 2508 - 2510</p>	E9
<p>Schröder, A.; Wippermann, K.; Mergel, J.; Lehnert, W.; Stolten, D.; Sanders, T.; Baumhöfer, T.; Sauer, D.U.; Manke, I.; Kardjilov, N.; Hilger, A.; Schloesser, J.; Banhart, J.; Hartnig, Ch. Combined local current distribution measurements and high resolution neutron radiography of operating Direct Methanol Fuel Cells Electrochemistry Communications 11 (2009), 1606 -</p>	V7
<p>Schröter, A.; Kiselev, M.A.; Hauß, T.; Dante, S.; Neubert, R.H.H. Evidence of free fatty acid interdigitation in stratum corneum model membranes based on ceramide [AP] by deuterium labelling. Biochimica et Biophysica Acta: Biomembranes 1788 (2009), 2194 - 2203</p>	V1
<p>Schröter, A.; Kessner, D.; Kiselev, M.A.; Hauß, T.; Dante, S.; Neubert, R.H.H. Basic nanostructure of stratum corneum lipid matrices based on ceramides [EOS] and [AP]: a neutron diffraction study Biophysical Journal 97 (2009), 1104 - 1114</p>	V1
<p>Seelert, H.; Dani, D.N.; Dante, S.; Hauss, T.; Krause, F.; Schafer, E.; Frenzel, M.; Poetsch, A.; Rexroth, S.; Schwassmann, H.J.; Suhai, T.; Vonck, J.; Dencher, N.A. From protons to OXPHOS supercomplexes and Alzheimer's disease: Structure-dynamics-function relationships of energy-transducing membranes Biochimica et Biophysica Acta: Bioenergetics 1787 (2009), 657 - 671</p>	V1
<p>Shtangeeva, I.; Alber, D.; Bukalis, G.; Stanik, B.; Zepezauer, F. Multivariate statistical analysis of nutrients and trace elements in plants and soil from northwestern Russia Plant and Soil 322 (2009), 219 - 228</p>	NAA
<p>Sikolenko, V.; Efimov, V.; Efimova, E.; Sazonov, A.; Ritter, C.; Kuzmin, A.; Troyanchuk, I. Neutron diffraction studies of structural and magnetic properties of niobium doped cobaltites Journal of Physics: Condensed Matter 21 (2009), 1 - 7</p>	NMI3: 1171 NMI3: 1170
<p>Skoulatos, M.; Goff, J.P.; Geibel, C.; Kaul., E.E.; Nath, R.; Shannon, N.; Schmidt, B.; Murani, A.P.; Deen, P.P.; Enderle, M.; Wildes, A.R. Spin correlations and exchange in square-lattice frustrated ferromagnets EPL-Europhysics Letters 88 (2009), 57005 -</p>	
<p>Smrcok, L.; Kucharik, M.; Tovar, M.; Zicak, I. High temperature powder diffraction and solid state DFT study of β-cryolite (Na₃AlF₆) Crystal Research and Technology 44 (2009), 834 - 840</p>	E9 NMI3: 1261
<p>Sobolev, O.; Le Forestier, L.; Gonzalez, M.A.; Russina, M.; Kemner, E.; Cuello, G. J.; Charlet, L. Hydration of Na⁺, Ni²⁺, and Sm³⁺ in the Interlayer of Hectorite: A Quasielastic Neutron Scattering Study Journal of Physical Chemistry B 113 (2009), 13801 - 13812</p>	V3 IHP: 1322

<p><i>Sosman, L.P.; Yokaichiya, F.; Bordallo, H.N</i> Raman and magnetic susceptibility studies of hexagonal elpasolite Cs₂NaAlF₆:Cr³⁺ <i>Journal of Magnetism and Magnetic Materials</i> 321 (2009), 2210 - 2215</p>	
<p><i>Stock, C.; Buyers, W.J.L.; Rule, K.C.; Chung, J.-H.; Liang, R.; Bonn, D.; Hardy, W.N.</i> Magnetic field resonantly enhanced free spins in heavily underdoped YBa₂Cu₃O_{6+x} <i>Physical Review B: Condensed Matter</i> 79 (2009), 184514/1 - 8</p>	V2 NMI3: 1285
<p><i>Strobl, M.</i> Future prospects of imaging at spallation neutron sources <i>Nuclear Instruments and Methods in Physics Research Section A</i> 604 (2009), 646 - 652</p>	
<p><i>Strobl, M.; Hilger, A.; Kardjilov, N.; Ebrahimi, O.; Keil, S.; Manke, I.</i> Differential phase contrast and dark field neutron imaging <i>Nuclear Instruments and Methods in Physics Research Section A</i> 605 (2009), 9 - 12</p>	V12a
<p><i>Strobl, M.; Kardjilov, N.; Hilger, A.; Jericha, E.; Badurek, G.; Manke, I.</i> Imaging with polarized neutrons <i>Physica B - condensed matter</i> 404 (2009), 2611 - 2614</p>	V7
<p><i>Strobl, M.; Kardjilov, N.; Hilger, A.; Kuhne, G.; Frei, G.; Manke, I.</i> High-resolution investigations of edge effects in neutron imaging <i>Nuclear Instruments and Methods in Physics Research Section A</i> 604 (2009), 640 - 645</p>	V7
<p><i>Strobl, M.; Manke, I.; Kardjilov, N.; Hilger, A.; Dawson, M.; Banhart, J.</i> Advances in neutron radiography and tomography <i>Journal of Physics D-Applied Physics</i> 42 (2009), 243001 -</p>	V7
<p><i>Szytula, A.; Kaczorowski, D.; Gondek, L.; Arulraj, A.; Baran, S.; Penc, B.</i> Magnetic properties of NdAu₂Ge₂ <i>Journal of Magnetism and Magnetic Materials</i> 321 (2009), 3402 - 3405</p>	E6 NMI3: 1256
<p><i>Takada, K.; Onoda, M.; Choi, Y.N.; Argyriou, D.N.; Izumi, F.; Sakurai, H.; Takayama-Muromachi, E.; Sasaki, T.</i> 2 x 2 Superstructure in Sodium Cobalt Oxide Superconductors <i>Chemistry of Materials</i> 21 (2009), 3693 - 3700</p>	E9
<p><i>Thiedmann, R.; Hartnig, C.; Manke, I.; Schmidt, V.; Lehnert, W.</i> Local Structural Characteristics of Pore Space in GDLs of PEM Fuel Cells Based on Geometric 3D Graphs <i>Journal of The Electrochemical Society</i> 156 (2009), B1339 - B1347</p>	V7
<p><i>Thielemann, B.; Rugg, C.; Kiefer, K.; Ronnow, H.M.; Normand, B.; Bouillot, P.; Kollath, C.; Orignac, E.; Citro, R.; Giamarchi, T.; Lauchli, A.M.; Biner, D.; Kramer, K.W.; Wolff-Fabris, F.; Zapf, V.S.; Jaime, M.; Stahn, J.; Christensen, N.B.; Grenier, B.</i> Field-controlled magnetic order in the quantum spin-ladder system (H₂pip)₂CuBr₄ <i>Physical Review B: Condensed Matter</i> 79 (2009), 20408 -</p>	
<p><i>Thielemann, B.; Rugg, C.; Ronnow, H.M.; Lauchli, A.M.; Caux, J.S.; Normand, B.; Biner, D.; Kramer, K.W.; Gudel, H.U.; Stahn, J.; Habicht, K.; Kiefer, K.; Boehm, M.; McMorro, D.F.; Mesot, J.</i> Direct Observation of Magnon Fractionalization in the Quantum Spin Ladder <i>Physical Review Letters</i> 102 (2009), 107204 -</p>	V2
<p><i>Tolinski, T.; Hoser, A.; Rols, S.; Kowalczyk, A.; Szlaferek, A.</i> Crystal field states in CeCu₄Al <i>Solid State Communications</i> 149 (2009), 2240 - 2243</p>	

<p><i>Triolo R.; Kardjilov N.; Giambona G.; Lo Celso F.; Benfante V.; Tusa S.; Ruffo I.</i> Archaeometric Applications of X-ray and Neutron Techniques <i>Atti Accademia Scienze Lettere Arti Palermo XXV (2009), 133 - 148</i></p>	<p>NMI3 II: 1551 NMI3 II: 1299</p>
<p><i>Triolo, A.; Russina, O.; Fazio, B.; Appetecchi, G.B.; Carewska, M.; Passerini, S.</i> Nanoscale organization in piperidinium-based room temperature ionic liquids <i>Journal of Chemical Physics 130 (2009), 164521 -</i></p>	
<p><i>Troyanchuk, I.O.; Bushinsky, M.V.; Karpinsky, D.V.; Mantyskaya, O.S.; Fedotova, V.V.; Prochnenko, O.I.</i> Structural transformations and magnetic properties of Bi(1-x)Ln(x)FeO(3) (Ln = La, Nd, Eu) multiferroics <i>Physical Status Solidi B 246 (2009), 1901 - 1907</i></p>	<p>E9 NMI3: 1347</p>
<p><i>Troyanchuk, I.O.; Karpinskii, D.V.; Bushinskii, M.V.; Chobot, A.N.; Pushkarev, N.V.; Prohnenko, O.; Kopcewicz, M.; Szymczak, R.</i> Crystal and magnetic structures of the Bi_{1-x}Sr_xFeO_{3-δ} and Bi_{1-x}A_xFe_{1-x}Mn_xO₃ (A = Sr, Ca) solid solutions <i>Crystallography Reports 54 (2009), 1172 - 1178</i></p>	<p>E9 NMI3: 1347 NMI3: 1306</p>
<p><i>Ustinov, A.; Olikhovska, L.; Glavatska, N.; Glavatskyy, I.</i> Diffraction features due to ordered distribution of the twin boundaries (110), <110> in orthorhombic Ni-Mn-Ga crystals <i>Journal of Applied Crystallography 42 (2009), 211 - 216</i></p>	<p>E1/E2</p>
<p><i>Weber, F.; Aliouane, N.; Zheng, H.; Mitchell, J.F.; Argyriou, D.N.; Reznik, D.</i> Signature of checkerboard fluctuations in the phonon spectra of a possible polaronic metal La_{1.2}Sr_{1.8}Mn₂O₇ <i>Nature Materials 8 (2009), 798 - 802</i></p>	
<p><i>Wimpory, R.C.; Ohms, C.; Hofmann, M.; Schneider, R.; Youtsos, A.G.</i> Statistical analysis of residual stress determinations using neutron diffraction <i>International Journal of Pressure Vessels and Piping 86 (2009), 48 - 62</i></p>	
<p><i>Xiao, D.; Hines, L.G.; Li, S.F.; Bartsch, R.A.; Quitevis, E.L.; Russina, O.; Triolo, A.</i> Effect of Cation Symmetry and Alkyl Chain Length on the Structure and Intermolecular Dynamics of 1,3-Dialkylimidazolium Bis(trifluoromethanesulfonyl)amide Ionic Liquids <i>Journal of Physical Chemistry B 113 (2009), 6426 - 6433</i></p>	
<p><i>Yokaichiya, F.; Krimmel, A.; Tsurkan, V.; Margiolaki, I.; Thompson, P.; Bordallo, H.N.; Buchsteiner, A.; Stusser, N.; Argyriou, D.N.; Loidl, A.</i> Spin-driven phase transitions in ZnCr₂Se₄ and ZnCr₂S₄ probed by high-resolution synchrotron x-ray and neutron powder diffraction <i>Physical Review B: Condensed Matter 79 (2009), 64423 -</i></p>	<p>E9</p>
<p><i>Zheludev, A.; Garlea, V.O.; Tselik, A.; Regnault, L.-P.; Habicht, K.; Kiefer, K.; Roessli, B.</i> Excitations from a chiral magnetized state of a frustrated quantum spin liquid <i>Physical Review B: Condensed Matter 80 (2009), 214413/1 - 6</i></p>	<p>V2</p>

AUTHOR INDEX

AUTHOR INDEX

Author	Page	Author	Page	Author	Page
A					
Abdul-Redah, T.	78	Ebrahimi, O.	8, 10, 11, 91, 93	Habicht, K.	47, 48, 49, 51
Aldridge, L. P.	88, 92	Eckert, J.	114	Hartmann, M.	80
Anderson, K.	3	Eder, N.	135	Hauß, Th.	83, 102, 105, 106, 152
Argyriou, D.	29, 66, 97	Efimov, V.	76	Heintze, C.	153
Arlt, T.	155	Ehlers, G.	54	Hellweg, T.	116, 126
Arulraj, A.	35, 72	Eisenhardt, S. U. H.	51	Henry, P.	40, 81, 97
Aynajian, P.	48	Engelbrecht, T.	103, 106	Hilger, A.	5, 6, 61, 156, 158, 159, 160, 162, 165
B					
Baran, S.	38, 75	Epp, J.	136	Himsl, D.	80
Behrens, M.	82	Evers, F.	119, 127	Hirsch, Th.	136, 139
Bellissent-Funel, M.-C.	112	F			
Boldyreva, E.	101	Farajian-Sohi, M.	144	Hoch, C.	68
Broholm, C.	43	Fiebig, M.	16	Hoffmann, J.-U.	15, 17, 18, 20
Bryant, G.	107	Fischer, J.	99, 113	Hofmann, M.	145
Buchsteiner, A.	103, 105, 106, 107, 152	Fouquet, P.	3	Hong, T.	44
Bunn, J.	162	Freire, P. T. C.	98, 108	Hoser, A.	15, 19, 37, 38, 39, 72, 73, 74, 75
C					
Calbucci, V.	138	Friederichs, O.	71, 150	I	
Campana, M.	120	Früh, J.	123	Iles, G.	23
Carradó, A.	137	Fujioka, J.	32, 33	Islam, N.	30, 34, 46, 53, 69
Chang, L. J.	15	G			
Chatterji, T.	22, 23	Garcia-Moreno, F.	6	Izaola, Z.	87, 110
Chmielus, M.	21, 142, 143, 159	Gardner, J.	54	J	
Choi, H.-C.	60	Garvey, Ch.	107, 128	Jalarvo, N.	89
Christensen, N. B.	51	Gaulin, B.	45	Jiao, X.	98
Comyn, T.	17	Gavrilov, V.	72	Jonke, J.	135
Czeslik, C.	119, 127	Geisler, M.	161	Josic, L.	156
Czub, J.	35, 87	Gerischer, S.	20, 28, 31, 36, 38	K	
D					
Da Silva Pedro, S.	67	Gibmeier, J.	145	Kallfaß, C.	68
Da Silva Rocha, A.	139	Giere, P.	165	Kandemir, T.	5
Dahint, R.	9, 121, 122, 125	Gil, A.	39	Kaneko, K.	19
Davies, C. M.	146	Gilbert, E. P.	109	Karakas, N.	8, 10, 11, 91, 93
Dawson, M.	4, 5, 6, 156, 158, 160, 161, 162, 166	Glancy, P.	45	Kardjilov, N.	4, 5, 6, 61, 155, 156, 157, 158, 160, 161, 162, 165, 166, 167
Demeter, J.	58, 59	Glavatskyi, I.	17, 18, 21, 65	Karimova, O.	70
Dencher, N. A.	105	Goldman, A.	29	Katsaros, F. K.	104
Dobner, B.	103, 106	Goll, G.	25	Katsavounis, S.	74
Dobron, P.	135	Gondek, L.	35, 87, 157	Kearley, G. J.	109
Doodoo, S.	118	Grigera, S.	20	Keiderling, U.	153, 154
Dreismann, C. A. C.	78	Grohol, D.	26	Keimer, B.	32, 33
E					
H					

AUTHOR INDEX

Author	Page	Author	Page	Author	Page
Kim, K.-Y.	60	Migliardo, F.	111	Q	
Kimber, S.	29, 66, 77	Mihalik, M.	37	Quintero Castro, D. L.	30, 46, 53
Kißner, S.	82	Minkov, V.	97	R	
Klemke, B.	20	Miyasaka, S.	32, 33	Raitman, E.	72
Knoll, W.	115	Mjasischev, D.	72	Ray, A.	88, 92
Köhler, R.	117, 119, 123, 124	Morris, J.	20, 55	Rayaprol, S.	73
Kolasinska, M.	117	Moskvin, E.	3, 54, 55	Reehuis, M.	30, 32, 33, 34, 66, 68, 69
Kongshaug, C.	89	Mufit, N.	19	Rehm, C.	92
Konieczko-Dziadula, M.	93	Mukherji, D.	154	Reichart, Ch.	119
Körner, J.	129	Müllner, P.	21, 142, 143, 159	Reichenauer, G.	152, 161
Kosmidou, K.	74	N		Reinhardt, M.	125
Krastev, R.	117, 123, 124	Naberezhnov, A.	65, 84	Remhof, A.	71, 85, 150
Kratz, K.	129	Nagy, B.	56	Robinson, J. S.	147
Kreuzer, M.	9, 121, 122, 125, 127	Natali, F.	115	Rolfs, K.	61, 149
Kreyssig, A.	29	Neubert, R.	103, 106	Roennow, H. M.	51
Krüger, P.	155	Neumann, Ch.	165	Ross, K.	45
Kubo, H.	27	Niazi, A.	53	Rovira-Esteva, M.	86, 90, 100
Kühl, S.	82	Nikseresht, N.	42	Ruff, J.	45
Kuhn, R.	155	Nitschke-Pagel, Th.	133	Ruffo, I.	166
Kursula, P.	115	Nunes, R.	139	Ruiz-Martin, M. D.	86, 90, 100
Kuzmin, A.	76	Nunes-Bordallo, H.	67, 88, 90, 92, 97, 98, 99, 101, 108, 113	Rule, K.	20, 43, 45, 50, 52, 54, 55
L		O		Russina, M.	77, 109, 110, 111, 112
Lake, B.	30, 34, 46, 50, 53, 69	Ohms, C.	148	Rysiakiewicz-Pasek, E.	65
Larsen, J.	51	Onimaru, T.	27	S	
Le, D.	47	Orendáč, M.	36	Sales, M.	51
Lee, J. S.	60	Orendáčová, A.	28, 31, 36	Sampathkumaran E. V.	73
Lee, Y. S.	26	P		Sanders, T.	155
Lees, M. R.	15	Palkowski, H.	137	Sapalidis, A. A.	104
Lefmann, K.	51	Pappas, C.	3	Saramago, B.	124
Lehmann, E.	156	Paramanik, D.	59	Sato, T.J.	26
Lehmann, Th.	165	Pardo, L. C.	86, 90, 100	Scherb, T.	77, 110
Lenne, Th.	107	Parshin, P.	84	Scherdel, Ch.	152
Lerch, M.	78	Paul, A.	56, 57	Schier, H.	68
Levy, D.	41	Paulke, A.	159, 165	Schmidt, B.	105
Liesegang, M.	91	Penc, B.	38, 39, 75	Schneider, R.	21, 142, 143, 159
Lorrmann, V.	152	Penunadu, D.	7, 158, 162	Schöbel, M.	135
M		Pérez-Hernández, N.	114	Schorr, S.	79
Magazù, S.	111	Peters, J.	115	Schröder, A.	155
Manescu, A.	138	Popravski, R.	65	Schubert, H.	68
Manke, I.	4, 5, 6, 61, 160	Preu, J.	102	Schumacher, G.	77, 110
Martelli, P.	85	Prokes, K.	26, 27, 28, 29, 31	Seidel, S.-O.	7, 8, 10, 11, 91, 92, 93, 129
Masuda, T.	52			Selvaraj, N. B.	157
Matan, K.	26			Serra, J.	77, 110
Mat'áš, S.	25, 26, 28, 31, 36				
Meier, D.	16				

AUTHOR INDEX

Author	Page	Author	Page
Sharifi, M.	83		
Siemensmeyer, K.	36		
Sikolenko, V.	76		
Siouris, I. M.	74		
Siruguri, V.	73		
Skoulatos, M.	42, 47, 48, 49, 51		
Smallwood, A.	88, 92		
Sokolova, A. V.	109		
Sosman, L. P.	67		
Stehle, R.	126		
Steitz, R.	9, 56, 58, 60, 118, 119, 120, 121, 122, 125, 127		
Stephan, C.	79		
Steriotis, T. A.	104		
Stevenson, T.	17		
Stockert, O.	19, 25		
Strobl, M.	4, 5, 7, 9, 61, 92, 128, 160		
Strunz, P.	154		
Stüßer, N.	72		
Su, Y.	15		
Süllow, S.	43		
Sumin, V.	151		
Szytula, A.	39		
T			
Takabatake, T.	27		
Tamaki, M.	156		
Tarasenko, R.	36		
Teichert, A.	58, 59, 60, 120		
Temst, K.	58		
Tennant, A.	20, 55		
Thomas, P.	88, 92		
Tokura, Y.	32, 33		
Tolan, M.	119, 127		
Toth, S.	50		
Tovar, M.	65, 78, 82		
Treimer, W.	8, 10, 11, 91, 93, 129		
Tremsin, A.	4		
Triolo, R.	166		
Tsapatsaris, N.	77, 110, 111, 114		
Tumanov, N.	101		
U			
Umeo, K.	27		
Ulbricht, A.	153		
Ulrich, C.	32, 33		
		V	
		v. Klitzing, R.	118
		v. Nessen, K.	116
		Van Bael, M. J.	58
		Venter, A.	151
		Visser, D.	167
		Vogtt, K.	112
		W	
		Wallacher, D.	56, 71, 77, 80, 82, 83, 85, 89, 110, 150
		Wark, M.	83
		Warszynski, P.	117
		Wellert, S.	116, 126
		Wheeler, E.	34, 46, 69
		Wieder, F.	166
		Wiener, M.	152
		Wimporoy, R. C.	133, 136, 137, 138, 139, 141, 142, 143, 144, 145, 146, 147, 148, 151
		Wolter, A.	43
		Woracek, R.	158
		Y	
		Yokaichiya, F.	67, 79, 98, 101
		You, C.-Y.	60
		Z	
		Zarbakhsh, A.	120
		Zheludev, A.	44